Studies of DNA binding of Lanthanide Platinum Complexes

by

Luca Scarpantonio

A thesis submitted to

The University of Birmingham

For the degree of

DOCTOR OF PHILOSOPHY

This thesis is dedicated to Fredi, who passed me the passion for Physics and Chemistry.

Acknowledgements

I would like to thank my supervisor Dr. Zoe Pikramenou who gave me the opportunity to join her group for my PhD four years ago. She has been always present for help, suggestions, support and my experience in her group has been determinant for my scientific formation. I wish to thank all the people that I met in Zoe group, those who helped me at beginning of my PhD and those who shared with me great time in the lab in the last years. I would like to thank the people working at the Analytical Facilities of the School of Chemistry for the technical support received during the last four years. I am particularly grateful to Dr. Neil Spencer, Peter Ashton and Graham Burns for their availability and for their precious friendships. I wish to thank all the Italian community that I have met here in UK, particularly Antonio Perreca, Ludovico Carbone, Cosimo Ducani and Alessio Terenzi. Furthermore, I wish to thank the best neighbours I could ever meet in UK, Andrea and Giacomo, who shared with me lot of fun and amazing dinners. Finally, I wish to thank the wonderful family of [redacted] Natalia, Andrea and Damian for supporting me during the writing up time. This work is dedicated to my cousin Fredi, my Family and those people who will be my best friends for ever. Thanks to Carlos, Lucia, Giorgio and Susana who have been simply like a family for me during the last years in England and certainly I will miss the time spent with them. Special thanks go to my friends Adornino and Giustino and to my housemate-brother Dario for their constant support and unique friendship.

Abstract

Using supramolecular principles, we have been designing luminescent lanthanide complexes with a defined hairpin bis-intercalator in order to obtain luminescent probes able to recognise DNA.

The complexes are comprised of platinum(II) terpyridine, which acts as a DNA recognition site and is brought together with a ”remote” luminescent lanthanide unit. All the synthetic approaches were based on the accessibility of the lanthanide-platinum complexes by the self-assembly of different components in a one pot reaction. Thus, we have been able to isolate a water soluble heterometallic complex based on thiophenol linkage named **[LnPt$_2$]Cl$_2$**. The complex has a relatively weak lanthanide luminescence, which increases upon addition of DNA. Photophysical and DNA binding properties of the lanthanide-platinum complex were investigated by UV-vis absorption, luminescent studies and circular and linear dichroism. Oligonucleotides of twelve bases were also used to investigate the intercalation **[LnPt$_2$]Cl$_2$** and **[Pt(tpy)(PhS)]Cl**. This led to a discovery of the optimal conditions for the 2D-NMR experiment of the Dickerson-Drew sequence toward interaction with **[LnPt$_2$]Cl$_2$** and the mono-intercalator **AATP** used as control compound. Using bidimensional NMR techniques, we investigated the binding site for **[LnPt$_2$]Cl$_2$** and **AATP** upon interaction with Dickerson-Drew sequence.

The sulphur lanthanide-platinum linkage in **[LnPt$_2$]Cl$_2$** was replaced with an acetylide one in order to introduce new photophysical features. Thus the the self assembly procedures based on DTPA-bis(amido-acetylide) and a platinum(II) terpyridine led us to isolate a new lanthanide-platinum complex named **[LnC≡CPt$_2$] (CH$_3$SO$_3$)$_2$**.

The photophysical properties and the DNA binding properties toward interaction with CT-DNA were investigated. The complex named **[LnC≡CPt$_2$](CH$_3$SO$_3$)$_2$** exhibited a

relatively strong lanthanide luminescence that increased upon addition of DNA. The bi-functional metal complex **[EuLPt](PF$_6$)** (where Pt = platinum-2,2':6'2"-terpyridine and L = asymmetric DTPA bisamide ligand with a thiopheno pendant arm and a quinoline moiety) was synthesised and the interaction of **[EuLPt](PF$_6$)** with CT-DNA was examined by luminescence spectroscopy, linear and circular dichroism studies and thermal denaturation studies. The **[EuLPt](PF$_6$)** retained the ability to increase its luminescence upon the addition of CT-DNA. The binding properties of the complexes were tested toward interaction with plasmid DNA by gel electrophoresis and properties such as the unwinding angle were measured. The bis-interclators **[LnPt$_2$]Cl$_2$** and **[LnC≡CPt$_2$](CH$_3$SO$_3$)$_2$** showed the ability to uncoil DNA almost as well as cisplatin and at low concentrations, while almost double the amount of mono-intercalators, such as **[EuLPt](PF$_6$)** is required to observe the same uncoiling effect.

List of publications

Luminescent Heterometallic Complexes Lanthanide based for DNA Recognition
L. Scarpantonio, M. C. Solomons, N. Spencer and Z.Pikramenou
Manunscript in preparation

1H-NMR structural analysis of Platinum-Lanthanide heterometallic complex for DNA recognition
L.Scarpantonio, N. Spencer and Z. Pikramenou
Manunscript in preparation

Luminescent Lanthanide complexes based on Platinum acetylide for bis-intercalative DNA recog-
nition.
L. Scarpantonio and Z. Pikramenou
Manunscript in preparation

Conference presentations

Cost meeting D39
"Metallodrugs that act through noncovalent interactions."
Birmingham, UK. October 2007.

Cost meeting D38
"Metal-Based Systems for Molecular Imaging Applications"
Lisbon . Portugal. April 2008.

Cost meeting D38
"Metal-based imaging probes for cellular and molecular imaging applications"
Dublin, September 2008.

Supra-Nano 2008
"Joint RSC Meeting of UK Macrocycles and Supramolecular Chemistry Group and Chemical Nanoscience and Nanotechnology Group"
Birmingham, December 2008.

COST D39
"Metallo-Drug Design and Action WG 01 : Bioorganometallic Drugs"
Zurich, Switzerland, April 2009.

ISABC 10
"10*th* International Symposium on Applied Bioinorganic Chemistry"
Debrecen, Hungary, September, 2009

EUROBIC 10*th*
"10*th*th European Biological Inorganic Chemistry Conference"
Thessaloniki, Greece, June 2010.

Abbreviations

δ	Chemical Shift
λ_{em}	Emission Wavelength
λ_{exc}	Excitation Wavelenght
ν	Frequency
τ	Luminescence lifetime
τ_m	mixing time
ε	Molar Extinction Coefficient
J	Coupling Constant
A	Adenine
AATP	4-acetoamidothiophenolato platinum 2,2':6',2"-terpyridine
AETE	Absorption Energy Transfer Emission
C	Cytosine
CD	Circular Dichroism
CT-DNA	Calf Thymus DNA
DCM	Dichloromethane
DMF	Dimethylformamide
DNA	Deoxyribonucleic acid
dppz	1,4,7,10-tetraazacyclododecane-N,N',N",N"'-tetraacetic acid dipyrido[3,2-a:2',3'-c]phenazine
DTPA	Diethylenetriamine pentaacetic acid
DTPA-BATP	1,11-(bis(4-aminothiophenol)-1,11-dioxo-3,6,9- triaza-3,6,9-triscarboxymethyl) undecane
EAP	4-ethynylaniline platinum 2,2':6',2"-terpyridine
ESI	Electrospray
FRET	Fluorescence Resonance Energy Transfer
G	Guanine
HEPES	4-(2-Hydroxyethyl)piperazine-1-ethanesulfonic acid, N-(2-Hydroxyethyl)piperazine-N'-(2-ethanesulfonic acid)
HPLC	High-Performance Liquid Chromatography
HSQC	Heteronuclear Single Quantum Correlation

J	Total Atomic Angular Momentum
K_b	Binding Constant
LD	Linear Dichroism
Ln	Lanthanide
MALDI	Mass to Charge ratio Matrix-Assisted Laser Desorption Ionization
Me	Methyl
MeCN	Acetonitrile
MeOH	Methanol
MLCT	Metal to Ligand Charge Transfer
MS	Mass Spectrometry
NIR	Near-Infrared
NMR	Nuclear Magnetic Resonance
NOE	Nuclear Overhauser Effect
NOESY	Nuclear Overhauser Effect Spectroscopy
OD	Optical density
PENDANT	Polarisation ENhancement During Attached Nucleus Testing
phen	1,10-phenanthroline
phi	9,10-phenanthrene quinone diimine
PMT	Photo Multiplier Tube
ppm	parts per milion
pzpt	3-(pyrazin-2-yl)-as-triazino[5,6-f]1,10-phenanthroline
ROESY	Rotating-Frame NOE Spectroscopy
T	Thymine
t	triplet
T_m	Melting Temperature
TOCSY	Total Correlation Spectroscopy
TOF	Time of Fly
tpy	2,2':6',2"-terpyridine
UV	Ultraviolet
Vis	Visible
YAG	Yttrium aluminium garnet
Z_{eff}	Effective Nuclear Charge

[Pt(tpy)C≡C]BF_4

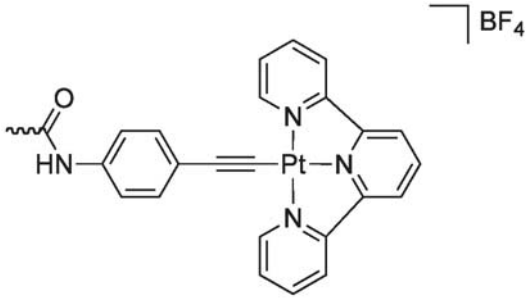

[Pt(tpy)C≡C]CH_3SO_3

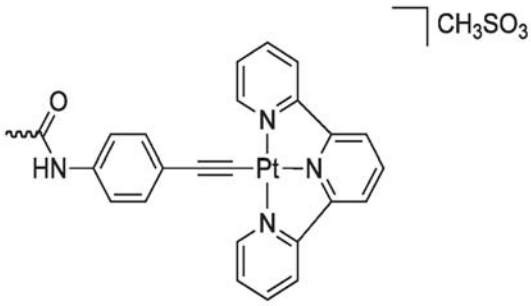

Contents

Chapter 1

General Introduction

From a chemistry point of view, DNA (deoxyribonucleic acid) can be defined as a polymer, where four alternating monomers (nucleotides) with backbones made of deoxyribose (adenine (A) , guanine (G), thymine (T) and cytosine (C)) are connected together by phosphodiesteric bonds. The DNA has intriguing properties from a materials application point of view[1] and it is crucial for life from a biological point of view, since it contains all the informations that all living organisms use to define their function and control their development. Many diseases can originate from DNA damaging, therefore the ability to specifically target different DNA regions is very attractive from a variety of research fields. Since the beginning DNA research has a high economic impact as well. In fact only ten years ago (June 26th 2000) quite a famous race ended, where the private and public sectors were challenging each other to sequence the human genome made of three billion bases, which should have opened a new era with personally designed drugs.[2] The ability to understand gene sequences and their manipulations, allowed in 20 years of studies to generate artificial bacterial life from a chemically synthesised genome.[3]

1.1 The DNA structure

The DNA structure was first elucidated by Watson and Crick in the 1950s which introduced the double-stranded helix model (B-DNA).[4] However DNA can exist in many possible conformations which include A-DNA and Z-DNA forms, although, only B-DNA and Z-DNA have been directly observed in functional organisms.[5] A number of non-B DNA structures have been discovered (approximately one new conformation every 3 years for the past 35 years) and include the following: triplexes, left-handed DNA, bent DNA, cruciforms, nodule DNA, flexible and writhed DNA, slipped structures, and sticky DNA (Figure 1.1).[6]

Name	Conformation	PDB ID
Cruciform	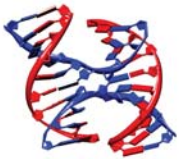	1L4J
Triplex		134D
Hairpin	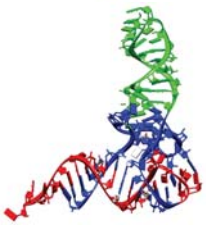	6NTA
Quadruplex		1K8P

Figure 1.1: Non-B DNA conformations involved in rearrangements.[6]

Since the B-DNA is the most common conformation in living organisms, this work will be mainly focused on this conformation, in which the base pairs form a central hydrogen-bonded π-stack running anti-parallel to the helical axis between the two strands of the sugar-phosphate back bone. Each base forms hydrogen bonds with its complementary opposite base; an A-T combination forms two hydrogen bonds and G-C combination three hydrogen bonds (Figure 1.2).

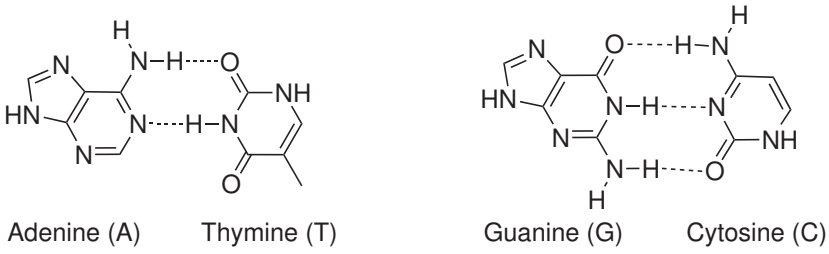

Figure 1.2: The structure of DNA base pairs showing Watson-Crick hydrogen bonding.

The B-DNA is characterised by ten bases per helical turn with a ride per base pair 3.4 Å; as a result of this geometrical constriction the DNA phosphate backbone forms two distinct grooves; a wide major groove and a narrow minor groove. Figure 1.3 shows a side-on representation of a typical B-form helix with the major and minor grooves clearly visible. The B-DNA structure is the most common but is not the unique helix which is possible to be made.

Indeed other less common DNA double helices such as the right-handed A-DNA form and the left-handed Z-DNA form can be created (Figure 1.3).[7] In this thesis we will mainly focus on the detection of the B-DNA structure paying particular attention to the employment of metal-complexes as luminescent probes.

Figure 1.3: A representation of the main double helix DNA conformations. Images from the RCSB PDB.[8] (www.pdb.org).

1.2 DNA binding modes

The specific recognition of DNA sequences, for example of genes, is of crucial importance in the development of therapeutic molecules able to act on the gene regulation and carcinogenesis in biological systems. The DNA is the major target for drug interaction as it is the origin point of most important cellular processes of replication, transcription and translation. These processes are vital for cell growth and division. Small ligand molecules bind to DNA and artificially modulate and or inhibit the functioning of DNA. These small ligand molecules act as drugs when the modulation or inhibition of DNA function is required to cure or control a disease. Enormous advances and efforts have been made to study the ways in which ligands (drug molecules) bind to DNA. Both covalent and non covalent binding modes are observed for DNA drug binding. Covalent binding leads to irreversible changes in the structure of DNA, inhibition of DNA processes and subsequent cell death. Cisplatin, a famous anticancer drug is a coordinative binder. It makes intra/inter strand crosslinks via the chloro groups with the nitrogen atoms in the DNA bases.[9][10]

Supramolecular chemistry offers the possibility of non covalent DNA binding which induces reversible changes and includes groove binders and intercalators.[11] The major groove has been successfully targeted with synthetic peptides containing zinc fingers[12] or oligonucleotides Zinc forming triple stranded DNA respectively (Figure 1.4).[13]

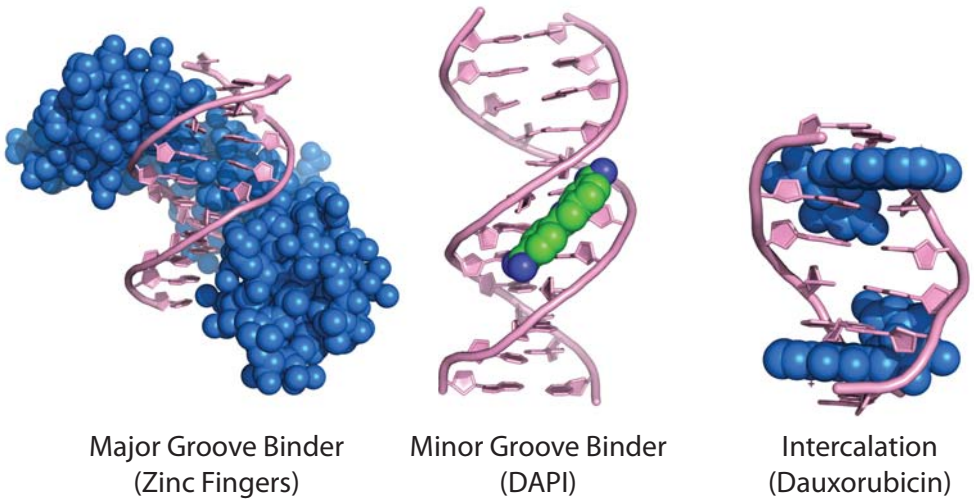

Figure 1.4: The major binding modes through which small molecules may interact with the DNA double helix. Images from the RCSB PDB.[8] (www.pdb.org).

Hannon and coworkers have reported a metallosupramolecular cylinders able to target the DNA double helix in the major groove, and they are the first truly synthetic agent to target only the major groove (Figure 1.5).[14]

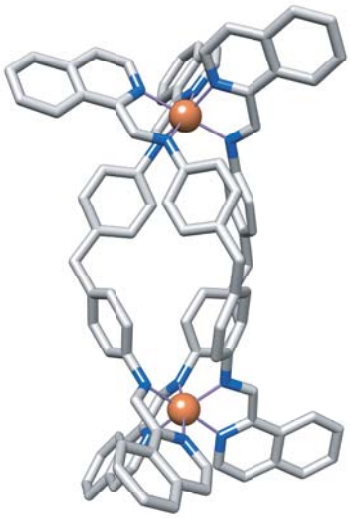

Figure 1.5: A dinuclear Fe(II) supramolecular helix which binds in the major groove of DNA.[15] [16].

Recently, the same group explored the possibility of attaching peptides to metallosupramolecular cylinders in order to create sequence-specific DNA binding agents targeted to the less-exploited DNA major groove. The parent cylinders were tetracationic triple stranded (Fe(II)) and the peptide selected for conjugation to the cylinder was the tripeptide Gly - Gly - Ser - $CoNH_2$. The two glycine residues were selected in order to provide the minimal steric bulk close to the cylinder, whereas the serine residue at the C-terminal was chosen based on its known frequent occurrence in protein motif–DNA base contacts. The binding experiments of the peptide-functionalized cylinders upon interaction with DNA, indicated that the Fe(II) cylinder retained its ability to coil DNA, albeit to less extent compared to the unsubstituted analogue.[17]

The DNA double helix minor groove can be targeted with organic synthetic molecules. Usually such agents are relatively small and positively charged with selectivity towards AT regions, where the narrow size of the groove makes them fit tighter than in a minor groove generated by GC sequences. Examples of these molecules are the DAPI and bis-benzimidazoles from the Hoechst family (Figure 1.6).[18] [19]

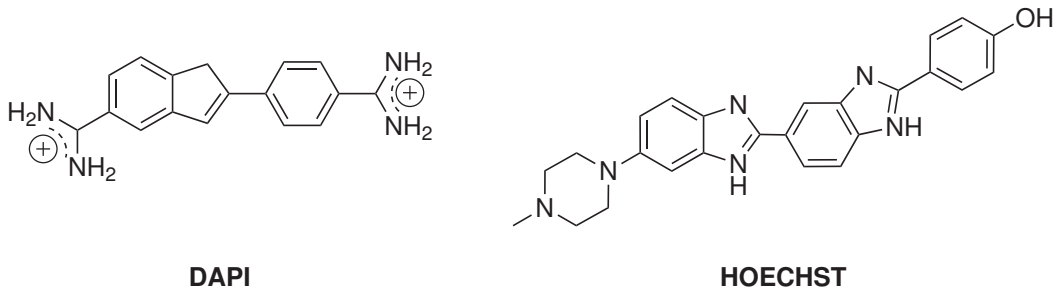

Figure 1.6: Synthetic molecules targeting the DNA minor groove.

Another example of a molecule able to wrap itself around the B-DNA helix is Distamycin A, a natural antibiotic used commercially against bacterial and viral infections. It is a long cationic molecule with methylpyrroles that bind specifically in AT rich regions.[18] Dervan *et al*. reported a modified structure of Distamycin A, with modifications of the pyrrole and imidazole sequences which allow the recognition of different DNA sequences *via* the minor groove (Figure 1.7).[18]

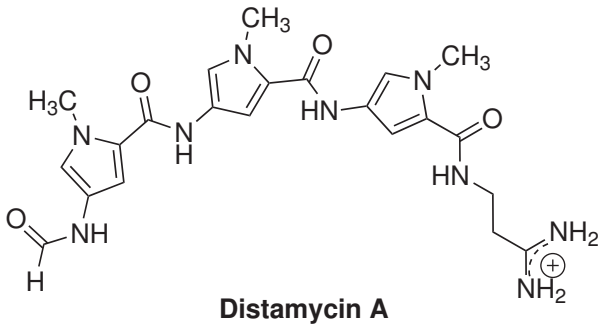

Figure 1.7: The structure of the minor groove binding agent Distamycin A.[18]

In this thesis we mainly focus on the third way of binding DNA, that is intercalation. This involves the introduction of planar aromatic molecules between the bases.[11] Intercalation is a phenomena that was first proposed in the1960s and can occur through either the major and or minor grooves opening the gap between base pairs to produce unwinding of the DNA double helix.[20] Due to the DNA backbone rigidity and the nearest-neighbour exclusion model which regulates the intercalation phenomena, only one molecule is allowed to intercalate every two gaps. An example of a molecule with intercalative properties is ethidium bromide, a carcinogenic compound used in molecular biology and biochemistry techniques as a fluorescent reference compound (Figure 1.8).[21]

A new binding mode occurs through the recognition of DNA junctions which play important

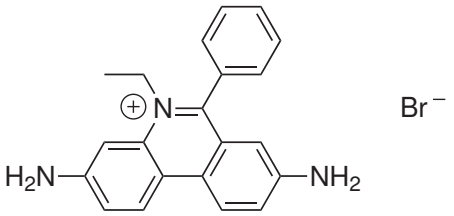

Ethidium Bromide

Figure 1.8: The structure of the intercalative binding agent Ethidium Bromide.

biological functions.[22] The simplest example involves only three strands of DNA known as a DNA three way junction or Y-shaped junction. Hannon *et al*. described the structure of a cationic metallosupramolecular complex that could bind in the internal cavity of a three way junction.

The X-ray diffraction of the complex with palindromic sequence showed that the cylindrical geometry with a dimension similar to zinc fingers, perfectly fits the cavity created by the three way junction structure (Figure 1.9).[23]

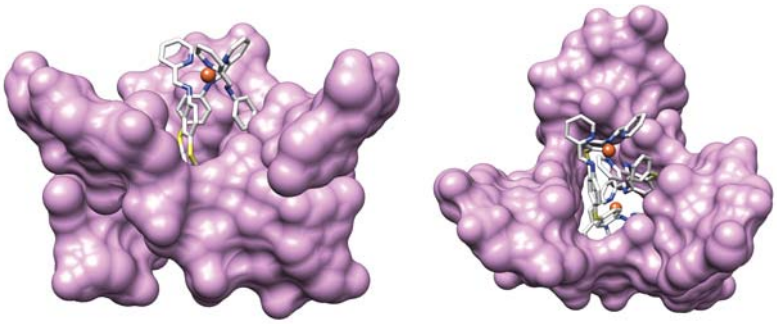

Figure 1.9: The refined structure of the three way junction interacting with the Hannon cylinder. Images from the RCSB PDB[8] (www.pdb.org) of PDB ID 1FX8.

1.3 Metallo-intercalators for DNA recognition

An ongoing effort toward unlocking biological information contained within DNA is the pursuit of molecules that can specifically interact with, label, or cleave oligonucleotide sequences. Despite the fact that in nature the binding and recognition of DNA in cells generally belongs to organic

moieties, the transition metal complexes are well suited for DNA interaction, since the electropositive metal centre is interently attracted to the negatively charged phosphate backbone of DNA. The metal centre also serves as a three dimensional structural scaffolds, which can be adjusted to fit into the base stacks and grooves of targeted DNA sequences.[24] Initial studies in this field started with Lippard *et al*. which discovered the ability of platinum(II) terpyridine to stack between DNA base pairs.[25] Since that several metal complexes with d^6 and d^8 have been prepared, and their use as luminescent probes for biomolecules is one of the major applications. Metal complexes as luminescent labels have advantages over organic dyes such as a longer excited state-lifetimes, larger stoke shifts, reduced self-quenching, tunable ground-state and excited-state energies and their sensitivity to the local environment which make them interesting as biosensors.[1]

Example of d^6 metal complexes are the Λ- and Δ-$[Ru(phen)_3]^{2+}$ which were characterised by an extensive debate on its binding mode (Figure 1.10).[26] In 2007 Barton *et al*. reported the ability of the complex to bind *via* hydrophobic interaction with the minor groove and partial intercalation of the phenantroline.[27]

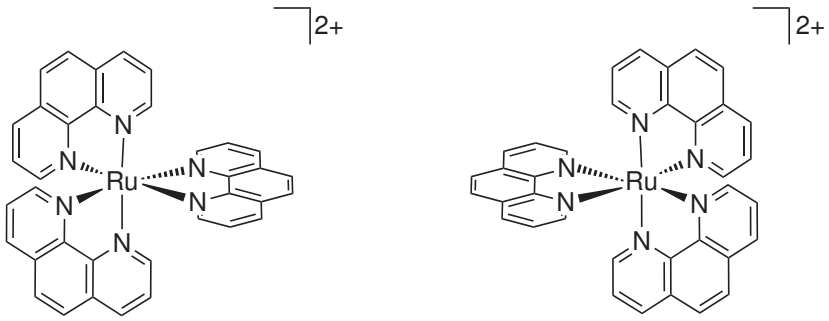

1 Λ-$[Ru(phen)_3]^{2+}$ **2** Δ-$[Ru(phen)_3]^{2+}$

Figure 1.10: Structure of Δ and Λ $[Ru(phen)_3]^{2+}$.

The d^6 metal complexes bring one more feature in comparison to the square planar d^8, which is the chirality. Indeed an octahedral complex can exist as Δ or Λ isomers, and differences in recognition mode were found. Preferential association between the Δ isomer with the right handed B-DNA was confirmed, and the enantioselectivity is believed to arise from steric interactions between the nonintercalated ligands of the Λ enantiomer with the DNA backbone. No enantioselectivity was observed in experiments conducted with left handed Z-DNA, probably due to the altered groove

dimensions.

Barton and coworkers confirmed their model of interaction by using a ruthenium complex using the 4,7-diphenyl-1,10-phenanthroline (DIP) as ligand (Figure 1.11). The introduction of phenyl groups on the phen ligand increased the steric interactions between the Λ enantiomer and the phosphate backbone, as well as enhancing the extent of intercalation.[28]

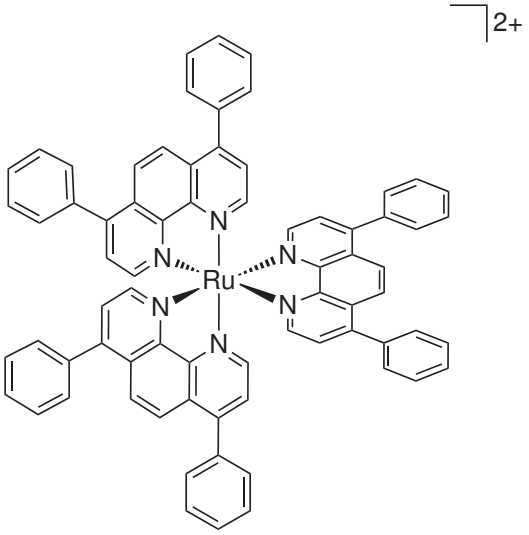

3 Λ-[Ru(4,7-diphenyl-1,10-phen)$_3$]$^{2+}$

Figure 1.11: Structure of Λ-[Ru(4,7-diphenyl-1,10-phen)$_3$]$^{2+}$.

It was successively found that increasing the surface area for intercalative stacking by a complex leads to a substantial increase in intercalative binding affinity. As a result, metallo-intercalators which contain an extended aromatic heterocyclic ligand can provide powerful tools to probe DNA.[26]

One of the most employed ligands are those based on dipyrido[3,2-a:2',3'-c]phenazine (dppz) which have been used to prepare several Ru(II) complexes known as molecular light switches for DNA, where a luminescent signal is observed only in the presence of DNA (Figure 1.12).

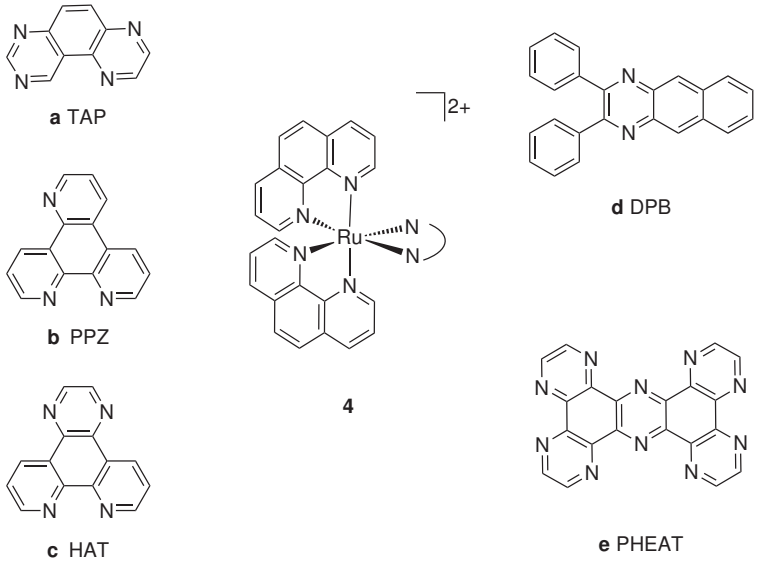

Figure 1.12: dppz-like intercalating ligands used to obtain switch on complexes of Ru(II).

In aqueous solution these complexes do not emit due to the ability of water to deactivate the excited state through hydrogen bonding with the intercalating unit. However upon interaction with DNA the luminescence is turned on, since the intercalating unit is shield from the bulk solvent.

Other derivatives were developed by Turro *et al*., which used tridentate ligands in order to obtain hetero- (**5**) or homoleptic (**6**) complexes bearing terpyridine as an ancillary ligand. Both complexes showed interaction with DNA *via* intercalation but only complex **6** showed luminescent enhancement upon binding to DNA (Figure 1.13).

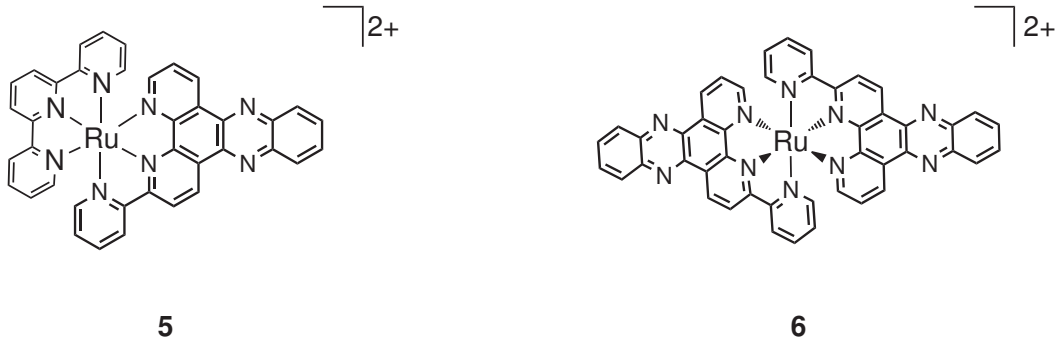

5 **6**

Figure 1.13: Structure of $[Ru(tpy)(pydppz)]^{2+}$ and $[Ru(pydppz)_2]^{2+}$.

Thomas *et al*. reported the synthesis[29] and use of **7** as a luminescent complex which switches on upon interaction with DNA. However complex **7** was found to act as a structure-sensitive DNA probe, since the luminescence colour upon interaction with double helix DNA was different from the

luminescence colour upon interaction with G-quadruplex (Figure 1.14).[30]

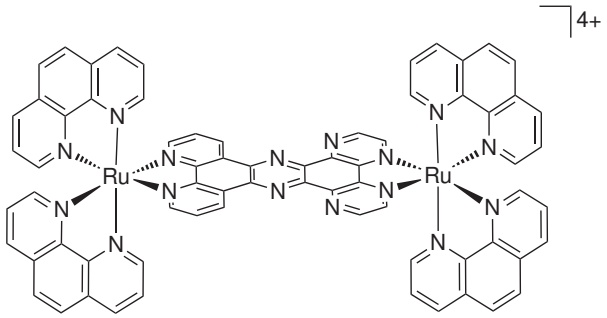

7

Figure 1.14: Structure of $[Ru_2(phen)_4PHEAT]^{4+}$.

Recently the same group reported the successfully employment of $[Ru_2(phen)_4PHEAT]^{+4}$ as a light switch complex for *in cellulo* nuclear DNA staining agent. Despite of the hydrophilicity the molecule, the complex was found to be able to cross the cell membrane and localise in the cell nucleus. Interestingly the complex showed different emission wavelengths depending upon the DNA region targeted, which the authors ascribe to its ability to discriminate G-quadruplex structure from the usual B-DNA.[31]

An original ligand system for Ru(II) have been developed by Lincoln *et al.* who synthesised a semi-rigid binuclear ruthenium complex (Figure 1.15).[32]

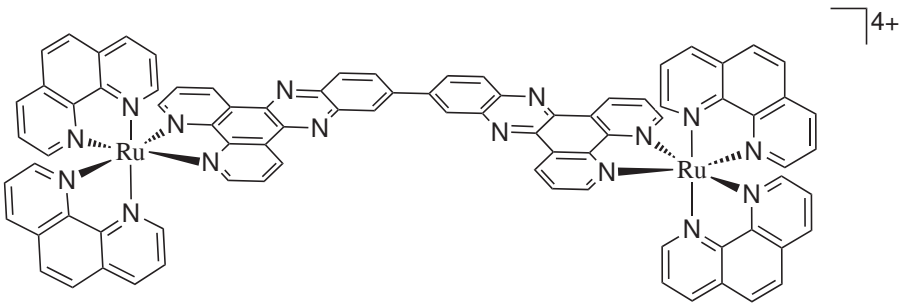

8

Figure 1.15: Structure of $\Delta\Delta$-$[L_2Rudppz(1l\text{-}1l')dppz)RuL_2]^{4+}$ (L = 1,10-phenanthroline, dppz = dipyrido[3,2-A : 2',3'-C]phenazine).

Complex **8** was found to bind DNA *via* a new DNA binding mode, known as threading intercalation.[33] Due to the bulky geometry a considerable transient conformational change is required

to thread through the base stack. Only after the complete intercalation is it possible to observe luminescence arising from the ^{3}MLCT, characterised by a high quantum yield upon interaction with poly(dAdT).[34]

Dinuclear Ru(II) complexes have been developed by Norden *et al*. and Aldrich-Wright, where the rigid aromatic bridge was replaced with a flexible alkyle chain and bis-intercalation behaviour was observed. However studies to understand the binding and specificity of these complexes are still ongoing.[35]

While Ru(II) is mainly used to obtain luminescent probes for DNA and perhaps to employ them as a stain in cell biology, Rh(III) can be used to induce DNA damage as photocleavage. In particular Barton *et al*. have developed an entire series of site-specific DNA binders. One such example is the Δ-[Rh(DIP)$_2$phi]$^{3+}$ (**9**) which was found to bind preferentially to a palindromic sequence, and inhibit site specifically the DNA binding of a protein.[26] Interestingly the Λ-[Rh(DIP)$_2$chrysi]$^{3+}$ (**10**) can not interact with palyndromic sequence and instead was found to probe the Z-form of DNA, a left handed form of the helix (Figure 1.16). This specificity might be due to the phenyl groups that are able to overlap in a cooperative arrangement only in the presence of the palindromic sequence.[26]

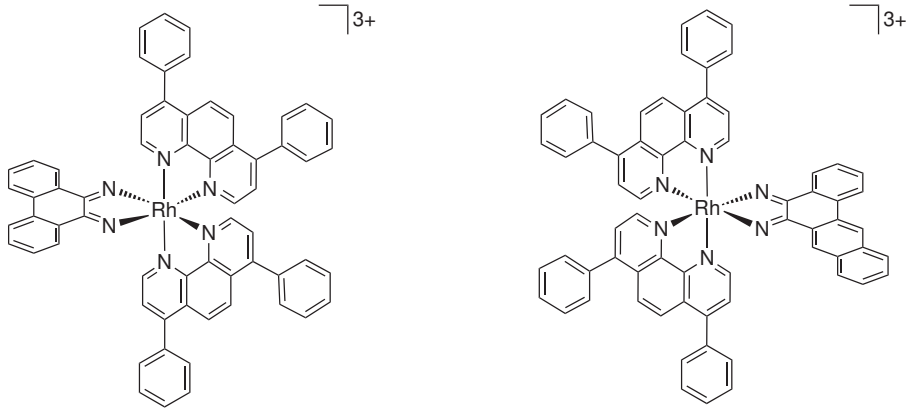

9 **10**

Figure 1.16: Structure of Δ-[Rh(DIP)$_2$phi]$^{3+}$ (**9**) and Λ-[Rh(DIP)$_2$chrysi]$^{3+}$ (**10**).

Barton and co-workers have been working on a new class of intercalators, better specified as metallo-insertors. In fact they found that by extending the aromaticity of the intercalating unit, it is possible to selectively detect DNA mismatches. Using a series of Rh(III) chrysenequinone diimine complexes (Figure 1.16), with different ancillary ligands, they proved that while the ancillary lig-

ands acts on the binding strength, the selectivity and cell membrane permeability belongs to the chrysenequinone which has a high selectivity for base mismatched binding sites.[36] Based on rhodium, the same group proposed a dual modal probe (**11**), where an organic fluorophore has been introduced onto one of the phenantroline ligands (Figure 1.17).

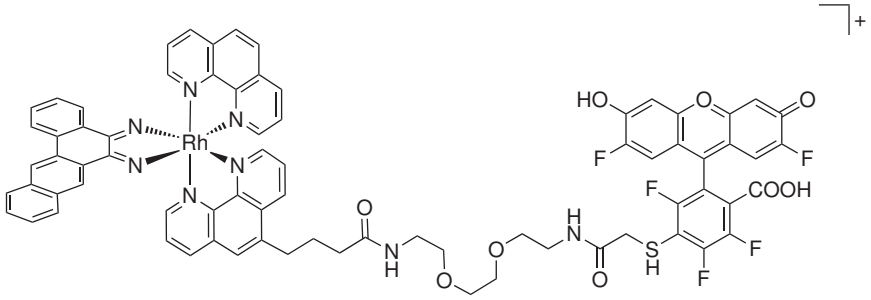

11

Figure 1.17: Luminescent probe for mismatch detection developed by Barton and co-workers.

In the presence of a mismatched DNA sequence the Rh(III) complex binds *via* insertion, and the anionic fluorophore is electrostatically repelled away from the metal complex thus attenuating intramolecular quenching and increasing fluorescence signal. However the unbounded probe still showed fluorescence and is the most fluorescent species.[37]

1.3.1 Platinum terpyridine metallo-intercalators for DNA recognition.

In the 1970's it was already known that terpyridine was able to form stable square planar complexes with metals having a d^8 as Pt(II) Pd(II) and Au(II). However after Lippard reported that the $[Pt(tpy)Cl]^+$ was able to intercalate between DNA base pairs,[25] the platinum(II) terpyridine has become an important reagent to study biomolecules due to their propensity to bind by selective modes. In particular luminescence arising from platinum(II) square planar complexes has been an area of growing interest, since the tuning of the photophysical properties can lead to a wide range of applications as bio-sensors.

Due to its d^8 electronic configuration, the platinum(II) terpyridine has a slightly distorted square planar geometry (D_{2d}) which makes it suitable to intercalate between the DNA base pairs. However the square planar geometry can be responsible for promoting radiationless decay and hence low efficiency in the photophysical processes. For example this geometry is characterised by an open

axial position which is free to interact with polar molecules (i.e. solvent). Indeed quite often polar solvents are promoters of the radiationless decay of the platinum(II) terpyridine excited state.[38] On the other hand, quite an important role is played by the distorted square planar geometry adopted by the platinum(II) terpyridine, that is responsible for the thermal activation of the $d-d$ transitions and for the quenching of the excited state by non radiative pathways.[39,40]

In order to obtain luminescent platinum(II) metal complexes, particular attention has been dedicated to the thiolate derivatives used as co-ligands for the Pt(II) terpyridine. Since in most cases the luminescence quenching arises from the thermal activation of the $d-d$ transitions, this can be avoided by using a of a strong σ and π electron donor, such as the thiolate ligands that modify quite dramatically the energy levels of *d* orbitals.

Omary *et al*. proposed platinum(II) terpyridine derivatives where varied substituted aryl sulphur co-ligands were used confirming that by tuning the σ and π electron donor properties, it is possible to activate the platinum(II) luminescence (Figure 1.18).[41]

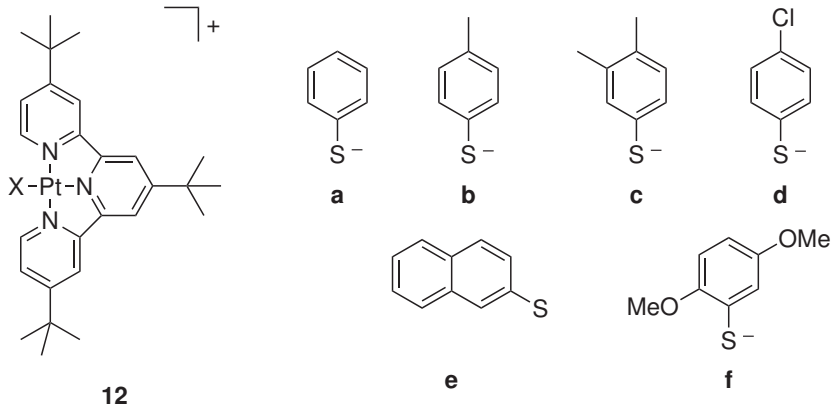

Figure 1.18: Structure of [Pt(tpy)(tertBu-)SR]$^{+}$ derivatives investigated for their photophysical properties.

They observed that changing the electron donating and withdrawing electron properties by substitution of the co-ligand, were responsible for the red and blue shifts of the charge transfer band absorption, respectively. This effect was assigned to the different abilities of the co-ligand to delocalise the π^* excited state which is generated during the transition from CT (thiolate/Pt(II)) $\rightarrow \pi^*$).

Other platinum(II) terpyridine derivatives with aryl thiolate co-ligands were reported by Che and co-workers. These which were found to be luminescent in fluid solution at room temperature with the exclusion of **13a** (Figure 1.19).[42]

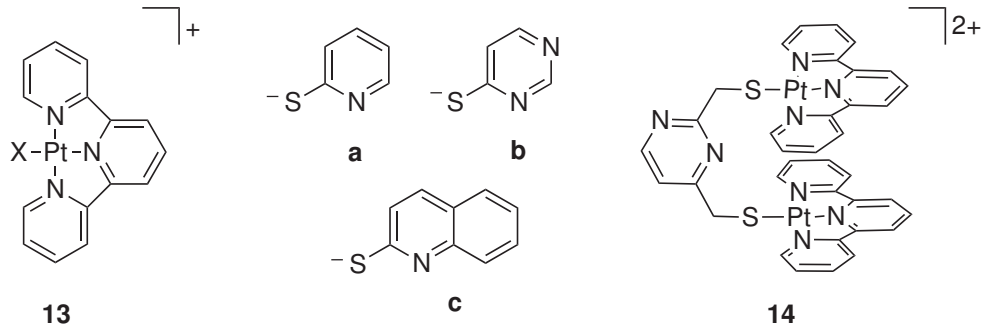

Figure 1.19: Structure of $[Pt(tpy)SR]^{+}$ derivatives investigated for their photophysical properties.

The same group reported other examples of aryl thiol derivatives of platinum(II) terpyridine which were able to interact with DNA (Figure 1.20).[43]

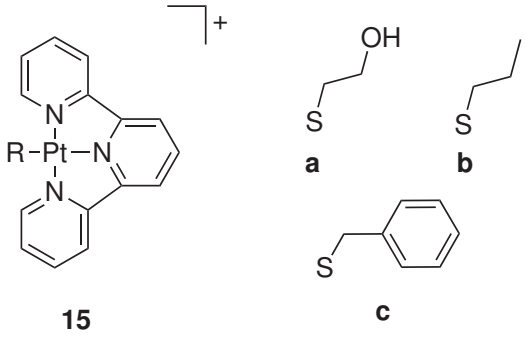

Figure 1.20: Structure of $[Pt(tpy)thiolates]^{+}$.

Altough intercalation has been proven and is widely accepted as a binding mode for Pt(tpy) complexes to DNA, stereochemical details of this process are needed to understand the real effect of intercalation on the backbone DNA geometry. Complex **15a** was used as DNA label to investigate the X-ray fiber diffraction of CT-DNA. Thus, the results obtained were able to support the Chroters theory,[44] where platinum terpyridine are evenily distributed by 10.2 Åthroughout the DNA backbone, and this is also known as the ”neighbour exclusion model”.[45]

One novel platinum(II) terpyridine derivative, designed by Wong and co-workers, incorporates a crown ether (Figure 1.21). However complex **11** was not found to be emissive, in both solution and solid state.[46]

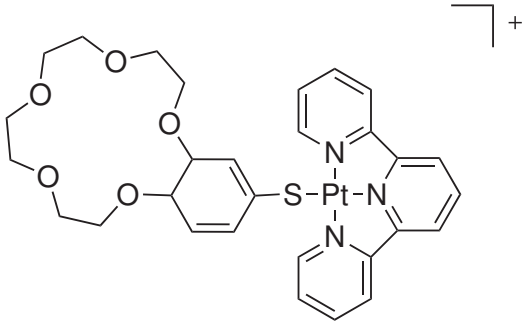

16

Figure 1.21: Structure of [Pt(tpy)mercapto-crown-ether]$^{+}$.

In order to better understand the photophysical properties of the platinum(II) terpyridine, various functional groups were tested as co-ligands. However not all of them were able to activate the platinum luminescence. In figure 1.22 we summarised which ligands are able to activate the platinum(II) emission, although the solvent condition may be different between each one.

Number	R_1	R_2	R_3
a	Cl	Cl	Cl
b	t-Bu	t-Bu	CH_2COMe
c	t-Bu	t-Bu	CH_2COPhe
d	CN	H	Cl
e	NMe_2	H	Cl
f	SMe	H	Cl
g	H	H	Cl
h	CN	H	Cl
i	NMe_2	H	Cl
j	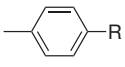	H	Cl

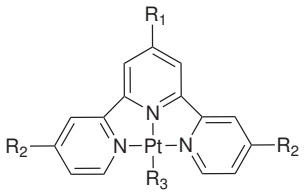

17

Number	R_1	R_2	R_3
k		H	Cl
l	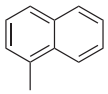	H	Cl
m	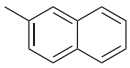	H	Cl
n	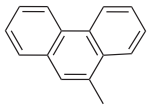	H	Cl
o	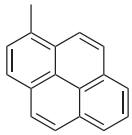	H	Cl

Figure 1.22: Selected luminescent Pt(II) terpyridine complexes in DCM, MeCN or DMF solution at 25 °C.[47]

After summarising these studies, it appeared clearly that not always a strong σ and π donor as the co-ligand aryl thiolate will produce a luminescent platinum(II) terpyridine complex. A recent review from McMillin shows how the combination of co-ligand and the modification introduced onto the terpyridine are important in creating the conditions required to avoid the thermal activation of the metal centred (MC) transitions in the platinum(II) terpyridine.[48]

Some of the platinum(II) terpyridine complexes have been investigated in conjunction with DNA. Wakelin and McFadyen used the simple platinum(II) terpyridine thiophenol (**18**) to study the affinity with a variety of different strains of DNA, showing that the complex had a high affinity for sites containing at least one CG base-pair (Figure 1.23).[49]

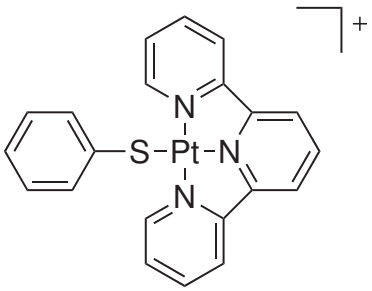

18

Figure 1.23: Structure of [Pt(tpy)thiophenol]$^{+}$.

Luminescent platinum complexes working as a DNA light switch were reported by McMillin *et al*., where the hydroxyl group was used as co-ligand (Figure 1.24).[50]

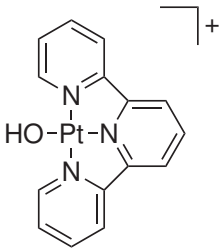

19

Figure 1.24: Structure of [4-hydroxylPt(tpy)]$^{+}$.

In aqueous buffer solution complex **19** is not emissive due to the formation of hydrogen bonds, which probably weakens electronic donation to platinum. Moreover the employment of polar solvent can introduce a non radiative quenching of the platinum(II) terpyridine excited state, *via* axial interaction. However, the effect of the axial interaction can be reduced by the presence of DNA. Indeed due to the intercalation of the platinum terpyridine unit between the DNA bases, the out-of-plane interaction with the solvent was blocked, which resulted in the luminescence of complex **18** being switched on.

Dinuclear platinum(II) terpyridine complexes such as **20** and **21** were isolated by Goto *et al*., which investigated their ability to bind DNA(Figure 1.25).[51]

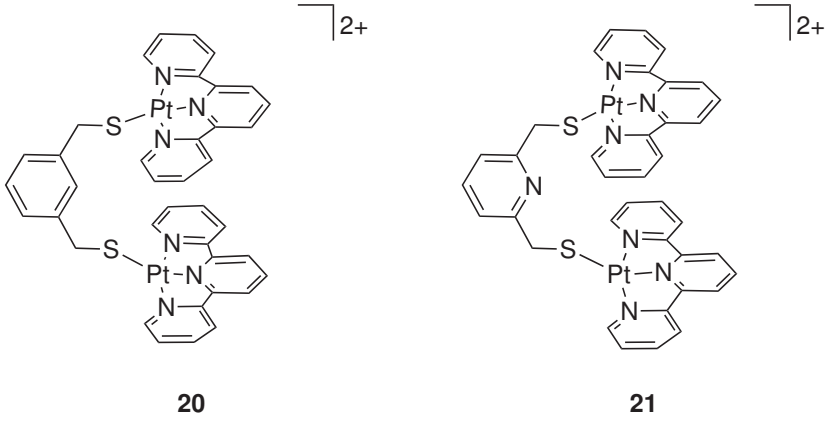

20 **21**

Figure 1.25: Structure of [Pt(tpy)dithiouracil]$^{2+}$ (**20**) and [Pt(tpy)(μ-N,S-thioacetimine]$^{2+}$ (**21**).[51]

Both complexes **20** and **21** are characterised by two platinum(II) terpyridine units linked together by a relatively short linker, which brings the DNA intercalative units quite close to one another ($\sim$ 4Å). While complex **20** was found to be unstable in aqueous solutions, complex **21** was found to bind quite strongly to the CT-DNA with the ability to distort the DNA due to the relatively close distance between the intercalating units.

Another study has developed a thiolate system to attach a carborane derivative, either singularly or in a bis arrangement (Figure 1.26).[52]

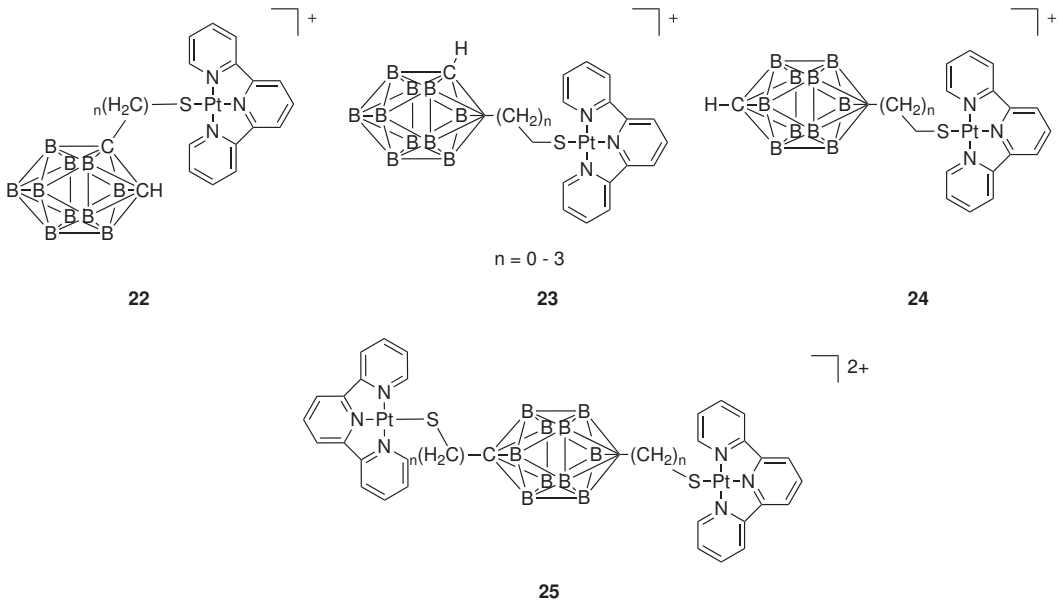

22 **23** **24**

25

Figure 1.26: Structure of [Pt(tpy)thiolates]$^{+}$.[52]

The mono- and dinuclear platinum(II) terpyridine complexes both show the retained ability to interact with DNA,[53] and when tested for anti-cancer activity by *in vitro* screening against leukaemia

cell line, they were characterised by a similar cytotoxicity as cis-platinum.[54,52]

Dinuclear platinum(II) terpyridine complexes bearing a non rigid aliphatic chain were originally reported by Mcfadyen *et al*. (Figure 1.27).[55]

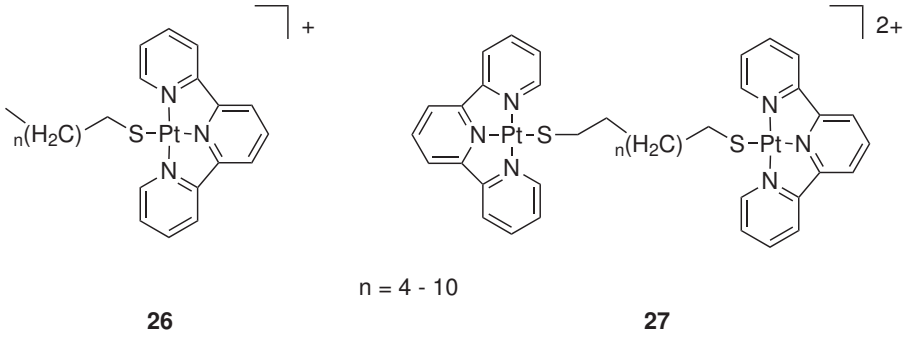

Figure 1.27: Structure of mono- and dinuclear platinum(II) terpyridine complexes with long thiolate chain as co-ligand.[55]

However, since these dinuclear complexes are characterised by non-stacked terpyridine units and because of the very flexible chain used as a linker, they can interact with DNA in multiple ways including the bis-intercalation. Indeed the problem of the flexible linker for these complexes appears clearly upon interaction with DNA, where a mixture of different intercalated species can be originated.[40]

Different co-ligand from the thiolate were successively proposed and particular interest turned onto the acetylide ligands. A more detailed discussion about their use as co-ligand in platinum(II) terpyridine complexes unit is discussed in chapter 4. Another platinum(II) terpyridine co-ligand tested was the 4-picoline derivative by Lowe *et al*. which reported the complex **28** as a potent DNA intercalator, characterised by a DNA binding constant almost a thousand times stronger than the analogous complex **19** (Figure 1.28).[56]

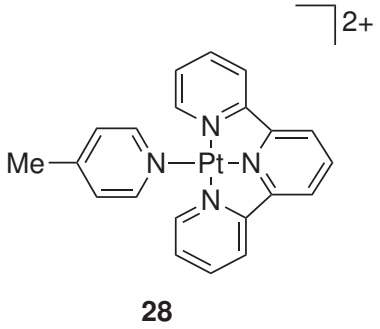

Figure 1.28: Structure of $[Pt(tpy)4\text{-picoline}]^{2+}$.

Recently, platinum(II) terpyridine was found to strongly interact with G quadruplex being able to stabilise this structure,[57] while quite an interesting result is the recent combination of the platinum(II) terpyridine moiety with distamycin to obtain a sequence-selective metallo-intercalator (Figure 1.29).[58]

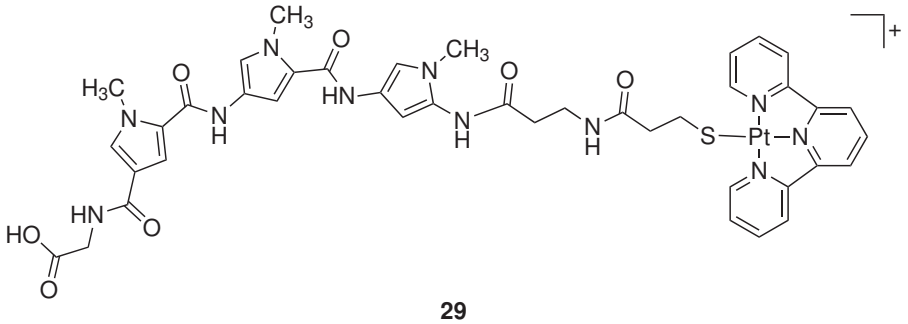

29

Figure 1.29: Structure of [Pt(tpy)diastamycin]$^{+}$ investigated for their photophysical properties.

Interesting multinuclear platinum(II) architectures were proposed by Williams *et al*. who proposed the tetraplatinated artificial oligopeptide (**30**) which appears to bind as a bis-intercalator (Figure 1.30).[59]

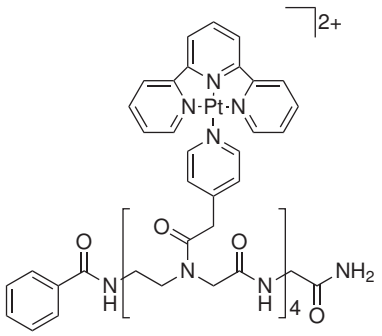

30

Figure 1.30: Structure of tetraplatinaated cyclic peptide tetraplatinated oligopeptide which interacts with DNA *via* intercalation.

These particular oligopeptides, which are analogous to peptide nucleic acids (PNAs), were synthesised to mimic DNA and RNA structures in order to improve their binding abilities to biomacromolecules.

Thus, bipyridine moiety was introduced into the center of a peptide backbone , which was tethered with two Pt(II) terpyridine complexes. Addition of Fe(II), Cu(II) or Zn(II) to this bypiridine oligopeptide promotes the assembly of hetero-multimetallic dendrimer (Figure 1.31).[60]

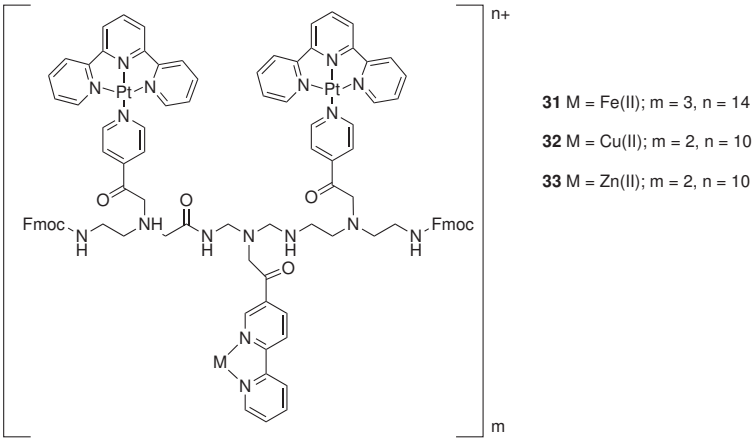

Figure 1.31: Chemical structure of metal containing artificial peptides.[47]

Tanaka and coworkers reported an example were the Pt(tpy) complexes were used for assisted synthesis of a 24-membered cyclic peptide with repeating unit of [glucine-L-cysteine] (Figure 1.32). Thiol groups in cysteine were connected to square planar Pt(II) terpyridine complexes, and the positively charged platinum complexes were responsible fot the alignment on the periphery of the macrocyclic peptide scaffold. Once the cyclic peptide are generated the Pt(tpy) units can be removed simply by treatment with TFA. Thus, in this case the Pt(tpy) complexes can be regarded as both protecting and promoting groups for peptide cyclization.[61]

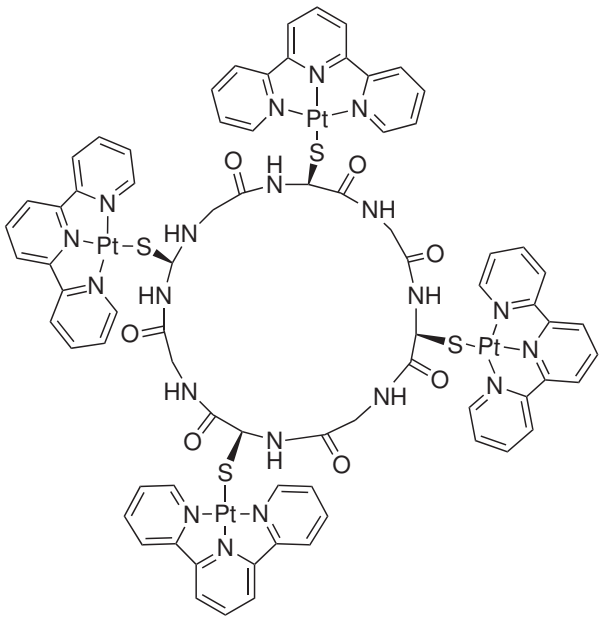

34

Figure 1.32: Structure of tetraplatinated oligopeptide.

1.4 Lanthanide properties

The lanthanide elements (Ln) form a separate group of elements in the periodic table called the "*f*-block" which is located between the *s* and *d* blocks in the sixth period. Due to the population of the *f* orbitals in their ground state, lanthanides exhibit unique magnetic and photophysical properties, which distinguish them from the transition metals. The lanthanide chemistry is highly uniform across the period, and the +3 oxidation state is the most common, as any further ionisation results in the f electrons being held too tightly to gain any energetic benefit from reaction. There are, however, some cases where the +2 and +4 oxidation states are also observed.[62]

Lanthanide ions are characterised by large ionic radii, adopting coordination numbers from 6 to 12, although the most common ones are 8 and 9.[63] Due to the nature of *f* orbitals (directional and disperse), the increasing number of electrons in the 4*f* shell is not balanced by the corresponding increase of the nuclear charge. Hence moving across the lanthanide period, the Z_{eff} increases and consequently the *f* orbitals are well shielded by the filled *5s* and *5p* and behave as if they were core atomic orbitals. For this reason Ln(III) complexes behave in the same way as the free ions, forming pure electrostatic bonds. Due to this ionic behaviour, lanthanide ions are highly labile and require strongly coordinating polydentate ligands to form stable complexes.

Because of the paramagnetism of nearly all of the lanthanide ions, Y(III) is commonly used as an alternative metal ion (i.e. NMR spectroscopy). The reason can be found in the electronic configuration of Y(III) which has an inert noble gas electron configuration, resulting in almost identical coordination chemistry to that of lanthanide ions.

The lanthanides exhibit a number of features in their chemistry and their magnetic and luminescent properties are particularly interesting for a wide number of applications in material and science biology.[64] In this thesis we will focus mainly on the use of lanthanides as luminescent probes for biology.

1.4.1 Optical properties

The fascinating lanthanide ions optical properties originate from their electronic configuration. Indeed the filled 'outer' *5s* and *5p* orbitals efficiently shield the *4f* electrons from surrounding ligands, with the result that crystal field splittings are of the order of 100 cm^{-1}. A consequence of the lack of crystal field effects in the lanthanides is that the vibrational level (thermal motion) of the ligands has very little effect upon them (as is not the case in the 3d situation), so the *f-f* absorption bands in the spectra are very narrow, almost as narrow as for free (gaseous) ions. However the *f - f* transitions are forbidden by Laporte (parity, $\Delta L \neq 0$) and by the orbital angular momentum selection rule ($\Delta l = \pm 1$) selection rules, that prohibits the redistribution of electrons in the *4f* subshell and also forbids *f - f* transitions, while certain transitions are also forbidden by the spin conservation selection rule ($\Delta S = 0$).

Table 1.1: Selected luminescent properties of Ln(III) ions.[65]

Ln[a]	G	I	F	λ/μm or nm[b]	gap/cm^{-1} [b]	τ^{rad}/ms [b]
Ce	$^2F_{5/2}$	5d	$^2F_{5/2}$	tunable, 300-450		
Pr	$^3H_4$	$^1D_2$	$^3F_4$,$^1G_4$,$^3H_4$,$^3H_5$	1.0,1.44,600,690	6940	(0.05[c]-0.35)
		$^3P_0$	^3H_J(J=4-6)	490,545,615	3910	(0.003[c]-0.02)
		$^3P_0$	^3F_J(J=2-4)	640,700,72		
Nd	$^4I_{9/2}$	$^4F_{3/2}$	^4I_J(J=9/2-13/2)	900,1.06,1.35	5400	0.42(0.2-0.5)
Sm	$^6H_{5/2}$	$^4G_{5/2}$	^6H_J (J=5/2-13/2)	560,595,640,700,775	7400	6.26
		$^4G_{5/2}$	^6F_J (J=1/2-9/2)	870,887,926,1.01,1.15		
		$^4G_{5/2}$	$^6H_{13/2}$	877		
Eu	$^7F_0$	$^5D_0$	^7F_J (J=0-6)	580, 590, 615, 650	12300	9.7(1-11)
				720, 750, 820		
Gd	$^8S_{7/2}$	$^6P_{7/2}$	$^8S_{7/2}$	315	32100	10.9
Tb	$^7F_6$	$^5D_4$	^7F_J(J=6-0)	490,540,580,620	14800	9.0(1-9)
				650,660,675		
Dy	$^6H_{15/2}$	$^4F_{9/2}$	^6H_J(J=15/2-9/2)	475,570,660,750	7850	1.85(0.15-1.9)
		$^4F_{15/2}$	^6H_J(J=15/2-9/2)	455,540,615,695	1000	3.22[b]
Ho	$^5I_8$	$^5S_2$	^5I_J (J=8,7)	545,750	3000	0.37(0.51[c]
		$^5F_5$	$^5I_8$	650	2200	0.8[c]
		$^5F_5$	$^5I_7$	965		
Er	$^4I_{15/2}$	$^4S_{3/2}$	^4I_J(J=15/2,13/2)	545,850	3100	0.7[c]
	$^4F_{9/2}$	$^4I_{15/2}$		660	2850	0.6[c]
	$^4I_{9/2}$	$^4I_{15/2}$		810	2150	4.5[c]
	$^4I_{13/2}$	$^4I_{15/2}$		1.54	6500	0.66(0.7-12)
Tm	$^3H_6$	$^1D_2$	$^3F_4$,$^3H_4$,$^3F_3$,$^3F_2$	450,650,740,775	6650	0.09
	$^1G_4$	$^3H_6$,	$^3F_4$,$^3H_5$	470,650,770	6250	1.29
	$^3H_4$	$^3H_6$	800	4300	3.6[c]	
Yb	$^2F_{7/2}$	$^2F_{5/2}$	$^2F_{7/2}$	980	10250	2.0(0.5-2.0)[c]

[a]G = ground state; I = main emissive state; F = final state; gap = energy difference between I and the highest SO level of F.

[b]Values for the aqua ions, otherwise stated, and ranges of observed lifetimes in all media, if available, between parentheses.

[c]Doped in Y_2O_3 or in $YLiF_4$ (Ho), or in $YAl_3(BO_3)^4$ (Dy).

[d]Complexes with organic ligands: 0.5-1.3 ms; solid-state inorganic compounds: $\sim$ 2 ms.

Lanthanide luminescence can be observed as the result of the deactivation process arising from an electronic excited state, which upon relaxation to the ground state can only emit a photon; hence the lanthanide electronic states are not thermally activated. The gap between the energy levels involved in the lanthanide luminescence are responsible for the characteristic wavelengths of emission.

According to table 1.4.1,[65] four lanthanide(III) ions are emissive in the visible region of the light spectrum (Eu^{3+}, Tb^{3+}, Dy^{3+}, Sm^{3+}) and three of them in the near-infrared region (NIR) (Nd^{3+}, Er^{3+}, Yb^{3+}). Due to a lack of thermally accessible excited states, lanthanides are characterised by a relatively long lifetime, which is often within μs or ms range. This provides an advantage for lanthanide based emitters over organic or transition metal complexes, typically characterised by a much shorter lifetimes (from ns to μs). The long-lived emission facilitates the use of time gated methods, which allow lanthanide luminescence to be distinguished from the shorter lived background fluorescence of many organic or biological systems.[66,64,67]

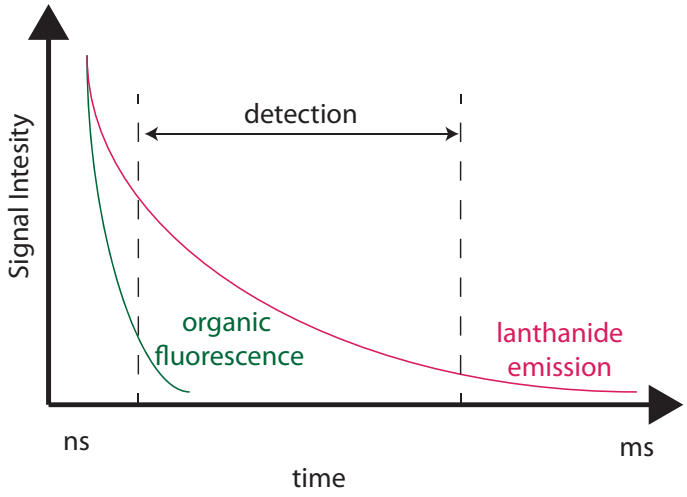

Figure 1.33: Schematic depiction of the time-resolved gating technique.

Thus properties of lanthanide ions can find useful application as long as an efficient method exists that allows to circumvent the low absorption molarity coefficient, characteristic for the metals of the series. This problem is often overcome by use of the antenna effect, where a chromophore is used to absorb light and transfer energy to the lanthanide centre *via* an intramolecular energy transfer process. This effect is known as the ”antenna effect” and if this process is efficient a strong lanthanide based luminescence can be observed (Figure 1.34).

The Jablonski diagram in figure 1.34 shows the excitation to the ligand singlet excited state (S_1) arising from the singlet ground state (S_0) by absorption of a photon. The next process is the relaxation of the S_1 state through the vibrational levels followed by an intersystem crossing to the lower energy triplet state (T_1). At this stage intramolecular energy transfer to the excited state of the lanthanide

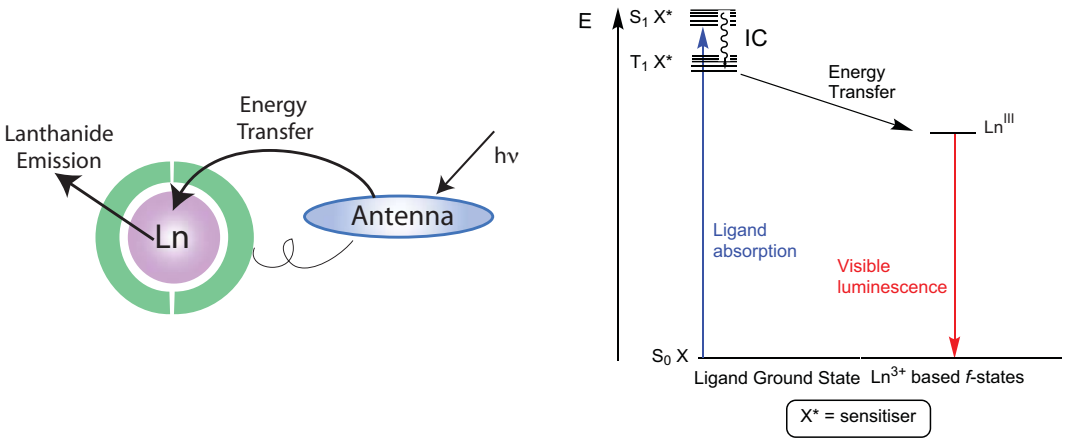

Figure 1.34: Schematic representation of the lanthanide sensitisation process.

may occur which populates the emissive level of the metal, from which radiative decay to the ground state results in emission of characteristic wavelengths of light (Figure 1.34).

A variety of organic ligand systems have been used as sensitisers.[68] [69] Ligand systems employed to sensitise lanthanide emission need to satisfy the following criteria

i) large absorption coefficient

ii) suitable energy levels to facilitate efficient ligand to metal energy transfer

iii) full wrapping of the lanthanide ion in order to avoid any possible interaction with solvent (i.e. water).

Energy transfer can occur by two principle mechanisms and they are referred to as short range (Dexter) and long range (Forster). Short range interactions require intermolecular orbital overlap to enable direct exchange of electrons between donor and acceptor. Therefore this process can only occur over intermolecular or interatomic distances. While long range energy transfer occurs *via* dipole-dipole interactions and can therefore be induced at further distances through space, with the rate dependent over $1/R^6$.

However the lanthanide luminescent excited states are susceptible of quenching upon interaction with certain group such as C–H, N–H and O–H (i.e water). Indeed the ability of a given bond to quench luminescence is related to the frequency of the vibrational overtones of the bond in question. In this way the rate of energy transfer to bond vibrational states is dependent upon the number of the

vibrational overtone best associated with the energy level of the lanthanide excited state, including how well matched these levels are. For example, the lower energy vibrational overtone ($\nu = 3$) of an O–H bond, deactivates the Eu(III) $^5D_0$ excited state far more efficiently than the higher energy vibrational overtone ($\nu = 5$) of an O–D bond (Figure 1.35). This explains why luminescence lifetimes of lanthanide complexes are generally longer in deuterated solvent as D_2O rather than H_2O (Figure 1.35).[70]

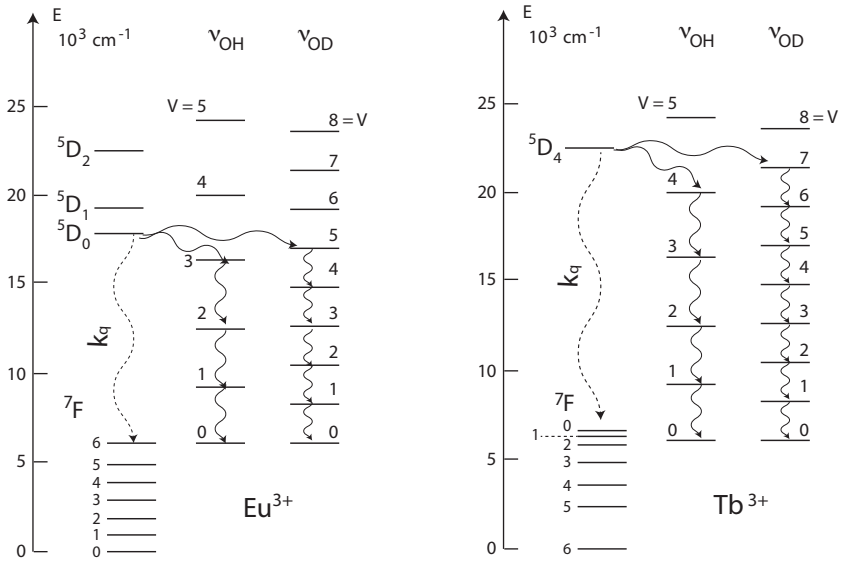

Figure 1.35: Radiationless deactivation of the excited state of Eu^{3+} and Tb^{3+} ions by O–H and O–D oscillators.

Application of an empirical formula determined by Horrocks Jr.[71] allows to calculate the number of coordinated water (q) molecule to the lanthanide ion.

$$q = A'_{Ln(III)}(k_H - k_D)$$

where $\mathbf{A}_{Ln(III)}$ is an empirically determined factor (i.e 1.05 for Eu^{3+} and 4.2 for Tb^{3+}), $\mathbf{k}_H$ and $\mathbf{k}_D$ are the decay rate in ms^{-1}, for the species in protonated and deuterated solvent respectively. Calculations of **q** may also be performed in other solvents such as methanol by simply doubling the **A** parameter as the methanol molecule is assumed to be half a water molecule in terms of quenching contribution.[72] [73]

1.5 Luminescent lanthanide complexes as probes for DNA

Lanthanide metal complexes find a wide range of applications in biology which include luminescence microscopy[65,67,74], energy transfer studies[75], NMR shift reagents and contrast agents for MRI.[76]

An area of research interest is the use of lanthanides as luminescent probes in DNA assays. Several polyaminocarboxylate chelates, such as diethylenetriaminepentaacetic acid (DTPA), covalently attached to a number of possible antenna molecules and have been widely used due to their ease of synthesis and good chelation properties (Figure 1.36).

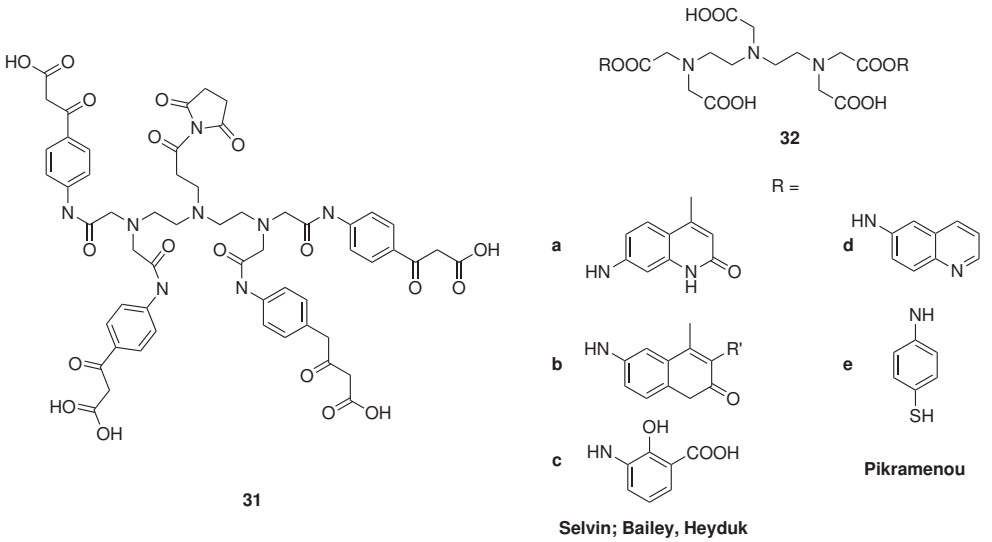

Figure 1.36: Some DTPA lanthanide chelators.[75] [77] [78]

These ligands can provide an eight coordinate environment for lanthanide encapsulation, binding through five hard oxygen donors and three medium-hard nitrogen donors, including coordination arising from the amide groups.[79] Lanthanide complexes obtained from DTPA derivatives are usually stable thermodynamically with a typical binding constant (K) between 10^{14} and 10^{19} M^{-1}. Only slight effects on the kinetic stability can be observed upon introduction of amide groups on DTPA, making these complexes suitable candidates for *in vivo* applications.[80]

The DTPA lanthanide derivatives have been successfully used as donors for fluorescence resonance energy transfer (FRET) experiments, which is a widely used technique to measure the distance between two points approximately separated by 10 - 100 Å.[75] Europium and terbium were successfully employed as donors in FRET experiments due to their long lifetime ($\sim 100\,\mu$s), which allows elimination of any prompt fluorescence arising from the organic molecules that are usually character-

ised by nano-second lifetimes. Further advantages of using lanthanides in FRET experiments arises from the anisotropic energy transfer process, with efficiency depending only on the distance between donor and acceptor and not from the relative orientation.[75]

An example was reported in 2000 by Selvin *et al.* and more recently from Laitala *et al.* which reported an example of DNA quantification using lanthanide chelates in a non overlapping resonance energy transfer assay (nFRET) (Figure 1.37).[75] [81]

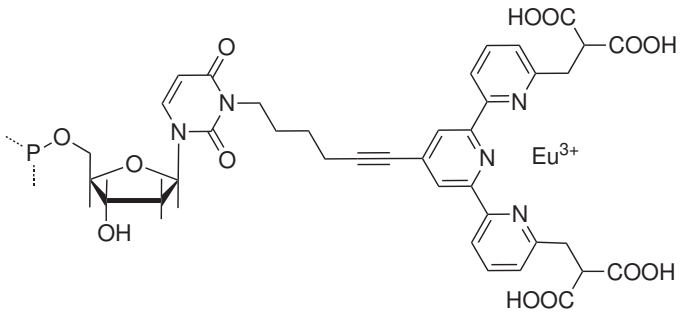

32

Figure 1.37: Structure of phosphoramidite ligand for nFRET.

Complex **32** was attached to the 3' end of a 3'-TAC TTA TAT CTA TGT CTTC-5' and the final product hybridised with a second oligonucleotide bearing an organic fluorophore. Upon hybridisation of the two strands, an energy transfer between the europium(III) $^5D_0$ excited state (donor) and the organic moiety (acceptor) is realised. Since in the unhybridised form the donor and the acceptor are in close proximity an efficient energy transfer can also be observed. However the hybridisation process pulls apart the donor and the acceptor producing changes in the energy transfer efficiency and lifetime of the acceptor; the different forms are therefore distinguished simply by using time resolved experiments.

The DTPA lanthanide complexes have been successfully combined with single-stranded oligonucleotides that are able to form a loop-stem structure upon hybridisation. This class known as molecular beacons and they are able to fluoresce when they bind to a target DNA or RNA sequence.[82] This luminescent probes are usually characterised by a loop that contains a probe sequence that is complementary to a target sequence in a nucleic acid, and the stem is formed by the annealing of complementary arm sequences that are located on either side of the probe sequence. The probe se-

quence is embedded between two "arm" sequences, which are complementary to each other. Under assay conditions, the arms bind to each other to form a double-helical stem hybrid that encloses the probe sequence, forming a hairpin structure. A reporter fluorophore is attached to one end of the oligonucleotide and a nonfluorescent quencher is attached to the other end of the oligonucleotide.

The stem hybrid brings the fluorophore and quencher in close proximity, allowing energy from the fluorophore to be transferred directly to the quencher through contact quenching. At assay temperatures, when the probe encounters a target nucleic acid, it forms a relatively rigid probe-target hybrid that is longer and more stable than the stem hybrid. Consequently, the molecular beacon probe undergoes a conformational reorganization that forces the stem hybrid to dissociate, and results in the separation of the fluorophore and the quencher, restoring fluorescence (Figure 1.38).[83][84]

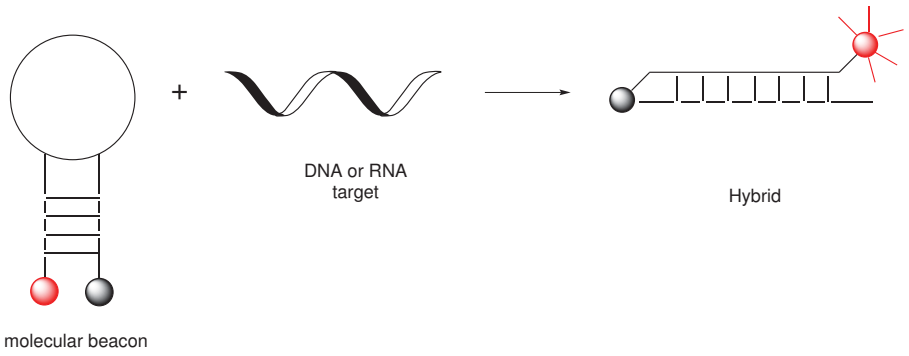

Figure 1.38: Scheme for molecular beacons.

Due to the lanthanide properties, molecular beacons became of great interest when employed as a fluorophore for real time detection of DNA/RNA hybridization in living cells and in diagnostic clinical assays. Recently the molecular beacons were used for coating nanoparticles in the presence of a complementary oligonucleotide with a quencher. Upon delivery of the nanoparticle in a cell nucleus, the oligonucleotide was released which consequently turns on the lanthanide luminescence (Figure 1.39).[85]

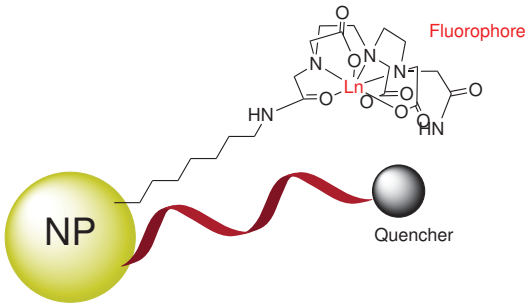

Figure 1.39: Fluorescent probe based on molecular beacons.

In this thesis we want to investigate the DNA binding properties of a luminescent lanthanide heterometallic properties, which combines the photophysical properties of lanthanides with the DNA recognition properties of a metallo-intercalator, such as the platinum terpyridine unit. In particular, we will investigate the DNA binding properties of $LnPt_2$ and how the binding affects the B-DNA conformation. In this sense we performed binding studies on oligonucleotides using also NMR techniques as NOESY and ^{31}P NMR. The importance of the hairpin geometry will be also investigated using new DTPA derivatives that brings new features, such as new luminescent properties to the final hairpin complex.

1.5.1 Outline of thesis

The versatile coordination chemistry of transition metals and lanthanides can be used to form stable complexes with a wide range of organic ligands. Using the metal centre as a template, it is possible to control the final geometry of the complex in order to enhance its binding properties to bio-molecules. Moreover an appropriate choice of the organic ligand allows to control their photophysical properties, which can be easily tuned to obtain long-lived luminescence. These characteristic make them ideal components in the development of new luminescent biomolecule labels. Our approach uses the principles of supramolecular self-assembly chemistry to generate heterometallic complexes to use as DNA luminescent probes.

In chapter 2 we investigated the DNA binding properties of a trimetallic bis-intercalator named [$LnPt_2$] upon interaction with calf thymus and polynucleotide DNA. Further studies involved the use of oligonucleotides and plasmid DNA (pBR322), where was showed clearly the ability of the complex to uncoil DNA.

Chapter 3 reports the ability of [$LnPt_2$] to interact with the Dickerson-Drew sequence, which was investigated by *via* ^{1}H and ^{31}P-NMR. Using the same experimental conditions, we compared the NMR studies of [$LnPt_2$] with those studies performed on the same oligonucleotide sequence, but upon interaction with the mono-intercalator complex [(4'-amidothiopenol)Pt(tpy)]Cl (AATP).

In chapter 4 we tried to resemble the hairpin complex [$LnPt_2$] using a new DTPA-bis(amide) derivative in order to introduce new photophysical feature as the luminescence from both platinum and lanthanide metal centre. Hence we describe the synthesis of the DTPA-bis(acetylide) and the synthesis of the relative trimetallic complex bearing two platinum terpyridine groups. Photophysical and DNA binding studies were therefore investigated and comparative studied were performed on the relative mono-intercalator [(4'-ethynylaniline)Pt(tpy)](CH_3SO_3).

In the last chapter we use a previously reported asymmetric DTPA-bis(amide) to synthesise a novel lanthanide luminescent probe.[77] Photophysical properties and DNA binding studies were than investigated which showed the ability to interact with DNA *via* monointercalation.

References

[1] Yang, H.; Metera, K. L.; Sleiman, H. F. *Coord. Chem. Rev.* **2010**, *254*, 2403.

[2] *The Economist* **2010**, *395*, 3.

[3] Gibson, D. G. et al. *Science* **2010**, *329*, 52.

[4] Watson, J. D.; Crick, F. H. C. *Nature* **1953**, *171*, 737.

[5] Ghosh, A.; Bansal, M. *Acta Crystallogr. D Biol. Crystallogr.* **2003**, *59*, 620.

[6] Bacolla, A.; Wells, R. D. *J. Biol. Chem.* **2004**, *279*, 47411.

[7] Blackburn, G. M. *Nucleic Acids in Chemistry and Biology*; Royal Society of Chemistry, 2006.

[8] Berman, H.; Westbrook, J.; Feng, Z.; Gilliland, G.; Bhat, T.; Weissig, H.; Shidyalov, I.; Bourne, P. *Nucleic Acid Res.* **2000**, *28*, 235.

[9] Lippard, S. J. *Acc. Chem. Res.* **1978**, *11*, 211.

[10] Schwietert, C. W.; McCue, J. P. *Coord. Chem. Rev.* **1999**, *184*, 67.

[11] Hannon, M. J. *Chem. Soc. Rev.* **2007**, *36*, 280.

[12] Jantz, D.; Amann, B. T.; Gatto, G. J.; Berg, J. M. *Chem. Rev.* **2004**, *104*, 789.

[13] (a) Ros, T. D.; Spalluto, G.; Prato, M.; Saison-Behmoaras, T.; Boutorine, A.; Cacciari, B. *Curr. Med. Chem.* **2005**, *12*, 71; (b) Thoung, N.; Helene, C. *Angew. Chem., Int. Ed. Engl.* **1993**, *32*, 666.

[14] Lippert, B. *Cisplatin : chemistry and biochemistry of a leading anticancer drug*; Wiley-VCH, Zürich, 1999.

[15] Kerckhoffs, J. M. C. A.; Peberdy, J. C.; Meistermann, I.; Childs, L. J.; Isaac, C. J.; Pearmund, C. R.; Reudegger, V.; Khalid, S.; Alcock, N. W.; Hannon, M. J.; Rodger, A. *Dalton Trans.* **2007**, 734–742.

[16] Hannon, M. J.; Claire, L. P.; Jackson, A.; Hamblin, J.; Errington, W. *Chem. Commun.* **1997**, 1807–1808.

[17] Cardo, L.; Hannon, M. J. *Inorg. Chim. Acta* **2008**, *362*, 784.

[18] Dervan, P. B. *Bioorg. Med. Chem.* **2001**, *9*, 2215.

[19] Hawley, T. S.; Herbert, D. J.; Eaker, S. S.; Hawley, R. G. *Methods Mol. Biol.* **2004**, *263*, 219.

[20] Lerner, L. S. *J. Mol. Biol.* **1961**, *3*, 18.

[21] Peberdy, J. C.; Malina, J.; Khalid, S.; Hannon, M. J.; Rodger, A. *J. Inorg. Biochem.* **2007**, *101*, 1937.

[22] Lilley, D. M.; Clegg, R. M. *Annu. Rev. Biophys. Biomol. Struct.* **1993**, *22*, 299.

[23] (a) Oleksi, A.; Blanco, A. G.; Boer, R.; Uson, I.; Aymami, J.; Rodger, A.; Hannon, M. J.; Coll, M. *Angew. Chem., Int. Ed.* **2006**, *45*, 1227; (b) Boer, D. R.; Kerckhoffs, J. M. C. A.; Parajo, Y.; Pascu, M.; Uson, I.; Lincoln, P.; Hannon, M. J.; Coll, M. *Angew. Chem., Int. Ed. Engl.* **2010**, *49*, 2336.

[24] Haas, K. L.; Franz, K. J. *Chem. Rev.* **2009**, *109*, 4921.

[25] Jennette, K. W.; Lippard, S. J.; Vassilades, G. A.; Baueri, W. R. *Proc. Nat. Acad. Sci. U.S.A.* **1974**, *71*, 3829.

[26] Erkkila, K. E.; Odom, D. T.; Barton, J. K. *Chem. Rev.* **1999**, *99*, 2777.

[27] Zeglis, B. M.; Pierre, V. C.; Barton, J. K. *Chem. Commun.* **2007**, 4565.

[28] Barton, J. K.; Basile, L. A.; Danishefsky, A.; Alexandrescu, A. *Proc. Natl. Acad. Sci. U. S. A.* **1984**, *81*, 1961.

[29] Bolger, J.; Gourdon, A.; Ishow, E.; Launay, J. P. *Inorg. Chem.* **1996**, *35*, 2937.

[30] (a) Rajput, C.; Rutkaite, R.; Swanson, L.; Haq, I.; Thomas, J. A. *Chem. Eur. J.* **2006**, *12*, 4611; (b) Liu, Y.; Turner, D. B.; Singh, T. N.; Angeles-Boza, A. M.; Chouai, A.; Dunbar, K. R.; Turro, C. *J. Am. Chem. Soc.* **2009**, *131*, 26.

[31] Gill, M. R.; Garcia-Lara, J.; Foster, S. J.; Smythe, C.; Battaglia, G.; Thomas, J. A. *Nat. Chem.* **2009**, *1*, 662.

[32] Norden, B.; Lincoln, P.; Akerman, B.; Tuite, E. *Met. Ions Biol. Syst.* **1996**, *33*, 177.

[33] Nordell, P.; Lincoln, P. *J. Am. Chem. Soc.* **2005**, *127*, 9670.

[34] (a) Westerlund, F.; Lincoln, P. *Biophys. Chem.* **2007**, *129*, 11–17; (b) Nordell, P.; Westerlund, F.; Reymer, A.; El-Sagheer, A. H.; Brown, T.; Norden, B.; Lincoln, P. *J. Am. Chem. Soc.* **2008**, *130*, 14651.

[35] Onfelt, B.; Lincoln, P.; Nord□n, B. *J. Am. Chem. Soc.* **2001**, *123*, 3630.

[36] Ernst, R. J.; Song, H.; Barton, J. K. *J. Am. Chem. Soc.* **2009**, *131*, 2359.

[37] Zeglis, B. M.; Barton, J. K. *J. Am. Chem. Soc.* **2006**, *128*, 5654–5655.

[38] Connick, W. B.; Geiger, D.; Eisenberg, R. *Inorg. Chem.* **1999**, *38*, 3264.

[39] (a) McMillin, D. R.; Moore, J. J. *Coord. Chem. Rev.* **2002**, *229*, 113; (b) Sauvage, J. P.; Collin, J. P.; Chambron, J. C.; Guillerez, S.; Coudret, C.; Balzani, V.; Barigelletti, F.; Decola, L.; Flamigni, L. *Chem. Rev.* **1994**, *94*, 993.

[40] Cummings, S. D. *Coord. Chem. Rev.* **2009**, *253*, 449.

[41] Chen, W.-H.; Reinheimer, E. W.; Dunbar, K. R.; Omary, M. A. *Inorg. Chem.* **2006**, *45*, 2770.

[42] Tzeng, B. C.; Fu, W. F.; Che, C. M.; Chao, H. Y.; Cheung, K. K.; Peng, S. M. *J. Chem. Soc., Dalton Trans.* **1999**, 1017.

[43] Kurosaki, H.; Yamakawa, N.; Sumimoto, M.; Kimura, K.; Goto, M. *Bioorg. Med. Chem. Lett.* **2003**, *13*, 825.

[44] Crothers, D. M. *Biopolymers* **1968**, *6*, 575.

[45] Bond, P. J.; Langridge, R.; Jennette, K. W.; Lippard, S. J. *Proc. Natl. Acad. Sci. U. S. A.* **1975**, *72*, 4825.

[46] Yam, V. W. W.; Tang, R. P. L.; Wong, K. M. C.; Ko, C. C.; Cheung, K. K. *Inorg. Chem.* **2001**, *40*, 571.

[47] Eryazici, I.; Moorefield, C. N.; Newkome, G. R. *Chem. Rev.* **2008**, *108*, 1834.

[48] McGuire, R.; McGuire, M. C.; McMillin, D. R. *Coord. Chem. Rev.* **2010**, *254*, 2574.

[49] Wakelin, L. P.; McFadyen, W. D.; Walpole, A.; Roos, I. A. *Biochem. J.* **1984**, *222*, 203–215.

[50] Peyratout, C. S.; Aldridge, T. K.; Crites, D. K.; Mcmillin, D. R. *Inorg. Chem.* **1995**, *34*, 4484.

[51] Kurosaki, H.; Yamakawa, N.; Sumimoto, M.; Kimura, K.; Goto, M. *Bioorg. Med. Chem. Lett.* **2003**, *13*, 825.

[52] Todd, J. A.; Turner, P.; Ziolkowski, E. J.; Rendina, L. M. *Inorg. Chem.* **2005**, *44*, 6401.

[53] Todd, J. A.; Rendina, L. M. *Inorg. Chem.* **2002**, *41*, 3331.

[54] Woodhouse, S. L.; Ziolkowski, E. J.; Rendina, L. M. *Dalton Trans.* **2005**, 2827.

[55] Mcfadyen, W. D.; Wakelin, L. P. G.; Roos, I. A. G.; Hillcoat, B. L. *Biochem. J.* **1986**, *238*, 757.

[56] McCoubrey, A.; Latham, H. C.; Cook, P. R.; Rodger, A.; Lowe, G. *FEBS Lett.* **1996**, *380*, 73.

[57] Suntharalingam, K.; White, A. J. P.; Vilar, R. *Inorg. Chem.* **2010**, *49*, 8371.

[58] van Holst, M.; Pevelen, D. L.; Aldrich-Wright, J. *Eur. J. Inorg. Chem.* **2008**, 4608.

[59] Levine, L. A.; Morgan, C. M.; Ohr, K.; Williams, M. E. *J. Am. Chem. Soc.* **2005**, *127*, 16764.

[60] Gilmartin, B. P.; Ohr, K.; McLaughlin, R. L.; Koerner, R.; Williams, M. E. *J. Am. Chem. Soc.* **2005**, *127*, 9546.

[61] Tanaka, K.; Shionoya, M.; Shigemori, K. *Chem. Commun.* **1999**, 2475.

[62] (a) Douglas, B. E.; McDaniel, D. H. *Concepts and models of inorganic chemistry*; John Wiley & Sons Inc.: New York, 1965; (b) Evans, W. J. *Coord. Chem. Rev.* **2000**, *206*, 263; (c) Lide, D. R.; Weast, R. C. *Handbook of chemistry and physics : A ready reference book of chemical and physical data, 84th*; CRC Press, Boca Raton, Fla., 2003.

[63] (a) Parker, D.; Dickins, R.; Puschmann, H.; Cossland, C.; Howard, J. A. K. *Chem. Rev.* **2002**, *102*, 1977; (b) Cotton, S. *Lanthanides and Actinides*; Macmillan Education, 1991.

[64] Eliseeva, S. V.; Bunzli, J. C. G. *Chem. Soc. Rev.* **2010**, *39*, 189.

[65] Bunzli, J. C. G. *Chem. Rev.* **2010**, *110*, 2729.

[66] (a) Mathis, G. *Clin. Chem.* **1995**, *41*, 1391; (b) Hanaoka, K.; Kikuchi, K.; Kojima, H.; Urano, Y.; Nagano, T. *J. Am. Chem. Soc.* **2004**, *126*, 12470.

[67] Montgomery, C. P.; Murray, B. S.; New, E. J.; Pal, R.; Parker, D. *Acc. Chem. Res.* **2009**, *42*, 925.

[68] Leonard, J.; Nolan, C.; Stomeo, F.; Gunnlaugsson, T. In *Topics in Current Chemistry*; Vincenzo, B., Sebastiano, C., Eds.; Springer Berlin / Heidelberg, 2007; Vol. 281; pp 1–43.

[69] Mewis, R. E.; Archibald, S. J. *Coord. Chem. Rev.* **2010**, *254*, 1686.

[70] Bunzli, J. C. G.; Choppin, G. R. *Lanthanide Probes in Life, Chemical and Earth Sciences*; Elsevier Science Ltd., 1990.

[71] Horrocks, W. D.; Sudnick, D. R. *Accounts. Chem. Res.* **1981**, *14*, 384.

[72] Holz, R. C.; Chang, C. A.; Horrocks, W. D. *Inorg. Chem.* **1991**, *30*, 3270.

[73] Wolbers, M. P. O.; van Veggel, F. C. J. M.; Snellink-Ruel, B. H. M.; Hofstraat, J. W.; Geurts, F. A. J.; Reinhoudt, D. N. *J. Chem. Soc. Perk. T. 2* **1998**, 2141.

[74] Muller, G. *Dalton Trans.* **2009**, 9692.

[75] Selvin, P. R. *Annu. Rev. Bioph. Biom.* **2002**, *31*, 275.

[76] Louie, A. *Chem. Rev.* **2010**, *110*, 3146.

[77] Lewis, D. J.; Day, T. M.; MacPherson, J. V.; Pikramenou, Z. *Chem. Commun.* **2006**, 1433.

[78] Glover, P. B.; Ashton, P. R.; Childs, L. J.; Rodger, A.; Kercher, M.; Williams, R. M.; Cola, L. D.; Pikramenou, Z. *J. Am. Chem. Soc.* **2003**, *125*, 9918.

[79] (a) Konings, M. S.; Dow, W. C.; Love, D. B.; Raymond, K. N.; Quay, S. C.; Rocklage, S. M. *Inorg. Chem.* **1990**, *29*, 1488; (b) Bligh, S. W. A.; Chowdhury, A. H. M. S.; Mcpartlin, M.; Scowen, I. J.; Bulman, R. A. *Polyhedron* **1995**, *14*, 567; (c) Georgopoulou, A. S.; Ulvenlund, S.; Mingos, D. P.; Baxter, I.; Williams, D. J. *J. Chem. Soc.-Dalton Trans.* **1999**, 547.

[80] Prata, M. I. M.; Santos, A. C.; Neves, M.; Geraldes, C. F. G. C.; de Lima, J. J. P. *J. Inorg. Biochem.* **2002**, *91*, 312.

[81] Laitala, V.; Hemmila, L. *Anal. Chem.* **2005**, *77*, 1483.

[82] Tyagi, S.; Kramer, F. R. *Nat. Biotechnol.* **1996**, *14*, 303–308.

[83] Heyduk, T.; Heyduk, E. *Nat. Biotechnol.* **2002**, *20*, 171.

[84] Krasnoperov, L. N.; Marras, S. A. E.; Kozlov, M.; Wirpsza, L.; Mustaev, A. *Bioconjugate Chem.* **2010**, *21*, 319.

[85] Bryson, J. M.; Fichter, K. M.; Chu, W. J.; Lee, J. H.; Li, J.; Madsen, L. A.; McLendon, P. M.; Reineke, T. M. *Proc. Natl. Acad. Sci. U.S.A.* **2009**, *106*, 16913.

Chapter 2

Heterometallic Luminescent Lanthanide Complex for DNA Recognition

2.1 Introduction

Gaining a greater understanding of the structural and functional properties of living systems is a key challenge in biology and medicine.[1] DNA is one of the target molecules in this field as it codes and stores the genetic information which an organism requires to function. Currently, one of the most popular DNA sequencing methods uses different fluorescent dyes, each of which fluoresces at a different wavelength, to label each of the different bases.[2,3] One inherent problem with this type of protocol is the prevalence of the long lived fluorescence arising from the organic molecules present *in vivo*; this is often referred to as autofluorescence. Recent chemical research has focused on using complexes containing metal ions as the source of luminescence. Both transition metals emit at higher wavelengths with a longer lifetime than organic fluorophorophores, allowing the possibility to filter out any autofluorescence to a give a clean and sharp emission signal.[4]

Several chiral octahedral complexes arising from the *d*-block metals have been studied as structural and reactive luminescent probes for nucleic acids. Typical examples includes the Δ and Λ isomers of $[Ru(phen)_3]^{+2}$ or $[Rh(NH_3)_4phi]^{+3}$ which are known to bind to the DNA minor groove.[5] However, there are not so many examples of water soluble lanthanides which are suitable for studying interaction and luminescent sensing of DNA. These complexes have been reported by Parker *et al*. who usually modify the lanthanide tetramide ligand (DOTA) with planar aromatic moieties which

are both DNA recognition sites and also lanthanide sensitisers. An example of this class of lanthanide complexes is the tetraamide based lanthanide complex which has a phenanthridium group as a chromophore (Figure 2.1).[6]

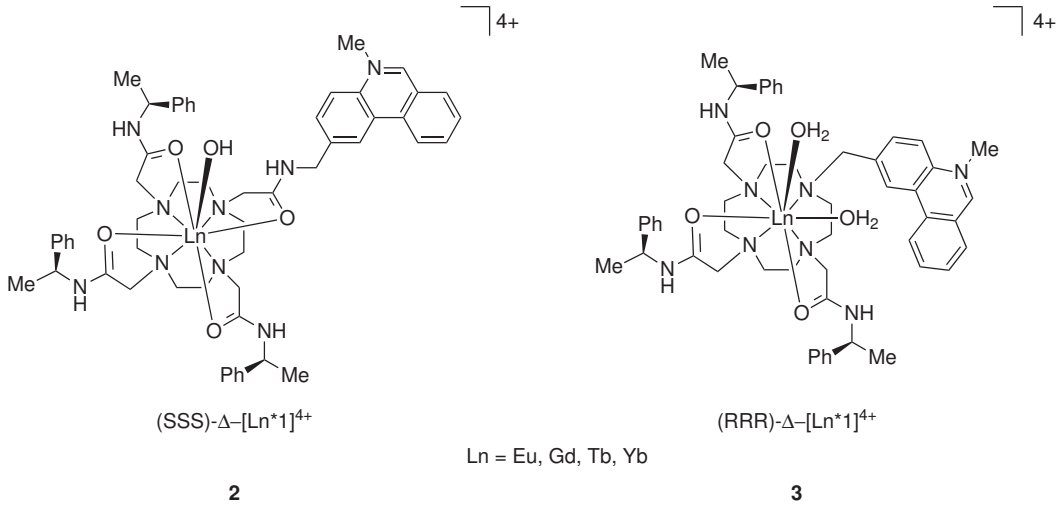

Figure 2.1: Lanthanide DOTA based complexes bearing a phenanthridium as chromophore.[6]

Complexes **2** and **3** bearing europium as metal centre, were expected to bind to DNA *via* intercalation of the phenanthridinium moiety. The photophysical studies performed on complex **2** showed a decrease in the magnitude of the europium luminescence upon interaction with DNA. Further studies with oligonucleotides $[(CG)_6]_2$ and $[(AT)_6]_2$, showed that charge-transfer mediated deactivation of the phenanthridinium singlet excited state occurred up to 20 times more efficiently for GC base-pairs than for AT, and both Δ and Λ-tetramide isomers. The increased distance between the sensitiser (phenanthridium) and the lanthanide lead to a final complex with the lanthanide emission being deactivated through non-radiative pathways upon interaction with the DNA. However in this case, the deactivation process of the lanthanide emissive excited state was observed to be more efficient for the Δ-isomer.[7]

The same research group tested other chromophores in order to obtain a luminescent intercalative DNA lanthanide probe. In 2002 the phenanthridinium chromophore was replaced with a phenanthroline group (**4**) and with a traazatriphenylene (**5**) (Figure 2.2).[7]

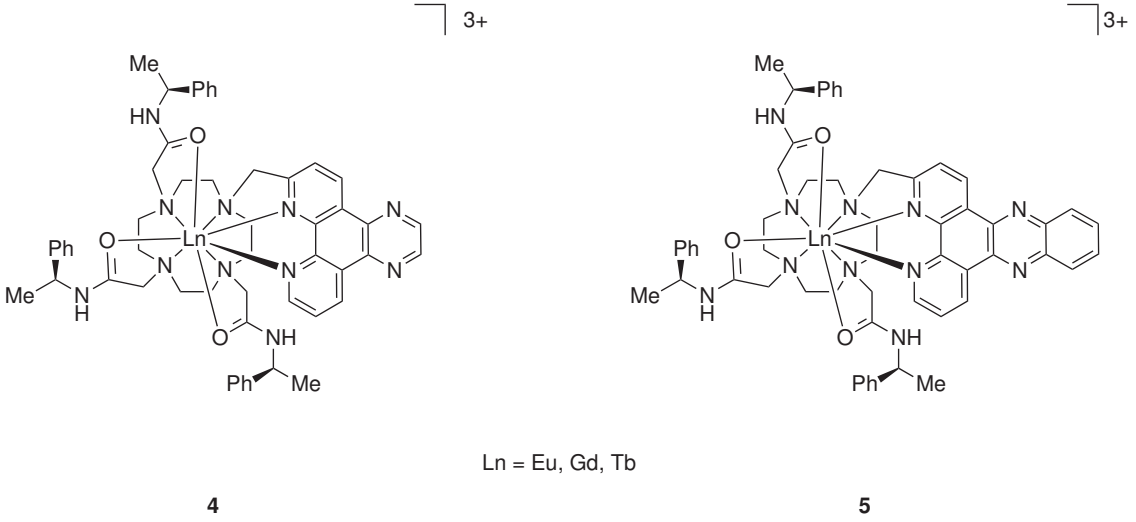

Figure 2.2: Lanthanide DOTA based complexes bearing phenanthroline (**4**) and traazatriphenylene (**5**) as chromophore.

Circular dichroism studies and luminescence studies were carried out for Δ and Λ isomers for complexes **4** and **5** upon interaction with poly(dAdT) and poly(dGdC). However for both isomers they observed the quenching of the lanthanide based luminescence upon addition of DNA. A stronger quenching effect was observed upon interaction of the complexes with poly (dGdC) rather than poly (dAdT) which is consistent with the stronger apparent binding constant of the complex for sequences containing cytosine and guanine. Based on time resolved luminescent experiments, they observed that the presence of DNA activates a quenching mechanism where guanine and cytosine are able to deactivate the S^1 excited state of the traazatriphenylene; and as a consequence the lanthanide luminescence is deactivated.[7] This class of complexes are particularly interesting as they allow to take advantage of the relatively long emission lifetimes to perform time resolved fluorescence microscopy experiments (TRFM). In particular complex **5** was used to treat cell lines and the cell uptake was monitored by TRFM (λ_{exc} = 350 nm). At high concentration the complex was found to localise in the cell nucleus of HEK 239,[1], 3T3[2] , COS[3] and CHO[4] cell lines.[8]

The europium derivatives of DOTA bearing naphthalene and phenanthroline (**6**) were also synthesised; both Δ and Λ enantiomers of complex **6** and **7** were studied upon DNA binding (Figure 2.3).

[1]Human Embryonic Kidney 293 cells
[2]3-day transfer, inoculum 3×10^5 standard fibroblast cell line
[3]COS is an acronym, derived from the cells being CV-1 (simian) in Origin, and carrying the SV40 genetic material
[4]Chinese hamster ovary (CHO) cells

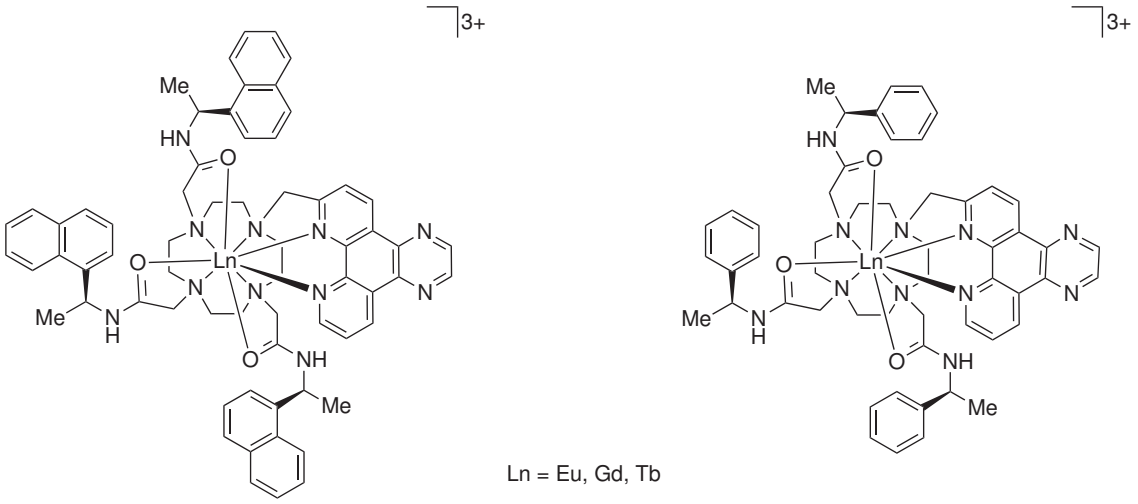

6 **7**

Figure 2.3: Lanthanide DOTA based complexes bearing phenanthroline naphthalene as chromophore.[9]

Upon excitation of complex **7** at 340 nm, a 350% luminescent enhancement was observed upon binding to the poly(dGdC) ($\Delta \approx \Lambda$) and calf thymus DNA (CT-DNA) while the poly(dAdT) showed only a 200% increase ($\Delta > \Lambda$). Moreover, for both isomers an increase in the luminescence lifetime was observed independently of the DNA type employed during the experiment.

However these results were not confirmed when luminescent DNA binding studies were performed on complex **6**, which showed a general quenching of the europium emission upon the binding to DNA. Hence the naphthalene seems to play an important role for the lanthanide luminescent enhancement upon interaction with DNA.

A tetramide ligand bearing coumarin and rhodamine was successively proposed as a sensitiser for both visible (Eu(IIII) and Tb(III)) and the NIR (Nd(III) and Yb(III)) lanthanide emitters (Figure 2.4).[10] However, the visible lanthanide emission resulted non luminescent upon interaction of the complex with DNA, when excitation occurred through the coumarin.

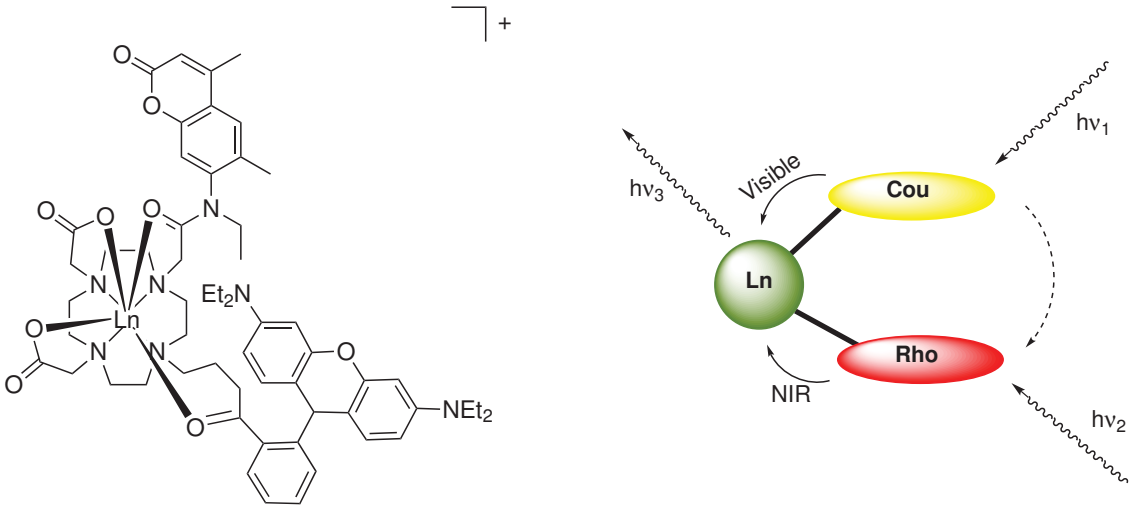

Ln = Nd, Yb

8

Figure 2.4: Structure of $[Ln(Cou)(Rho)]^{+}$ (Cou = Coumarin and Rho = Rhodamine).[10]

An energy transfer cascade could be realised only when the visible lanthanide emitters were replaced with the Nd(III). The direct excitation of the coumarin allows an energy transfer to the rhodamine which is able to transfer energy to the central lanthanide. The cascade process was interrupted upon addition of DNA, since it quenches the coumarin excited state. Conversely the Nd(III) emission was always observed upon selective excitation of the rhodamine chromophore, which is not affected by the interaction with DNA.[10]

In 2010 Parker *et al.* reported a new lanthanide metal complex based on DOTA ligand, where the 3-azaxanthone is employed as an antenna system to sensitise Tb(III) and Eu(III) (Figure 2.5).[11] Absorption and luminescence experiments of complex **9** were performed upon interaction of calf thymus DNA and polynucleotides such as poly(dAdT) and poly(dGdC). While the absorption spectrum do not show any hypochromism or spectral shift, the luminescence intensity and lifetime were tremendously reduced by half upon interaction with DNA.

Using the Tb(III) derivative of complex **9** as a staining agent for a TRFM experiment with HeLA[1] cells, it was possible to investigate the cell uptake mechanism, which showed that the complex was able to cross the cell membrane only during their mitosis process.[11] [4]

[1]Cell line derived from cervical cancer cells taken from Henrietta Lacks.

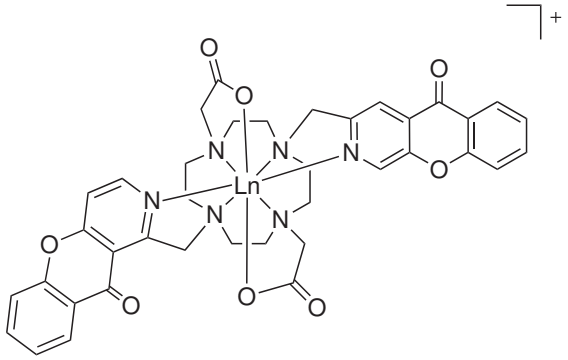

Ln = Eu, Gd, Tb

9

Figure 2.5: Structure of [LnDOA2-bis((1-azaxanthone)]$^{+}$.

Recently Vazquez *et al*. employed the tetramide luminescent lanthanide complexes of Eu(III) and Tb(III) in order to investigate the photophysical properties of the bis-4-amidobenzamidine (**10**), which was previously reported to exhibit a remarkable fluorescence emission enhancement upon binding to A/T-rich sites in ds-DNA when excited at 329 nm (Figure 2.6).[12]

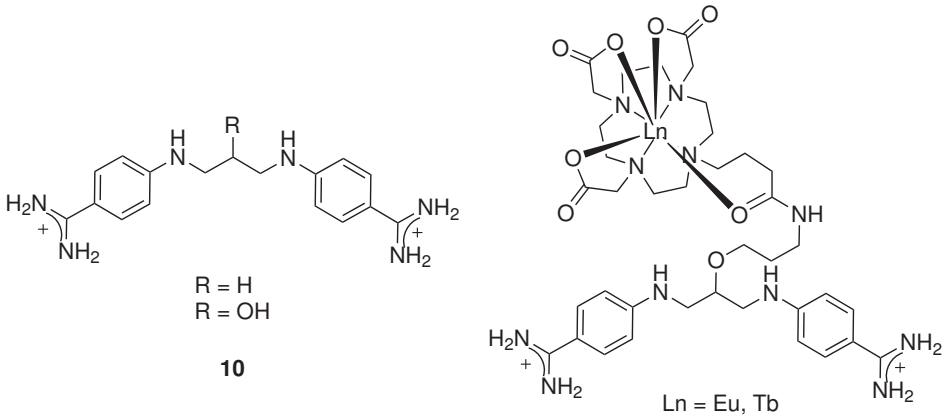

R = H
R = OH

10

Ln = Eu, Tb

11

Figure 2.6: Structure of [Ln-DOTA-bis(4-aminobenzamidine)].[13]

The bis-4-amidobenzamidine(**10**) has been coupled with [Ln-DOTA] to obtain complex **11**, and employed as an antenna system to sensitise the lanthanide emission. Indeed upon excitation of the bis-aminobenzamidine at 329 nm, energy transfer occurs to the lanthanide excited state.

The initially poor lanthanide emission in aqueous media becomes enhanced upon addition of the *ds*DNA, and a four fold increase in luminescence magnitude was observed for complex **11** upon interaction with duplexes containing the -AATTT- sequences.[13]

2.1.1 Luminescent heterometallic lanthanide complexes for DNA sensing

Attention has been given to the development of heterometallic luminescent architectures, where transition metal complexes can be used as recognition site whilst simultaneously being used as antenna systems to sensitise lanthanide luminescence *via* energy transfer. Indeed heterometallic lanthanide complexes have been proposed for use in a variety of applications including catalysis[14], magnetic devices[15] liquid crystal materials, and sensor design.[16]

Parker *et al*. developed an heterometallic complexes (Figure 2.7) where a Pd(II) porphyrin complex used as a chromophore to sensitise the lanthanide luminescence (Figure 2.7).[17]

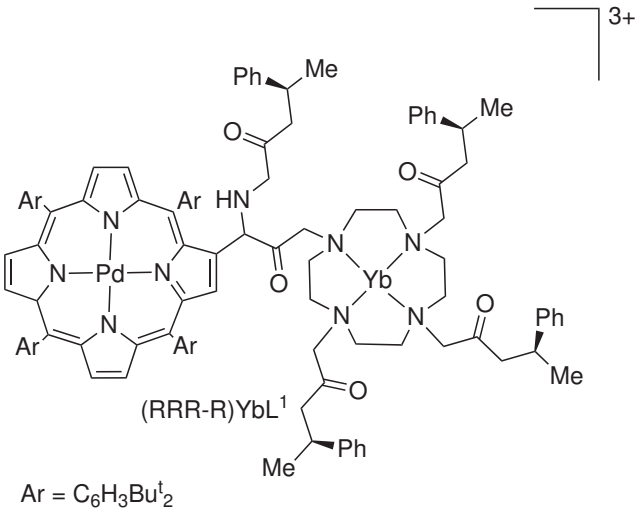

12

Figure 2.7: Structure of $[YbPd]^{3+}$.

Since the Pd(II)-porphyrin excited state is efficiently quenched by oxygen, and the luminescence of NIR lanthanide emitters is deactivated by O–H oscillators, consequently the heterometallic complex is non emissive in the presence of an aqueous buffer.[18] Addition of DNA allows shielding of the Pd(II)-porphyrin from oxygen by its intercalation between the DNA bases. As a consequence an enhancement in luminescence arising from the Pd(II)-porphyrin and the lanthanide was observed. Preliminary results from photophysical studies showed a preferred binding to alternating sequence of cytosine and guanine rather then adenine and thymine.[17]

Efficient sensitisation of NIR-emitting Ln(III) ions is particularly pertinent for biological application, since tissue is transparent to the higher excitation wavelengths required to sensitise near-infrared

emission. Typically the lanthanide sensitisation process proceeds through a MLCT level which is inherently lower in energy than then the triplet energy level arising from the organic chromophores and relatively close to the lanthanide luminescent excited state.[19] The MLCT level usually varies greatly and can be modulated by the combination of the transition metal and ligand system employed. Examples in literature cover a range of chromophores and derivatives including Re(I), Ru(II), Pt(II), Fe(II), Cr(III) and Ir(III) metal centres.[20]

Gunnlaugsson et al. reported an example of a heterometallic complex able to sensitise near-infrared emitting Ln(III) ions by energy transfer upon excitation through the MLCT band of the complex (Figure 2.8).[21][22]

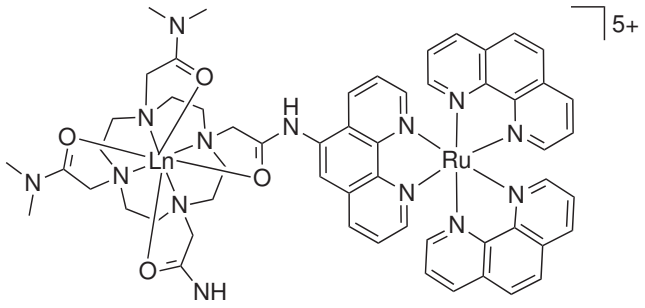

12

Ln = Yb, Nd, Gd

Figure 2.8: Ln-DOTA Ru(II)$(bpy)_2$ structure.

Recently the same group reported that complex **12** changes its luminescent properties upon binding to *ds*DNA.[23] In fact upon addition of calf thymus DNA to complex **12**, a luminescence enhancement of 30% for ytterbium and 27% for neodymium was observed upon excitation of the ruthenium based ^{3}MLCT band. However the luminescence arising from the lanthanide ion was "switched off" upon interaction of **12** with *ss*DNA, clearly indicating that energy transfer from ^{3}MLCT to the lanthanide exited state was inhibited upon binding to *ss*DNA.

This particular behaviour was only observed for the Yb(III) complex and not for Nd(III), which shows no change in luminescence upon binding to DNA.[24] Competitive binding studies with ethidium bromide showed the ability of complex **12** to behave as an intercalator, where the phenantroline ligand it stacks between the DNA base pairs.

2.1.2 Project overview

This chapter explores the DNA binding studies of luminescent metallohairpins notated as [$LnPt_2$], obtained using a versatile self-assembly approach which combines a lanthanide ion with planar aromatic platinum(II) metal arm. The system is based on a derivative of the diethylenetriaminepentaacetic acid (DTPA) with bisamide thiophenol moieties, bearing a hard binding core to encapsulate the lanthanide ion and soft thiolates sites to attach Pt(II) terpyridine units.

The design offers a luminescent label as well as sites for intercalation, which could be used to sensitise lanthanide emission *via* organic chromophores or charge transfer bands, all in one discrete moiety.

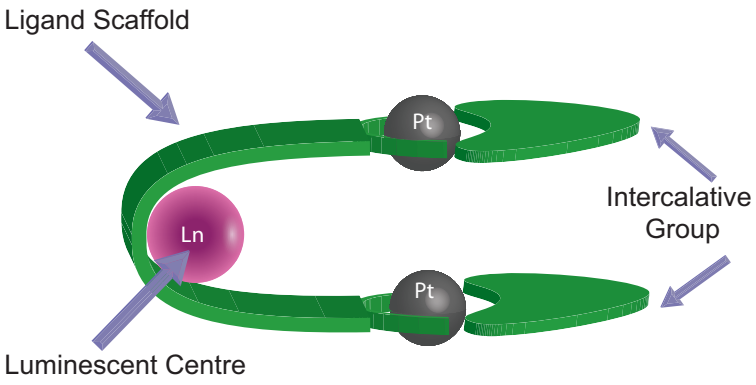

Figure 2.9: A schematic diagram of the hairpin complex [$LnPt_2$].

The intercalation of any compound into the DNA duplex causes the DNA helical structure to stiffen. Planar aromatic ligands (i.e. ethidium bromide) can intercalate between the base pairs and hence these interactions can be studied using a variety of absorption techniques. Due to the combination of the square planar geometry with the electronic properties of a d^8 metal centre, the platinum(II) terpyridine moieties can act both as chromophores and as DNA recognition sites *via* intercalation.

The [$NdPt_2$] complex was first characterised and reported by Glover *et al.* who discovered the ability of the complex to bind to calf-thymus (CT-DNA). The terpyridiplatinum(II) ligands were able to form an extended π-π stacking interaction with DNA base pairs (Figure 2.10), as perhaps demonstrated by previously reported linear dichroism studies.[25]

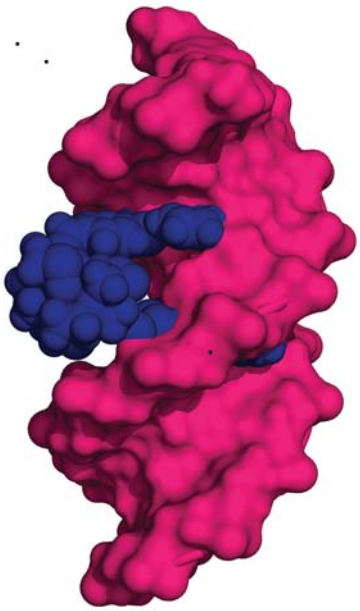

Figure 2.10: A 3D model of the [$LnPt_2$] complex binding to B-DNA.

Photophysical studies of [$LnPt_2$] were also reported by Solomons,[26] who replaced the initial Nd(III) ion with lanthanides able to emit in the visible (Ln = Eu, Tb) and NIR (Nd, Yb, Er). However only the [$EuPt_2$] and the [$NdPt_2$] were successively investigated upon binding to DNA.

In this chapter we report the preparation of [$LnPt_2$] (Ln = Eu, Nd) with improved solubility in water. There are mainly two reasons to improve the water solubility: firstly to examine the NMR properties upon binding to DNA (which will be detailed in chapter 3) and secondly to investigate in more detail the photophysical properties upon binding to DNA. There are two possible strategies that can be used to improve the water solubility of [$LnPt_2$], either the modification of the terpyridine ligand with hydrophilic groups or simply metathesised PF_6^- with an ion that has a bigger affinity for water (i.e. Cl^-).

2.2 Results and discussion

2.2.1 Synthesis of $[LnPt_2]Cl_2$

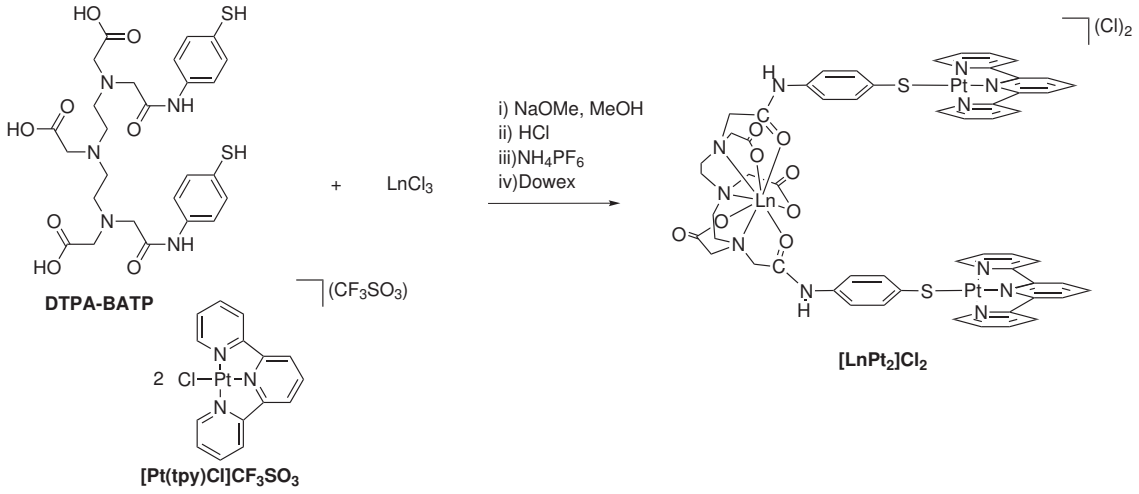

Scheme 2.1: Synthetic route of $[LnPt_2]Cl_2$ complexes.

The synthesis of $[NdPt_2](PF_6)_2$ has been previously reported by P. Glover[25] and successively with the same method by M. Solomons[26], who isolated the $[LnPt_2](PF_6)_2$ (with Ln = Tb(III), Eu(III), Gd(III), Nd(III), Yb(III), Er(III)).

The heterometallic complexes can be made by self assembly using stoichiometric amounts of the three components DTPA-BATP, $[Pt(tpy)Cl](CF_3SO_3)$ and $LnCl_3 \cdot 6H_2O$ in a 1:2:1 ratio. A variety of different approaches, both sequential and one-pot synthetic routes, have been successfully employed to isolate these complexes. However, the procedure predominantly employed here involved prior assembly of the ligand in order to allow isolation of $[LPt_2]$ to confirm the first step was successful. Firstly, DTPA-BATP was deprotonated with sodium methoxide and combined with $[Pt(tpy)Cl](CF_3SO_3)$ to form the Pt–S bond linkage. The complexes were formed *in situ* by increasing the pH to 5 in order to deprotonate the carboxylate coordination sites and the lanthanide ion was then added as the hydrated chloride. Finally, a metathesis reaction was performed using a saturated methanolic solution of ammonium hexafluophosphate to precipitate the desired complex (Scheme 2.1). Despite of +2 charge of both $[LnPt_2](PF_6)_2$ and $[LPt_2](PF_6)_2$, they were sparingly soluble in water; we needed to increase the solubility of these complexes in water in order to follow their DNA binding by ^{1}H-NMR spectroscopy.

In order to preserve the photophysical and intercalative properties of [$LnPt_2$] and its high DNA binding constant, the $(PF_6)^-$ anion was metathesised to Cl^- by ion exchange chromatography.

Ion exchange chromatography was performed on Dowex 1×8 resin, where a polystyrene resin includes quaternary salts of ammonium which can be considered as an immobilised positive charge, and each of them are neutralised with a chloride *via* ionic interaction (Figure 2.11).

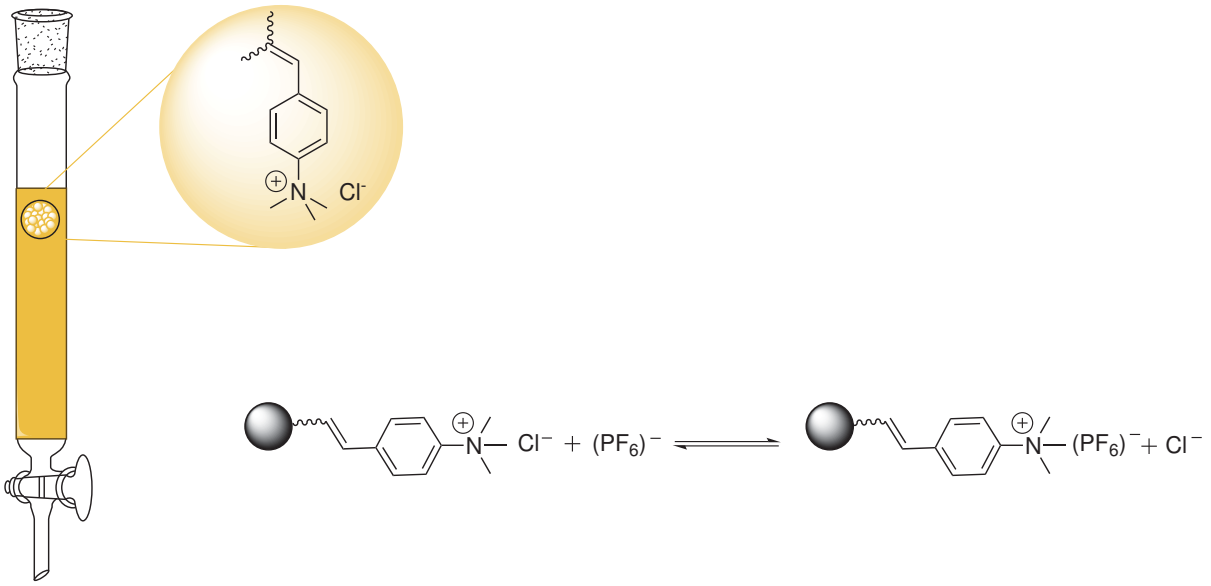

Figure 2.11: Principle of ion exchange chromatography.

The [$LnPt_2$]$(PF_6)_2$ and its precursor [LPt_2]$(PF_6)_2$ sample were initially dissolved in deionised water in the presence of a few Dowex beads. When the sample is eluted through the ionic exchange column, an equilibrium of $(PF_6)^-$ in the solution and on solid phase is taking place. As is characteristic of the chromatography techniques, every single step of the elution is characterised by a new equilibrium. Due to the high loading Cl^- of the resin, the equilibrium will favour the release of Cl^- while the $(PF_6)^-$ will be retained.

The resulting chloride salts of the complexes were soluble in water and in methanol, and all complexes were fully characterised and as expected the results were in agreement with the $(PF_6)^-$ salt ones. The ^{1}H NMR of [LPt_2]Cl_2 shows a singlet at 4.19 ppm characteristic for the central $\mathbf{CH_2}$ of the DTPA (Figure 2.12), while the multiplet peaks at 3.69 and 3.44 ppm are consistent with the aliphatic chain and the $\mathbf{CH_2COO^-}$ groups respectively. The multiplet at 8.49 ppm corresponds to **H6** of the platinum(II) terpyridine unit, which overlaps with the **H4'**. The multiplets between 8.45

and 8.25 ppm can be assigned to **H4**, **H3** and **H3'** of the terpyridine unit while the doublet of doublets at 7.56 ppm arises from the **H5**. The **Hb** and the **Ha** arising from the thiophenol group are observed respectively at 7.48 and 7.33 ppm. Protons on the thiophenol unit and in particular **Hb** are quite diagnostic to monitor the progress of the reaction due to their upfield shift from 7.31 ppm to 7.48 ppm upon coordination of the sulphur to the platinum.

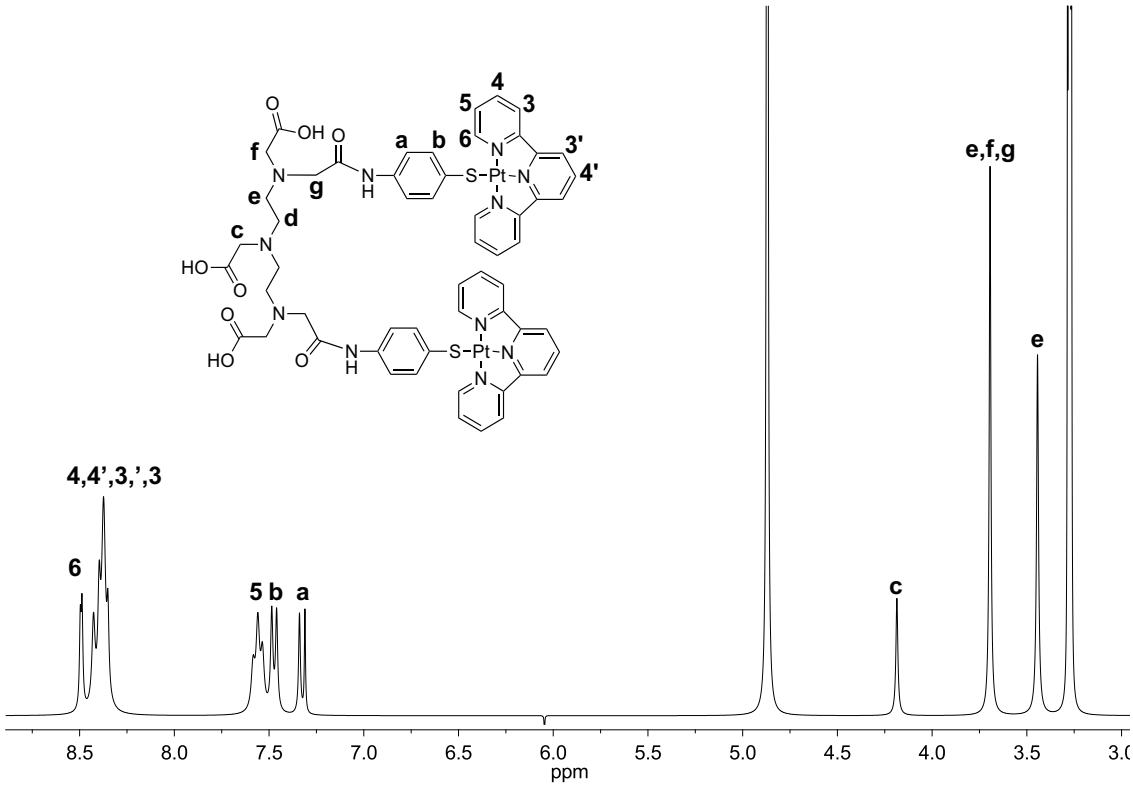

Figure 2.12: ^{1}H-NMR at 300 MHz of $[LPt_2]Cl_2$ in D_2O/d_4-methanol.

The $[LPt_2]Cl_2$ and $[LnPt_2](PF_6)_2$ (Ln = Eu, Nd) were further characterised by electrospray and MALDI-TOF mass spectrometry which reveals peaks corresponding to a number of species for the same heterometallic complex, and in both techniques the complexes are usually observed with the loss of both Cl^-(Figure 2.13). All the electrospray spectra for the $[LnPt_2]$ complexes were also characterised by the presence of a secondary peak at m/z = 464 that is assigned to the $[Pt(tpy)Cl]^+$. However, since the UV-vis and elemental analysis are consistent with the presence of these species, the $[Pt(tpy)Cl]^+$ is likely to be the product of fragmentation processes taking place during the ionisation process in the electrospray techniques.

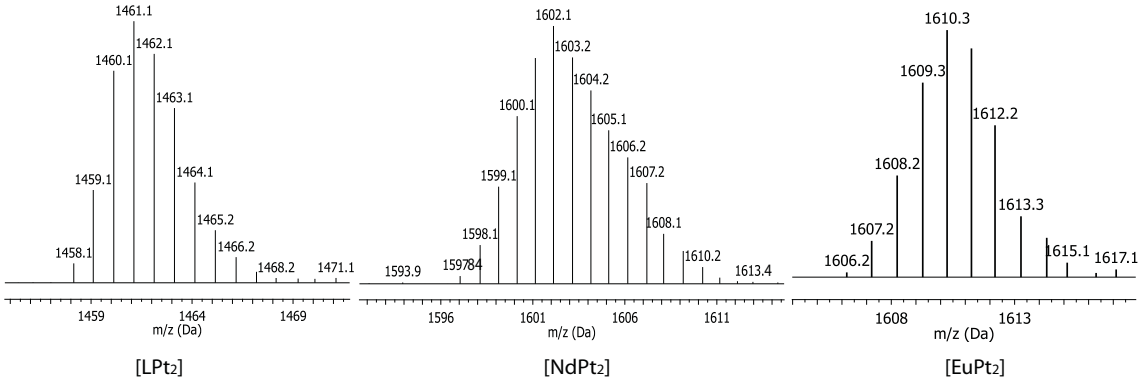

Figure 2.13: MALDI-TOF mass spectra of $[LPt_2]$ (left), $[NdPt_2]^+$ and $[EuPt_2]^+$.

Due to lanthanide paramagnetism we synthesised the diamagnetic analogue of $[LnPt_2]$ using Y(III) which was used for ^{1}H-NMR assignment of the heterometallic complex (Figure2.14). The chemical shift of the terpyridyl ligand are in the same region as the $[LPt_2]Cl_2$ complex.

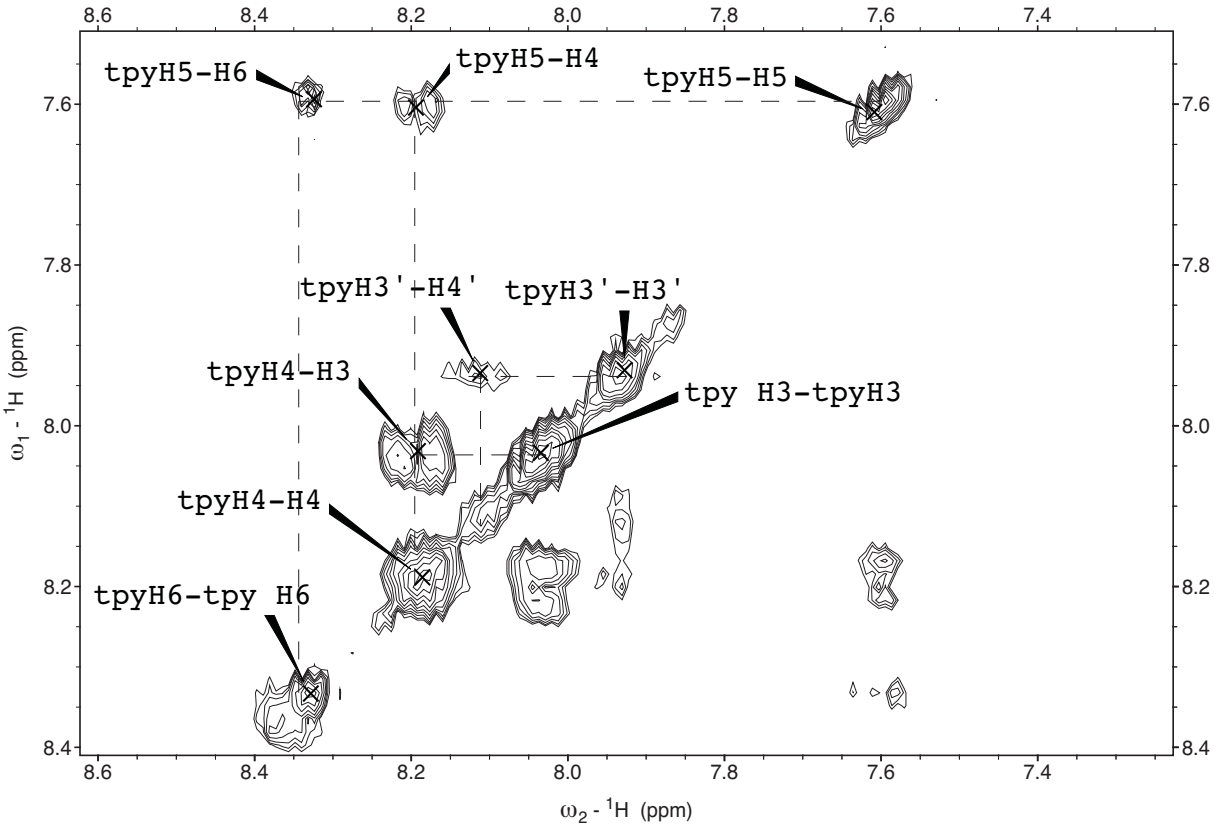

Figure 2.14: ^{1}H-^{1}H COSY NMR at 400 MHz for the aromatic region of $[YPt_2]Cl_2$ in D_2O.

The **H6** is identified at 8.35 ppm while **H5** and **H4** are respectively at 7.60 and 8.20 ppm. There is a considerable broadening of the proton resonances in the aliphatic region. This can be ascribed

to the presence of a number of rotamers that lead to the broadening of the aliphatic region in the ^{1}H-NMR spectrum of the complex.[27] Due to its diamagnetic properties and relatively high solubility in water, $[YPt_2]Cl_2$ is a good candidate to be used in the DNA binding studies by NMR spectroscopy (see Chapter 3).

2.2.2 Photophysical studies

The photophysical properties of $[LnPt_2]Cl_2$ (Ln = Eu, Nd, Gd) were investigated, and figure 2.15 shows the absorption spectrum of $[LnPt_2]Cl_2$ in methanol. The absorption band at 250 nm is observed as a result of the $\pi \rightarrow \pi^*$ transitions in the phenyl ring, while the $\pi \rightarrow \pi^*$ intraligand terpyridine transitions were observed at 280 nm, 330 and 345 nm. At 380 nm a shoulder appears which was assigned to a mixed state arising from the terpyridine $\pi \rightarrow \pi^*$ and MLCT transitions. A broad transition band was observed in the region between 400 and 700 nm with a maximum at 540 nm which is characteristic of the ligand-ligand charge transfer (LLCT) from the ground state of the thiolate moiety into the π^* orbitals of the terpyridine groups. This band is responsible for the deep purple colour of the complex and it is diagnostic for the complex formation. Similar LLCT charge transfer bands have previously been observed in S-Pt-tpy complexes.[28]

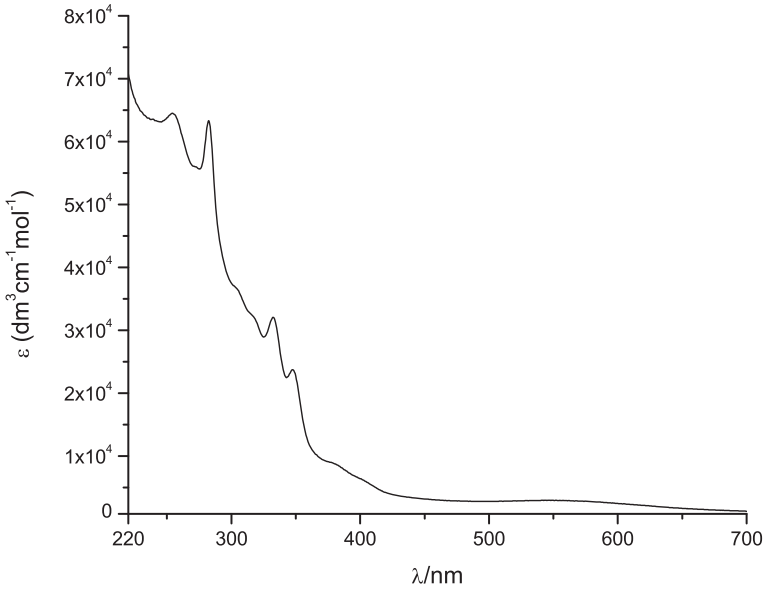

Figure 2.15: Absorption spectrum of 10 μM $[EuPt_2]Cl_2$ in methanol.

2.2.2.1 77 K emission studies of [$GdPt_2$]

There are mainly two reasons to use Gd(III) ions for low temperature studies; one is due to the heavy atom effect of Gd(III) which increases the rate of the intersystem crossing from the single to the triplet state within the ligand and thus enhances the observation of the triplet state phosphorescence; the second reason is due to the fact that the luminescent energy level of Gd(III) is too high to receive any energy transfer from the ligand. Thus the 77 K emission experiment of [$GdPt_2$]$(PF_6)_2$ in a rigid matrix provides a good environment to observe the phosphorescence ligand transitions.

The [$GdPt_2$]$(PF_6)_2$ sample was kindly provided by Solomons, and it was used in a MeOH/EtOH 1:5 rigid matrix at 77 K. When excited at 330 nm a phosphorescence in the region between 450 - 600 nm was observed (Figure 2.16), that can be assigned as derived from the [π(tpy)$\rightarrow$ $\pi*$(tpy)] triplet excited state.

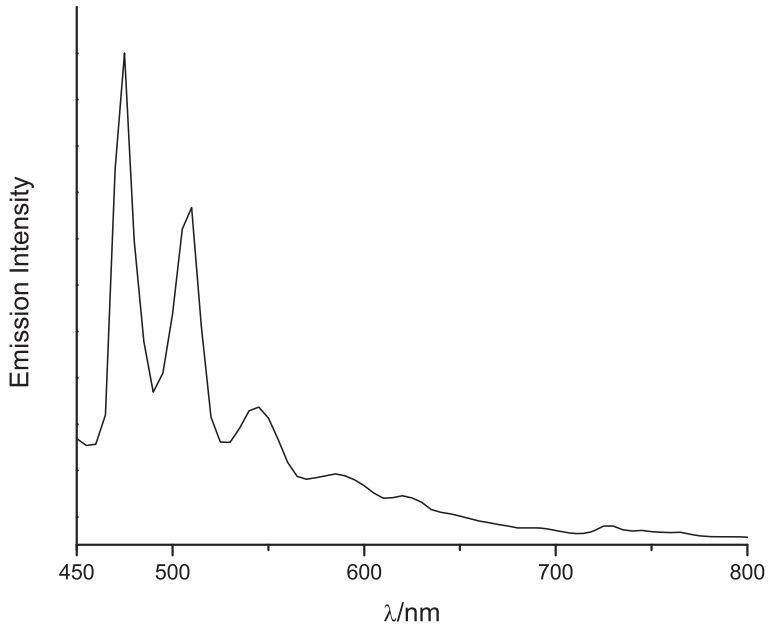

Figure 2.16: Emission spectrum of [$GdPt_2$]$(PF_6)_2$ in MeOH/EtOH 1:5 rigid matrix at 77 K with λ_{exc} at 330 nm.

Table 2.1 lists the phosphorescence transitions, with the lowest one at 470 nm which is attributed to the ground state of the ligand triplet state (0 - 0 transition). A calculation of the vibrational energy levels from the structured emission spectrum of [$GdPt_2$]$(PF_6)_2$ reported in table 2.1, shows a spacing of about 1480-1420 cm^{-1} that is typical of the C=C or C=N stretching frequencies of the tridentate ligand.[29,30,31]

The broad emission bands observed in the region of $\sim$ 630 nm, can be ascribed to the excimer that originates from the $\pi - \pi$ stacking of the platinum(II) terpyridine units in the rigid matrix.[32,33]

In 2006 Lianos *et al*. reported a complex where the terpyridine ligand was directly coordinated to the lanthanide ion, and the low temperature experiments show a phosphorescence band at 19880 cm^{-1} which was assigned to the terpyridine triplet state. This value is consistent with the transitions observed for the $[GdPt_2](PF_6)_2$ and confirms that the energy level of the terpyridine triplet state is not able to give an efficient energy transfer.

λ/nm	$\nu - \nu'$	Energy/cm^{-1}	E(cm^{-1})
470	0 - 0	21280	-
505	0 - 1	19800	1480
544	0 - 2	18380	1420

Table 2.1: List of $T_1 \rightarrow S_0$ phosphorescence transitions of $[GdPt_2]$ at 77 K.

The observed phosphorescence transitions are similar to other platinum(II) terpyridine complexes previously reported. For example Bekiari *et al*. reported a thiolate substituted platinum(II) terpyridine complex bearing a dithiobenzoquinone as co-ligand, characterised by a 77 K emission profile that resembles the one obtained with $[GdPt_2](PF_6)_2$.[34] The same profile was observed also by Solomons in a 77 K experiment for a platinum(II) terpyridine complex where the coligand was the 4-amidothiophenol.[26]

Similar values were also observed for other platinum(II) terpyridine complexes bearing a non thiolate coligand. For example the $[Pt(tpy)(MeCN)]^{2+}$ displays a phosphorescence transitions with emission at 480, 515 and 550 nm.[35]

Furthermore, it is interesting to mention that the 77 K emission spectrum of the [GdDTPA-BATP] (amidothiophenyl complex) shows a triplet ground state at 24000 cm^{-1} and vibronic transitions at 22730 and 21600 cm^{-1}.[36]

Another important consideration in this system is the influence of the LLCT band at 18500 cm^{-1} which could also be responsible for the energy level perturbations.

2.2.2.2 Emission studies of $[EuPt_2]Cl_2$

Typical Eu(III) luminescence was observed upon excitation of $[EuPt_2]Cl_2$ at 280 nm and red emission was observed as a result of the luminescent transitions $^5D_0 \rightarrow ^7F_J$ (J= 0, 1, 2, 3, 4) at 580, 590, 615, 650 and 695 nm, respectively (Figure 2.17).

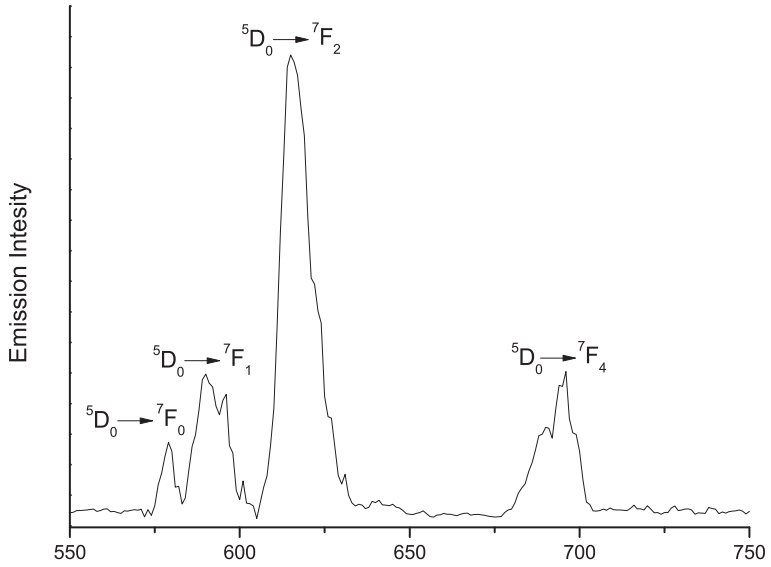

Figure 2.17: Emission spectrum of 10 μM $[EuPt_2]Cl_2$ in MeOH upon excitation at λ_{exc} = 280 nm, uncorrected for PMT response.

Emission spectra were also collected using different excitation wavelengths; 250, 280, 290, 330, 345 and 380 nm (Appendix to chapter 2 Figure 14), which are the values that correspond to the band maxima observed in the absorption spectrum. The emission spectra demonstrate that sensitisation can be achieved through the terpyridyl arms of the molecule; however the most intense emission is observed when the excitation wavelength is 290 nm. At this wavelength there is likely to be both phenyl centred $\pi \rightarrow \pi^*$ and terpyridine $\pi \rightarrow \pi^*$ centred absorption involved.

The excitation spectrum of $[EuPt_2]Cl_2$ was recorded monitoring the transition $^5D_0 \rightarrow ^7F_2$ at 615 nm. The spectrum displays one band which corresponds to the thiophenyl group at 280 nm and a very weak broad band between 345 and 380 assigned to the terpyridine $\pi \rightarrow \pi^*$ with some contribution of the MLCT transitions (Figure 2.18). In the excitation spectrum the LLCT is not observed which implies it does not contribute efficiently to energy transfer to Eu^{3+}.

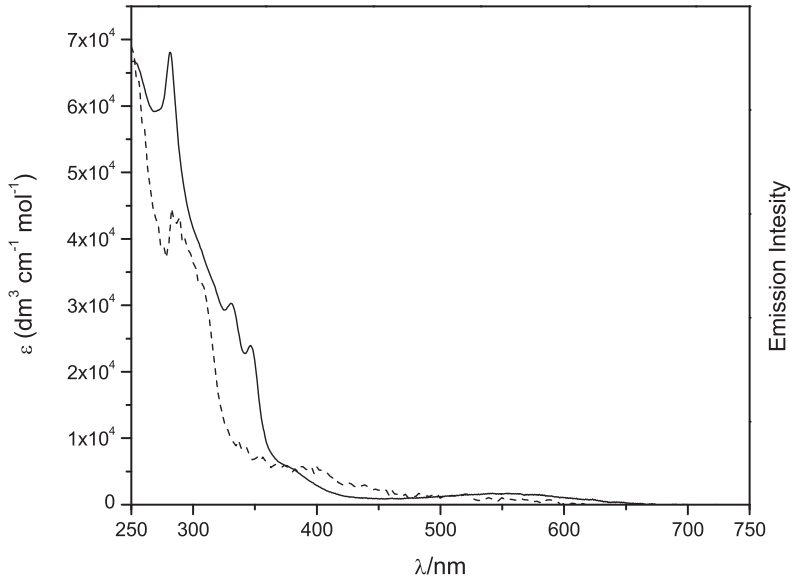

Figure 2.18: Absorption (solid line) and excitation (dashed line) spectra of 10 μM [$EuPt_2$]Cl_2 in methanol corrected for lamp intensity. λ_{em} = 615 nm.

Previously reported studies for the visible lanthanide emitters of [$LnPt_2$]$(PF_6)_2$ investigated the photophysical properties of [$TbPt_2$]$(PF_6)_2$ which resulted to be less emissive than [$EuPt_2$] $(PF_6)_2$.[26] An explanation can be found in the energy levels involved and in the distance between the chromophore and the lanthanide ion. Indeed considering the close proximity of the triplet excited state of the ligand (21280 cm^{-1}) and the excited luminescent level of Tb(III) (20545 cm^{-1}), it can be seen that they are divided by an energy gap of only 735 cm^{-1} that is too small to avoid back energy transfer followed by vibrational deactivation. The luminescent excited state of Eu(III) is suitably placed (17300 cm^{-1}) to receive energy transfer from both thiophenyl and terpyridine moieties, although the thiophenol moiety dominates the process as it is closer to the luminescent centre. According to reports, the energy transfer from sensitiser to lanthanide are usually a very fast process. An example was reported by Nocera and coworkers, using acetylacetonate (acac) to sensitise Tb(III) encapsulated in a macrocyclic cage of cryptand. The energy transfer between the $^3\pi$ and Tb(III) occured within few picoseconds.[37] We have not been able to monitor the rate of energy transfer in thisshort timescale in our system.

Furthermore, we also tested the excitation through the LLCT band at 540 nm and as expected the

LLCT transition did not lead to any Eu(III) based luminescence, since the charge transfer band has light absorption in the same spectral region.[25].

In figure 2.19 a Jablonski diagram summarises the photophysical processes that occur in [$EuPt_2$]. Both chromophore the amidothiophenyl (S_1X_1) and the terpyridine (S_1X_2) moieties were shown to be able to sensitise the Eu(III) emission. Furthermore, the triplet state of the terpyridine (T_1X_2) is suitably placed to receive energy from the higher phenyl levels as well. This coupled with the luminescent energy level of Eu(III), means that either ligand triplet state can effect sensitisation and a mixed pathway appears to be the most efficient method.

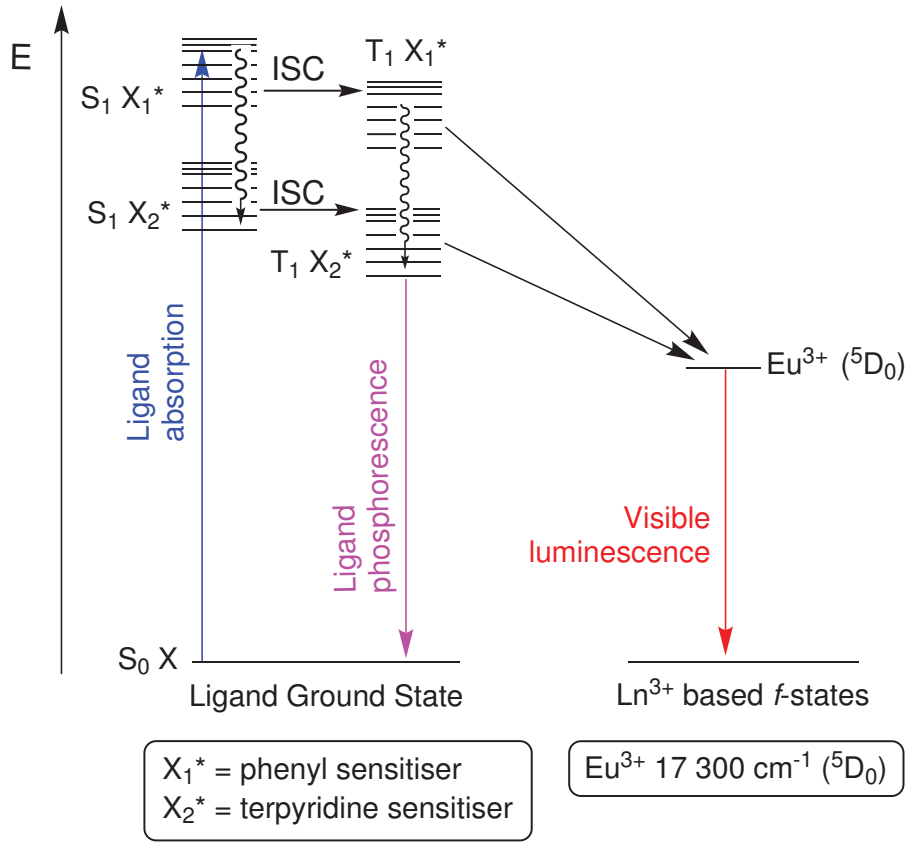

Figure 2.19: A schematic AETE energy level diagram for sensitising visible emission in the [$EuPt_2$]Cl_2 ligand system.

2.2.2.3 Emission studies of [$NdPt_2$]Cl_2

Photophysical studies with NIR lanthanide emitters of [$LnPt_2$]$(PF_6)_2$ (Ln = Nd, Yb, Er) were previously reported by Solomons.[26] These studies were performed using d_6-DMSO as solvent, in order to reduce the number of bond oscillators, namely C–H and O–H, which are able to quench the relevant near-infrared *f-f* transitions. When a deuterated solvent is employed the Franck-Condon vibrational

overlap integrals are reduced and hence a less efficient energy relaxation pathway is realised leading to a minimised quenching effect (see chapter 1, page 27).[38] However DMSO as solvent can not be used in DNA binding studies, since it may induce conformational changes on the B-DNA structure. Since we isolated a more water soluble form of $[LnPt_2]Cl_2$ (Ln = Nd), we reinvestigated these properties using D_2O in order to maximise the emission intensity from the lanthanide. Excitation of the $[NdPt_2]Cl_2$ complex through the terpyridine $\pi \rightarrow \pi^*$ region at 337 nm gave a relatively intense neodymium luminescence in the near-infrared region. Characteristic emission bands were at 880 nm ($^4F_{3/2} \rightarrow {}^4I_{9/2}$) and 1330 nm ($^4F_{3/2} \rightarrow {}^4I_{13/2}$) with the strongest one at 1060 nm ($^4F_{3/2} \rightarrow {}^4I_{11/2}$) (Figure 2.20).

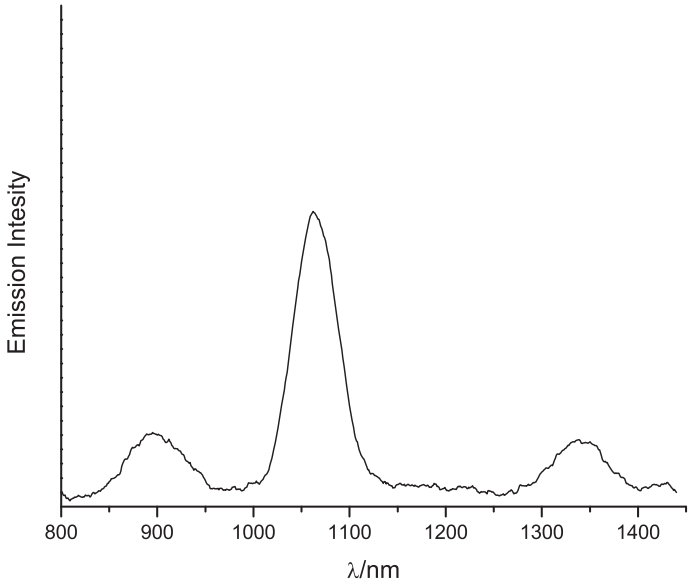

Figure 2.20: Emission spectrum of 15 μM $[NdPt_2]Cl_2$ in D_2O, uncorrected. λ_{em} = 337 nm.

Weak neodymium(III) emission could be observed upon excitation at 280 and 380 nm, while the excitation of the LLCT band at 540 nm did not show any emission due to the weak concentration of the sample. Figure 2.21 shows the excitation spectrum of $[NdPt_2]Cl_2$ which indicate that a different sensitisation pathway operates for the $[NdPt_2]Cl_2$ compared to the $[EuPt_2]Cl_2$.

When $[NdPt_2](PF_6)_2$ salt was used in d^6-dmso, due to the higher solubility of the complex, Nd^{3+} emission was observed upon excitation at 540 nm (18500 cm^{-1}, LLCT)

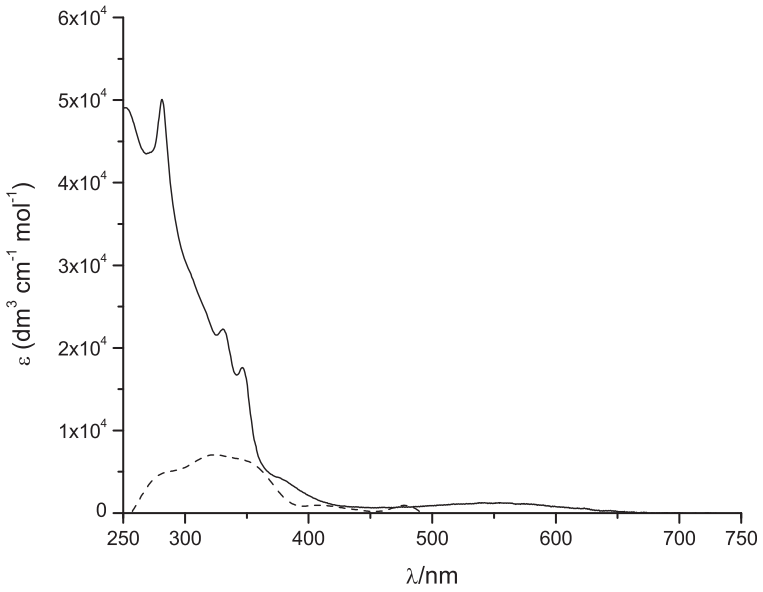

Figure 2.21: Absorption (solid line) and excitation (dashed line) spectra of 15 μM $[NdPt_2]Cl_2$ in D_2O corrected for lamp intensity. λ_{em} = 1060 nm.

Examples of energy transfer from charge transfer state to Nd^{3+} have been previously reported by Faulkner and coworkers. Using Ru(II)/Nd(III) dyads incorporating two bipyridyl metal-binding site separated by an aromatic spacer and a sensitisation of the ^{3}MLCT, the authors were able to measure a rate constant (k_{EnT}) for a Ru(II)$\rightarrow$Nd(III) energy transfer of 1.9×10^7 s^{-1}.[39]

In Figure 2.22 we summarised in a Jablonski's diagram the photophysical processes that occur in $[NdPt_2]$. Both chromophore the amidothiophenyl (S_1X_1) and the terpyridine (S_1X_2) moieties were shown to be able to sensitise the Nd(III) emission, although the terpyridine (S_1X_2) moieties are more efficient. As reported for the $[EuPt_2]$, the triplet state of the terpyridine (T_1X_2) is suitably placed to receive energy from the higher phenyl levels as well.

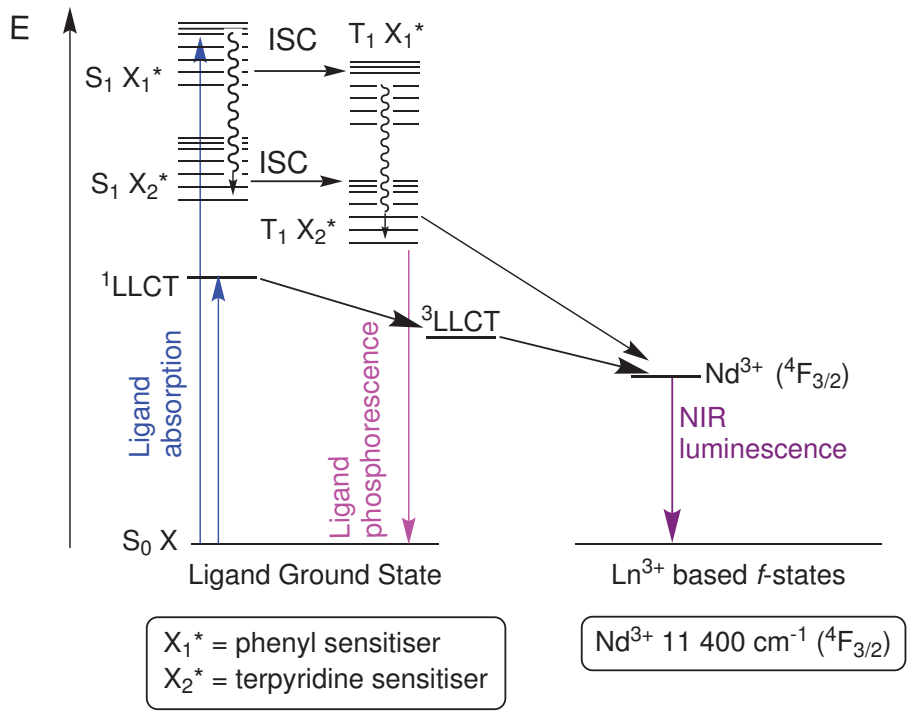

Figure 2.22: A schematic AETE energy level diagram for sensitising visible emission in the $[EuPt_2]Cl_2$ ligand system.

Moreover, the ^{1}LLCT band may be suitably placed for energy transfer to near-infrared lanthanides. However, due to the relatively low solubility of the complex in D_2O we were not able to detect any Nd(III) emission upon excitation of the LLCT band. Thus the terpyridine moiety was found to be more efficient than the ^{1}LLCT to sensitise the Nd(III) emission, especially in the case of low concentrations as required for DNA binding studies in water.

2.2.3 DNA binding studies

The binding of $[LnPt_2]Cl_2$ (Ln = Y, Eu, Nd) to DNA (CT-DNA, poly(dAdT) and poly(dGdC) was initially investigated by luminescence studies, DNA melting point, and here CD and LD are mentioned together as dichroism studies.

2.2.3.1 Luminescent studies

The excitation wavelength selected was 330 nm, where the DNA absorption is the least and excitation of the chromophore is still efficient for energy transfer to the lanthanide. The excitation at 330 nm is a compromise, which in first instance leads to a weak europium emission from the complex in solution. However, upon addition of CT-DNA to a solution of $[EuPt_2]Cl_2$ it is possible to observe an increase of the lanthanide emission intensity. The emission spectra of $[EuPt_2]Cl_2$ on its own and in presence of DNA was recorded upon excitation at 330 nm (Figure 2.23), and by integration of the emission peak area we found the luminescence intensity increased by 2.5 upon interaction with CT-DNA.

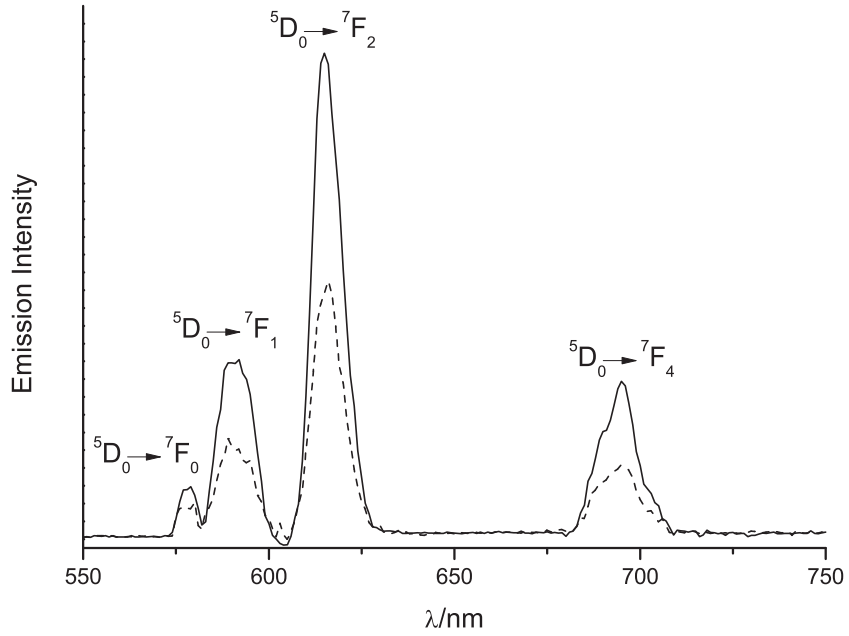

Figure 2.23: Emission spectra of solution of $[EuPt_2]Cl_2$ (dashed line) (20 μM) and $[EuPt_2]Cl_2$ in presence of CT-DNA (solid line) (80 μM) in H_2O, 10 mM HEPES and 10 mM NaCl. λ_{exc} = 330 nm.

The same emission experiments were performed with poly (dAdT) DNA and we observed changes similar to those recorded upon interaction with CT-DNA. The Eu(III) emission was initially weak but was enhanced by double upon interaction of the complex with poly(dAdT) (Figure 2.24).

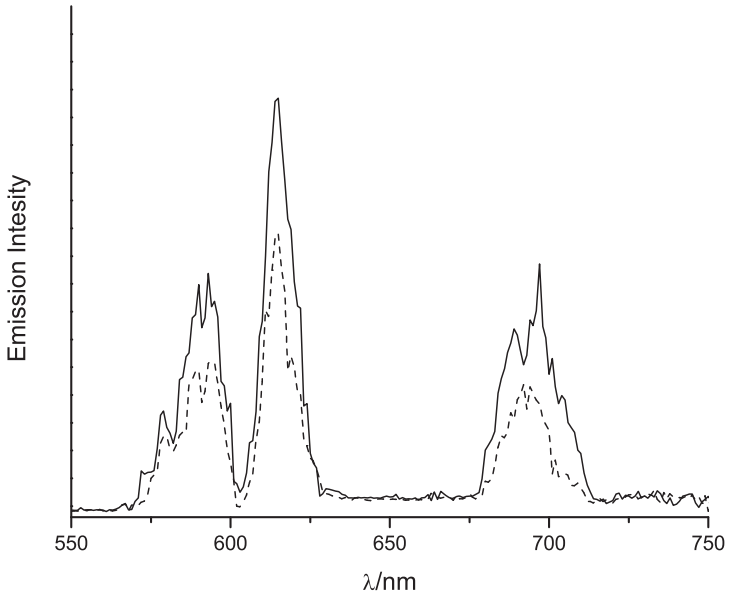

Figure 2.24: Emission spectra of solution of $[EuPt_2]Cl_2$ (dashed line)(20 μM) and $[EuPt_2]Cl_2$ in presence of poly(dAdT) (80 μM) in H_2O, 10 mM HEPES and 10 mM NaCl. λ_{exc} = 330 nm.

The emission spectra of $[EuPt_2]Cl_2$ and poly(dGdC) was characterised by a weak europium based emission for the complex alone. However, once again the addition of poly(dGdC) led to an increase of the emission signal. Integration of the emission peak area showed the luminescence increased by only 1.2 times upon addition of poly(dGdC) DNA (Figure 2.25).

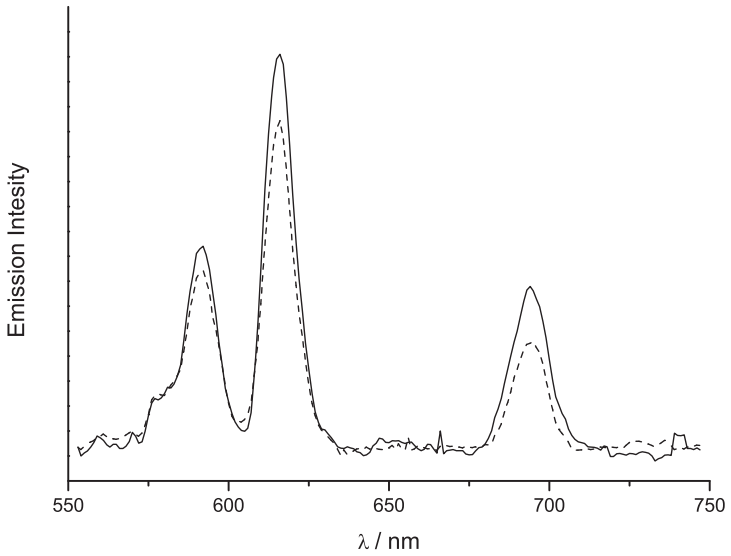

Figure 2.25: Emission spectra of solution of $[EuPt_2]Cl_2$ (dashed line)(20 μM) and $[EuPt_2]Cl_2$ in presence of poly(dGdC) (80 μM) in H_2O, 10 mM HEPES and 10 mM NaCl. λ_{exc} = 330 nm.

In the first instance it appears that the $[EuPt_2]Cl_2$ luminescence response depends on the base composition of the DNA sequence. In fact by evaluation of the area of the emission peak, it was seen that a pronounced luminescence enhancement was generated upon interaction of $[EuPt_2]Cl_2$ with

DNA sequences characterised by alternating sequence of adenine and thymine, while smaller Eu(III) luminescence enhancement were observed for sequences based on alternate sequences of guanine and cytosine (Figure 2.26).

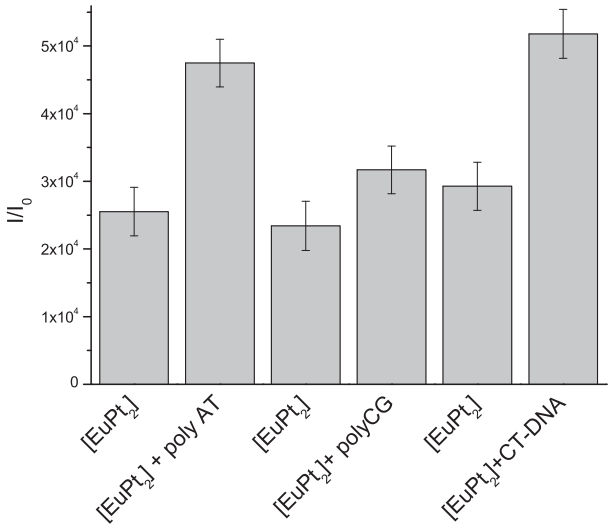

Figure 2.26: Comparison plot for luminescence response of $[EuPt_2]Cl_2$ upon interaction with CT-DNA, poly(dGdC) and poly(dAdT) in H_2O, 10 mM HEPES and 10 mM NaCl. Integration of the peak area at λ_{em} = 615 nm.

The same trend in fluorescence enhancement was observed when the near infrared emitting complex $[NdPt_2]Cl_2$ was employed as a luminescent probe for the sensing of CT-DNA, poly(dAdT) and poly(dGdC).

The excitation wavelength for the photophysical studies with the near-infrared complexes was maintained at 330 nm as DNA absorption at this wavelength is smaller. The $[NdPt_2]Cl_2$ displayed the characteristic near-infrared emission with its characteristic emission bands observed at 890, 1060 and 1332 nm corresponding to the $^4F_{3/2} \rightarrow {}^4I_J$ (J = 9/2, 11/2, 13/2) transitions. As seen for $[EuPt_2]Cl_2$, the $[NdPt_2]Cl_2$ showed an initial emission characterised by weak intensities, however upon addition of CT-DNA the complex showed an emission signal with doubled intensity (Figure 2.27).

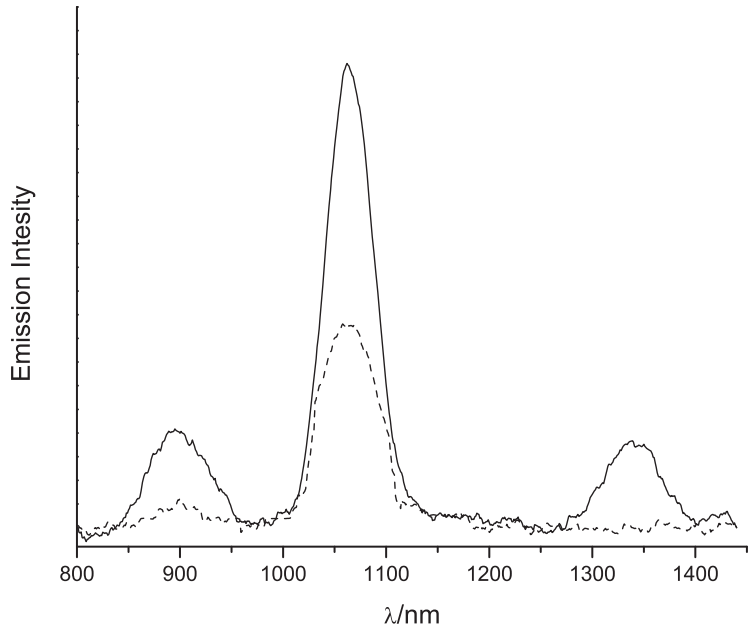

Figure 2.27: Emission spectra of solution of $[NdPt_2]Cl_2$ (20 μM) (dashed line) and $[NdPt_2]Cl_2$ in presence of CT-DNA (solid line) (80 μM), 10 mM HEPES and 10 mM NaCl, in D_2O uncorrected λ_{exc} = 330 nm.

Similar emission experiments were reported by Solomons using poly (dAdT) and poly (dGdC) DNA. Despite the initial weak emission, a luminescent enhancement that was 1.4 times stronger was observed upon addition of poly(dAdT), while a 1.6 times increase in the magnitude of emission was observed upon addition of poly(dGdC).[26]

The addition of CT-DNA and polynucleotide DNA showed an increase in emission intensity on both $[EuPt_2]Cl_2$ and $[NdPt_2]Cl_2$. In both cases the initial emission intensity was relatively weak and became greatly enhanced upon interaction with DNA. Since the selected excitation wavelength for these experiments (330 nm) corresponded to transitions within the planar terpyridine arms of the molecule, the observed luminescence enhancement has to be related with the intercalative interaction of the platinum(II) terpyridine unit.

Thus both the visible and near-infrared $[LnPt_2]Cl_2$ complexes can act as luminescent labels to detect intercalative DNA recognition with different DNA sequences. However, there is no discernible difference in the proportions of emission intensity response with different sequences of DNA, and therefore selectivity can not be monitored using photophysical techniques.

Circular dichroism

The DNA binding of $[EuPt_2]Cl_2$ was investigated by Circular Dichroism (CD) which uses circularly polarised light to measure the difference in molar absorption coefficients for left and right circularly polarised light at varying wavelengths. Consequently only chiral compounds will exhibit a CD signal, hence DNA has a characteristic CD signal. In comparison, an achiral ligand is able to absorb polarised light only when non-degenerate couplings between the electric dipole transition moment of the complex and those of the DNA bases are realised.[40] Thus any CD signal that arises in the spectroscopic region of the complex can only be ascribed to the degeneration of the energy level obtained when platinum(II) terpyridine moieties intercalates between the DNA base pairs.

The CD spectrum of CT-DNA recorded in aqueous buffer solution (Figure 2.28), shows a negative and positive signal respectively at 245 and 330 nm, characteristic of the B-DNA conformation adopted by CT-DNA. Upon aliquot additions of $[EuPt_2]Cl_2$, an increase of the positive and negative signals can be observed, confirming that the B-DNA conformation of the CT-DNA is retained, followed by a new positive band between 300 and 340 nm. This bad is the result of the induced circular dichroism (ICD) effect, and according with the UV-vis spectrum they can be assigned to $\pi \rightarrow \pi^*$ transitions of platinum terpydine units.[40]

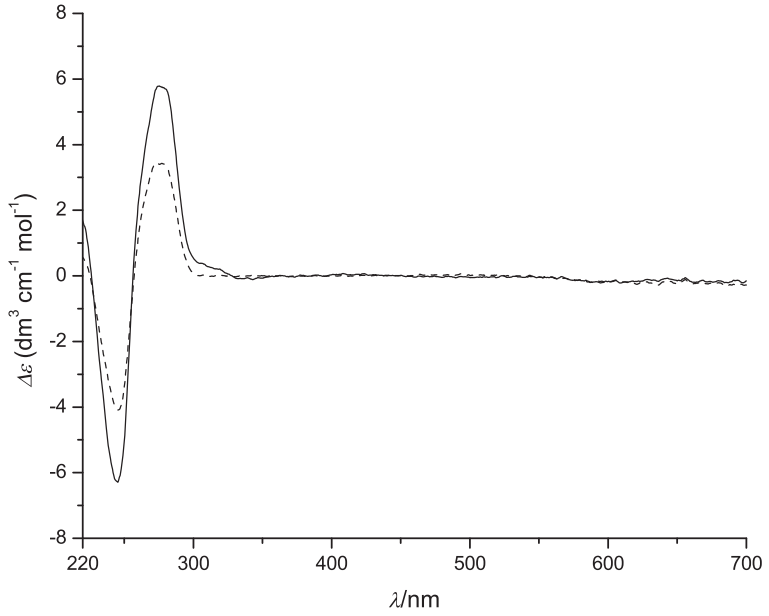

Figure 2.28: CD spectra of CT-DNA (dashed line) with addition of $[EuPt_2]Cl_2$ (solid line) (5:1) in H_2O 10 mM HEPES and 10 mM NaCl.

Under the same experimental conditions we recorded the CD spectrum for polynucleotide DNA, and figure 2.29 shows the characteristic spectra for poly(dAdT). The negative and the positive signals are observed respectively at 245 and 260 nm, which are indicative of the B-DNA conformation adopted by the polynucleotide DNA in the aqueous buffer solution. Addition of the $[EuPt_2]Cl_2$ to the poly(dAdT) solution is characterised by a reduction of the signal intensity at 250 nm followed by hypsochromic shift of 8 nm; while the positive signal at 262 nm showed an increase in the magnitude of the signal.

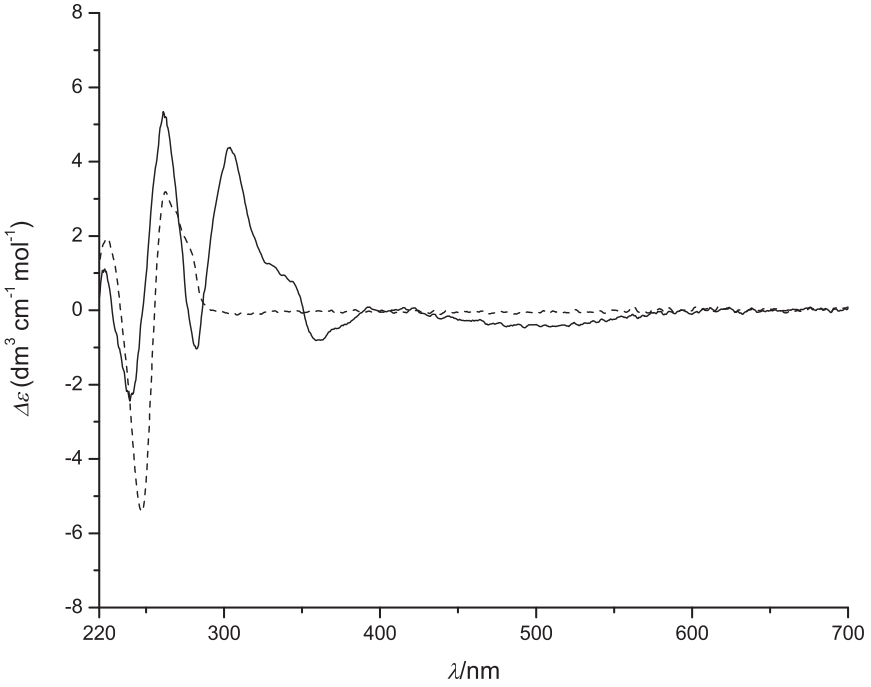

Figure 2.29: CD spectra of poly(dAdT) (dashed line) with addition of $[EuPt_2]Cl_2$ (solid line) (5:1) in H_2O 10 mM HEPES and 10 mM NaCl.

A significantly positive ICD signal is observed between 300 and 340 nm which is characteristic for the $\pi \rightarrow \pi^*$ transition with its transition moment being aligned parallel to the DNA base pairs. Furthermore a negative ICD signal is observed at 360 nm and between 450 and 560 nm which relative to the LLCT transition region of the spectra.

The poly(dGdC) DNA was also investigated by CD spectroscopy and upon addition of $[EuPt_2]Cl_2$ we observe a decrease of the negative signal at 250 nm followed by hypsochromic shift of 5 nm, which is consistent with the stiffening of the DNA helix upon intercalation of the two platinum(II) terpyridine unit (Figure 2.30).

The intensity of the positive band at 260 nm increases upon interaction with $[EuPt_2]Cl_2$, while a positive ICD signal appears in the region between 310 and 360 nm. This changes are consistent with the metal complex being able to bind polynucleotides, where a stronger interaction occurs with poly(dAdT) rather than poly(dGdC).

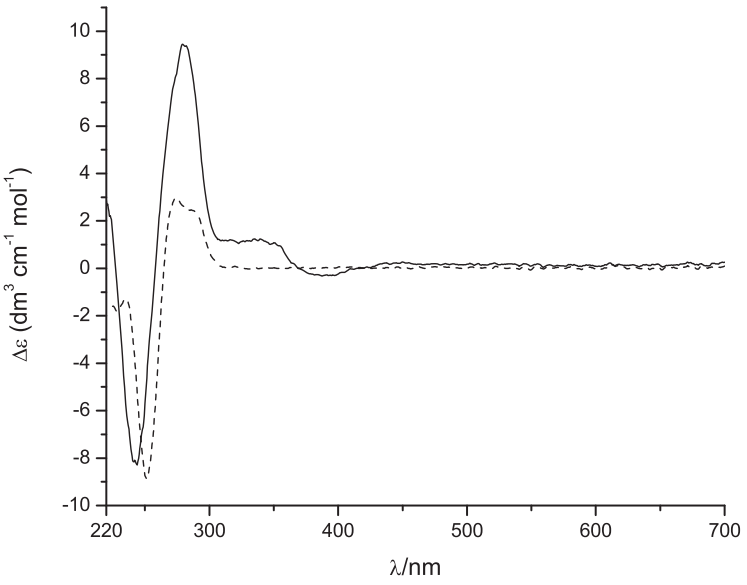

Figure 2.30: Circular dichroism spectra of poly(dGdC) in H_2O, 10 mM HEPES and 10 mM NaCl.

Linear dichroism

Modification of the DNA structure was further studied using flow linear dichroism (LD), where relatively long polymeric DNA (minimum length of ≈ 250 base pairs) is oriented by viscous drag in a couette cell. The extent of orientation can be found as the difference between the absorption of light linearly polarised parallel and perpendicular to a certain orientation, which usually matches with the orientation of the main B-DNA axis (Figure 2.31).[41]

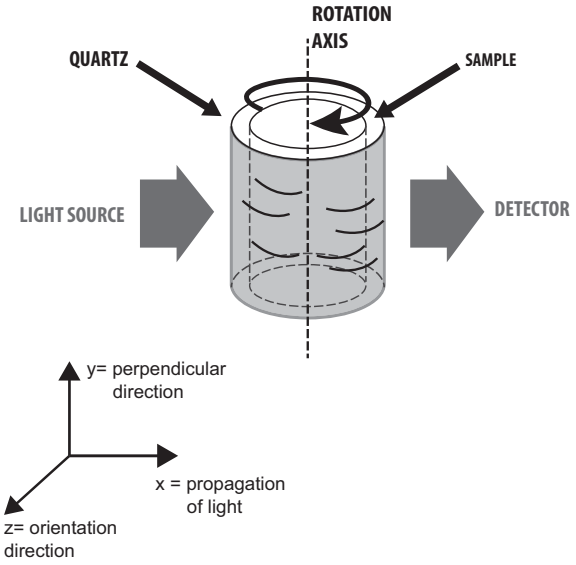

Figure 2.31: Schematic of a Couette flow cell showing flow orientation in a coaxial flow cell with radial incident light.[42]

In the LD spectrum the B-DNA conformation is characterised by a negative band in the region between 220 and 300 nm, which arises from the $\pi \rightarrow \pi^*$ transition of the bases being orthogonal to the main axis of the DNA helix. The magnitude of the LD signal is dependent on the degree to which the DNA is oriented, being reduced by effects such as DNA-bending, and it usually increases when molecules intercalate between the DNA base pairs. This latter effect is better known as stiffening of the DNA double helix.

We employed this technique to monitor the binding of $[EuPt_2]Cl_2$ upon interaction with CT-DNA (Figure 2.32). The LD spectrum of CT-DNA shows an increase in the intensity of the signal at 260 nm upon addition of the complex. This increase is attributed to the stiffening of the DNA double helix structure, as a result of the simultaneous stacking of the two platinum(II) terpyridine units between the DNA bases.

Similarly to the CD experiment, we observed ILD bands at 330 and 350 nm which are the characteristic transitions of the terpyridine moiety, while the broad ILD band observed at 380 nm can be assigned to the MLCT transition. An additional ICD band was observed at 540 nm which is relative to the LLCT band of the complex. All the ILD signals were characterised by a negative sign, which indicates that all the transitions moments are oriented in the plane of the platinum(II) terpyridine unit, that is consistent with the two intercalating units being perpendicular to the DNA axis. Moreover the platinum(II) terpyridine units are stacking between the DNA bases, since no LD signal can be

observed for the $[EuPt_2]Cl_2$ itself.

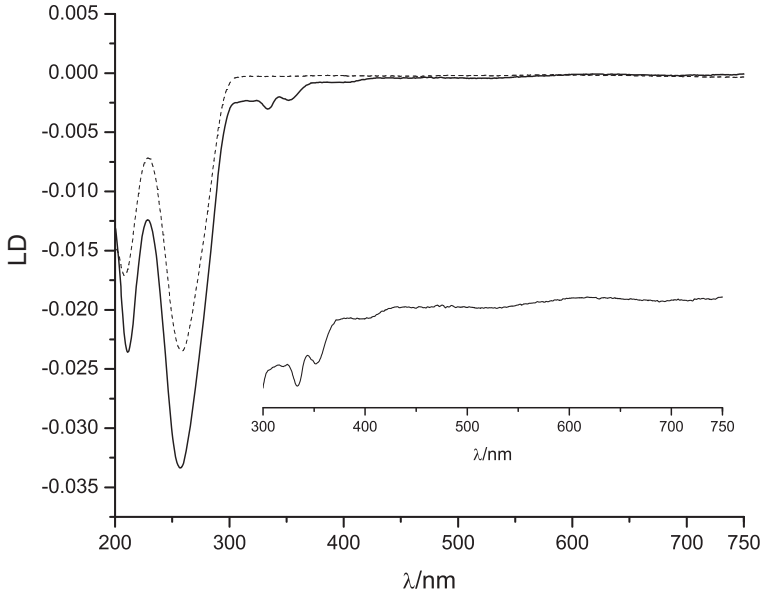

Figure 2.32: Linear dichroism of CT-DNA (dashed line) upon addition of $[EuPt_2]Cl_2$ (solid line) (5:1) in10 mM HEPES and 10 mM NaCl.

Flow linear dichroism was performed on a long chain of polynucleotides as poly(dAdT) with ($\approx$ 700 bases) (Figure 2.33), in order to study the interaction with $[EuPt_2]Cl_2$. Due to the relatively short length of the sequence,[40] the LD resulted in a very weak signal which nevertheless showed the characteristic negative signal of poly(dAdT) at 260 nm. The LD signal became increasingly negative upon addition of further amounts of $[EuPt_2]Cl_2$ which confirms the ability of the complex to intercalate between the base pairs and consequently produce the DNA stiffening as well. However due to the weakness of the signal it was not possible to record the ILD signal which would have been negative since the transitions might be polarised in the plane of the terpyridine.

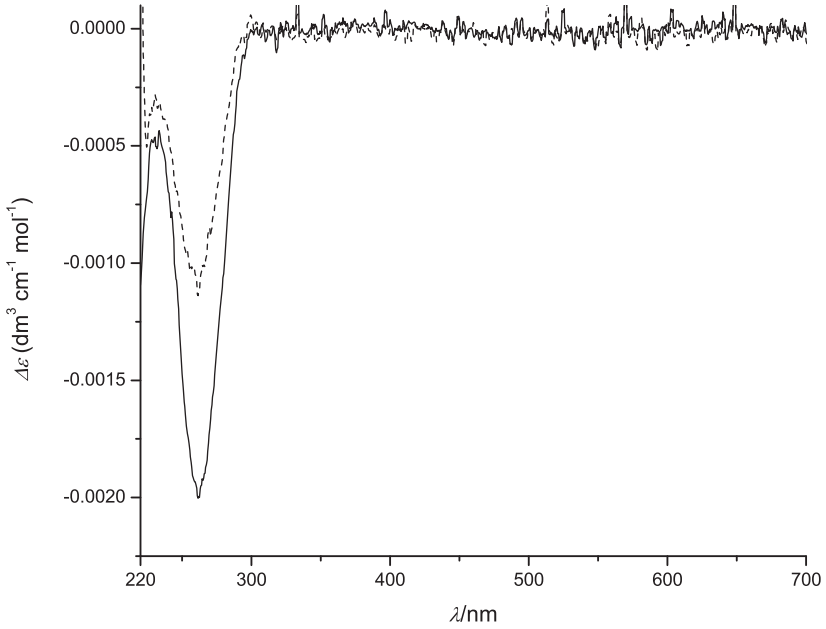

Figure 2.33: Linear dichroism of poly(dAdT) (dashed line) upon addition of $[EuPt_2]Cl_2$ (solid line) (5:1) in10 mM HEPES and 10 mM NaCl.

We attempted to detect the binding of $[EuPt_2]Cl_2$ with poly(dGdC) ($\approx$ 1000 bases) using LD spectroscopy, but we did not observe the expected stiffening effect (Figure 2.34). The region between 300 and 400 nm shows the ILD signal which is again negative and hence consistent with the orientation of the intercalating unit parallel to the plane of the DNA bases.

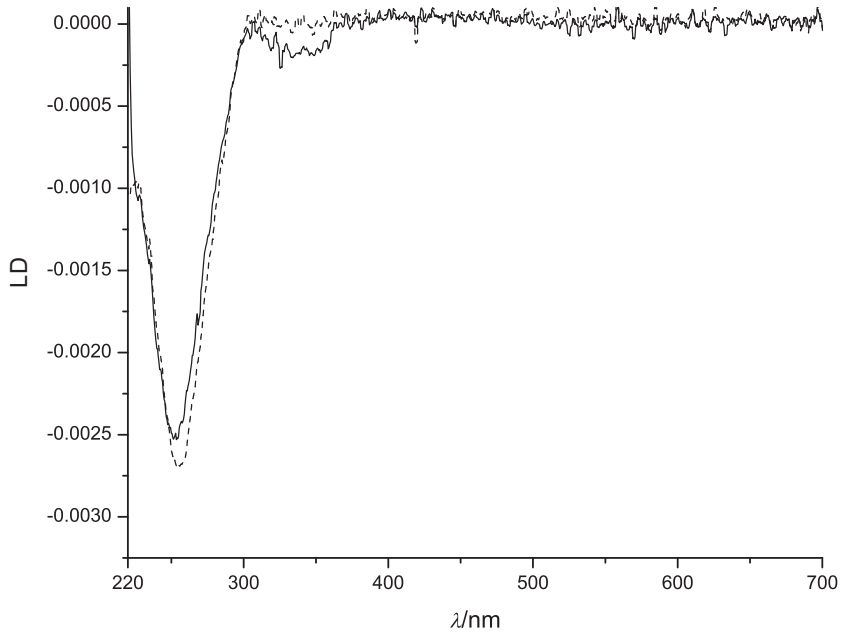

Figure 2.34: Linear dichroism of poly(dGdC) (dashed line) upon addition of $[EuPt_2]Cl_2$ (solid line) (5:1) in10 mM HEPES and 10 mM NaCl.

The comparison of the DNA binding studies performed until here shows that the terpyridine region of the $[EuPt_2]Cl_2$ interacts *via* an intercalative mode. Furthermore, stronger induced CD signals for the terpyridine and the LLCT region of the spectra were observed upon interaction of the $[EuPt_2]Cl$ complex with poly(dAdT), when compared to the interaction with poly(dGdC) under the same experimental conditions.

A similar behaviour was previously observed by Bierbach *et al*. when they reported the platinum(II) bis-acridine complex (Pt-bis(ACRAMTU)) which is also characterised by a 10 Å distance between the intercalating units, with a preferential binding for the AT sequences of DNA.[43] Thus more information on the $[LnPt_2]$ binding preferences might be obtained from binding studies performed on relatively short oligonucleotides.

2.2.4 Binding studies with oligonucleotides

Oligonucleotides of twelve basis (12-mer) and representing one complete turn of the B-DNA, were investigated upon interaction with $[EuPt_2]Cl_2$. oligonucleotides (Table 2.2).

Sequences	Abbreviation
d(5'-CGCG**CGCG**CGCG-3')$_2$	-CGCG-
d(5'-CGCG**CCGG**CGCG-3')$_2$	-CCGG-
d(5'-CGCG**AATT**CGCG-3')$_2$	-AATT-
d(5'-CGCG**ATAT**CGCG-3')$_2$	-ATAT-

Table 2.2: Oligonucleotide sequences employed for the binding studies of $[YPt_2]Cl_2$.

These duplexes were conveniently chosen since they were already fully characterised by X-ray or investigated by NMR and the structure refined by molecular dynamics,[44] and our particular interest was to monitor the binding of $[YPt_2]Cl_2$ upon interaction with -AATT- and -ATAT-.

2.2.4.1 Circular dichroism spectroscopy

The CD spectrum obtained in aqueous buffer solution for the -ATAT- 12-mer oligonucleotide (Figure 2.35), show a negative signal at 250 nm and a positive one at 280 nm, which is indicative of the B-DNA helicity. Upon addition of $[YPt_2]Cl_2$, we observed a decrease of the signal at 250 nm, while the positive band at 280 nm was slightly modified. On the other hand a new signal at 330 nm appears

which is assigned to $\pi \rightarrow \pi^*$ of the platinum(II) terpyridine units. Since $[YPt_2]Cl_2$ is achiral and is not able to absorb the circularly polarised light, the absorption band at 330 nm can only arise from a non degenerate coupling between the electric dipole transition moment of the ligand and those of the DNA bases. Degeneration of the energy level is obtained when platinum(II) terpyridine moieties intercalates between the DNA base pairs.

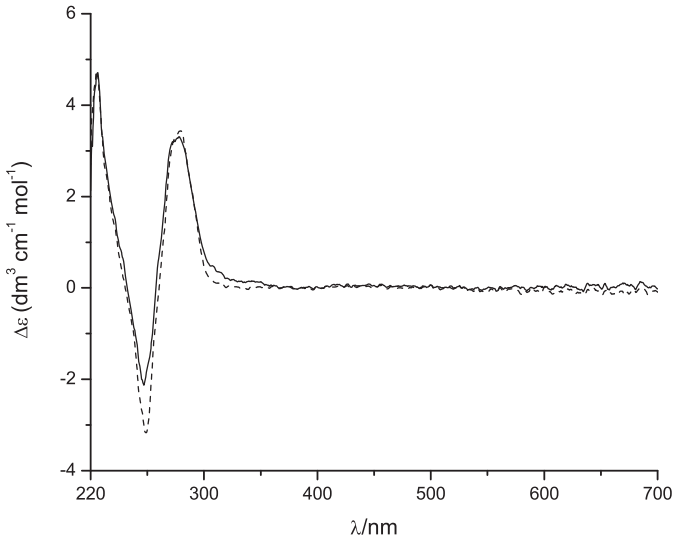

Figure 2.35: Circular Dichroism of d(5'-CGCGATATCGCG-3')$_2$ (dashed line) (10 μM) plus $[YPt_2]Cl_2$ (solid line). Spectra recorded using a ratio oligonucleotide: $[YPt_2]Cl_2$ 2:1 in 10 mM sodium phosphate buffer.

Under the same experimental conditions we recorded the CD spectrum for the -AATT- duplex. The negative and positive signals were observed respectively at 250 and 280 nm, which is consistent for a duplex with a B-DNA helicity. Aliquots additions of $[YPt_2]Cl_2$ to the 12-mer duplex shows a decrease in the intensity of the signals at 250 and 280 nm, while an ICD band is observed at 330 nm and it is assigned to the $\pi \rightarrow \pi^*$ with the transitions moment oriented in the plane of the platinum(II) terpyridine and hence consistent with the $[YPt_2]Cl_2$ intercalated into the 12-mer duplex (Figure 2.36).

In both sequences we observed the negative and positive signals respectively at 250 nm and 280 nm, are reduced in their intensity upon the binding of $[YPt_2]Cl_2$. In the first instance this can appear in contrast with what was observed on CD experiments performed on polynucleotide DNA, which showed an increase in intensity for the same bands. However an explanation can be found in the stiffening effect produced upon the binding of $[YPt_2]Cl_2$ to the 12-mer sequence.

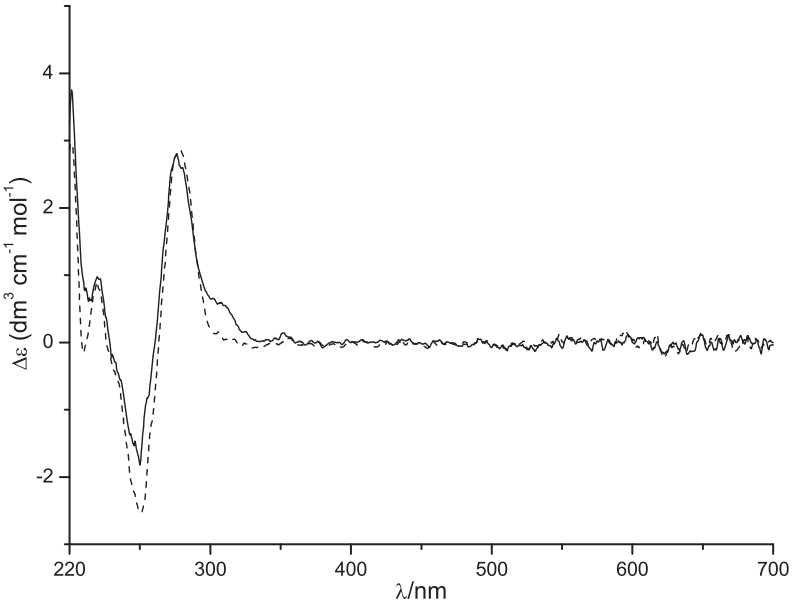

Figure 2.36: Circular Dichroism of d(5'-CGCGAATTCGCG-3')$_2$ (dashed line) (10 μM) plus [YPt$_2$]Cl$_2$ (solid line). Spectra recorded using a ratio oligonucleotide: [YPt$_2$]Cl$_2$ 2:1 in 10 mM sodium phosphate buffer.

Usually the B-DNA helix is characterised by a 10.5 bases per helical turn, however it is also known that intercalators are able to stiffen DNA. When the intercalation stiffens the double helix up to 10.2 bases per helical turn, the CD spectrum will show a decrease in intensity of both negative (λ_{max} = 250 nm) and positive (λ_{max} = 275 nm).[40]

Further circular dichroism spectroscopy studies were performed on the other 12-mer sequences, which contain only cytosine and guanine. Their spectra shows the negative and the positive band being consistent with the B-DNA conformation of the duplexes. The addition of [YPt$_2$]Cl$_2$ to the oligonucleotides does not modify the position or the intensities of the signals, is consistent with the B-DNA helicity left almost unmodified. Furthermore, a very weak ICD signal of the platinum(II) terpyridine unit at 330 nm was observed (Figure 2.37 and 2.38).

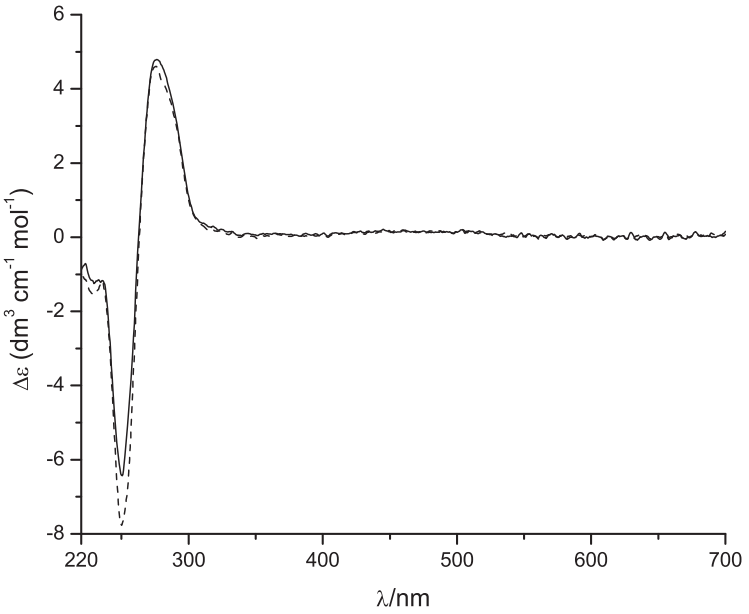

Figure 2.37: Circular Dichroism 10 μM d(5'-CGCGCCGGCGCG-3')$_2$ (dashed line) and d(5'-CGCGCCGGCGCG-3')$_2$ plus [YPt$_2$]Cl$_2$ (solid line) . Spectra recorded using a ratio oligonucleotide: [YPt$_2$]Cl$_2$ 2:1 in 10 mM sodium phosphate buffer.

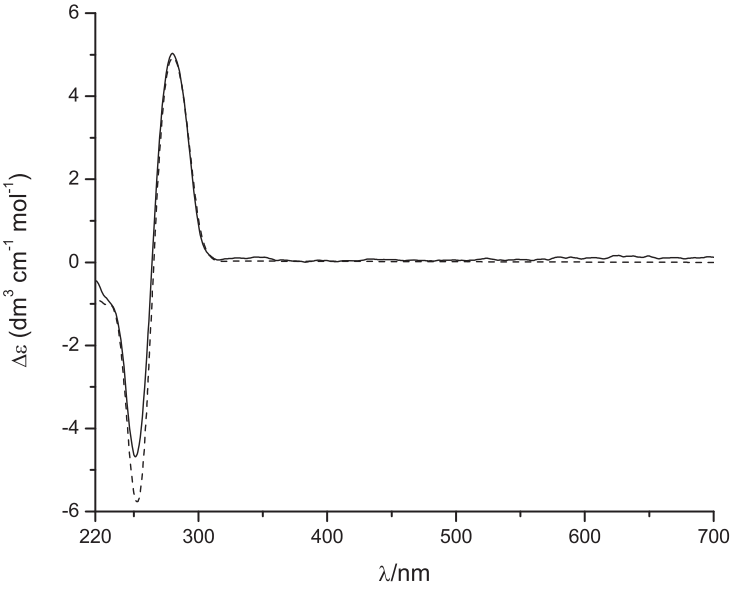

Figure 2.38: Circular Dicroism spectrum 10 μM d(5'-CGCGCGCGCGCG-3')$_2$ (dashed line) and d(5'-CGCGCGCGCGCG-3')$_2$ plus [YPt$_2$]Cl$_2$ (solid line). Spectra recorded using a ratio oligonucleotide: [YPt$_2$]Cl$_2$ 2:1 in 10 mM sodium phosphate buffer.

These results are in agreement with the previously reported experiment on poly(dGdC), which suggests that the binding to the GC alternating oligomer is less favourable, while the binding to adenine and thymine it might be favourite due to the weaker π-π stacking that these bases are able to realise when introduced in a DNA double helix structure.

2.2.4.2 Melting point experiments

At high temperatures double stranded DNA can be denatured to a randomly coiled single stranded DNA by making the hydrogen bonds between the base pairs of the helix less favourable.[45,46] Since DNA bases absorb UV light in the 260 nm region, it is possible to monitor the hyperchromicity effect *via* absorption of the UV light.

Melting point studies were performed with calf thymus DNA and on poly(dAdT) and poly(dGdC) upon their interaction with $[YPt_2]Cl_2$. Figure 2.39 shows the sigmoidal curve obtained by monitoring the UV absorption at 260 nm while the temperature was raised with a rate of 0.5 °C/min for calf thymus DNA.

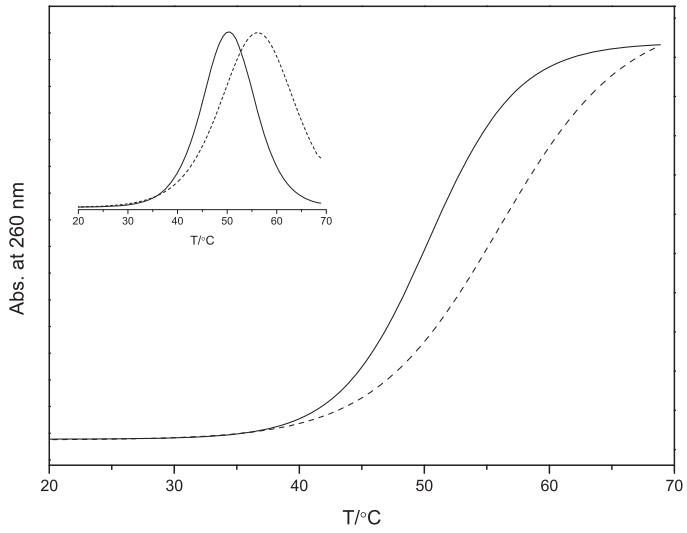

Figure 2.39: Melting point experiment for calf thymus DNA (solid line) (20μM) plus $[YPt_2]Cl_2$ (dashed line) (5:1) in 10 mM HEPES and 10 mM NaCl. Inset plot shows the first order derivate used to determine the T_m.

The experiment was repeated for the poly(dAdT) and the poly(dGdC) under the same conditions as CT-DNA. Since T_m is defined as the mid-point of the curve, at which 50% of the DNA is in duplex form and 50% is in a random coiled single strand form, we could determine this point by using the first order derivative method (Table 2.3).[47]

	°C		
Sequence	T_m	T_m + [YPt_2]	ΔT_m
CT-DNA	49	56	7
poly(dAdT)	58	68	10
poly(dGdC)	40	48	8

Table 2.3: Summary of T_m values for DNA melting experiments (within an error of ± 1°C) with CT-DNA, poly(dAdT) and poly(dGdC) in presence of [$EuPt_2$]Cl_2 (5:1) in 10 mM phosphate aqueous buffer.

These data are in agreement with the model of the intercalation, where the DNA double strand becomes more stabilised upon intercalation of the [$LnPt_2$]Cl_2 complexes due to the π-π stacking between the DNA bases and the platinum(II) terpyridine units, which is responsible for an increase in the melting point temperature. The same stabilising effect was observed upon interaction of the complex with poly (dAdT) and poly (dGdC).

However, the differences in ΔT_m between poly(dAdT) ad poly(dGdC) might be too small to assess a preference for poly(dAdT), but the overall trend appeared to be consistent with the results arising from the LD, CD and emission experiment where the binding to poly(dAdT) seems to be favourite (Table 2.3).

The melting point experiment was repeated with the 12-mer oligonucleotides to assess the intercalative properties of [$LnPt_2$]Cl_2 with oligonucleotides at pH 7.2. The DNA absorption band at 260 nm has been monitored while the temperature was increased at a rate of 0.5 °C/min. The usual sigmoid behaviour was observed for all the 12-mer duplexes with and without the complex (Figure 2.40). In particular, we observed a shift to higher temperatures for duplexes containing adenine and thymine, while only small changes in melting point were recorded for CG alternating oligomer duplexes.[47]

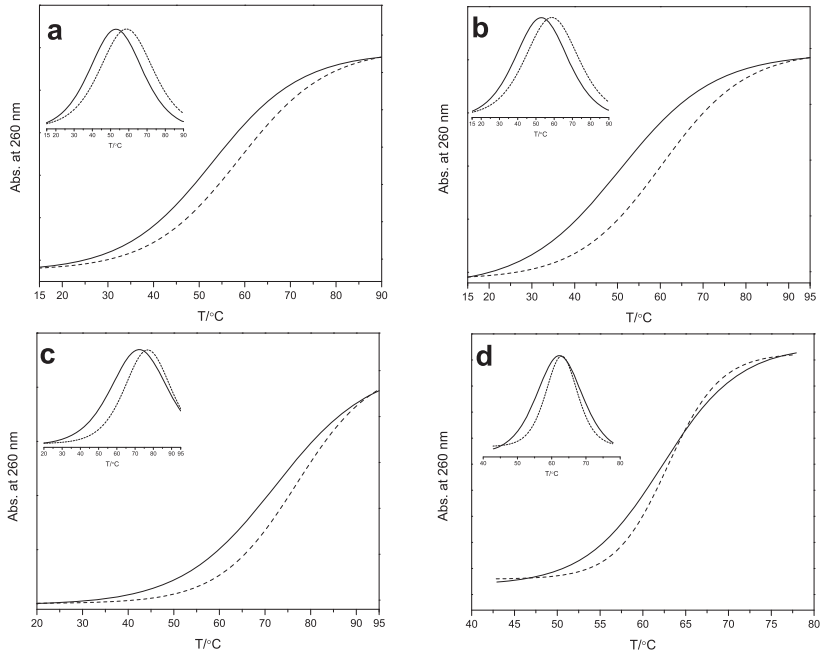

Figure 2.40: Melting point experiment for d(5'-CGCGAATTCGCG-3')$_2$ 20 μM (solid line) (**a**), d(5'-CGCGAATTCGCG-3')$_2$ 20 μM (**b**), d(5'-CGCGCGCGCGCG-3')$_2$ 20 μM (**c**) and d(5'-CGCGCCGGCGCG-3')$_2$ 20 μM (**d**) plus [YPt$_2$] 5 μM (2:1) (dashed line), in 20 mM sodium phosphate buffer.

Using the first order derivative method we could derive the melting point for the four sequences in agreement with the calculated ones (Table 2.4).[48]

These results indicates that the [YPt$_2$]Cl$_2$ is able to better stabilise sequences containing adenine and thymine. Indeed, duplexes with a sequence -AATT- and -ATAT- were stabilised up to 7 °C. On the other hand, only a minor stabilisation is observed for the 12-mer duplexes based on alternating cytosine and guanine.

	°C		
Sequence	T_m	T_m + [YPt$_2$]	ΔT_m
d(5'-CGCGATATCGCG-3')$_2$	50	57	7
d(5'-CGCGAATTCGCG-3')$_2$	51	58	7
d(5'-CGCGCCGGCGCG-3')$_2$	62	64	2
d(5'-CGCGCGCGCGCG-3')$_2$	64	68	4

Table 2.4: Summary of T_m values for DNA melting experiments of oligonucleotides with [YPt$_2$]Cl$_2$ (within an error of $\pm$1°C).

2.2.4.3 UV-Vis absorption

UV-vis absorption spectroscopy was used to determine the binding affinity of $[YPt_2]Cl_2$ toward the 12-mer oligonucleotides. The addition of duplexes to $[YPt_2]Cl_2$ resulted in a considerable hypochromicity effect of the intraligand $\pi \rightarrow \pi^*$ transition band. In particular we observed a hypochromicity of $\sim 25\%$ upon interaction of the complex with 12-mer duplexes having the -AATT- and -ATAT- sequence, while a $\sim 15\%$ hypochromicity effect was observed for the sequences with only alternating cytosine and guanine (Figure 2.41). Furthemore, in all the cases the LLCT band shows a bathochromic shift of ~ 20 nm upon additions of the 12-mer duplexes. This effect is attributed to the change in hydrophobic environment around the molecule upon interaction of the complex with the 12-mers.

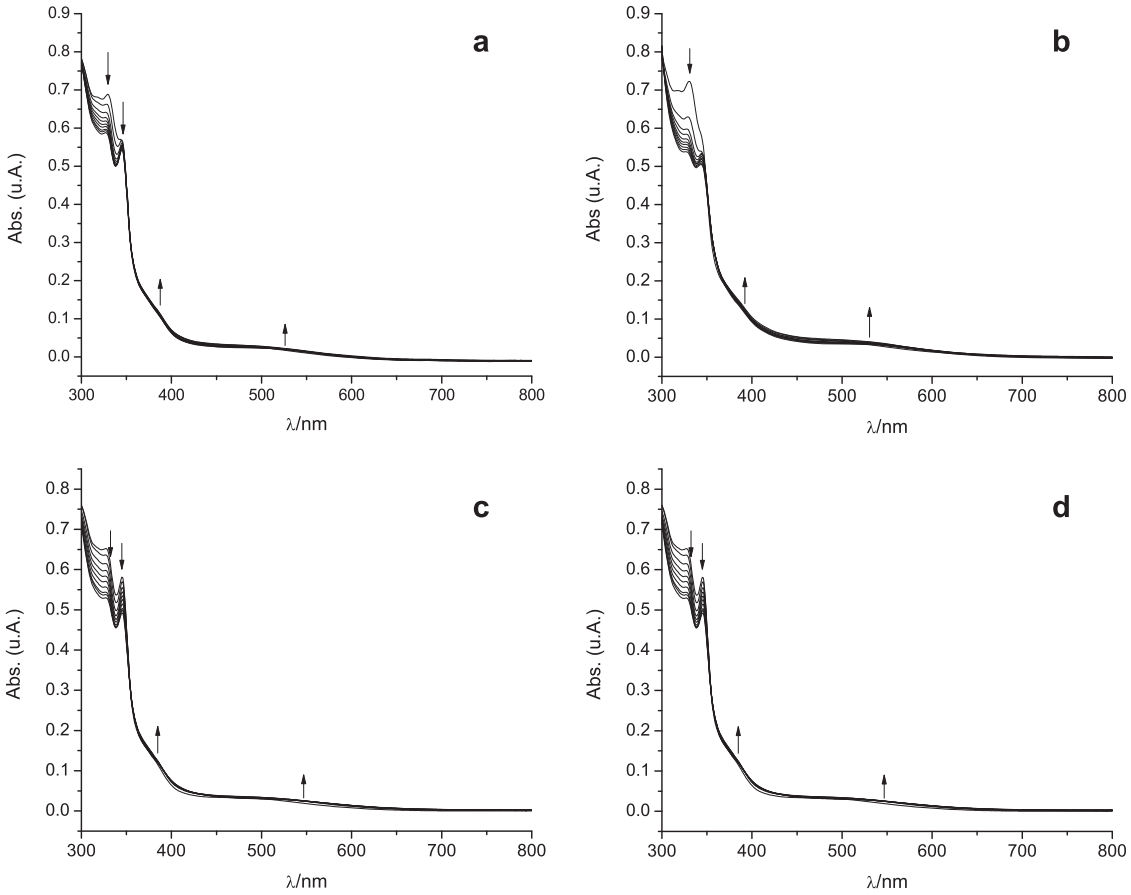

Figure 2.41: UV-vis titration of $[YPt_2]Cl_2$ 30 μM with d(5'-CGCGATATCGCG-3')$_2$ (**a**), d(5'-CGCGAATTCGCG-3')$_2$ (**b**), d(5'-CGCGCCGGCGCG-3')$_2$ (**c**) and d(5'-CGCGCGCGCGCG-3')$_2$ (**d**) in 20 mM sodium phosphate aqueous buffer. The arrows indicate the change upon increasing amount of 12-mer duplexes.

The hypochromism and the bathochromic shifts observed in the UV-vis absorption spectrum, are quite common effects for DNA metallo-intercalators and they have been previously observed for the $[Ru(bpy)_2(pztp)]^{2+}$,[49] $[Ru(bpy)(phi)_2]^{2+}$,[50] and platinum(II) terpyridine derivatives.[51,52,53]

2.2.4.4 Photophysical studies

Photophysical studies were performed on $[NdPt_2]Cl_2$ upon interaction with the 12-mer duplexes, using a deuterated buffer in order to prevent the quenching arising from the O–H bond oscillators. The characteristic emission bands of Nd(III) were observed at 890, 1060 and 1332 nm corresponding to the $^4F_{3/2} \rightarrow {}^4I_J$ (J = 9/2, 11/2, 13/2) transitions, when $[NdPt_2]Cl_2$ was excited at 330 nm. At this excitation wavelength the 12-mers duplexes have a reduced molar coefficient extinction, and it is the mid-point of the terpyridyl absorption bands. Although the photophysical experiments were performed in D_2O the initial luminescence arising from Nd(III) was weak (Figure 2.42).

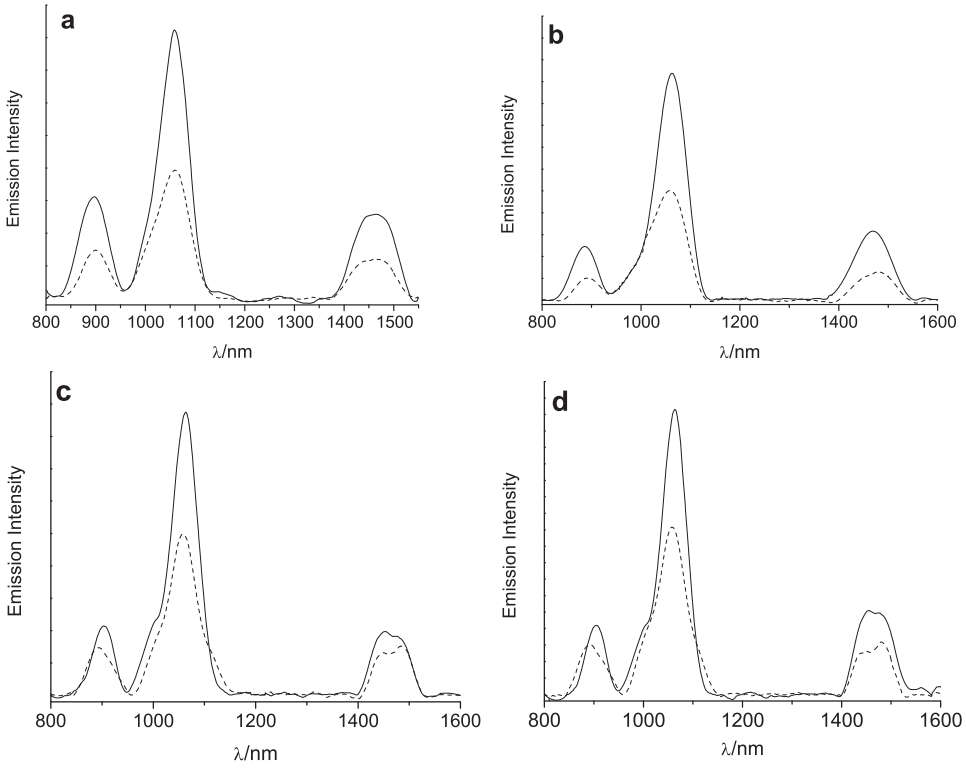

Figure 2.42: Emission experiment for $[NdPt_2]$ (dashed lines) (5 μM) upon addition of d(5'-CGCGAATTCGCG-3')$_2$ (20 μM) (**a**), d(5'-CGCGAATTCGCG-3')$_2$ (20 μM) (**b**), d(5'-CGCGCGCGCGCG-3')$_2$ (20 μM)(**c**) and d(5'-CGCGCCGGCGCG-3')$_2$ (20 μM) (**d**) (solid lines), in 10 mM sodium phosphate buffer D_2O based.

Upon interaction with the 12-mer duplexes, the $[NdPt_2]Cl_2$ showed a luminescent enhancement which was almost two times the original emission if the duplex contained the -ATAT- or the -AATT- fragment. Integration of the spectra area for $[NdPt_2]Cl_2$ emission showed an enhancement of luminescence by 1.5 times when compared to the initial emission of Nd(III).

2.2.5 Synthesis of [4'-acetamidothiophenolPt(tpy)]Cl (AATP)

The AATP complex was isolated following a previously reported procedure, where a methanolic solution of 4'-aminothiophenol was added to a solution of [Pt(tpy)Cl] (CF_3SO_3) in methanol and in the presence of sodium methoxide. A substitution reaction then takes place at the platinum(II) metal centre (Scheme 2.2). The final complex was isolated by a methathesis reaction by addition of ammonium hexafluorophosphate, which led to the desired complex.[26] The final complex showed a spare solubility in water, which was improved by exchange of the PF_6^- ion with Cl^- using the ionic exchange chromatography method. The PF_6^- salt of the complex was preliminarily dissolved in water in the presence of a minimum amount of Dowex beads. The solution was successively eluted through a Dowex column using water as eluent.

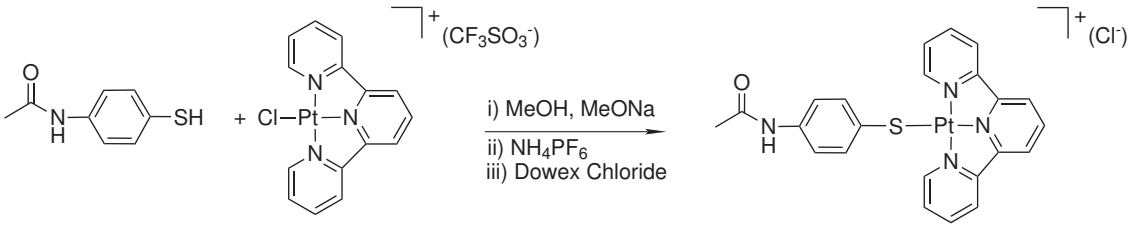

Scheme 2.2: Synthesis of AATP.

The chloride salt of the complex was nicely soluble in water and in methanol, and as a consequence displayed an improvement in spectra quality. The complex was fully characterised and as expected the results were in agreement with previously reported data for the PF_6^- salt of the complex.[26]

The ^1H NMR spectrum shows all the characteristic terpyridine and aryl shifts as expected in its aromatic region (Figure 2.43). The doublet centred at 8.52 ppm can be assigned to **H6**, the proton environment closest to the platinum metal centre. The triplet at 8.43 and at 8.32 ppm is assigned to

H4 and **H4'** respectively. The **H3'** and **H3** is observed as two doublets at 8.22 ppm and 8.18 ppm, while the **H5** signal is observed at 7.61 ppm and confirmed as a doublet of doublets with an integral value of two.

The aryl proton signals are appear as double signals at 7.45 and 7.01 ppm, which are assigned as **Hb** and **Ha**. At 1.93 ppm there is a singlet that can be assigned to the methyl group of acetoamide.

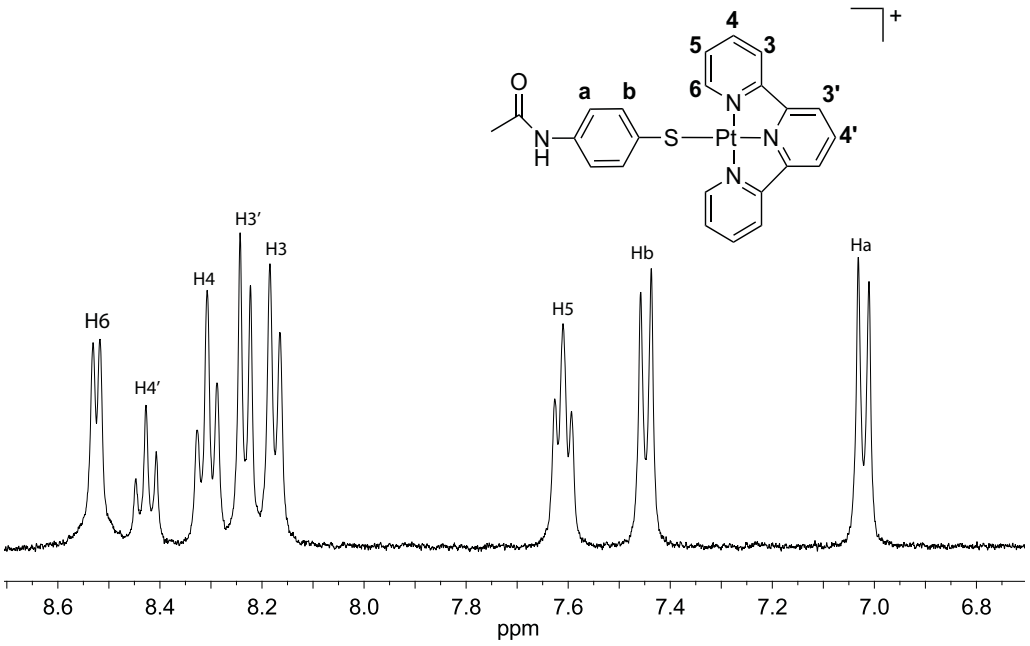

Figure 2.43: ^{1}H-NMR at 400 MHz of [4'-amidothiophenolPt(tpy)]Cl (AATP) in D_2O.

2.2.6 Photophysical studies

The absorption spectrum for AATP in methanol show the lowest band in the region at 250 nm which can be assigned to the $\pi \rightarrow \pi^*$ transitions within the phenyl group, while the bands at 280, 330 and 345 nm are $\pi \rightarrow \pi^*$ transitions within the terpyridine units (Figure 2.44). The shoulder centred at 380 nm arises from a mixed state which arises from the terpyridine $\pi \rightarrow \pi^*$ and MLCT transitions; while the broad lower energy band centred around 540 nm is assigned to the LLCT transition of the $\pi(ArS^-) \rightarrow \pi^*(tpy)$.

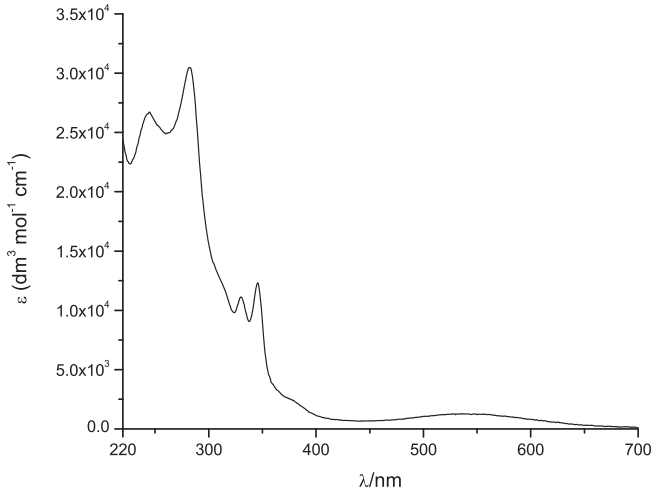

Figure 2.44: Absorption spectrum for AATP in MeOH (15 μM).

Emission studies of AATP at room temperature display an emission signal when the excitation occurs through the terpyridine absorption bands. The emission profile shows two maxima at 340 and 355 nm assigned to unresolved vibrational progression (~ 1300 cm^{-1}) that corresponds to the C=C and C=N stretching modes of the terpyridine (Figure 2.45).[54]

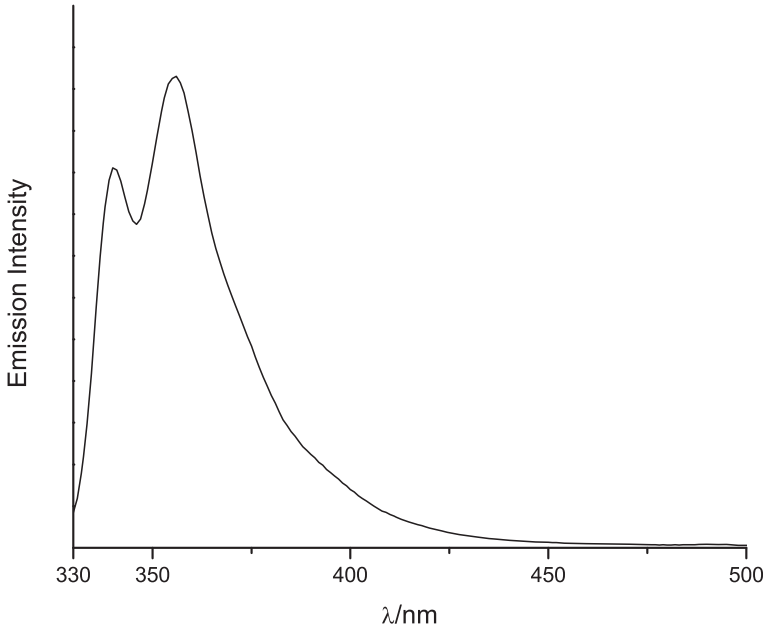

Figure 2.45: Emission spectrum of AATP in MeOH (15 μM). λ_{exc} =280 nm.

Excitation of the LLCT does not result in any platinum based luminescence was observed. This is also consistent with the examples in literature (see also chapter 1), where usually the lack of the platinum(II) based emission is ascribed to a deactivation process which involves the lower lying non-luminescent ^{3}LLCT.[55]

2.2.7 DNA Melting Point experiments

Since the acetamide arm of the molecule resembles the intercalator unit of [$LnPt_2$], we employed the AATP as a model in order to compare the effect upon DNA binding when the fourth ligand on platinum it is not a part of a rigid structure as in [$LnPt_2$].

DNA binding studies of AATP were previously investigated by linear and circular dichroism and melting point experiments, showing the ability of AATP to stack between the DNA base pairs of CT-DNA, poly(dAdT) and poly(dGdC).[26]

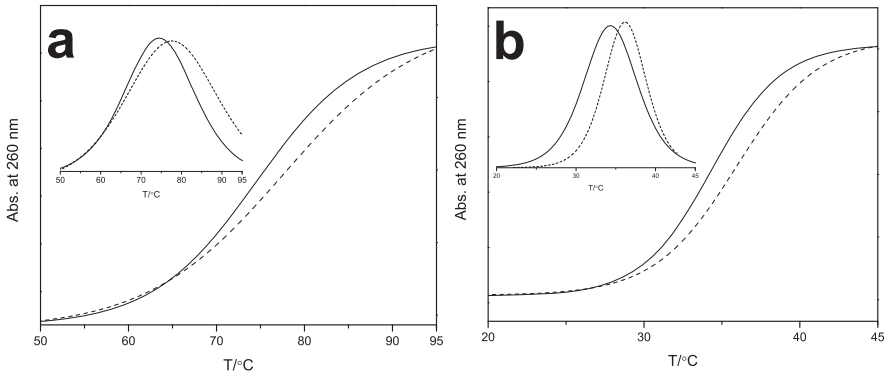

Figure 2.46: Melting point experiments of d(5'-CGCGCGCGCGCG-3')$_2$ (solid line) (10 μM) (**a**) and d(5'-CGCGATATCGCG-3')$_2$ (solid line) (10 μM) (**b**) plus of AATP (dashed line) (5 μM) in 10 mM sodium phosphate buffer. Inset plot shows the first order derivative.

The melting point experiment was performed with the 12-mer duplexes and AATP by monitoring the absorption band at 260 nm, while the temperature was raised by 0.5 °C/min. Figure 2.46 shows the characteristic sigmoidal behaviour, where the melting point values of d(5'-CGCGGCGCGCG-3')$_2$ and d(5'-CGCGATATCGCG-3')$_2$ correspond to the mid-point of the curve, at which point 50% of the DNA is in duplex form while the other 50% is in a random coiled single strand form.

An increase in of the melting point temperature for the 12-mer duplexes was observed upon interaction with AATP. This is consistent with an increased stabilisation of the 12-mer duplexes arising from the π-π stacking between the bases and the platinum(II) terpyridine unit. The largest increase

in T_m of the 12-mer duplex was observed for the -CGCG- upon addition of AATP (6 °C) while a ΔT_m of 2 °C was observed upon interaction of AATP with the -AATT- 12-mer duplex.

Sequence	ΔT_m
d(5'-CGCGATATCGCG-3')$_2$	3
d(5'-CGCGAATTCGCG-3')$_2$	2
d(5'-CGCGCCGGCGCG-3')$_2$	6
d(5'-CGCGCGCGCGCG-3')$_2$	5

Table 2.5: Summary of T_m values for DNA melting experiments of oligonucleotides with [$LnPt_2$].

The data reported in Table 1 is indicative of the ability of AATP to better stabilise the d(5'-CGCGGCGCGCG-3')$_2$ by increasing the melting point by 6 °C, while the melting temperature for d(5'-CGCGATATCGCG-3')$_2$ increased by 3 °C. These results are in agreement with Wang *et al*.[56] and more recently with McMillin *et al*,[57] where a better stabilisation of the DNA duplex arose from the interaction of the platinum terpyridine unit with CpG fragment of DNA, since a stronger π - π interaction can be formed between the terpyridine -CG- rather than between the -AT- bases.

2.2.7.1 UV-Vis absorption

UV-vis absorption spectroscopy was used to determine the binding affinity of AATP toward the 12-mer oligonucleotides. The addition of duplexes to AATP resulted in a considerable hypochromicity effect of the intraligand $\pi \rightarrow \pi^*$ transition band. In particular we observed a hypochromicity of $\sim 30\%$ upon interaction of the complex with 12-mer duplexes having the -AATT- and -ATAT- sequence, and a $\sim 20\%$ hypochromicity effect was observed for the sequences with only alternating cytosine and guanine (Figure 2.47).

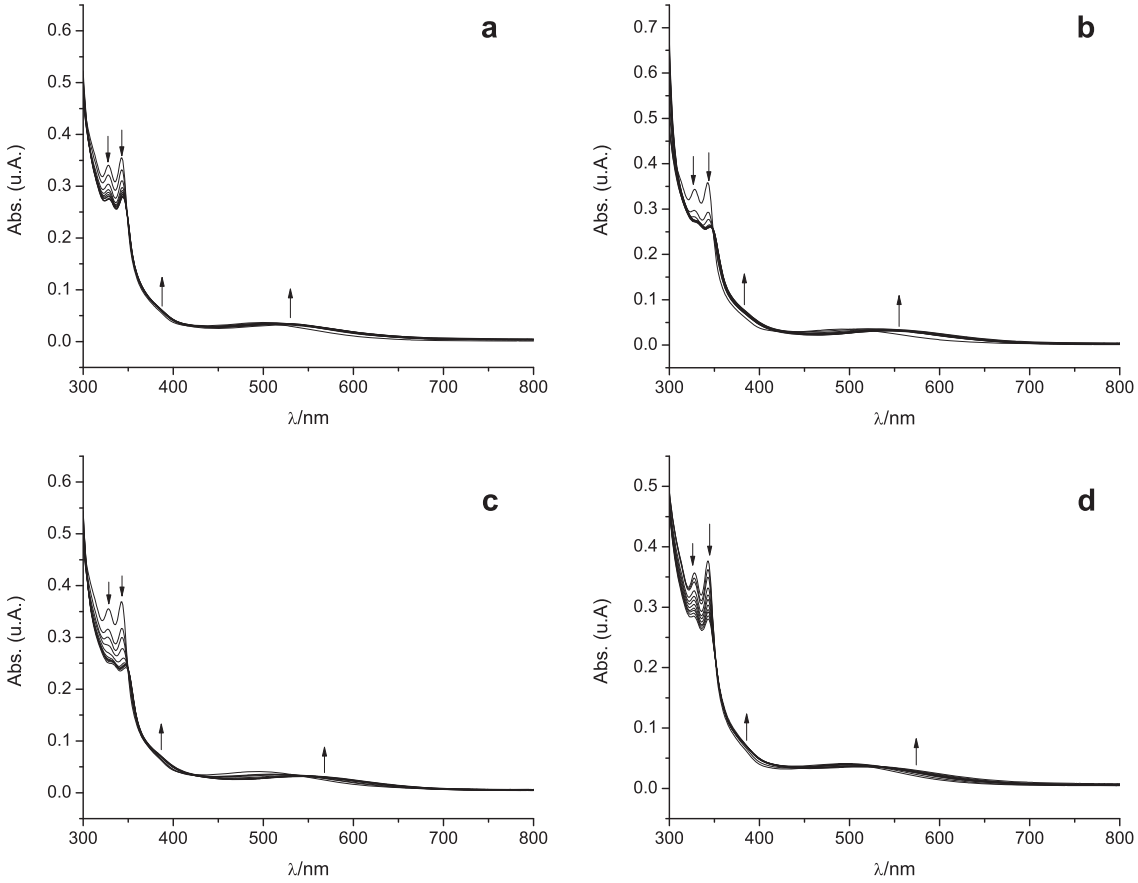

Figure 2.47: UV-vis titration of AATP 30 μM with d(5'-CGCGAATTCGCG-3')$_2$ (**a**), d(5'-CGCGATATCGCG-3')$_2$ (**b**), d(5'-CGCGCCGGCGCG-3')$_2$ (**c**) and d(5'-CGCGCGCGCGCG-3')$_2$ (**d**) in 20 mM sodium phosphate aqueous buffer. The arrows indicate the change upon increasing amount of 12-mer duplexes.

A bathochromic shift (of $\sim$ 5 nm) was also observed upon additions of the 12-mer duplexes to the AATP complex. Both this effect and the hypochromism one are well known in literature and they are characteristic for the intercalation of platinum(II) terpyridine complexes between the DNA base pairs.[51,52,53]

2.2.8 Gel Electrophoresis

Gel electrophoresis is a technique used in chemical biology for the separation of bio-molecules such as DNA, RNA and proteins.[58] The technique is based on the principle that DNA molecules have a specific net charge arising from the phosphate backbone, which can be used to cause their migration along with an appropriate gel matrix under the effect of an electric field applied to the gel.

Because DNA is negatively charged, the electric field drives the molecules toward the positive

electrode with a velocity of the migration (ν) that depends on the strength of the electric field (E) applied, the net charge of the molecule (z) and the frictional coefficient (f):

$$\nu = \frac{E \cdot z}{f}$$

The frictional coefficient f depends on the shape and mass of the migrating molecule and on the viscosity of the medium, which contrasts the mobility of the molecules throughout the matrix pores. Usually, the matrix is a cross linked polymer, that assumes the consistence of a gel, whose composition and porosity is chosen in accordance with the molecule to be analyses. Generally, agarose gels are used for molecules such as plasmid DNA. The scheme in figure 2.48 represents a typical agarose gel used to analyse a big molecule of DNA such as plasmid DNA. This is a type of double stranded circular DNA that occurs naturally in bacteria.

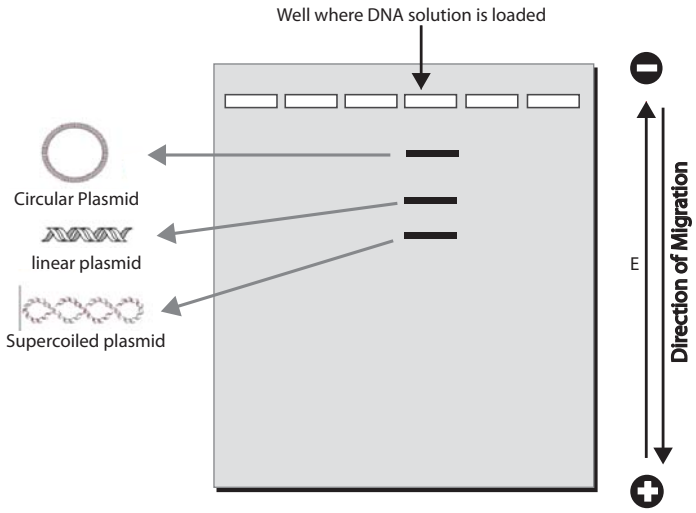

Figure 2.48: Representation of three different conformations of plasmid DNA that migrate with different rates on an agarose gel.

The plasmid DNA can assume a supercoiled conformation, where the DNA is compact with a twist built up or with a circular conformation. This conformation can be obtained upon enzymatic or artificial cut of one of the strands causing the opening to a relaxed circular structure. The linear conformation is obtained by cutting both strands of supercoiled or circular DNA. Solutions containing a mix of the three conformations of plasmid (circular, linear and supercoiled) are loaded in the gel wells and the electric field is applied at both ends of the gel, making DNA migrate to the positive

electrode.

The DNA migration rate in the gel matrix changes according to the DNA conformation. In this case the supercoiled plasmid runs faster than the circular plasmid and the linear conformation has an intermediate rate.

There are different methods to visualise the bands on the gel after the electrophoresis run is complete. If gel agarose is used as support, the gel can be stained by luminescent compounds that interact with the DNA. Typically ethidium bromide is used as a staining agent for its well known DNA intercalator and luminescence properties.

Gel electrophoresis studies performed on plasmid DNA upon addition of $[EuPt_2]Cl_2$ (Figure 2.49) show the ability of the complex to uncoil greatly the DNA, even at low concentrations. At 8:1 DNA/-complex ratio, the band relative to the negatively supercoiled DNA completely disappears. Higher relative quantities of complex produce a band possibly indicating the positively supercoiled plasmid. This is remarkable and might be indicative of a high DNA binding affinity.

At low DNA/complex ratios, a new and unexpected band with reduced migration in comparison to the relaxed conformation of the plasmid starts to form, and is clearly visible at 5:1 and 3:1 ratios. The observed reduced drag rate of the circular DNA is at least surprising and could be caused by the decrease on the neat amount of negative charge due to the high concentration of DNA-bound complex (double positively charged).

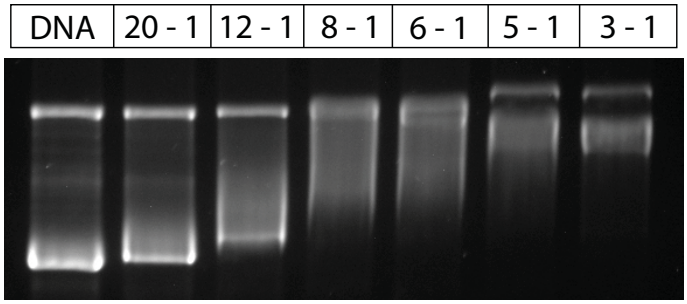

Figure 2.49: Gel image of pBR322 DNA treated with $[EuPt_2]Cl_2$.

A gel electrophoresis experiment for plasmid DNA upon interaction with AATP, was run parallel to the $[EuPt_2]Cl_2$ ones and under the same experimental conditions (Figure 2.50). The gel shows the retained ability of AATP to uncoil the plasmid DNA, but almost double amount of the AATP is required in order to obtain the same uncoiling effect of the $[EuPt_2]Cl_2$.

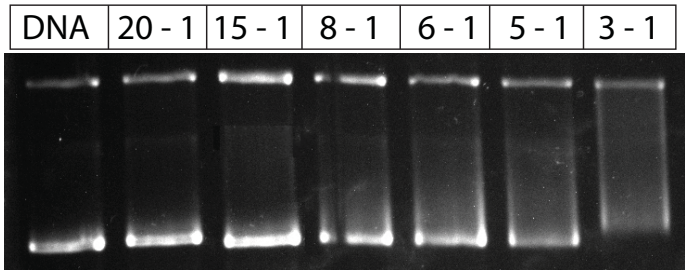

Figure 2.50: Gel image of pBR322 DNA treated with AATP.

Gel electrophoresis of supercoiled and open-circle plasmid DNA can be used to asses the unwinding angle of the DNA helix produced by binding of platinum(II) complexes.[59] [60] Upon binding of the complexes a retardation of the supercoiled band and an acceleration of the open circle band are observed.

Using the appropriate ratio complex : plasmid DNA, the two bands relative to the supercoiled and uncoiled DNA can co-migrate. This particular ratio can be used to assess the unwinding angle by applying the equation 4.1:[61]

$$\phi = -18 \times \frac{\sigma}{r_c} \tag{2.1}$$

where ϕ is the unwinding angle and σ the superhelicity constant, while r_c is the base complex ratio where supercoiled and relaxed DNA co-migrate. The σ used was -0.074 and it was determined from the unwinding angle of the 2-hydroxyethanethiolate derivative of the platinum(II) terpyridine complex (26°).[62] [59] The unwinding angle determined for $[EuPt_2]Cl_2$ was 15.4°, which is about double the value we found for the unwinding angle of AATP (7.5°).

The unwinding angle for $[EuPt_2]Cl_2$ is almost similar to the the cis-platinum one[63] (13°), and this might be due to the rigidity introduced by the DTPA lanthanide complex when it is used as a linking chain of the two platinum(II) terpyridine units.

2.3 Conclusions and future work

The energy level of the triplet state calculated for the $[GdPt_2]Cl_2$ system confirms that the ligand is able to sensitise the Eu(III) emission (17277 cm^{-1}), and that lanthanide emission can be sensitised by excitation through the triplet states of both phenyl and terpyridine ligand.

Photophysical studies with the visible emitter $[EuPt_2]Cl_2$ indicate that there is a luminescent enhancement upon addition of DNA, and it is noticeable that the effect is strongest with poly(dAdT). This was also confirmed by the near-infrared emitter $[NdPt_2]Cl_2$ with photophysical studies performed upon interaction with 12-mer duplexes, which showed that the strongest luminescent enhancement arises from interaction of the complex with d(5'-CGCGAATTCGCG-3')$_2$ and d(5'-CGCG ATATCGCG-3')$_2$.

A possible explanation for this behaviour is that the energy levels of the terpyridine transition are slightly modified upon intercalation between the DNA bases. This is in agreement with the UV-vis absorption spectrum, which shows the energy level of the LLCT band being lowered when the complex intercalates between the DNA bases.

The differences in the luminescent enhancement observed in the photophysical studies could be accounted for by assuming there is a difference in binding strength associated with intercalation between the different base pair combination. In fact, although the differences were relatively small, they were always reproducible by using different spectroscopic techniques, with the strongest induced CD and LD spectra observed for the interaction of the $[EuPt_2]Cl_2$ with poly(dAdT). Using 12-mer duplexes we performed further binding studies in presence of $[YPt_2]Cl_2$, which confirmed that the strongest interaction was achieved with 12-mer duplexes containing alternate sequences of adenine and thymine. The differences observed upon binding of the $[YPt_2]Cl_2$ to the 12 mer duplexes were small, but always reproducible through all the spectroscopic techniques that we used.

The DNA binding experiments performed on 12-mer duplexes upon addition of the AATP complex did not show the same trend as the one described for the $[LnPt_2]Cl_2$ complex. This can suggest that a strong interaction between the $[LnPt_2]Cl_2$ and the binding site can be a consequence of the characteristic structural rigidity of the complex. Thus if we consider that the π-π stacking occurring

between the adenine and thymine is weaker than a π-π interaction between cytosine and guanine,[64] the intercalation of a rigid structure it may be more favourable on the most flexible binding site of the duplex.

It is interesting then to investigate one of the 12-mer duplexes studied here, by using the 2D-NMR techniques. Chapter 3 reports the 2D-NMR experiment, where the interaction between the $[YPt_2]Cl_2$ and the Dickerson-Drew duplex is investigated by 2D-NOE techniques.

Since we isolated the water derivative $[LnPt_2]Cl_2$, it is important in the future to evaluate the binding strength of the metal complex using the Isothermal Titration Calorimetry (ITC). ITC is a quantitative technique that can be used to determine the binding affinity of a small molecule to a large macromolecule; other thermodynamic parameters can also be determined using Gibbs free energy relationships. The experiment monitors the total amount of heat released or absorbed during the interaction of two different species in solution, and hence binding events can be followed quantitatively.[65]

One crucial piece of evidence which remains outstanding is crystal data to further our understanding of the exact binding geometry of the bis-intercalator; thus far attempts to isolate a crystal of $[LnPt_2]$ suitable for X-ray diffraction have been unsuccessful. Furthermore an ideal piece of crystallographic evidence would be to determine a crystal structure of the hairpin complex included with DNA as observed previously with a Pt(tpy) derivative that was found to bind selectively between GC base pairs.[56] Such trials are part of an ongoing collaboration with Prof. Miquel Coll and Dr. Roeland Boer at the Institute for Research in Biomedicine in Barcelona.

2.4 Experimental

2.4.1 Synthesis of 1,11-(bis(4-aminothiophenol)-1,11-dioxo-3,6,9- triaza-3,6,9-triscarboxymethyl) undecane: DTPA-BATP

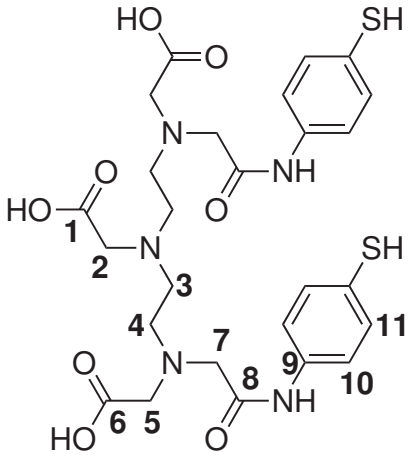

DTPA-BATP

4-Aminothiophenol (2.0 g, 16 mmol) was added to a stirred suspension of diethylenetriaminepenta acetic acid bis(anhydride) DTPA (1.02 g, 2.8 mmol) in pyridine (10 cm^3). The solution was stirred under nitrogen for 24 h at room temperature. A cloudy pale yellow solution was obtained. The solvent was removed under vacuum at 40 °C and a yellow oil was obtained. Water (8 cm^3) was added and a cloudy precipitate was afforded. The crude ligand was then isolated by lowering the pH to 3 via the dropwise addition of concentrated hydrochloric acid and then refrigerated to encourage precipitation. The precipitate was collected and washed with water (2 $\times$ 25 cm^3) and acetonitrile (2 $\times$ 25 cm^3). The resulting off-white suspension was then stirred vigorously in acetonitrile (2 $\times$ 50 cm^3) to afford an off-white powder. The product was then triturated to aid removal from the flask. The powder was collected by filtration and washed with acetonitrile (2 $\times$ 10 cm^3) and ether (2 $\times$ 20 cm^3). The crude product was isolated as an off-white powder.

The crude product was dissolved in pyridine (20 cm^3) and hydrazine monohydrate (3 cm^3) was added to the resulting solution and a clear yellow solution formed. The pyridine was then removed under vacuum at 40 °C to give a yellow oil. The product was then dissolved in water (8 cm^3) and filtered. A yellow/white cloudy solution was formed.

The solution was then acidified to pH 3 (from pH 8) by the dropwise addition of concentrated hydrochloric acid. There was a transition from a sticky off-white solid to a cloudy white suspension, which remained sticky as the precipitation proceeded. The organic layer was then washed with acetonitrile (2×25 cm^3) and then stirred in acetonitrile (2×50 cm^3) until a white powder had formed. The powder was collected by filtration, washed with acetonitrile (2×10 cm^3) and ether (2×20 cm^3) and dried *in vacuo* to afford the desired product (99 mg, 58%).

^{1}H NMR (300 MHz, [D4] MeOH, 24 °C), δ ppm: 7.30 (d, ^3J(H,H) = 8.6 Hz, 4H, H11); 7.05 (d, ^3J(H,H) = 8.6 Hz, 4H, H10); 4.22 (s, 2H, H2); 3.72 (s, 4H, H5); 3.69 (s, 4H, H7); 3.58 (t, ^3J(H,H) = 5.2 Hz, 4H, H4); 3.30 (t, ^3J(H,H) = 5.2 Hz, 4H, H3). ^{13}C-PENDANT $\{1H\}$ NMR (75 MHz, [D4]MeOH, 24 °C), δ ppm: 174.6, 171.5, 169.7 (COOH, C1, C6; CONH, C8); 136.9 (ArCNHCO, C9); 130.8 (ArCH,C10); 127.9 (ArCSH, C12); 122.3 (ArCH, C11); 59.1, 56.3 55.2, 55.0, 51.2 (CH2, C2,3,4,5,7). MS (ES$^+$) = m/z 608 $[M + H]^+$, 630 $[M + Na]^+$

This data agrees with that previously reported.[66]

2.4.2 Synthesis of [Pt(tpy)Cl] (CF_3SO_3)

$AgCF_3SO_3$ (0.054 g, 0.210 mmol) dissolved in dry acetonitrile (5 cm^3) was added to a suspension of $[PtCl_2(PhCN)_2]$ (0.100 g, 0.210 mmol) in dry acetonitrile (10 cm^3). The solution was heated under reflux at 90 °C for 6 h and underwent a colour change from clear yellow to clear and colourless with a white precipitate. The precipitate was removed by filtration and 2,2': 6',2"-terpyridine (tpy) (0.049 g, 0.210 mmol) added. A clear yellow solution resulted and was heated under reflux at 90 °C for 16 h. The volume of the solution was reduced *in vacuo* to afford an orange solid. The product was collected by filtration, washed with acetonitrile (20 cm^3), diethyl ether (2×20 cm^3) and dried under vacuum (70 mg, 80%).

^{1}H NMR (300 MHz, [D3] CD_3CN, 24 °C), δ ppm: 9.10-8.98 (m, 2H, H6); 8.55 (t, ^{3}J(H,H) = 8.1 Hz, 1H, H4); 8.46 (td, ^{3}J(H,H) = 8.1 Hz, ^{4}J(H,H) = 2Hz, 2H, H4'); 8.37-8.33 (m, 4H, H3/H3'); 7.84 (dt, ^{3}J(H,H) = 8.0 Hz, ^{3}J(H,H) = 2Hz, 2H, H5). ^{13}C PENDANT {1H} NMR (100 MHz, D_2O, 24 °C), δ ppm: 127.6, 122.72 (C2, C2'); 149.3 (C6); 141, 140.7 (C4', C4); 127.7 (C5); 126.7, 125.4 (C3, C3'). MS (ES^+) = *m/z* 464 [*M* - (CF_3SO_3)]$^+$. UV-Vis (CH_3OH:H_2O), 4:1): λ_{max} in nm (log ε) 540 (2.2), 380 (3.3), 330 (4.1), 280 (4.4), 253 (4.3)

2.4.3 Synthesis of $[LnPt_2]Cl_2$

A solution of DTPA-BATP (13 mg, 0.0205 mmol) and sodium methoxide (2.5 mg, 0.041 mmol) in methanol (5 cm_3) was added to a solution of [Pt(tpy)Cl] (CF_3SO_3) (25 mg, 0.041 mmol) in hot methanol (15 cm_3). The solution underwent a rapid colour change from clear yellow to deep purple. The solution was heated under reflux at 80 °C for 2 h. The solution was then cooled to room temperature and the volume was reduced to approximately 12 cm^3. Water (10 cm^3) was then added, following addition of a solution of $LnCl_3.6H_2O$ (0.0205 mmol) in methanol (2 cm^3), and the pH of the solution raised from 3 to 5 by the dropwise addition of aqueous sodium hydroxide (0.1 M) to give a clear red solution. The volume of the solvent was reduced to approximately 2 cm^3 and the anion exchanged with a saturated methanolic solution of ammonium hexafluorophosphate. A fine, deep purple precipitate began to form.

The flask was then transferred to the fridge and left overnight. The product was collected by filtration and washed with ethanol (20 cm^3), methanol (20 cm^3) and ether (20 cm^3), then dried under vacuum. A fine powder was obtained.The complexes were purified by size exclusion chromatography (Biobeads SX-3) eluted with DMF. The solvent was completely removed by vacuum and the final deep purple powder $[LnPt_2]$ $(PF_6)_2$ was dissolved in CH_3OH / H_2O (4:1); the anion was exchanged by peforming a column with an anion exchange resin, Dowex 1 X 8 chloride using water as eluent. The solvent was removed by vacuum to give $[LnPt_2]$ (Cl_2), which was dried in vacuo.

[YPt_2]Cl_2 was isolated as a deep purple solid, yield 53%. ^{1}H NMR (300 MHz, [D2] D_2O, 24 °C), δ ppm: 8.3 (br, H6); 8.15 (br, H4',H4); 8.0 (br, H3); 7.9 (br, H3'); 7.5 (br, H5); 7.1 (br, ArHb); 6.9 (br, ArHa); 4.16 (m, CH_2COO), 3.76 (br, CH_2); 3.71 (br, CH_2) . UV-Vis (MeOH): λ_{max} in nm (log ε) 540 (3.4), 379 (3.7), 347 (4.4), 330 (4.4), 281 (4.8), 242 (4.8). MS (MALDI) *m/z* = 1549 [M - 2Cl - H]$^+$; (ES$^+$) = *m/z* 773 [*M* - 2Cl]$^{+2}$. Analysis calc. (%) for $C_{56}H_{50}O_8N_{11}S_2Pt_2Y_1Cl_2 \cdot (H_2O)$: C, 39.6; H, 3.1; N,9.0 Found: C, 39.3; 3.2; N 8.8 UV-Vis (MeOH): λ_{max} in nm (log ε) 540 (3.4), 380 (3.7), 347 (4.4), 330 (4.4), 281 (4.8), 242 (4.8).

[$EuPt_2$]Cl_2 was isolated as a deep purple solid, yield 63%. MS (MALDI) *m/z* = 1610 [*M* - 2Cl - H]$^+$; (ES$^+$) = *m/z* 805 [M - 2Cl]$^{+2}$. Elemental analysis calculated (%) for $C_{56}H_{50}O_8N_{11}S_2Pt_2Eu_1Cl_2 \cdot (H_2O)$: C, 39.6; H, 3.1; N,9.0 Found: C, 39.3; H, 2.9; N, 8.7. UV-Vis (MeOH): λ_{max} in nm (log ε) 540 (3.4), 380 (3.7), 347 (4.4), 330 (4.4), 281 (4.8), 242 (4.8).

[$NdPt_2$]Cl_2 was isolated as a deep purple solid, yield 55%. MS (MALDI) *m/z* = 1602 [*M* - 2Cl - H]$^+$; (ES$^+$) = *m/z* 801.0 [M - 2Cl]$^{+2}$. UV-Vis (MeOH): λ_{max} in nm (log ε) 540 (3.3), 380 (3.7), 346 (4.3), 331 (4.4), 281 (4.7), 246 (4.7).

2.4.4 Synthesis of [LPt_2]Cl_2

To a solution of [Pt(tpy)Cl](CF_3SO_3) (25 mg, 0.042 mmol) in hot methanol (50 cm^3) was added a solution of DTPA-BATP (13 mg, 0.021 mmol) in methanol (5 cm^3) followed by sodium methoxide (2.5 mg, 0.042 mmol) in methanol (5 cm^3). The solution underwent a rapid colour change from yellow to a deep purple. The solution was heated under reflux for 2 hours, and was then allowed to cool to room temperature. The volume of the solvent was reduced to 25 cm^3 and water (25 cm^3) added and then the pH of the solution raised from 3 to 5 by dropwise addition of aqueous sodium hydroxide (0.1 M). The volume of the solvent was reduced to 2 cm^3 and the anion exchanged with a saturated methanolic solution of ammonium hexafluorophosphate giving a fine deep purple precipitate. The product was collected by filtration and washed with ethanol, methanol and ether. Further purification was performed by size exclusion chromatography using Biobeads SX-3 eluted with DMF.

The $[LPt_2]$ $(PF_6)_2$ was dissolved in CH_3OH / H_2O (4:1); the anion was exchanged by performing a column with an anion exchange resin, Dowex 1 X 8 chloride where the pH was raised to 5 by HCl. The solvent wasremoved by vacuum to give $[LPt_2](Cl_2)$.

$[LPt_2]Cl_2$ was isolated as a dark red/purple powder, yield 60%. ^{1}H NMR (300 MHz, [D4] MeOH, 24°C) δ ppm: 8.49 (br, H6); 8.45 - 8.25 (br, H4, H4', H3', H3); 7.48 (d, ^3J(H,H) = 8.3 Hz, ArHb); 7.33 (d, ^3J(H,H) = 8.3 Hz, ArHa); 4.19, (br, CH_2COO^-), 3.69 (br, CH_2), 3.44 (br, CH_2). MS (MALDI) *m/z* 1519 $[M - 2Cl - H]^+$, (ES^+) 773.8 $[M - 2Cl + Na]^{2+}$. UV-Vis (MeOH): λ_{max} in nm (log ε) 540 (3.4), 379 (3.7), 347 (4.4), 330 (4.4), 281 (4.8), 242 (4.8).

2.4.5 Synthesis of [(4-acetamidothiophenolato) platinum (2, 2' : 6', 2''-terpyridine)]Cl (AATP)

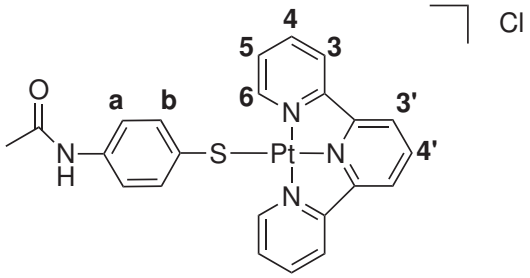

A solution of 4-acetamidothiophenol (6.8 mg, 0.041 mmol) and sodium methoxide (2.5 mg, 0.041 mmol) in methanol (7 cm^3) was added to a solution of [Pt(tpy)Cl] (CF_3SO_3) (25 mg, 0.041 mmol) in methanol (50 cm^3). The solution was then stirred under reflux for 3 h over which time a colour change from pale orange to deep purple was observed. The volume of solvent was then reduced to a minimum and the anion exchanged with a saturated methanolic solution of ammonium hexafluorophosphate. The precipitate was collected by filtration, washed with ethanol (20 cm^3) and methanol (20 cm^3), dried *in vacuo* and isolated as a fine blue/black powder. The [AATP] PF_6 was dissolved in CH_3OH / H_2O (4:1) and the anion was exchanged by performing a column with an anion exchange resin, Dowex 1 X 8 chloride. The solvent was removed by vacuum to give [AATP](Cl) with a yield of 76%

^{1}H-NMR (400 MHz, D_2O, 24°C), δ ppm: 8.52 (d, ^{3}J(H,H) = 5.3 Hz, 2H, H6); 8.43 (t, ^{3}J(H,H) = 7.5 Hz, H4); 8.33 (t, ^{3}J(H,H) = 7.5 Hz, H4'); 8.22 (d, ^{3}J(H,H) = 7.5Hz, 2H, H3'); 8.32 (d, ^{3}J(H,H) = 7.5 Hz, 2H, H3); 7.61 (dd, ^{3}J(H,H) = 7.5 Hz, 2H, H5); 7.45 (d, ^{3}J(H,H) = 8.3 Hz, 2H, Hb-Ar); 7.01 (d, ^{3}J(HH) = 8.3 Hz, 2H, Ha-Ar); 2.00 (s, 3H,CH_3). ^{13}C PENDANT {1H} NMR (100 MHz, D_2O,24°), δ ppm: 172 (CO); 158.2 (C2); 152.8 (C2'); 151.8 (C6); 142.1 (C4); 141.8 (C4'); 136.0 (CS); 134.0 (CNH); 132.5 (CHa); 128.7 (C5); 125.2 (C3); 123.7 (C3'); 120 (CHb); 22.9 (CH3). MS (ES^+) = *m*/*z* 594 [*M* - Cl]$^+$. UV-Vis (MeOH): λ_{max} in nm (log ε): 540 (3.3), 380 (3.5), 345 (4.1), 331 (4.4), 280 (4.5), 253 (4.5). Elemental analysis calculated (%) for $C_{23}H_{19}ClN_4OPtS$: C, 43.9; H, 3.0; Cl, 5.6; N, 8.9. Found: C, 43.7; H, 3.0; N, 8.7.

References

[1] Bunzli, J. C. G. *Chem. Rev.* **2010**, *110*, 2729.

[2] Ju, J. Y.; Ruan, C. C.; Fuller, C. W.; Glazer, A. N.; Mathies, R. A. *Proc. Natl. Acad. Sci. U. S. A.* **1995**, *92*, 4347.

[3] Teo, Y. N.; Wilson, J. N.; Kool, E. T. *J. Am. Chem. Soc.* **2009**, *131*, 3923.

[4] Montgomery, C. P.; Murray, B. S.; New, E. J.; Pal, R.; Parker, D. *Acc. Chem. Res.* **2009**, *42*, 925.

[5] (a) Eriksson, M.; Leijon, M.; Hiort, C.; Norden, B.; Graslund, A. *Biochemistry* **1994**, *33*, 5031; (b) Hudson, B. P.; Dupureur, C. M.; Barton, J. K. *J. Am. Chem. Soc.* **1995**, *117*, 9379; (c) Zeglis, B. M.; Pierre, V. C.; Barton, J. K. *Chem. Commun.* **2007**, 4565.

[6] Bobba, G.; Kean, S. D.; Parker, D.; Beeby, A.; Baker, G. *Perkin Trans. 2* **2001**, 1738.

[7] Bobba, G.; Frias, J. C.; Parker, D. *Chem. Commun.* **2002**, 890.

[8] Pandya, S.; Yu, J.; Parker, D. *Dalton Trans.* **2006**, 2757.

[9] Bobba, G.; Bretonniere, Y.; Frias, J. C.; Parker, D. *Org. Biomol. Chem.* **2003**, *1*, 1870.

[10] Bodi, A.; Borbas, K. E.; Bruce, J. I. *Dalton Trans.* **2007**, 4352.

[11] Law, G. L.; Man, C.; Parker, D.; Walton, J. W. *Chem. Commun.* **2010**, *46*, 2391.

[12] Vazquez, O.; Sanchez, M. I.; Costas, J. M.; Vazquez, M. E.; Mascarenas, J. L. *Org. Lett.* **2010**, *12*, 216.

[13] Vazquez, O.; Sanchez, M. I.; Mascarenas, J. L.; Vazquez, M. E. *Chem. Commun.* **2010**, *46*, 5518.

[14] Fischbach, A.; Perdih, F.; Sirsch, P.; Scherer, W.; Anwander, R. *Organometallics* **2002**, *21*, 4569.

[15] Winpenny, R. E. P. *Chem. Soc. Rev.* **1998**, *27*, 447.

[16] Binnemans, K.; Gorller-Walrand, C. *Chem. Rev.* **2002**, *102*, 2303.

[17] Beeby, A.; Dickins, R. S.; FitzGerald, S.; Govenlock, L. J.; Maupin, C. L.; Parker, D.; Riehl, J. P.; Siligardi, G.; Williams, J. A. G. *Chem. Commun.* **2000**, 1183.

[18] Werts, M. H. V.; Woudenberg, R. H.; Emmerink, P. G.; van Gassel, R.; Hofstraat, J. W.; Verhoeven, J. W. *Angew. Chem., Int. Ed. Engl.* **2000**, *39*, 4542.

[19] Jauregui, M.; Perry, W. S.; Allain, C.; Vidler, L. R.; Willis, M. C.; Kenwright, A. M.; Snaith, J. S.; Stasiuk, G. J.; Lowe, M. P.; Faulkner, S. *Dalton Trans.* **2009**, 6283.

[20] Chen, F. F.; Chen, Z. Q.; Bian, Z. Q.; Huang, C. H. *Coord. Chem. Rev.* **2010**, *254*, 991.

[21] Senechal-David, K.; Pope, S. J. A.; Quinn, S.; Faulkner, S.; Gunnlaugsson, T. *Inorg. Chem.* **2006**, *45*, 10040.

[22] Nonat, A. M.; Harte, A. J.; Senechal-David, K.; Leonard, J. P.; Gunnlaugsson, T. *Dalton Trans.* **2009**, 4703.

[23] dos Santos, C. M. G.; Harte, A. J.; Quinn, S. J.; Gunnlaugsson, T. *Coord. Chem. Rev.* **2008**, *252*, 2512.

[24] Nonat, A. M.; Quinn, S. J.; Gunnlaugsson, T. *Inorg. Chem.* **2009**, *48*, 4646.

[25] Glover, P. B.; Ashton, P. R.; Childs, L. J.; Rodger, A.; Kercher, M.; Williams, R. M.; Cola, L. D.; Pikramenou, Z. *J. Am. Chem. Soc.* **2003**, *125*, 9918.

[26] Solomons, M. Ph.D. thesis, University of Birmingham, Birmingham UK, 2008.

[27] (a) Lammers, H.; Maton, F.; Pubanz, D.; vanLaren, M. W.; vanBekkum, H.; Merbach, A. E.; Muller, R. N.; Peters, J. A. *Inorg. Chem.* **1997**, *36*, 2527; (b) Heineke, D.; Franklin, S. J.; Raymond, K. N. *Inorg. Chem.* **1994**, *33*, 2413; (c) Geraldes, C. F. G. C.; Urbano, A. M.; Hoefnagel, M. A.; Peters, J. A. *Inorg. Chem.* **1993**, *32*, 2426; (d) Rizkalla, E. N.; Choppin, G. R.; Cacheris, W. *Inorg. Chem.* **1993**, *32*, 582.

[28] Yam, V. W. W.; Tang, R. P. L.; Wong, K. M. C.; Ko, C. C.; Cheung, K. K. *Inorg. Chem.* **2001**, *40*, 571.

[29] Arena, G.; Calogero, G.; Campagna, S.; Scolaro, L. M.; Ricevuto, V.; Romeo, R. *Inorg. Chem.* **1998**, *37*, 2763.

[30] Büchner, R.; Cunningham, C. T.; Field, J. S.; Haines, R. J.; McMillin, D. R.; Summerton, G. C. *Dalton Trans.* **1999**, 711.

[31] Bailey, J. A.; Hill, M. G.; Marsh, R. E.; Miskowski, V. M.; Schaefer, W. P.; Gray, H. B. *Inorg. Chem.* **1995**, *34*, 4591.

[32] Arena, G.; Calogero, G.; Campagna, S.; Scolaro, L. M.; Ricevuto, V.; Romeo, R. *Inorg. Chem.* **1998**, *37*, 276.

[33] Hobert, S. E.; Carney, J. T.; Cummings, S. D. *Inorg. Chim. Acta* **2001**, *318*, 89.

[34] Bekiari, V.; Lianos, P. *Langmuir* **2006**, *22*, 8602.

[35] Moussa, J.; Wong, K. M. C.; Chamoreau, L. M.; Amouri, H.; Yam, V. W. W. *Dalton Trans.* **2007**, 3526.

[36] Lewis, D. J. Ph.D. thesis, University of Birmingham, Birmingham, 2006.

[37] Yu, J. A.; Lessard, R. B.; Bowman, L. E.; Nocera, D. G. *Chem. Phys. Lett.* **1991**, *187*, 263.

[38] Beeby, A.; Parker, A. W.; Simpson, M. S. C.; Phillips, D. *J. Photochem. Photobiol. B: Biol.* **1992**, *16*, 73.

[39] Lazarides, T.; Sykes, D.; Faulkner, S.; Barbieri, A.; Ward, M. D. *Chem. Eur. J.* **2008**, *14*, 9389.

[40] Rodger, A.; Norden, B. *Circular and Linear Dichroism*; 1997.

[41] Galindo, M. A.; Olea, D.; Romero, M. A.; Gomez, J.; del Castillo, P.; Hannon, M. J.; Rodger, A.; Zamora, F.; Navarro, J. A. R. *Chem. Eur. J.* **2007**, *13*, 5075.

[42] Hicks, M. R.; Kowalski, J.; Rodger, A. *Chem. Soc. Rev.* **2010**, *39*, 3380.

[43] Choudhury, J. R.; Bierbach, U. *Nucleic Acids Res*. **2005**, *33*, 5622.

[44] (a) ShatzkySchwartz, M.; Arbuckle, N. D.; Eisenstein, M.; Rabinovich, D.; BareketSamish, A.; Haran, T. E.; Luisi, B. F.; Shakked, Z. *J. Mol. Biol*. **1997**, *267*, 595; (b) Coll, M.; Aymami, J.; Vandermarel, G. A.; Vanboom, J. H.; Rich, A.; Wang, A. H. J. *Biochemistry* **1989**, *28*, 210; (c) Vega, M. C.; Saez, I. G.; Aymami, J.; Eritja, R.; Vandermarel, G. A.; Vanboom, J. H.; A. Rich, M. C. *Eur. J. Biochem*. **1994**, *222*, 721; (d) Hare, D. R.; Wemmer, D. E.; Chou, S. H.; Drobny, G.; Reid, B. R. *J. Mol. Biol*. **1983**, *171*, 319; (e) Glaser, S. J.; Remerowski, M. L.; Drobny, G. P. *Biochemistry* **1989**, *28*, 1483.

[45] Wetmur, J. G. *Crit. Rev. Biochem. Mol. Biol*. **1991**, *26*, 227.

[46] Breslauer, K. J.; Frank, R.; Blöcker, H.; Marky, L. A. *Proc. Natl. Acad. Sci. U. S. A*. **1986**, *83*, 3746.

[47] Freifelder, D. *The DNA Molecule: Structure and Properties*; 1978.

[48] Kibbe, W. A. *Nucleic Acids Res*. **2007**, *35*, 43.

[49] Zou, X.-H.; Ye, B.-H.; Li, H.; Liu, J.-G.; Y. Xiong, L.-N. J. *J. Chem.l Soc., Dalton Trans*. **1999**, 1423.

[50] Hiort, C.; Lincoln, P.; Norden, B. *J. Am. Chem. Soc*. **1993**, *115*, 3448.

[51] Arena, G.; Scolaro, L. M.; Pasternack, R. F.; Romeo, R. *Inorg. Chem*. **1995**, *34*, 2994.

[52] Clark, M. L.; Green, R. L.; Johnson, O. E.; Fanwick, P. E.; McMillin, D. R. *Inorg. Chem*. **2008**, *47*, 9410.

[53] Suntharalingam, K.; White, A. J. P.; Vilar, R. *Inorg. Chem*. **2010**, *49*, 8371.

[54] Garino, C.; Gobetto, R.; Nervi, C.; Salassa, L.; Rosenberg, E.; Ross, J. B. A.; Chu, X.; Hardcastle, K. I.; Sabatini, C. *Inorg. Chem*. **2007**, *46*, 8752.

[55] (a) Castellano, F. N.; Pomestchenko, I. E.; Shikhova, E.; Hua, F.; Muro, M. L.; Rajapakse, N. *Coord. Chem. Rev*. **2006**, *250*, 1819; (b) Cummings, S. D. *Coord. Chem. Rev*. **2009**, *253*, 1968.

[56] Wang, A. H. J.; Nathans, J.; Vandermarel, G.; Vanboom, J. H.; Rich, A. *Nature* **1978**, *276*, 471.

[57] Clark, M. L.; Diring, S.; Retailleau, P.; McMillin, D. R.; Ziessel, R. *Chemistry* **2008**, *14*, 7168.

[58] Jin, L. T.; Choi, J. K. *Electrophoresis* **2004**, *25*, 2429.

[59] Jennette, K. W.; Lippard, S. J.; Vassilades, G. A.; Baueri, W. R. *Proc. Nat. Acad. Sci. USA* **1974**, *71*, 3829.

[60] Ramos-Lima, F. J.; Vrana, O.; Quiroga, A. G.; Navarro-Ranninger, C. N.; Halamikova, A.; Rybnickova, H.; L. Hejmalova, V. B. *J. Med. Chem.* **2006**, *49*, 2640.

[61] Bauer, W. R. *Annual Rev. of Biophys. and Bioeng.* **1978**, *7*, 287.

[62] Newman, J. *Biopolymers* **1984**, *23*, 1113.

[63] Bellon, S. F.; Coleman, J. H.; Lippard, S. J. *Biochemistry* **1991**, *30*, 8026.

[64] Neidle, S. *DNA Structure and Recognition*; 1994.

[65] (a) Arya, D. P.; Micovic, L.; Charles, I.; Coffee, R. L.; Willis, B.; Xue, L. *J. Am. Chem. Soc.* **2003**, *125*, 3733; (b) Velazquez-Campoy, A.; Freire, E. *Biophys. Chem.* **2005**, *115*, 115.

[66] Lewis, D. J.; Day, T. M.; MacPherson, J. V.; Pikramenou, Z. *Chem. Commun.* **2006**, 1433.

Chapter 3

Probing the DNA binding site for [$LnPt_2$]metallo-intercalator by ^{1}H-NMR

3.1 Introduction

Over the years since NMR was first applied to solve problems in structural biology, it has undergone dramatic developments in both instrument hardware and methodology. Although potentially NMR gives the most detailed information on the structure of biomolecules in solution, the analysis of NMR spectra has been hampered by the difficulty of obtaining unambiguous resonance assignments. For proteins and oligonucleotides this situation has changed recently as two-dimensional NMR techniques have made it possible to translate the known primary structure of the molecule into resonance assignments via so-called sequential assignment methods.[1]

After the successful employment of NMR spectroscopy for protein structure determination, Feigon *et al*. (1982) were the first to use 2-D NMR in the study of a double-stranded oligonucleotides, observing some interesting intra- and internucleotide Nuclear Overhauser Effects (NOE). Later on Scheek reported a systematic method for the sequential resonance assignments in ^{1}H NMR spectra of oligonucleotides by two-dimensional NMR spectroscopy.[2]

Thus, the NMR and X-ray diffraction offers the opportunity to investigate the binding site of small duplexes with extremely high resolution. However, even if the X-ray diffraction can offers the highest spatial resolution ($\sim$ 3 Å) it is limited to solid state studies, while by NMR it is possible to determine the structure of duplexes simply using an appropriate water buffered solution. Moreover NMR can be used to extract information on the geometry dynamics yielding indispensable physi-

cochemical data.[3] We will focus mainly on the use of the NMR techniques to explore the DNA binding of intercalators, which can be classified into organic intercalators (i.e. anthracyclines, acridines) and metallointercalators like platinum(II) terpyridine complexes. Where possible, views of NMR restrained molecular dynamic refined structures are selected to illustrates the various binding mode.

3.1.1 NMR studies of organic based DNA intercalators.

One of the first applications of NMR to investigate the binding of small molecules to DNA was reported by Jacobsen *et al*. in 1995 using the fluorescent DNA bis-intercalative 1,1'-(4,4,8,8-tetramethyl-4,8-diazaundecamethylene)bis[4-(3-methyl-2,3-dihydrobenzo1,-3-thiazolyl-2-methylidene) quinolinium] tetraiodide alternatively known as TOTO (Figure 3.1).[4]

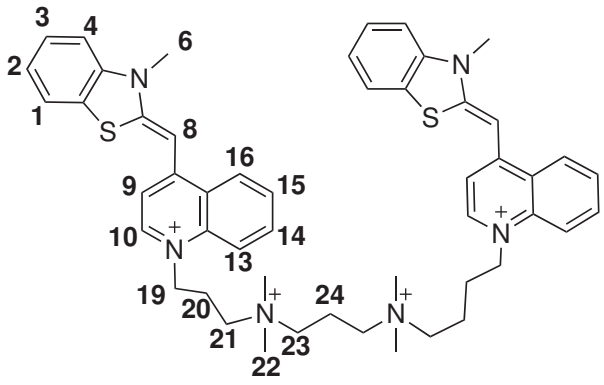

Figure 3.1: Schematic representation of 1,1'-(4,4,8,8-tetramethyl-4,8-diazaundecamethylene) bis[4-(3-methyl-2,3-dihydrobenzo1,-3 -thiazolyl-2-methylidene)quinolinium] tetraiodide (TOTO).

Binding studies performed by NMR spectroscopy of TOTO upon interaction with a series of oligonucleotides showed a preferential binding for -CTAG- sites. Indeed, NOESY spectrum recorded in D_2O and water, allows to follow NOE connectivity occurring between the H6/H8 of the aromatic bases and the H1', H2' and H2" of the deoxyribose. Disruption of the NOE pathway can be observed between C-T and A-G of the -CTAG- site, which is consistent with a bis-intercalation of the two thiazole orange units. The intercalation sites were conclusively defined when NOE interaction between the protons on the oligonucleotide and thiozole orange was found. Even if not all the 4 base pair (bp) possibilities have been investigated, the authors argue that the TOTO binds selectively to the -CTAG- and estimates a 100-fold preference for binding a sequence containing -CTAG- than any

other site present on that oligonucleotide. The binding preference is attributed to the thiozole orange, since the charged alkyl-amino linker is non-sequence selective.[5] [6]

Full characterization of the interaction was achieved when the NOE data connectivity was employed in restrained molecular dynamics (Figure 3.2)

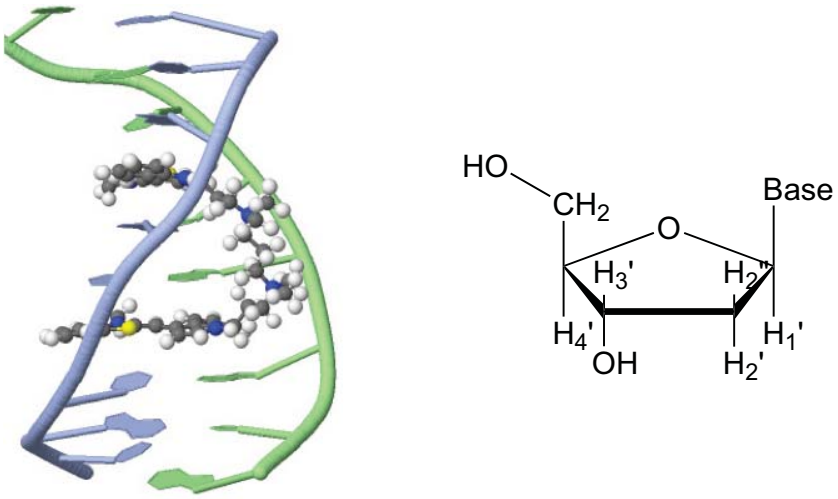

Figure 3.2: The refined structure of TOTO-d(5'-CCGACTGATGC-3')$_2$. Image from the RCSB PDB.[7] (www.pdb.org) of PDB ID 108D.

The restrained molecular dynamics calculations indicate the poly(propylenamine) linker chain located in the minor groove of dsDNA while the benzothiazole ring system is twisted relative to the quinoline. The site selectivity of TOTO for the CTAG-CTAG site is explained by its ability to adapt to the base pair propeller twist of dsDNA in order to optimize stacking and the hydrophobic interaction between the thymidine methyl group and the benzothiazole ring.

Using a derivative of acridine, an established DNA intercalator,[8] Garcia *et al.* in 1997 has demonstrated the ability of DTAc and ATAc (Figure 3.3) to selectively intercalate between the DNA base pairs. They proposed the basic scheme for creating these tailor-made molecules, which contain several units designed for specific functions.

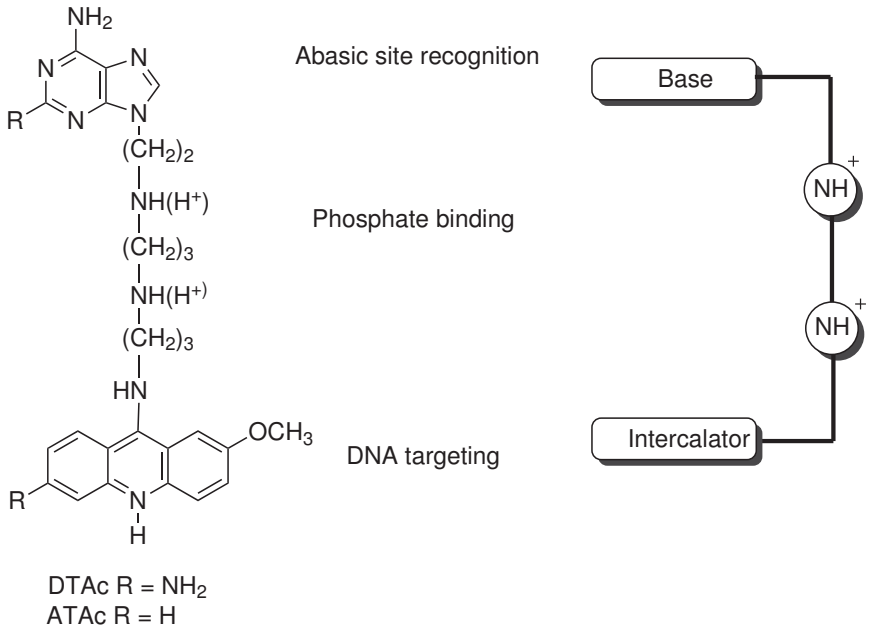

Figure 3.3: Schematic representation of DTAc and ATAc units.

A number of molecules of this type have been prepared but only DTAc and ATAc showed a DNA binding constant of $K_{aff} = 10^4\ M^{-1}$ upon interaction with calf thymus of DNA, which makes them suitable for NMR investigation. The difference between DTAc and ATAc was an amino group introduced onto the adenine unit of DTAc (Figure 3.3). Due to hydrogen bonding DTAc results in stronger binding to the oligonucleotide and sharper peaks on the ^{1}H-NMR are observed.[9]

A synthetic DNA fragment d(5'-CGACXCACGC-3')·d(5'-GCGTGTGCG-3') and high field ^{1}H-NMR spectroscopy were employed in order to investigate the nature and the geometry of the adduct formed between DTAc and ATAc and a mismatched DNA. A change of nearly 0.3 ppm in chemical shifts and the absence of NOE couplings from H6/H8 aromatic protons to H1', H2' and H2" of the sugar, suggested the C3·dG20 and A4·dT19 as the preferred intercalation site for DTAc and ATAc.

The binding site for the acridine unit was confirmed by a presence of intermolecular NOE couplings between the aromatic protons of the acridine and the aromatic protons of the DNA bases. However due to severe overlap on the NOESY spectrum, it was only possible to assign the adenine base interacting in the abasic site of the sequence. Further information about the orientation of the linked base inside the abasic site was obtained by restrained molecular dynamics, which shows a preferred Hoogsteen orientation rather than Watson-Crick conformation.[10]

Dauno- and doxorubicin are also popular organic anticancer drugs, having anthracycline as the intercalating unit (Figure 3.4). However they are characterised by a lack of activity against resistant cancer cells, which seems to be associated with the interaction between the drugs and the transport protein. Thus, in 1997 Wang *et al.* proposed to link together the antracycline units of a daunorubicins derivative using a sugar moiety, which increases the binding affinity with the transport proteins (Figure 3.4).

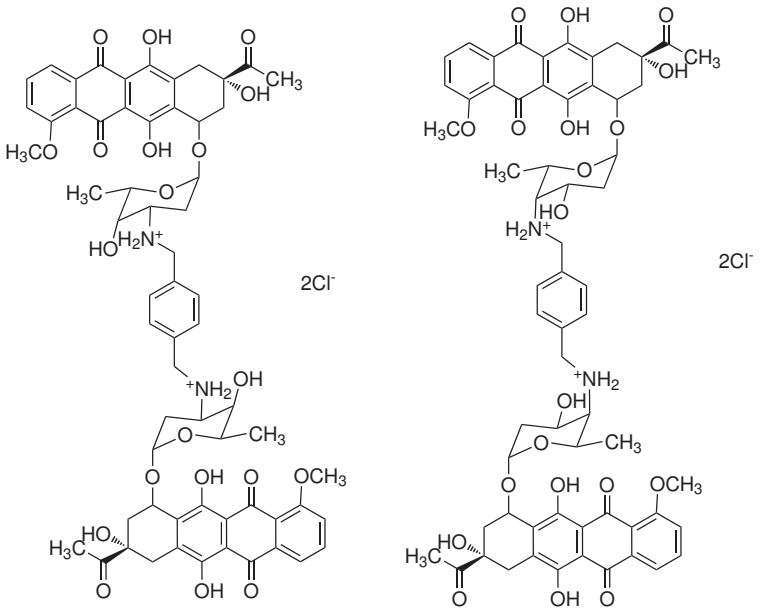

Figure 3.4: Molecular structure of WP631 at left and WP652 at right.

A particularly high binding constant of 10^{11} M^{-1} was recorded for WP631 upon interaction with calf thymus DNA.[11] The binding site and sequence preferences of WP631 and WP652, were investigated by ^{1}H-NMR upon interaction with a set of oligonucleotides, where a preference for the -CGTACG- and -TGTACA- respectively was observed. The changes in chemical shifts and the dis-

ruption in the NOE connectivity are evidence for intercalation of WP631 between the symmetric CG units; while the WP652 prefers the intercalation between TG and TA (Figure 3.5).[11]

As a consequence of the bis-intercalation, the oligonucleotide assumes a distorted B-DNA structure where one of the aglycon rings is protruding into the major groove and the two daunosamines plus the p-xylenyl group tether occupying the entire minor groove.

In this case the NMR experiment yielded detailed informations about the binding sites for WP631 and WP652, and allowed to conclude that from the changes on how linked are the antracycline moieties (C4' or C3') will affect the final geometry of the molecule, and hence a different binding selectivity can be observed upon interaction with oligonucleotide.

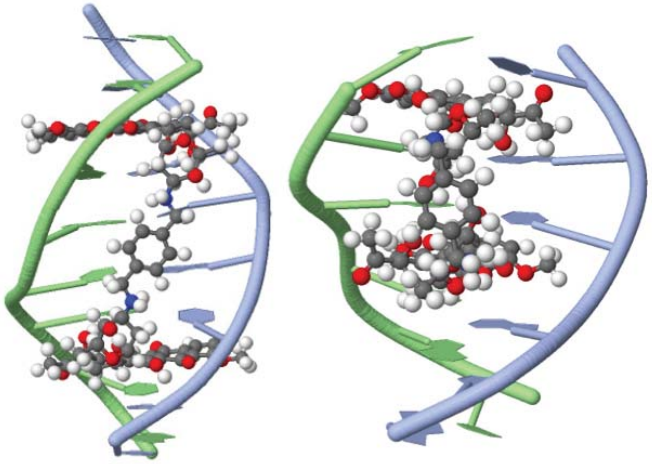

Figure 3.5: The refined structure of WP631-d(ACGTACGT)$_2$ and WP652-d(TGTACA)$_2$. Images from the RCSB PDB[7] (www.pdb.org) of PDB ID 1AL9 and 1AMD.

3.1.2 NMR studies of DNA metallointercalators.

Over the past twenty five years, increasing interest has focused on a new class of non-covalent DNA-binding agents: metallointercalators. In these molecules, the metal centre acts in essence as an anchor, holding in place a rigid, three-dimensional scaffold of a ligand that potentially can bear recognition elements, which in case of the metallo-intercalators are mainly extended flat aromatic molecules. The employment of transition metals in DNA recognition can introduce several benefits such as rich photophysical and electrochemical properties and this extends their utility far beyond that of the passive molecular recognition agents. Moreover the metallo-intercalators are structurally rigid molecules with well-defined symmetry that make them suited for the recognition of certain DNA sequences.

Ruthenium and rhodium have been the most investigated metal complexes by NMR upon interaction with DNA due to their octahedral geometry, which make them suitable for DNA intercalation via the major groove.

Platinum metal centre have also been investigated as it guarantees a square planar geometry of the complex.

Research group such as Barton and co-workers or Nordén and co-coworkers, have been focusing their attention on rhodium and ruthenium complexes. In particular they were interested in studying how to control the binding selectivity for the minor or the major groove of DNA. In 1994 Barton published DNA binding studies of Δ-[Rh(NH_3)$_4$phi]$^{3+}$ and successively (1995) of its analogues Δ-α-[Rh[(R,R)-Me_2-trien]phi]$^{3+}$ (Figure 3.6), upon interaction with small oligonucleotides.[12]

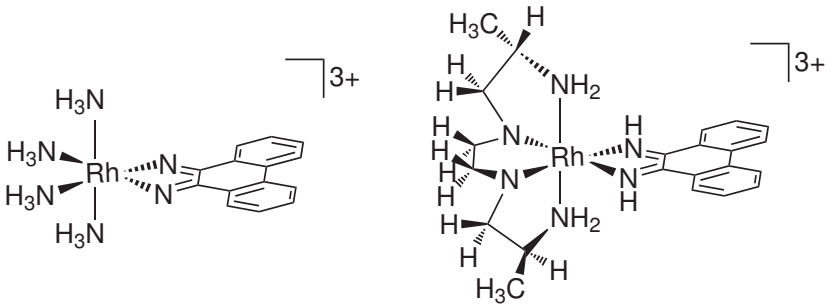

Figure 3.6: Structure of Δ-[Rh(NH_3)$_4$phi]$^{3+}$ and its analogues Δ-α[Rh[(R,R)-Me_2-trien]phi]$^{3+}$ on the right.

^{1}H-NMR studies show the protons from the ancillary ligands having NOE coupling with the protons on the major groove. Furthermore, on the NOESY spectrum there was an absence of NOE resonances from the H6-H8 aromatic protons to the sugar protons of the binding site. These results led them to conclude that the ancillary ligand was playing an important role on the groove selection, while the aromatic phi ligand was stacking between the base pairs. In the mean time but working independently, Nordén studied two other systems based on ruthenium octahedral metal complexes (Figure 3.7).[13,14]

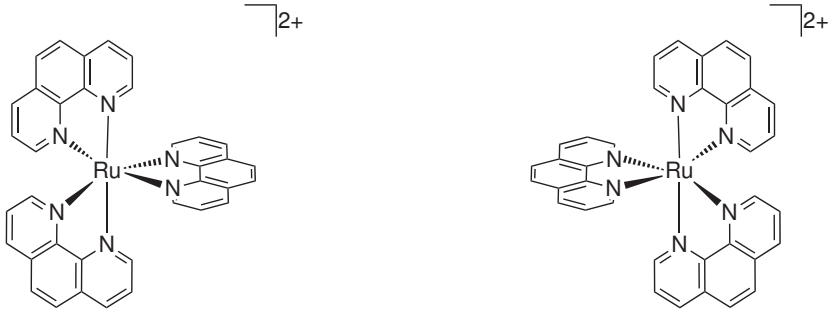

Λ-[Ru(phen)$_3$]$^{2+}$ Δ-[Ru(phen)$_3$]$^{2+}$

Figure 3.7: Structure of Δ and Λ [Ru(phen)$_3$]$^{2+}$.

The Δ and Λ-[Ru(phen)$_3$]$^{2+}$ were also investigated by ^{1}H-NMR while interacting with the decamer oligonucletide d(5'-CGCGATCGCG-3')$_2$. The one dimesional ^{1}H-NMR spectrum recorded upon addition of the complex to DNA, shows clearly the metal complex in rapid exchange compared to the NMR timescale, leading to an NMR spectrum with sharp peaks.

More detailed information was obtained from the NOESY spectrum, where it was found that there was a lack of NOE couplings between the ancillary ligand of [Ru(phen)$_3$]$^{2+}$ and the protons of the major groove, while both of Δ - and Λ-[Ru(phen)$_3$]$^{2+}$ bind to the minor groove of the 10-mer as evidenced by the intermolecular NOE interaction. Barton and collaborators demonstrated enantioselectivity associated to the Δ complexes, upon binding the B-DNA structure. However the same enantioselectivity was not shown for Λ complexes upon interaction with Z-DNA.

Using the NMR it was possible to understand that the dimension, the geometry and the functionality of the ancillary ligands plays an important role towards the selectivity of octahedral complexes in binding the major or the minor groove of different DNA geometries.[15]

This led Barton and co-workers to design several octahedral complexes based on rhodium, and investigate their DNA interaction by ^{1}H-NMR (Figure 3.8).[16]

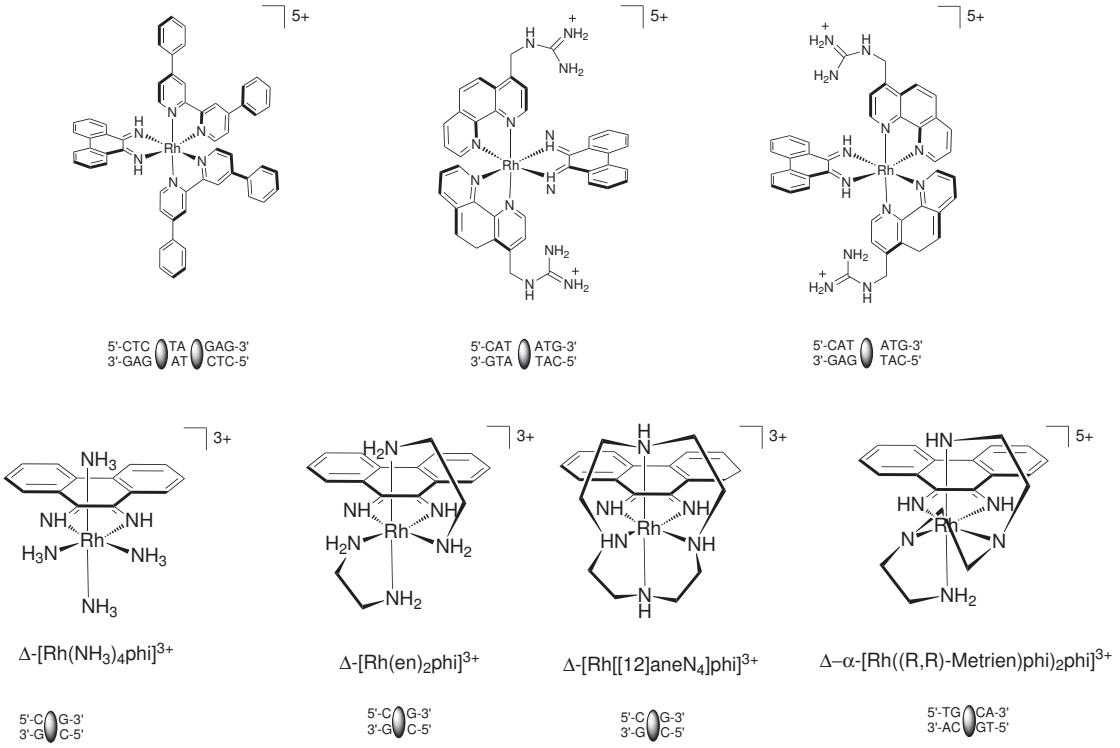

Figure 3.8: Chemical structure of rhodium-phenanthrenequinone studied by Barton.[15]

Complexes containing a bulky ancillary ligand showed a preference for major groove binding. The high selectivity and binding constant could be ascribed to the ability of the ancillary ligand to form hydrogen bonding with phosphate groups arising from the major groove of the duplex (i.e. Δ-α[Rh(R,R)-Me$_2$trien(phi)]$^{3+}$). However this approach can be very demanding and not always leads to the expected results.[15]

The designed complexes able to recognise selectively major versus minor groove of DNA by intercalation is still a growing field, and the ^{1}H-NMR investigation plays an important role for elucidation of the interaction between these complexes and the binding site. Collins *et al*. demonstrated by ^{1}H-NMR and NOE experiments that both Δ and Λ-[Ru(dmphen)$_2$dppz]$^{2+}$ (Figure 3.9) bind the hexanucleotide d(GTCGAC)$_2$ in the minor groove. This binding mode was strongly suggested from the intermolecular NOE cross-peaks between the dmphen and the d(GTCGAC)$_2$ protons, which were only observed between the minor groove basis G4A5.[17]

A key role is played not only by the ancillary ligand but the extension of the aromatic intercalating unit is an important parameter. ^{1}H-NMR studies previously reported by Norden showed an increased

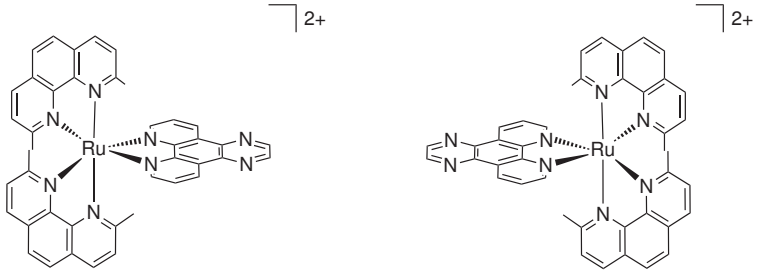

Λ-[Ru(dmphen)$_2$dpq]$^{2+}$ Δ-[Ru(dmphen)2dpq]$^{2+}$

Figure 3.9: Structure of Δ and Λ-[Ru(dmphen)$_2$dppq]$^{2+}$ complexes.

selectivity versus the duplex minor groove when one of the phenantroline ligand in [Ru(phen)$_3$]$^{2+}$ was substituted with the dipyrido[3,2-a:2',3'-c]phenazine (ddpz) to obtain the [Ru(phen)$_2$ddpz]$^{2+}$.[13]

Recently Thomas *et al*. reported the NMR investigations on the DNA binding mode of the octahedral complexes using achiral ruthenium complex as [Ru(tpm)(dppz)py]$^{3+}$, which is based on dppz ligand. ^{1}H-NMR spectroscopy based on NOE experiments are strongly consistent with the intercalation into G2-A3 from the minor groove side of the two chosen octamer d(AGAGCTCT)$_2$ and d(CGAGCTCG)$_2$.[18]

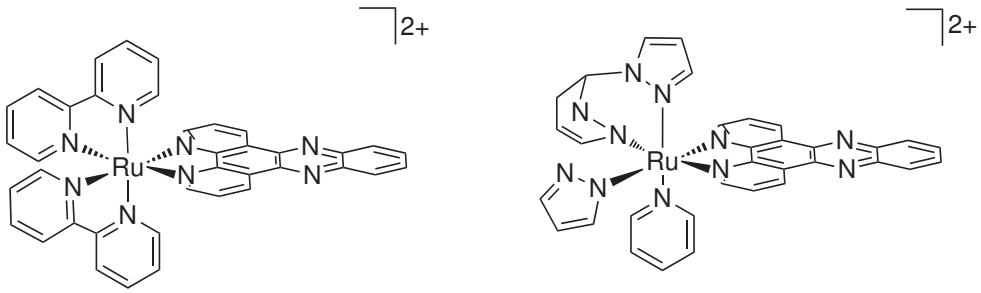

[Ru(bpy)$_2$(dppz)]$^{2+}$ [Ru(tpm)(dppz)py]$^{2+}$

Figure 3.10: The structure of [Ru(bpy)$_2$(dppz)]$^{2+}$ and [Ru(tpm)(dppz)py]$^{3+}$.

A lot of investigations has been done in structural biology and most of this involved NMR as technique, but still not clear how to control the intercalation and how to control the selective binding on the major groove, with the scientific community still debating the DNA groove selection rules. However at this stage the contribution of NMR led to an understanding that the ancillary ligands and the final isomer configuration of the complex play a key role upon the interaction with DNA.

Bierbach *et al*. used the NMR spectrscopy to investigate the d^8 metallo-intercalators Pt-ACRAMTU and Pt-bis(ACRAMTU) upon interaction with 8-mer oligonucleotides.[19] [20] These complexes use

the acridine as the DNA recognition unit, while the metal centre in one case coordinate the DNA base and in the Pt-bis(ACRAMTU) it is only responsible for the rigidity and the final geometry of the bis-intercalator (Figure 3.11).

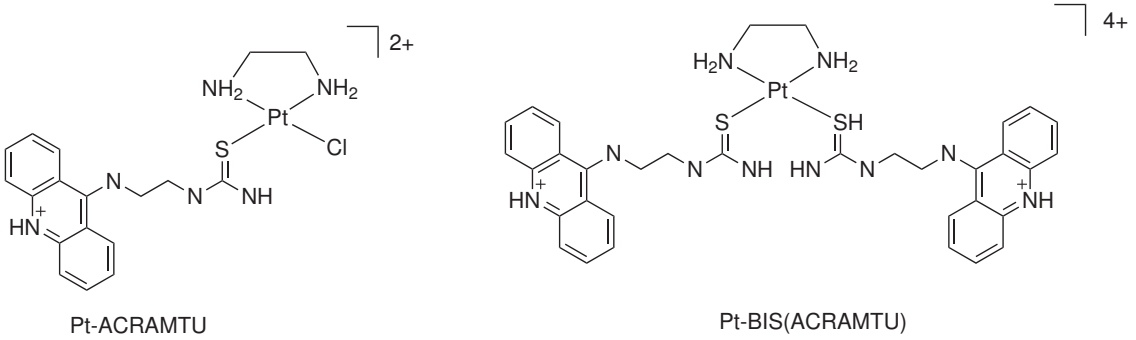

Figure 3.11: Structure of Pt-ACRAMTU and Pt-bis(ACRAMTU).

According to their previous studies on acridine as an intercalating unit[19], in 2005 they reported NMR studies of Pt-(ACRAMTU) upon interaction with d(5'-CCTCGTCC-3')·d(5'-GGACGAGG-3').

The NOESY spectrum showed a clear interruption in the NOE pathway between the bases C4/G5 and C12/G13 on the complementary strand. NOE couplings were missing at the top and the bottom of the intercalating binding site that is consistent with a distortion of the double helix upon acridine intercalation.[21]

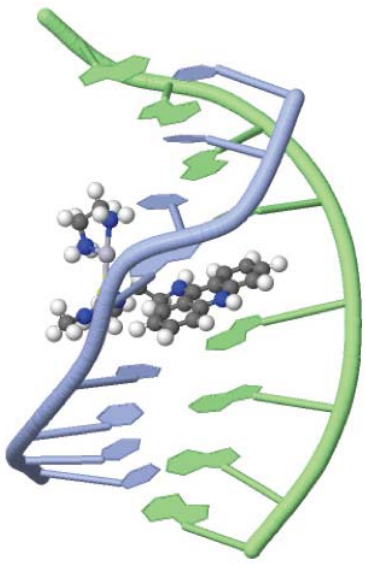

Figure 3.12: The refined structure of Pt-ACRAMTU. Image from the RCSB PDB[7] (www.pdb.org) of PDB ID 1XRW.

The Pt-ACRAMTU is characterised by the presence of one chloride as co-ligand, and which

make it able to platinate the N7 on the base G5. This could be observed in the ^{1}H-NMR since a characteristic downfield shift of 0.7 ppm was produced (Figure 3.12).[19] When the labile chloride ligand coordinated to platinum was replaced with a second acridine the Pt-bis(ACRAMTU) was isolated. ^{1}H-NMR studies based on a NOESY experiment showed a preferred intercalation on the 5'-TATA-3' when binding studies were performed on 8-mer d(GCTATAGC)$_2$. NOE couplings are clearly interrupted between T3H2' and A4H8 and between T5H2' and A6H8, as indicated by the complete absence of the corresponding cross-peak. Furthermore intermolecular NOE couplings were observed between the H1-H8 of acridine sand the H2'/H2" deoxyribose of both strands.

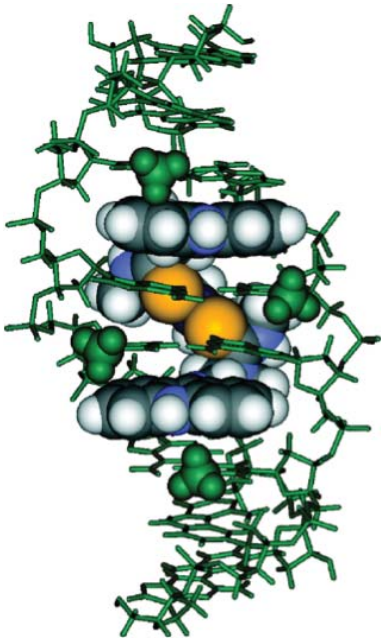

Figure 3.13: View of the major groove of an energy minimised Amber model of the duplex d(GCTATAGC)$_2$ based on NMR data.[20]

3.1.3 Project overview

This chapter aims to investigate how the luminescent metallohairpin [$LnPt_2$] complex interacts with DNA binding site. Based on the previous chapter results where optical spectroscopy have been used to evaluate the DNA at the binding of [$LnPt_2$], we chose the Dickerson-Drew[22] sequence in order to investigate the binding by ^{1}H-NMR spectroscopy.

The Dickerson-Drew sequence d(5'-CGCGAATTCGCG-3')$_2$ is one of the extensively studied sequences in structural biology due to its high relevance in biology, since it represents a binding site for the endonuclease restriction enzyme (EcoRI), which is able to make a staggered cut of the double-stranded DNA molecule by cutting between the G4 and A5 on both strands of the -GAATTC- sequence with an high level of discrimination (Figure 3.14).[23]

Figure 3.14: The refined structure of EcoRI interacting with the Dickerson-Drew sequence. Images from the RCSB PDB[7] (www.pdb.org) of PDB ID 2OXV.

In this chapter we investigated the Pt(tpy) moiety upon interaction with the Dickerson-Drew sequence by ^{1}H-NMR spectroscopy . The employment of proton correlated NMR techniques NOESY and TOCSY will allow us to describe more specifically the intercalation sites for the two platinum terpyridine units of [$LnPt_2$]. The [4'-amidothiophenolPt(tpy)]Cl (AATP) will be employed as a model of the intercalating units on [$LnPt_2$] in order to investigate any binding preference that can be induced by the rigid geometry of [$LnPt_2$].

3.2 Results and Discussion

While the luminescent properties of [$LnPt_2$] upon DNA interaction have been studied using the europium(III) ion, for the NMR experiments the luminescent europium has been replaced with yttrium. Introducing yttrium gives the advantage of reducing line-broadening in the spectra due to the paramagnetic effect characteristic for lanthanides. The [YPt_2]Cl_2 complex (Figure 3.15) bear two platinum metals, which are part of the DNA recognition unit on the complex. Not all the isotopes of platinum are NMR active, but only the ^{195}Pt is NMR active with spin 1/2. The abundance of the ^{195}Pt is estimated to be 33.8% compared to all the platinum isotopic distribution.[24] However the low concentration of the NMR active ^{195}Pt isotope may preclude the observation of any couplings between the protons of the DNA and the ^{195}Pt metal ion.

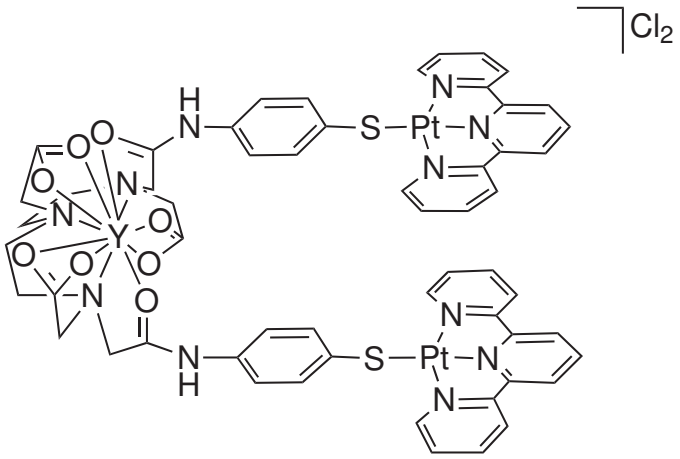

Figure 3.15: Structure of the [YPt_2]Cl_2complex.

In order to have a reasonably high concentration of [YPt_2]Cl_2 in the aqueous buffer solution used for the experiment, we used chloride as counterion. The complex was synthesised and isolated following the procedure reported in chapter 2.

The "Dickerson-Drew" oligonucleotide employed in the experiment was chosen based on the initial four oligonucleotide sequences employed in the optical spectroscopy binding studies discussed in the previous chapter. Since the previous results showed a preferred binding for oligonucleotide sequences containing adenine and thymine but selectivity was not observed between -AATT- and -ATAT- oligonucleotide units, we decided to investigate the "Dickerson-Drew" oligonucleotide by ^{1}H-NMR upon interaction with [YPt_2]Cl_2. The 12-mer d(5'-CGCGAATTCGCG-3')$_2$ sequence has been

previously characterised by ^{1}H-NMR from Hare *et al*.[25] Despite the improved signal dispersion at higher magnetic field strengths, the combination of substantial overlap and poor resolution, especially for ^{1}H nuclei, imposes major limitations on the assignments of spectra and of DNA and ligand DNA-complexes. For this reason the 2D and 3D NMR methods have emerged as the principal sources of both assignments and structural and dynamic information on such materials.

3.2.1 ^{1}H-NMR characterization of d(5'-CGCGAATTCGCG-3')$_2$

Since no previous DNA binding studies of platinum terpyridine derivatives using ^{1}H-NMR have been reported in the literature, the NMR spectrum of the d(5'-CGCGAATTCGCG-3')$_2$ is a good start point to understand the changes in ^{1}H-NMR resonances upon interaction with the metal complexes (Figure 3.16).

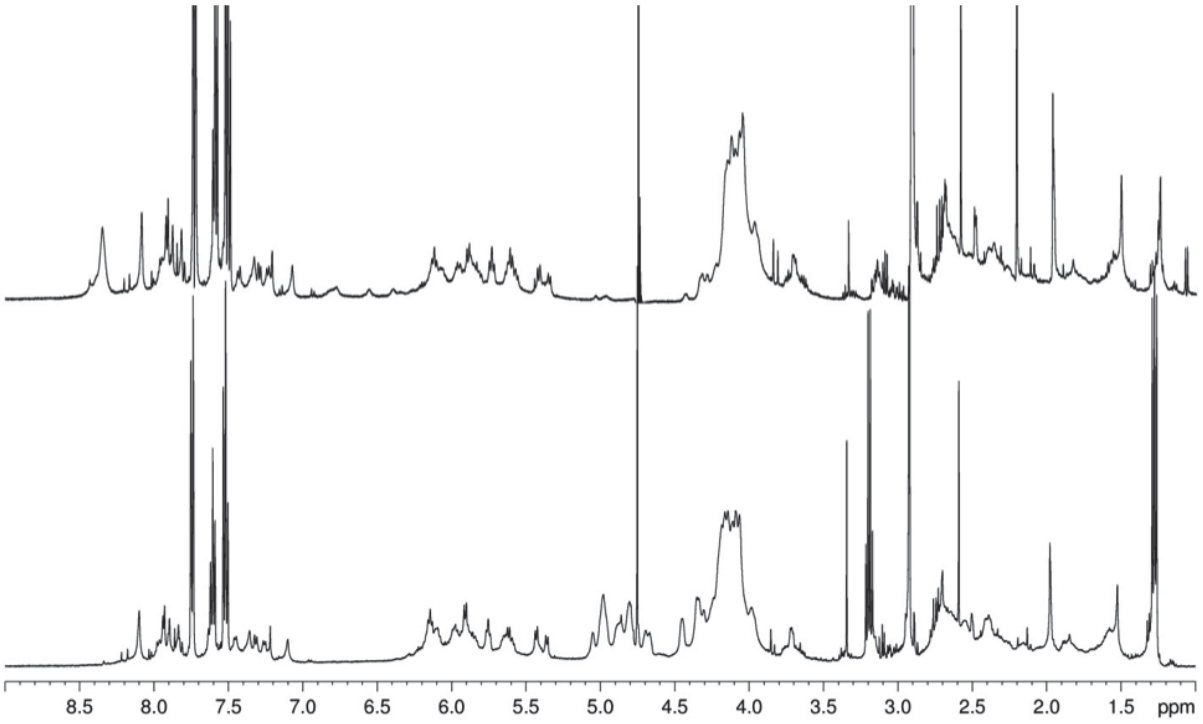

Figure 3.16: Overlay of the ^{1}H-NMR spectra recorded at 500 MHz of d(5'-CGCGAATTCGCG-3')$_2$ recorded in 90:10 (H_2O : D_2O)(top) and 99.99 % D_2O (bottom) at 24°C.

At room temperature conditions the bases arising from the duplex, are in a dynamic equilibrium where they continuously flip between the open and the closed form; as a consequence the amino and imino protons arising from the bases are able to exchange with the protons of the solvent (Figure 3.17).[26] [27]

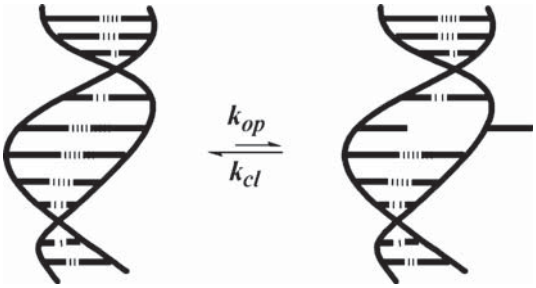

Figure 3.17: A schematic diagram of the equilibrium between opened and closed form of the DNA duplex.[27]

Thus ^{1}H-NMR of d(5'-CGCGAATTCGCG-3')$_2$ initially recorded using an aqueous sodium phosphate buffer (10 mM) containing D_2O (used for the magnetic field locking), allowed us to assign the exchangeable protons arising from adenines at 8.5 ppm by comparison with the ^{1}H-NMR recorded in 99.99% D_2O in which they are not present. The full deuterium exchange was obtained by applying three cycles of freeze-drying with D_2O directly in the NMR tube followed by the recording of the ^{1}H-NMR spectrum. This allowed us to distinguish between the exchangeable and non exchangeable protons. Furthermore, the exchangeable protons are very useful probes to eventually study how the metal-complex interaction affects the kinetic of the base flipping process.

3.2.2 Analysis of the ^{1}H-NMR assignment in DNA spectra

Three scalar-coupled spin systems (isolated from one other in terms of directing bonding) exist in DNA, namely sugar ring, H1', H2', H2", H3', H4',H5', cytosine H6, thymine CH3, CH6, adenine and guanine respectively AH8 and GH8 (Figure 3.18).

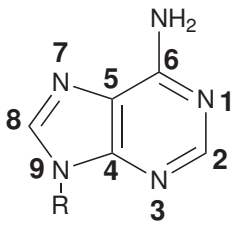

Adenine

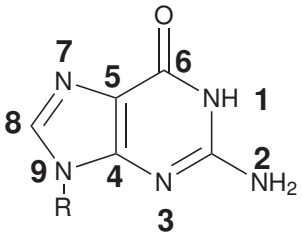

Guanine

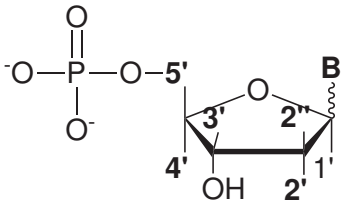

Deoxyribose

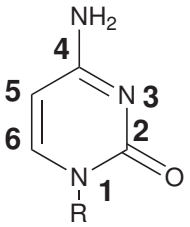

Cytosine

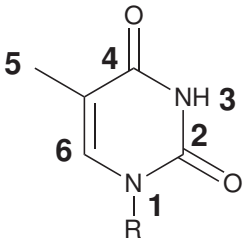

Thymine

5'-$C_1G_2C_3G_4A_5A_6T_7T_8C_9G_{10}C_{11}G_{12}$-3'

3-'$G_{12}C_{11}G_{10}C_9T_8T_7A_6A_5G_4C_3G_2C_1$-5'

Figure 3.18: Structure of bases showing the ^{1}H enumeration used for DNA structure elucidation.

In NOESY data sets, the off-diagonal resonances correlate nuclei that are affected from a spatial separation not bigger than 5 Å. The coupling is through space and not through the bonds, hence called dipolar-couplings. In order to cover most of the spatial distances with the magnetisation transfer in a NOE experiments on oligonucleotide, a relatively long time of irradiation called mixing time τ_m is required.

However because NOE enhancement is not linear with the increase of the mixing time and the distances between the protons of the DNA bases (CH6, GH8, AH8, TH6) is bigger than the maximum distance allowed for a NOE resonance, it is not possible to find a NOE pathway where the protons of the bases are directly connected to allow the complete characterization of the DNA sequence. Hence, the deoxyribose protons play a key role in the ^{1}H-NMR experiment on DNA sequences. Deoxyriboses units connect the bases together by two phosphodiester bonds at the extremity 5' and 3' of the sugar. Because of the secondary structure of DNA (B-DNA), the protons on the deoxyribose units are positioned geometrically at an acceptable distance for NOE interactions with the imino or amino protons of the bases to be observed. A schematic representation (Figure 3.19) shows how the sugar protons (H2', H2" and H1') are essential in order to see any NOE connectivity between the oligonucleotide bases.

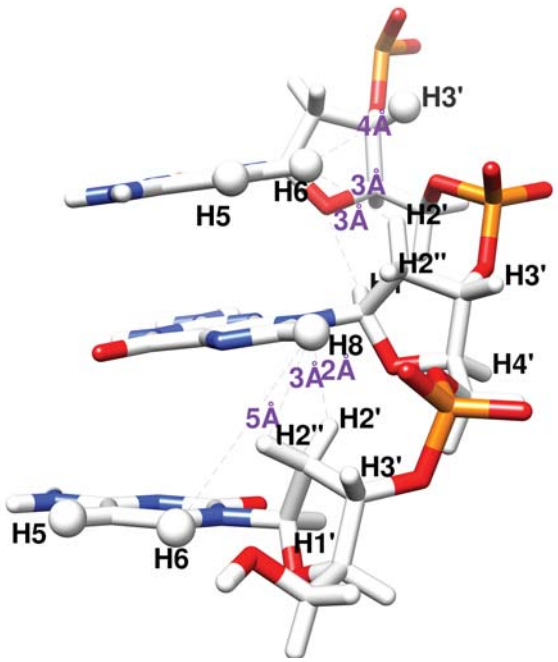

Figure 3.19: Representation of a GCG in B-DNA structure with distances in Å. Image from the RCSB PDB[7] (www.pbd.org) of PDB ID 1GIP.

In fact if we consider an initial fragment like G1C2G3, the distances between G1H8, C1H6 and G3H8 are in between 4.5 and 5 Å which indicate inefficient magnetisation transfer. While if we consider the proton distances between the base protons (H8 and H6) and the sugar protons (H1',H2',H2'), we obtain an average distance of 2.5 Å which is a suitable distance for NOE magnetisation transfer.

Hence the connection of the DNA bases can be followed by NOE coupling with protons of the sugar connected. The most sensible sugar protons are the H1', H2' and H2", while bigger distances are involved between the deoxyribose protons H3', H4', H5' and the imino/amino protons on the bases leading to quite a weak NOE signal, unless relatively long mixing times (τ_m) are employed. However, this may generate artefact signals arising from the NOESY spin-echo sequence and subsequently transformed into observable signals.[28][29]

3.2.2.1 Mixing Time

Incorrect choice of τ_m can cause a complete absence of observable signals since the enhancements have yet to grow to a detectable level, whilst an excessively long τ_m can mean the enhancements have decayed through relaxation. The motional properties of the molecule and hence the longitudinal relaxation times of the nuclei play the most significant role in dictating NOE growth and in turn dictate the selection of τ_m.[30] Above all, selection of τ_m for an NMR experiment involving DNA sequences has to maximise the initial build up rates of the NOEs (which in a large molecule is directly related to the inverse sixth power of the distance between the irradiated and observed protons) minimising the possibility of record signals as a results of the scalar coupling.[31] In order to find a reasonably good (τ_m) for the NOESY experiments on the 12-mer oligonucleotide d(5'-CGCGAATTCGCG-3')$_2$, a set of five τ_m were chosen to record the NOESY spectra. The intensity of NOE signal was measured by integration of the cross-peak and the resulting volume values were plotted against the mixing time (Figure 3.20). In order to maximise the NOE magnetisation transfer, according to the plot reported in figure 3.18 we recorded the 2D NOESY experiments using a τ_m of 400 ms.

3.2.3 NOESY spectrum of d(5'- $C_1G_2C_3G_4A_5A_6T_7T_8C_9G_{10}C_{11}G_{12}$-3')$_2$

Figure 3.21 shows a contour plot of the NOESY spectrum of d(5'-CGCGAATTCGCG-3')$_2$ where all the exchangeable protons have been fully swapped with deuterium and the residual water peak

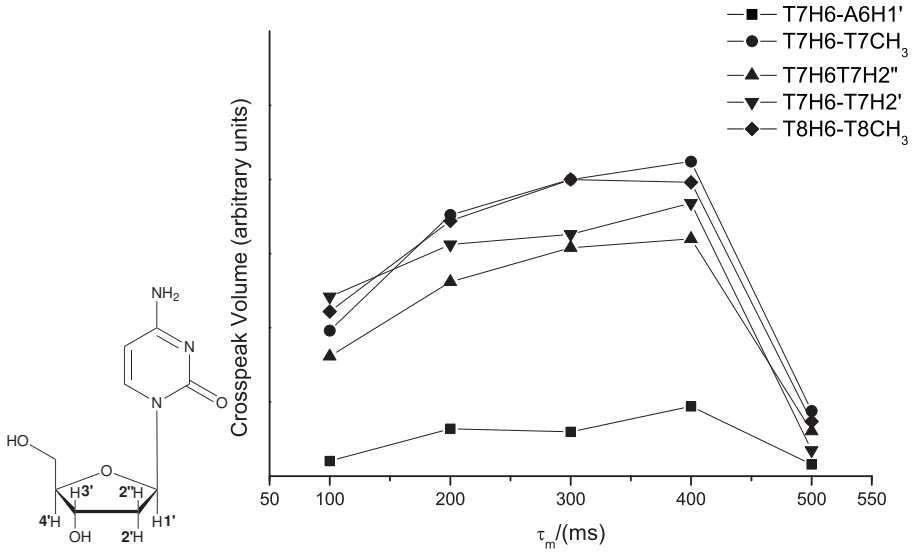

Figure 3.20: Time dependence of intensity (volume integrals) for five representative NOE cross-peaks.

suppressed.

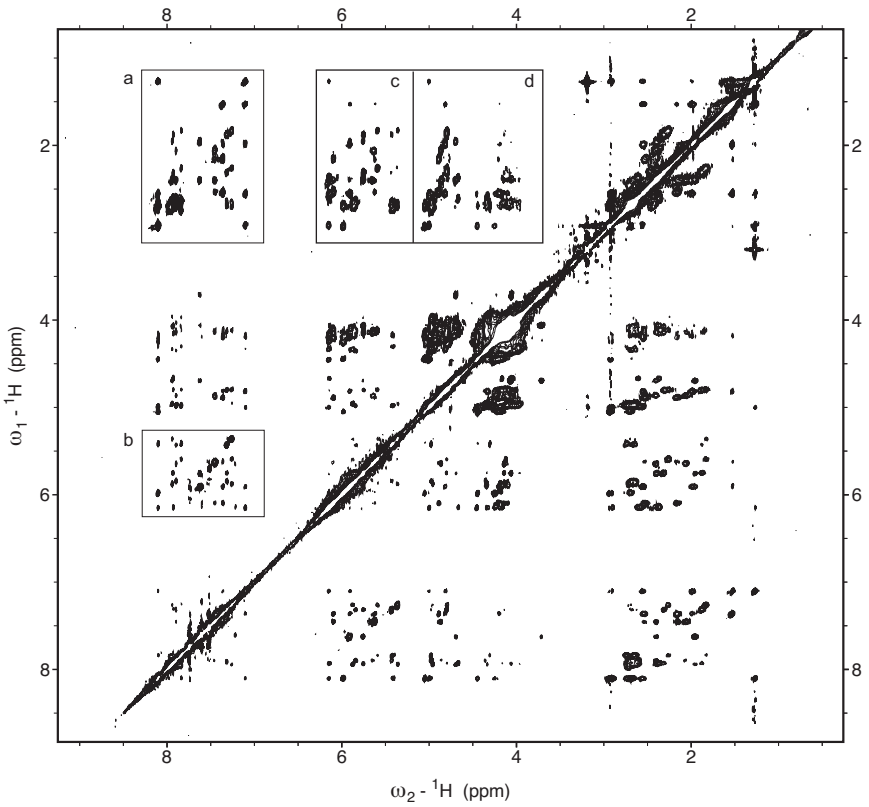

Figure 3.21: Contour plot of d(5'-CGCGAATTCGCG-3')$_2$ NOESY spectrum recorded at τ_m = 400 ms.

The diagonal spectrum, which looks similar to the usual 1D spectrum, arises from protons which do not relax with other protons during the mixing time, while most of the small peaks off the diagonal

are the major feature as a result of the dipolar coupling. In the first instance, the NOE spectrum appear to be particularly complicated, but a more detailed analysis shows that all the signals are divided into groups of resonances.[25]

Following the previous work from Hare *et al*., we can divide the spectra as reported in figure 3.21 in four areas:

a) The imino/amino protons of the bases have dipolar coupling with the H2' and H2" of the deoxyribose.

b) The imino/amino protons of the bases are in resonance with the H' of the sugar.

c) The protons of the sugar are spatially coupled as well, and in the region c resonances between H1' and H2', H2" are present.

d) Region d arises from the NOE coupling between the H2'/H2" and H3' of the sugar.

The easiest starting points on the NOESY spectra are the methyl groups on the thymine units of the sequence. The CH_3 groups arise to one of the most intense signals in the ^{1}H-NMR and they appear as a singlet at 1.26 ppm for T7CH_3 and at 1.53 ppm for T8CH_3. Once the two CH_3 have been assigned, the cross-peak in the aromatic region of the spectra is due to the coupling with the H6 respectively of T7 and T8. Because we know the oligonucleotide sequence, if we exclude all the cross-peaks that are related to the TH6, the only remaining resonances are from the terminal part of the sequence. Since the cytosine is the only base which has two vicinal protons, at this stage we can identify the C1H6 using TOCSY, and according to the previously published results we found the C1H6 at 7.63 ppm coupling with H2" and H2' of the sugar respectively at 2.40 and 1.95 ppm. Because the imino proton H8 of G2 has a dipolar coupling with the C1H2", we can find the coupling between the G2H8 and its own H2" at 2.65 ppm and then the coupling with C3H6 (Figure 3.22).

Following this assignment strategy, we found that all the signals can be assigned and show good agreement with those previously reported by Hare *et al*.[25] It is interesting to note that resonances follow an anticlockwise NOE connection, which confirm the oligonucleotide has a structure consistent with that of B-DNA.

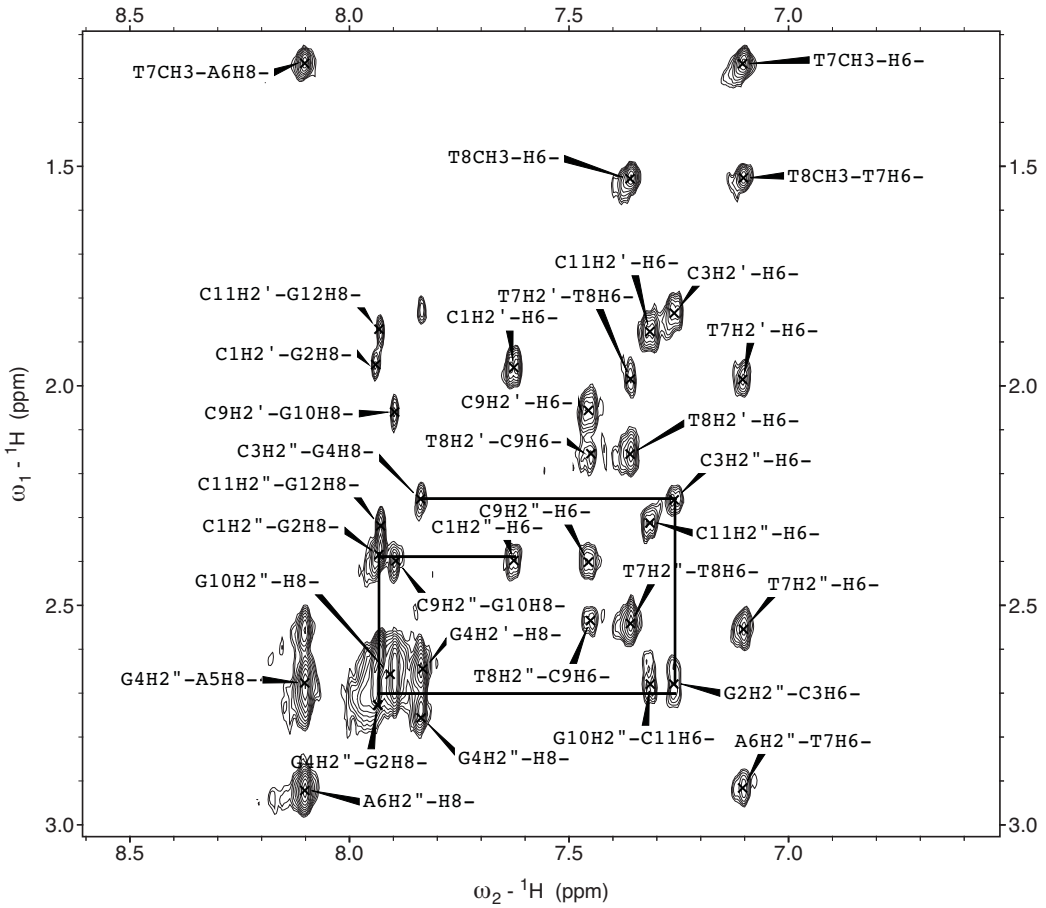

Figure 3.22: Expanded NOESY contour plot of the cross peaks between the GH8, CH6 region and the H2'-H2" and CH_3. The top of the spectrum identifies the two thymine methyl groups and the adjacent base protons, while the connectivities between the aromatic and the H2" protons of G2 and C1 are traced at the bottom.

3.2.3.1 NOE Couplings to H1'

It is possible to study the connectivity of the DNA bases in a 12-mer oligonucleotide using the proton H1' of the sugar, as H1' is spatially in the range for generating dipolar coupling with the adjacent imino/amino proton of the bases.

A convenient starting point to assign this part of the spectrum is the C1H6, which we can vertically find from the H2" and H2' assignment completed before and according to the previously published results the coupling with the H1' (C1H1') is at 5.71 ppm.[25] [32]

Following the strategy assignment described before, it is possible to assign all the couplings between the DNA bases and the H1' of the sugar (Figure 3.23).

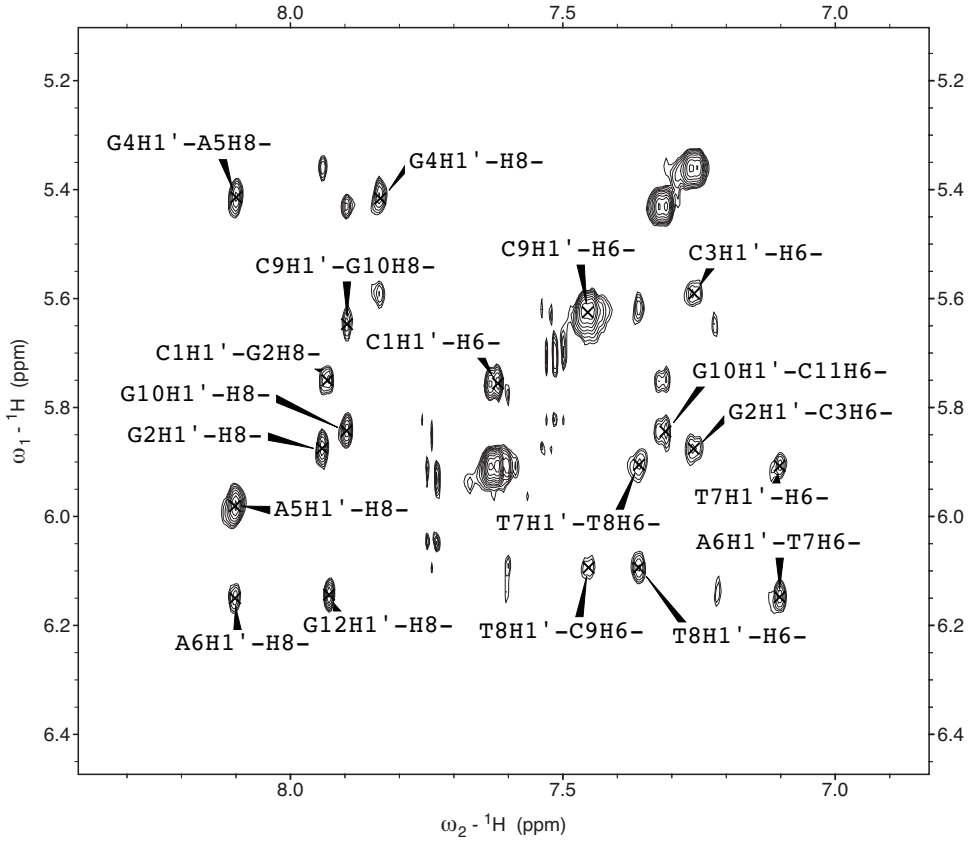

Figure 3.23: Expanded NOESY contour plot of the cross peaks between the GH8, CH6 region and the H1' of the sugar.

Some of the NOE couplings in the area b are not coupled with any of the sugar H1' protons, but they are the result of the dipolar coupling between the H5 and H6 of the cytosines. These could be confirmed by a TOCSY spectrum recorded at τ_m of 100 ms, which shows the scalar coupling of the vicinal H5 and H6 (Figure 3.24).

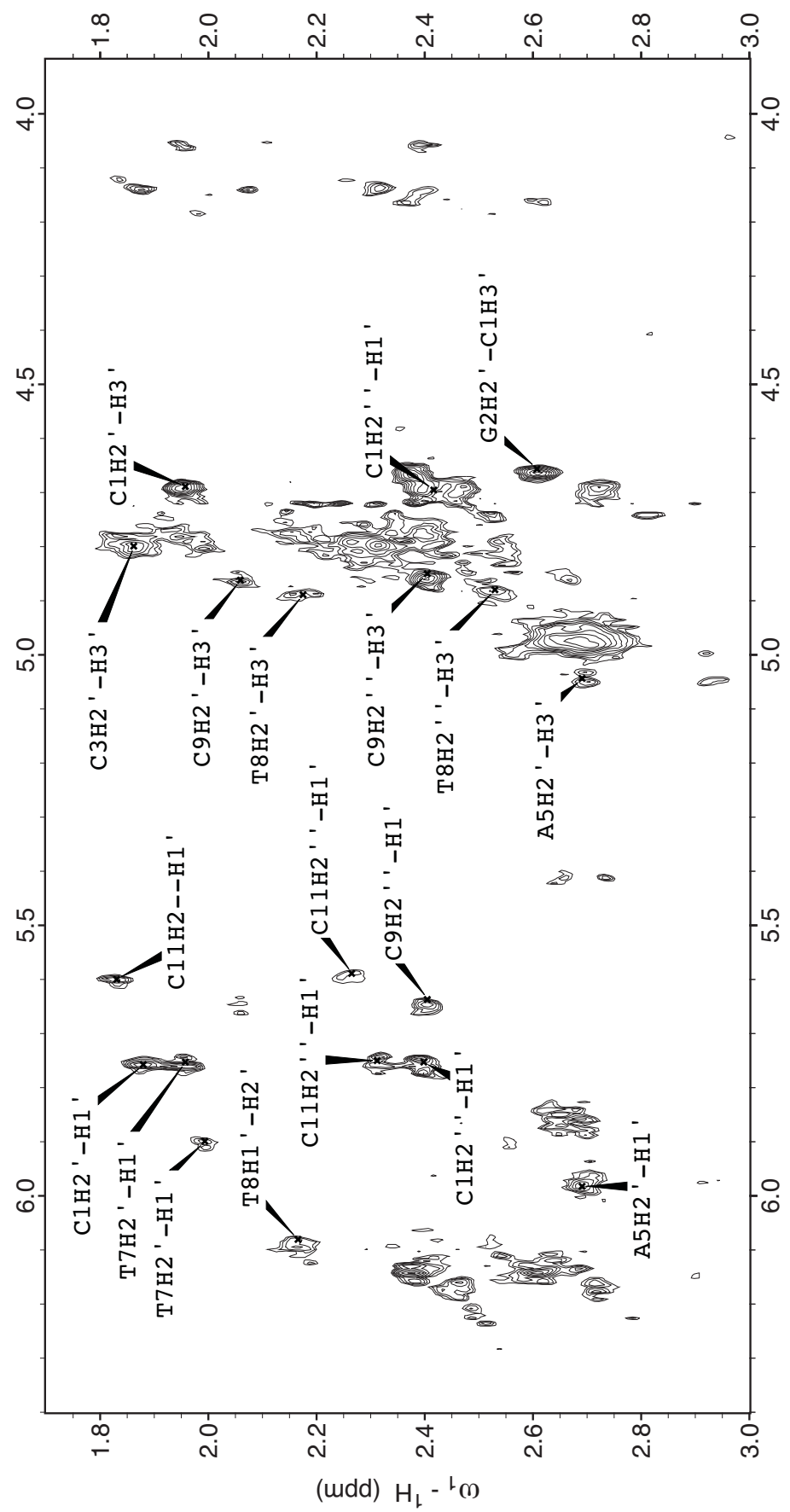

Figure 3.24: Part c and d of the TOCSY spectrum of d(5'-CGCGAATTCGCG-3')$_2$ recorded with 100 ms mixing time in 10 mM sodium phosphate buffer.

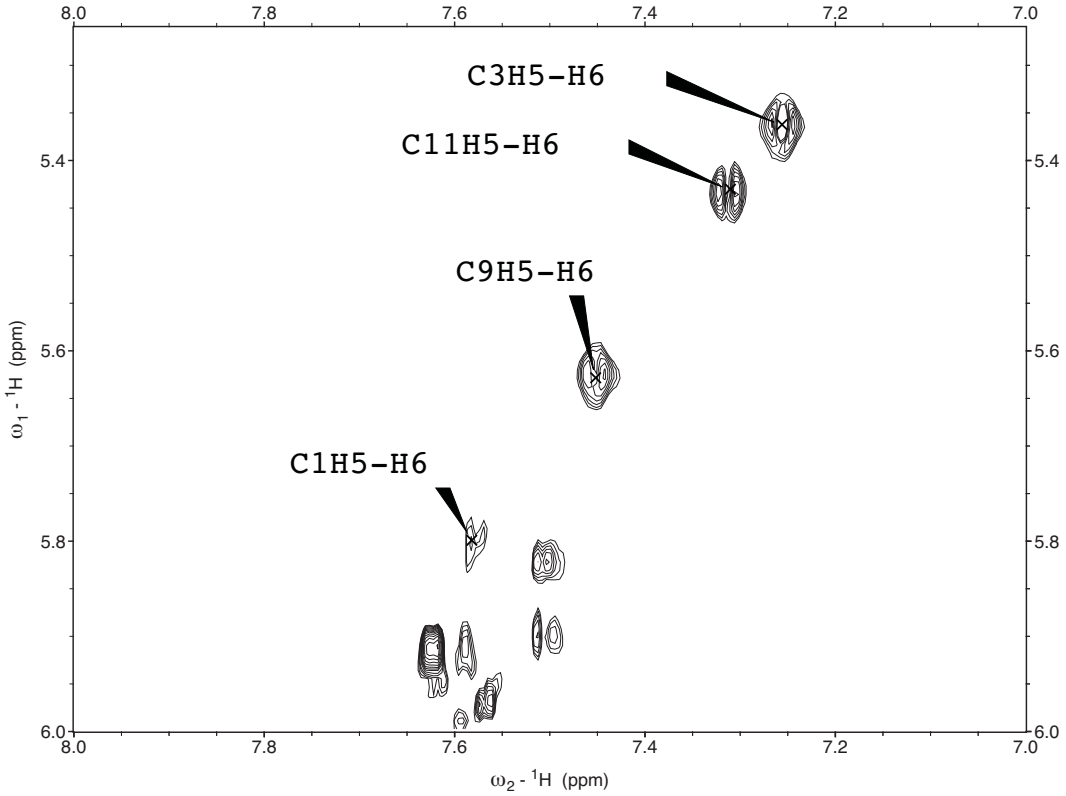

Figure 3.25: Expanded TOCSY contour plot of the cross peaks for region **b**.

The total correlation spectroscopy (TOCSY) is a technique that yields the homonuclear proton correlation spectra based on scalar couplings, but is also able to establish correlations between protons that sit within the same spin system. In other words, provided there is a continuous chain of spin-spin coupled protons, A-B-C-D- etc, the TOCSY sequence transfers magnetization of one proton to the next along the chain. TOCSY of oligonucleotide sequences offer the advantage of more informative spectra then ^{1}H-^{1}H COSY, which tend to produce severely overlapped spectra.[30]

TOCSY spectra find useful application when the NOE cross peaks in the region c and d need to be assigned. Located in this region are the dipolar couplings between the H1', H2', H2", H3' and H4' of the sugar ring. The NOESY spectrum of these two regions presents several overlaps; in particular the couplings of the guanines sugar protons are quite overlapped and difficult to distinguish (Figure 3.26)

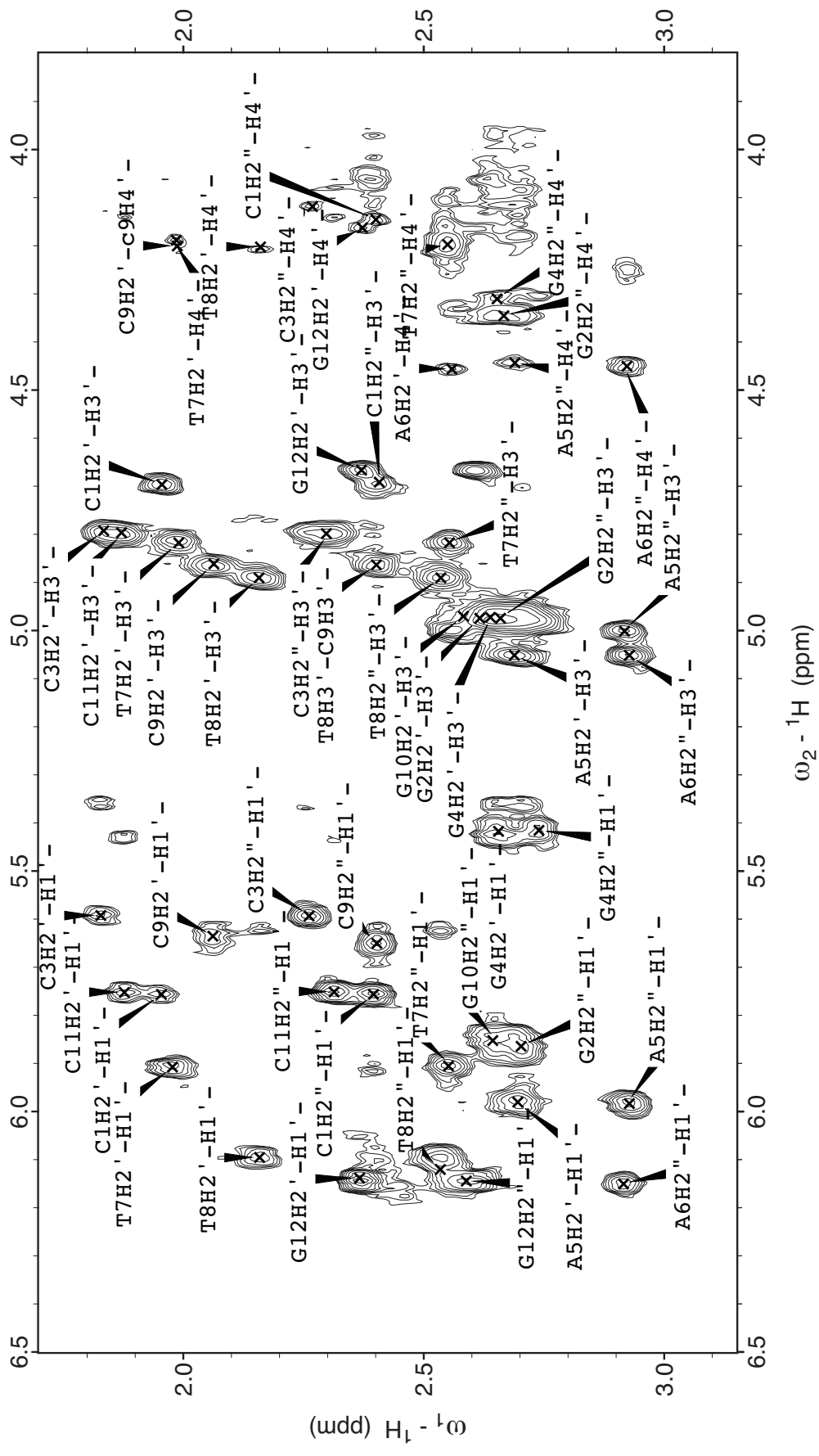

Figure 3.26: Expanded NOESY contour plot of the cross peaks for regions c and d recorded with 400 ms mixing time in 10 mM sodium phosphate buffer.

With the approach of combining information from NOESY and TOCSY spectra, we have been able to assign all the chemical shifts of the Dickerson-Drew 12-mer oligonucleotide. The results here shown are consistent for a B-DNA secondary structure for the 12-mer d(5'-CGCGAATTCGCG-3')$_2$ oligonucleotide. All the NOE chemical shifts that we summarised in (Table 3.1), were in good agreement with the previously published data from Hare *et al*.[25]

	H8	H6	H5	CH_3	H1'	H2"	H2'	H3'	H4'
C1	-	7.61	5.80	-	5.75	2.39	1.95	4.67	4.14
G2	7.93	-	-	-	5.87	2.67	2.61	4.97	4.34
C3	-	-	-	-	5.59	2.26	1.83	4.79	4.12
G4	7.83	7.26	5.36	-	5.41	2.72	2.64	4.97	4.31
A5	8.10	-	-	-	5.98	2.84	2.69	5.03	4.44
A6	8.10	-	-	-	6.14	2.92	2.55	5.05	4.45
T7	-	7.10	-	1.26	5.90	2.55	1.98	4.81	4.19
T8	-	7.36	-	1.52	6.10	2.53	2.16	4.89	4.20
C9	-	7.45	5.62	-	5.64	2.40	2.04	4.86	4.20
G10	7.89	-	-	-	5.84	2.65	2.58	4.97	4.34
C11	-	7.31	5.43	-	5.75	2.30	1.86	4.79	4.20
G12	7.92	-	-	-	6.12	2.58	2.36	4.66	4.16

Table 3.1: Chemical shifts of 125 assigned protons for d(5'-CGCGAATTCGCG-3')$_2$)

At this stage the main objective has been simply to assign protons to their respective NMR peaks in order to follow any changes during the addition of the [YPt$_2$]Cl$_2$ complex. However the results also contain a large amount of structural information, which can be further analysed employing the restricted molecular dynamics modelling that would lead to more detailed structural information about the Dickerson-Drew dodecamer.[32]

3.2.4 ^{1}H-NMR titration of d(5'-CGCGAATTCGCG-3')$_2$ with [YPt$_2$]Cl$_2$

In order to find the best condition in terms of ratio of DNA/complex we performed ^{1}H-NMR titration where aliquots of [YPt$_2$]Cl$_2$ were added from a stock solution into the NMR tube, which contained the 12-mer duplex d(5'-CGCGAATTCGCG-3')$_2$. Additions were performed in order to obtain ratio of DNA/complex from 10:1 to 2:1 and a 1D ^{1}H-NMR recorded (Figure 3.27). Upon additions of [YPt$_2$]Cl$_2$ changes in chemical shifts were observed particularly for the aromatic protons H8/H6 of the bases and H1', H2' and H2" of the sugar. The ratio 12-mer/complex 2:1 represent the upper limit of the titration where no further changes in chemical shift could be observed.

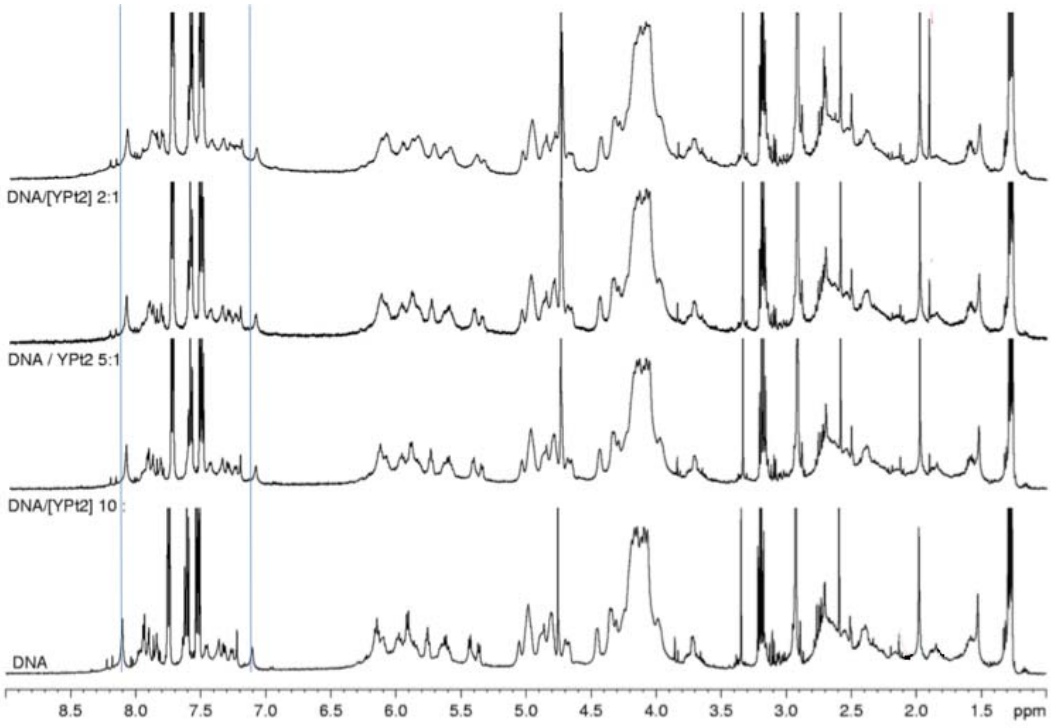

Figure 3.27: ^{1}H-NMR at 500 MHz of d(5-CGCGAATTCGCG-3')$_2$ upon addition of [YPt$_2$]Cl$_2$ in 10 mM phosphate buffer solution for a final ratio DNA:[YPt$_2$]Cl$_2$ of 1:0.5

The changes in chemical shift of the H8/H6 aromatic protons, upon addition of [YPt$_2$]Cl$_2$ are plotted in figure 3.28. Since changes occurs mainly between G4/A5 and between C9/G10, they are the possible binding site for [LnPt$_2$].

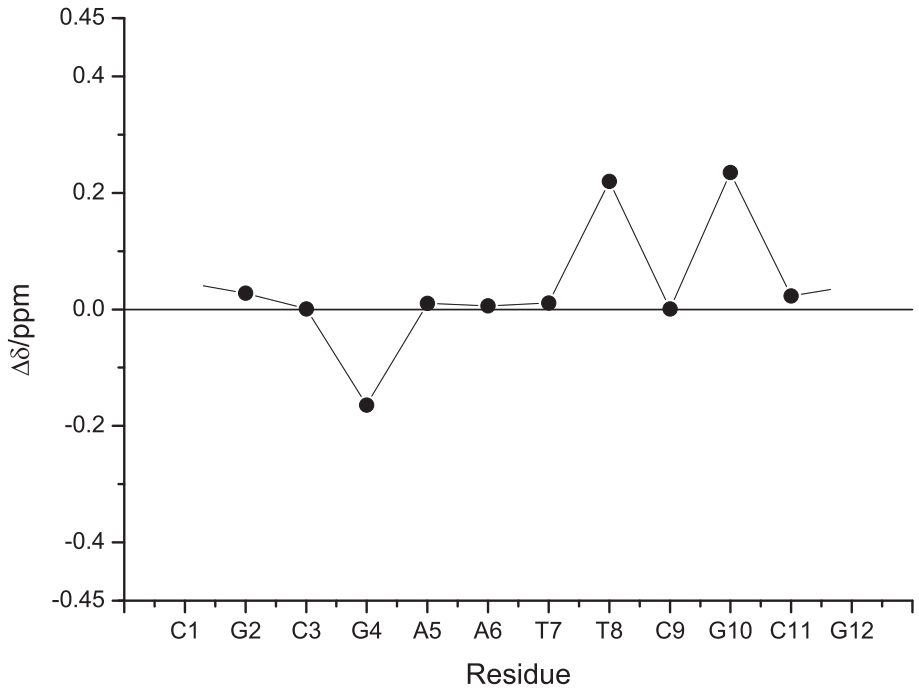

Figure 3.28: ^{1}H-NMR of $\Delta\delta$ for the aromatic protons of the bases (H6, H8); shifts to upfield region of the spectrum have *positive* sign while the shifts to downfield region has *negative* sign.

3.2.5 DNA binding studies by NOE

Determining the location of the $[YPt_2]Cl_2$ binding site could be achieved by taking into consideration the dipolar coupling from the H6/H8 aromatic protons to the sugar protons. Upon the bis-intercalative interaction of the $[YPt_2]Cl_2$ with DNA ideally we expect to see a decrease in intensity of NOE signals for the imino/amino protons that are part of the binding site; additionally we expect to see new NOE signals that possibly generate from the dipolar couplings between the platinum terpyridine intercalating units and the protons of the binding site. Due to the high overlap of the peaks on the diagonal spectra upon addition of $[YPt_2]Cl_2$ to the oligonucleotide, it is merely speculative to identify and assign any proton signal arising from the dipolar coupling between the H6/H8 of the bases or the sugar and the platinum terpyridine units. The line broadening produced on the ^{1}H-NMR spectra upon interaction of $[YPt_2]Cl_2$ with the 12-mer is due to the relatively slow kinetic exchange between free and interacting $[YPt_2]Cl_2$ in the NMR time-scale, which might be due to the high value of the binding constant which is characteristic for $[LnPt_2]$ upon interaction with CT-DNA.[33]

The binding site $[YPt_2]Cl_2$ on the oligonucleotide can be determined mainly by evaluation of the NOE connectivity in the NOESY spectra that have been recorded using a mixing time τ_m of 400 ms. Comparing the NOESY spectra recorded using a DNA/complex ratio of 2:1 (Figure 3.29) with the NOESY of the 12-mer on its own (Figure 3.21), many signals are reduced in their intensity while some of them are missing when we compare it with the one from the oligonucleotide itself (Figure 3.21).

In order to assign the cross-peaks, it is convenient to divide all the spectra into four areas: **a**, **b**, **c** and **d** which start from the area a, where the dipolar coupling is observed between the imino/amino protons and the H2', H2" of the sugar. However these regions are not to be considered independently from each other; in fact due to the severe overlap it is essential in some cases (i.e. G2, G4, G10 and G12) to consider all of them as a whole to reach an unambiguous assignment.

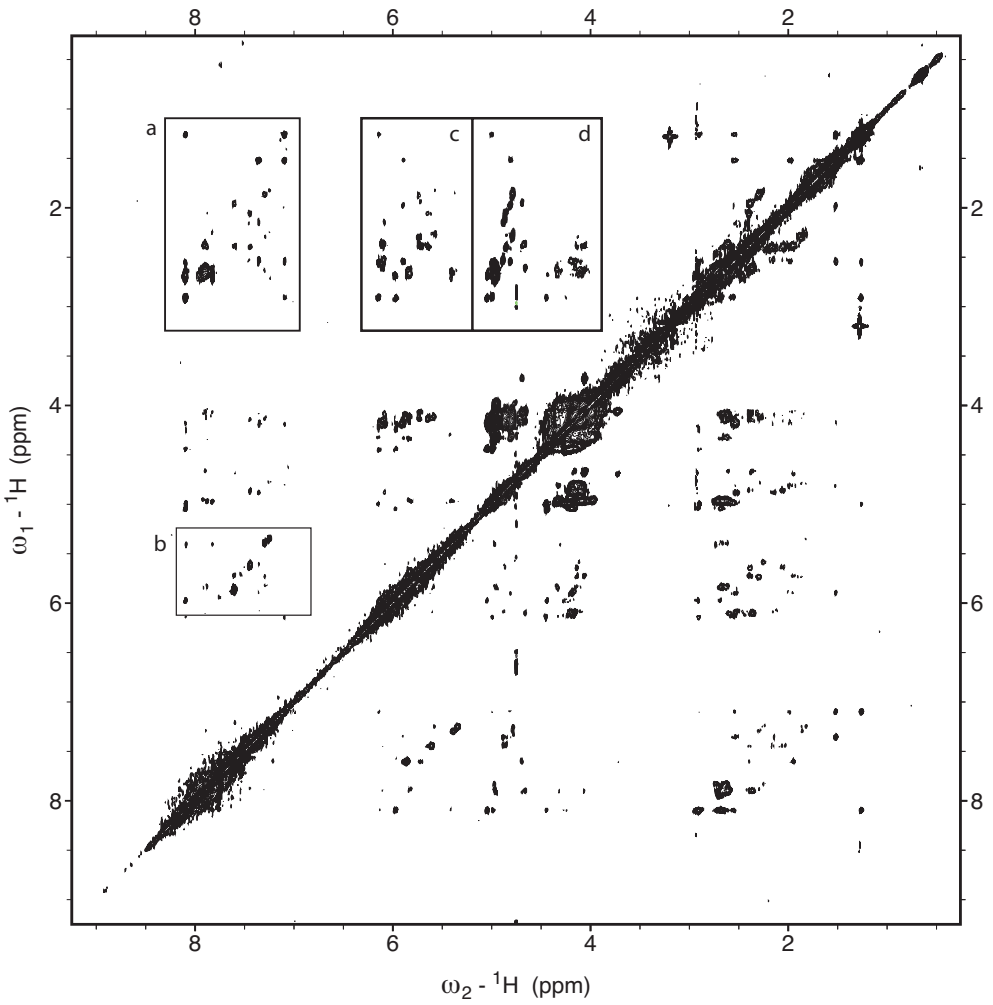

Figure 3.29: Contour plot of d(5'-CGCGAATTCGCG-3')$_2$ NOESY spectrum upon interaction with $[YPt_2]Cl_2Cl_2Cl_2$ using mixing time τ_m = 400 ms.

3.2.5.1 Area a: NOE couplings by H2" and H2'

Taking into consideration the assignments reported earlier for the 12-mer d(5'-CGCGAATTCGCG-3')$_2$, we can start conveniently from the NOE coupling of C1H6 with its H2", which is at the right distance to couple with G2H8 as well. Following the NOE couplings from the aromatic protons to the protons of the sugar, we assigned all the cross-peaks through an anticlockwise NOE pathway connection, which is consistent with a retained B-DNA conformation of the oligonucleotide upon interaction with the [YPt$_2$]Cl$_2$ (Figure 3.30).

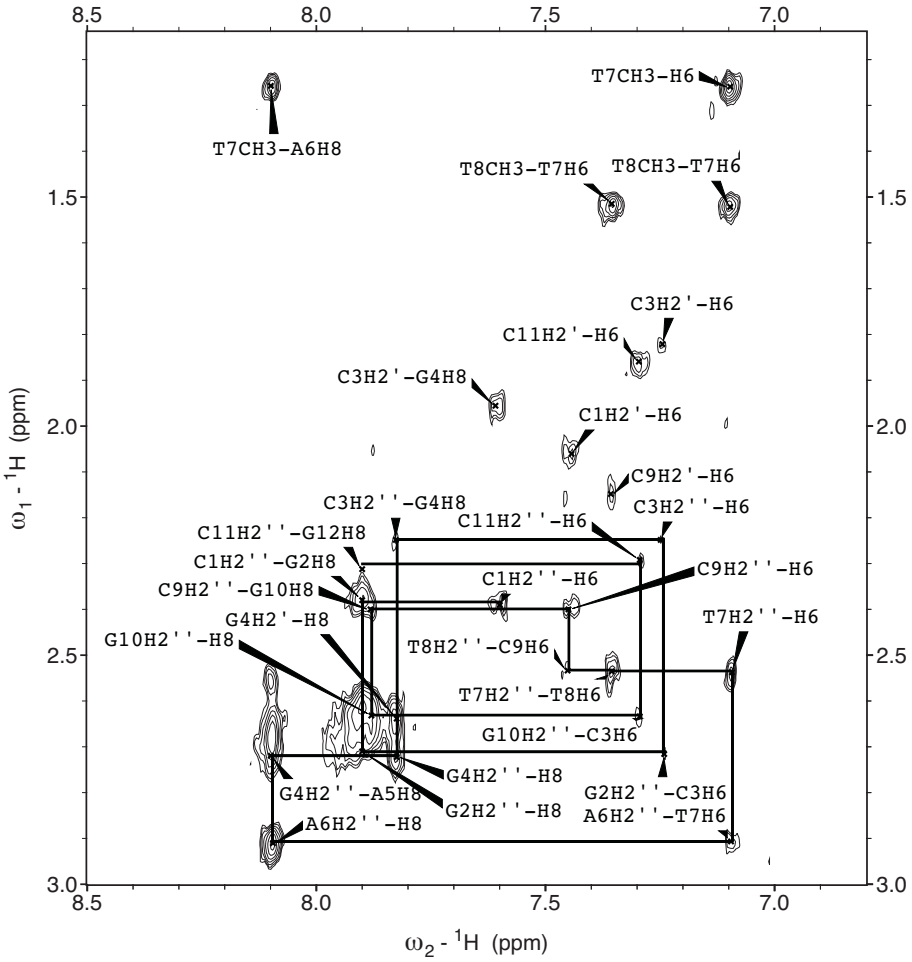

Figure 3.30: Expanded NOESY contour plot of the cross peaks between the GH8, CH6 region and the H2'-H2" and CH_3.

According to the chemical shifts reported in (Figure 3.28), the major changes to the area **a** of the spectra occurs in the central part where the H6 and H8 from cytosine and guanine couple with the H2" and H2' of the sugar respectively.

In fact NOE connectivity is dramatically reduced between the C3H6 and G4H8, which were

originally coupled by the C3H2" while the NOE intensity observed between the G2H2" and C3H6 is reduced. NOE connectivity is interrupted between the C11H6 and G10H8 as well, where originally these protons were coupling with the G10H2" while the coupling between C9H6 G10H8 via G10 H2" is still present even if the intensity of the NOE signal intensity is reduced. NOE couplings are interrupted between C9H6 and T7H8 due to the missed dipolar coupling between C9H6 and T8H2".

Dipolar couplings between C3H6 and G4H8 are missing in the region of H2' resonance, as the coupling between C9 and G10 is not present. Because the final 12-mer duplex is formed by two self-complementary palindromic single stranded unit, the G10 results to be the complementary base for C3 and consequently the C9 for G4. This suggests that at least one of the terpyridine unit of $[YPt_2]Cl_2$ completely covers the plane of the bases probably leading to a maximised π-π stacking between the DNA bases and the terpyridine. However while NOE interruption occurs between T8 and C9 in the H2' region, it is impossible to evaluate any NOE variation on the complementary strand about the coupling between A5H8 and G4H8 due to the severe overlap of the NOE resonances.

It is important to see that the central part of the 12-mer oligonucleotide remains essentially unchanged upon interaction with $[YPt_2]Cl_2$. In fact the methyl groups on thymine T7 and T8 are still able to couple between them with no changes in NOE couplings. However the 1D ^{1}H-NMR spectrum (Figure 3.27) showed changes in chemical shift for the H8 of T7, while the T8H8 was left unchanged by the interaction with $[YPt_2]Cl_2$. More information can be obtained by the assignment of part **b** of the NOESY spectrum.

3.2.5.2 Area b: NOE couplings by H1'

The region b of the NOESY spectrum is based on NOE couplings between the H6/H8 aromatic protons of the bases with the H1' of the sugar. In this part the NOE connectivity between the C3H6 and G4H8 was missing, while the NOE coupling between A6H8 and the G4H1' still occurs but it is sensibly reduced in its intensity (Figure 3.31).

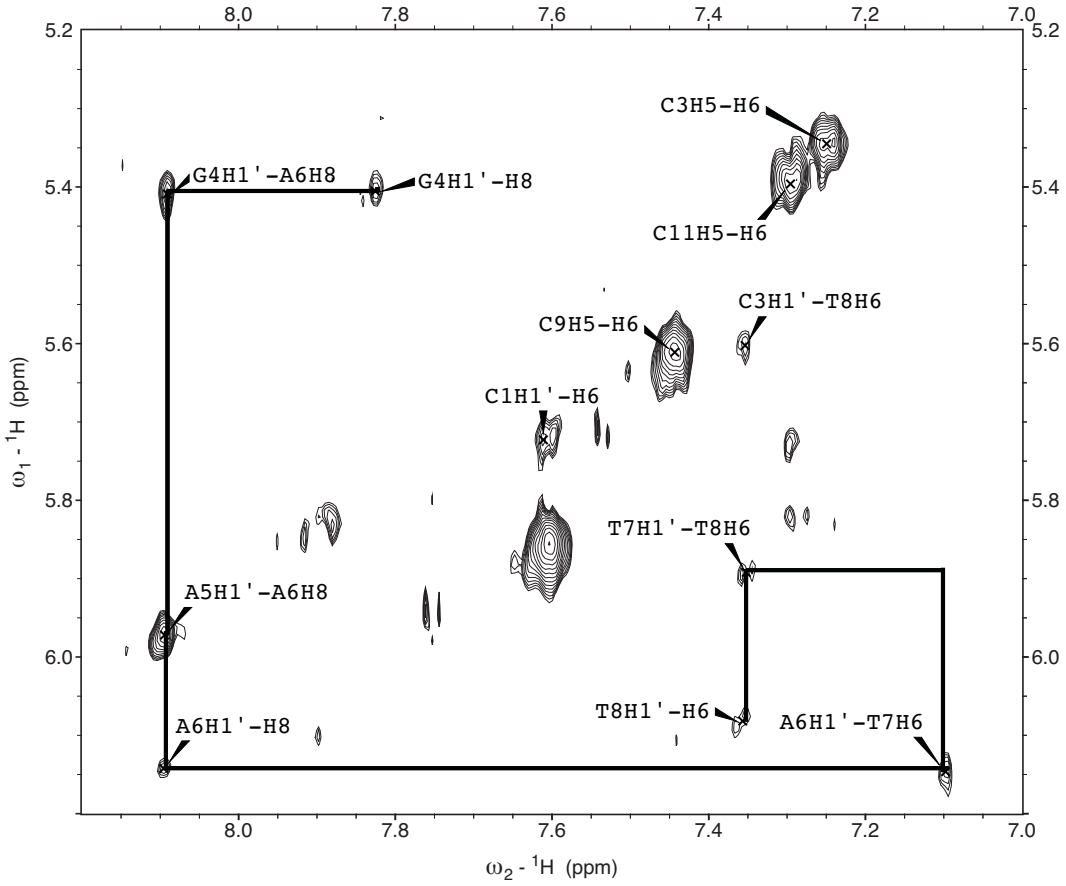

Figure 3.31: Expanded NOESY contour plot of the cross peaks between the GH8, CH6 region and the H1' of the sugar.

As already seen in the area a of the spectrum the NOE coupling between T8H1' and C9H6 has disappeared, as has disappeared the NOE coupling between the C1H6H1' and G12H1'. However the NOE resonances between the terminal bases of the 12-mer duplex and their sugar may be missing due to the β configuration of the anomeric bond on the sugar, which in a B-DNA structure that goes from 5' to 3' leads to a final structure for the duplex where the sugar is above the plane of the base and it is free to change its configuration.

The data discussed to this point appears to be consistent with a model where the two platinum terpyridine units stack between the bases C1G2/C11G12 and G4A5/T8C9, which confirms the bis-interclator behaviour of the $[YPt_2]Cl_2$. The intercalation between C1 and G2 is supported by the absence of NOE coupling from G2H2" to G2H8 and C3H6, due to possible produced conformational changes on G2H2" upon intercalation of the platinum terpyridine unit. The square planar geometry induced by the d^8 electronic configuration of the metal centre, it makes the platinum(II) terpyridine as an extended flat intercalating unit able to cover the DNA bases from both strands.[34]

In fact NOE interruption occurs on the complementary strand between G12 and C11, due to the missing dipolar coupling from G12H2" to the aromatic G12H8 and C11H6. A representative model of the intercalation site has been built using a Dickerson-Drew structure obtained by molecular dynamics based on NOE restriction from Clore *et al*., and an X-ray structure of the AATP used as model of the intercalation unit that has been previously reported by M. C. Solomons.[33]

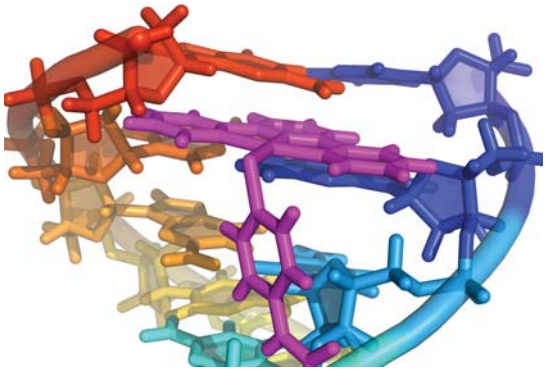

Figure 3.32: Model of the terpyridine intercalation based on image from the RCSB PDB[7] (www.pdb.org) of PDB ID 1GIP with AATP inserted in the intercalation site.

According to the previously published molecular mechanics model of [$LnPt_2$] where the two DNA recognition units are separated by 10 Å, we expect the second platinum terpyridine unit of [YPt_2]Cl_2 to intercalate between the G4A5/C9T8.[35] In fact the absence of the NOE coupling between the T8H2" and C9H6 is concomitant with the missing dipolar coupling between T8H1' and C9H6 and allows us to assign it as the second intercalation site. On the complementary strand, this intercalation site is confirmed from a strong reduction of the NOE intensity between A5H1' and G4H8. As before, we built a representative model for the second intercalation site of the molecule (Figure 3.33).

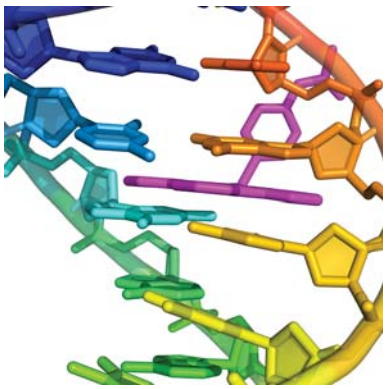

Figure 3.33: Model of the terpyridine intercalation based on image from the RCSB PDB[7] (www.pdb.org) of PDB ID 1GIP with AATP inserted in the intercalation site.

Since the models reported above have not been obtained by molecular dynamics, they do not take into consideration the stiffening effect that the bis-intercalator produced upon interaction with DNA, which was previously shown by linear dichroism and herein by the absence of NOE coupling between the H6/H8 of the aromatic protons arising from C3 and G4. Indeed the missing NOE couplings between C3-G4 and G10-C11 may be due to the DNA unwinding upon intercalation of the two platinum terpyridine units, which produces an increase in distance between the sugar protons and their bases.

Based on the molecular modelling structure previously reported, a representative model of the intercalation has been built where the intercalation between C1G2/G4A6 is happening from the minor groove side of the chain (Figure 3.34).

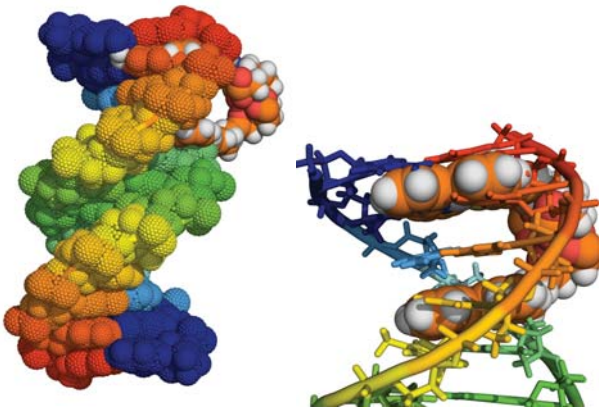

Figure 3.34: Model of the terpyridine intercalation based on image from the RCSB PDB[7] (www.pdb.org) of PDB ID 1GIP with AATP inserted in the intercalation site.

3.2.6 ^{1}H-NMR titration of d(5'-CGCGAATTCGCG-3')$_2$ with AATP

Additional ^{1}H-NMR experiments were performed on the 12mer d(5'-CGCGAATTCGCG-3')$_2$ using the mono-intercalator AATP as a mimic compound for the single intercalating unit of $[YPt_2]Cl_2$.

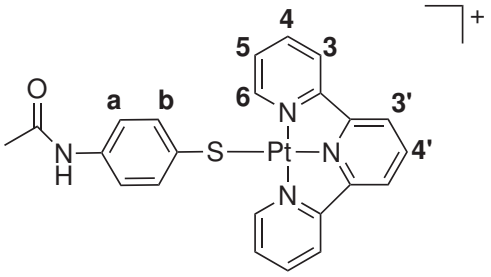

Figure 3.35: Structure of AATP.

In order to find the best condition in terms of ratio DNA/complex we performed ^{1}H-NMR titrations where aliquots of $[YPt_2]Cl_2$ were added from the stock solution into the NMR tube, which contained the 12-mer duplex d(5'-CGCGAATTCGCG-3')$_2$. Additions were performed in order to obtain ratio of DNA/complex from 10:1 to 2:1 and a 1D ^{1}H-NMR recorded (Figure 3.36).

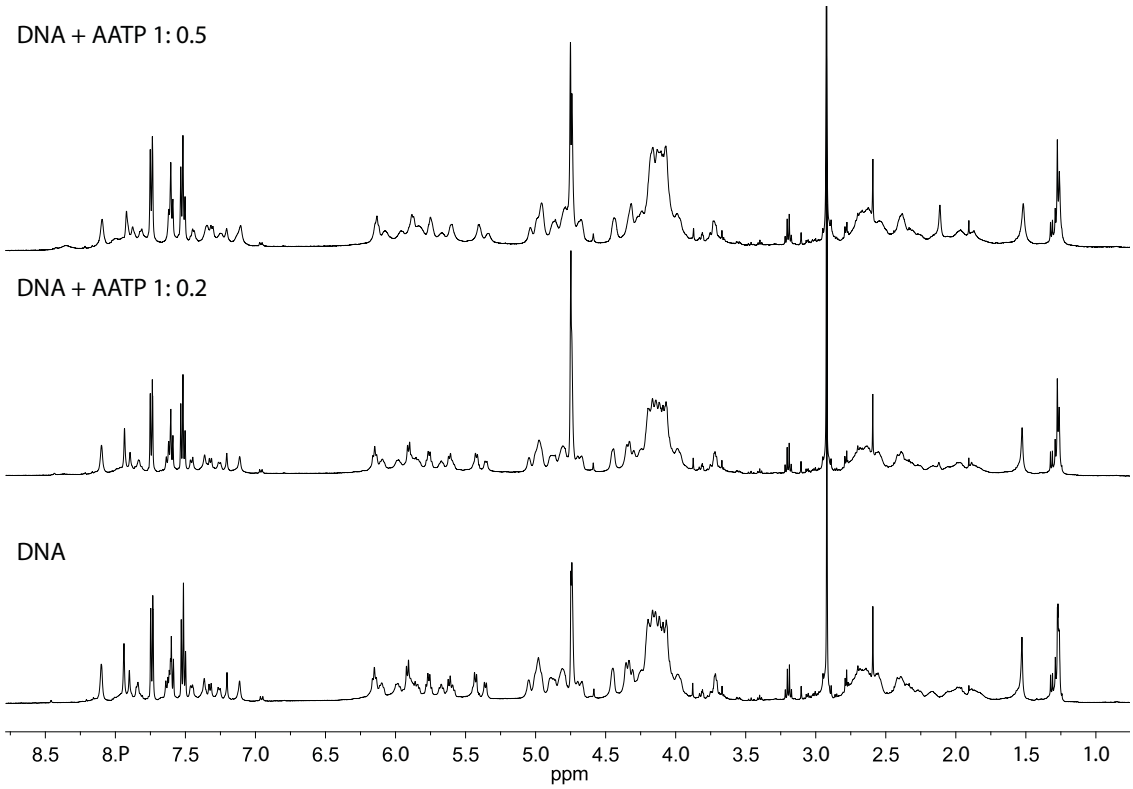

Figure 3.36: ^{1}H-NMR at 500 MHz of d(5'-CGCGAATTCGCG-3')$_2$ upon addition of AATP 10 mM phosphate buffer solution for a final ratio DNA : complex of 1:0.5.

Upon additions of $[YPt_2]Cl_2$ changes in chemical shifts were observed for the aromatic protons H8/H6 of the bases and H1', H2' and H2" of the sugar. The ratio 12-mer/complex 2:1 represent the upper limit of the titration where no further changes in chemical shift could be observed.

The addition of AATP to the 12mer duplex leads to a slight broadening of the 1D ^{1}H-NMR signals arising from the oligonucleotide. Changes in chemical shifts were only recorded for the imino/amino protons of the cytosine and guanine, while in contrast to the $[YPt_2]Cl_2$ interaction, the chemical shifts of adenine and thymine stays unchanged upon the interaction with the AATP (Figure 3.37).

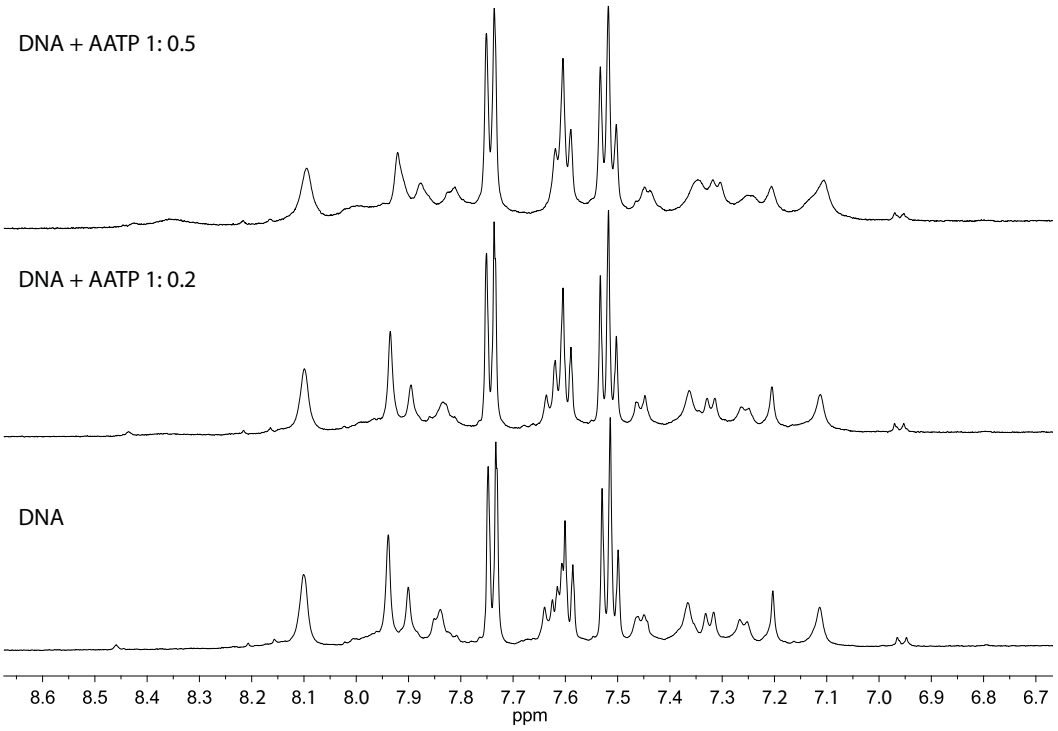

Figure 3.37: ^{1}H-NMR titration of d(5'-CGCGAATTCGCG-3')$_2$ exapnded on the region of the imino/amino protons of the bases.

Even if we speculate that the AATP is interacting in the region of the cytosines and guanines of the 12-mer duplex, it is not possible to describe in detail the interaction site due to the severe overlapping of the signals and the increased broadness of the spectrum. More information can be extracted from the NOESY spectrum that have been recorded with a mixing time τ_m of 400 ms (Figure 3.39). As reported before the NOESY spectra can be conveniently split into four areas. All the cross-peaks have been assigned following the usual strategy, obtaining a complete table of chemical shits. Differences in chemical shifts between the 12-mer itself and the 12-mer-AATP have been calculated and plotted

against the double strand residues (Figure 3.38).

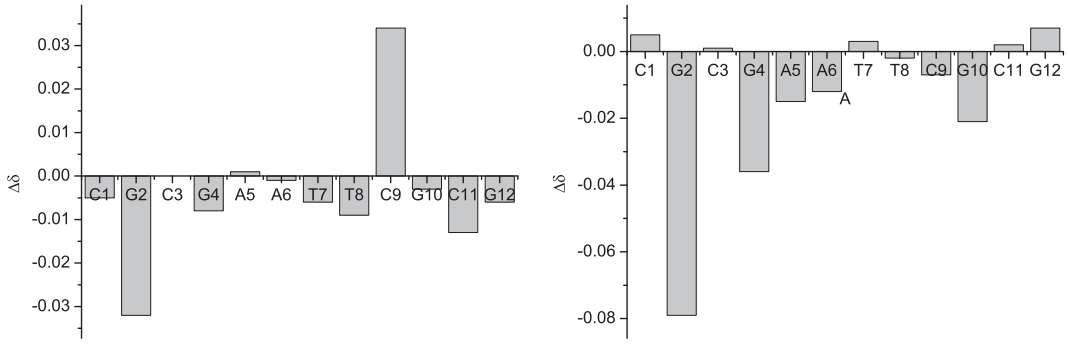

Figure 3.38: Chemical shift changes for selected base and deoxyribose protons (H1' on the left and H2" on the right); shifts to upfield region of the spectra have *negative* sign while the shifts to *downfield* region have positive sign.

Changes in chemical shifts are observed on the residues G3, G4 and on the complementary strand at C9 and G10. Thus according to the changes in chemical shifts a potential site of interaction for the AATP upon interaction with d(5'-CGCGAATTCGCG-3')$_2$ involves the G2 deoxyribose and the G4 sugar.

A better description of the intercalation site arises from the NOESY spectrum, where we expect to see the NOE couplings between the bases being interrupted by the intercalation of AATP.

In the first instance, the NOESY spectrum of d(5'-CGCGAATTCGCG-3')$_2$ appears more defined in the region of the diagonal spectrum. Thus, considering the chemical shift previously reported for AATP and the COSY spectra (Figure 3.36), we are able to distinguish the cross-peaks relative to the AATP residue from the oligonucleotides internal cross-peaks. Unfortunately due to the severe overlap between the terpyridine unit with the oligonucleotide main spectral diagonal, it was not possible to assign any NOE interaction between the terpyridine unit and the binding site on the oligonucleotide.

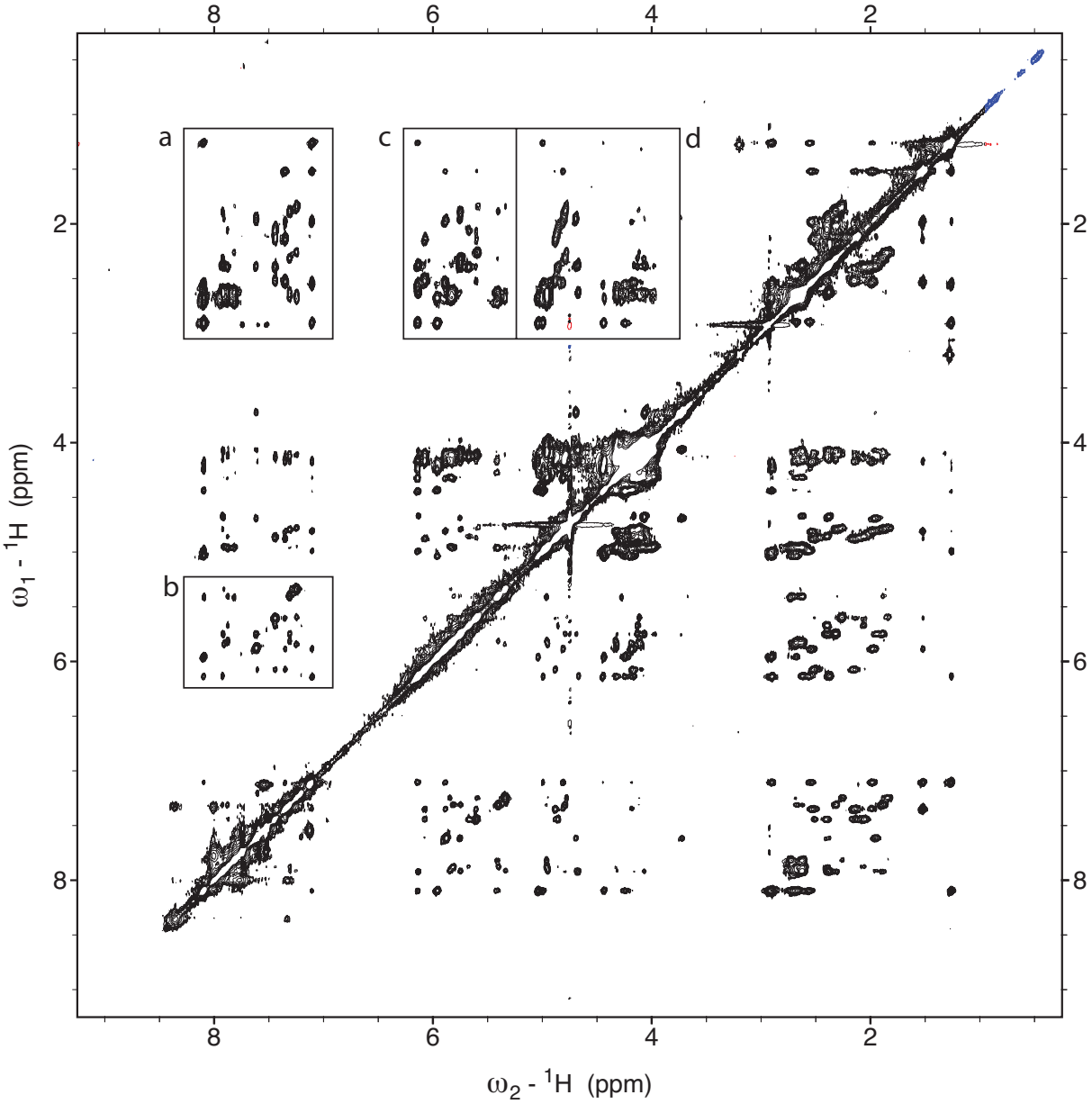

Figure 3.39: Contour plot of d(5'-CGCGAATTCGCG-3')$_2$ NOESY spectrum upon interaction with [AATP] using mixing time τ_m = 400 ms.

3.2.6.1 Area a: NOE couplings by H2" and H2'

Starting a detailed analysis of the NOESY spectrum in area a where NOE couplings arises from H2" and H2' of the sugars coupling with the DNA bases, we can see that interaction of the AATP with the 12-mer oligonucleotide is leading to a NOESY spectrum where some of the NOE couplings are missing.

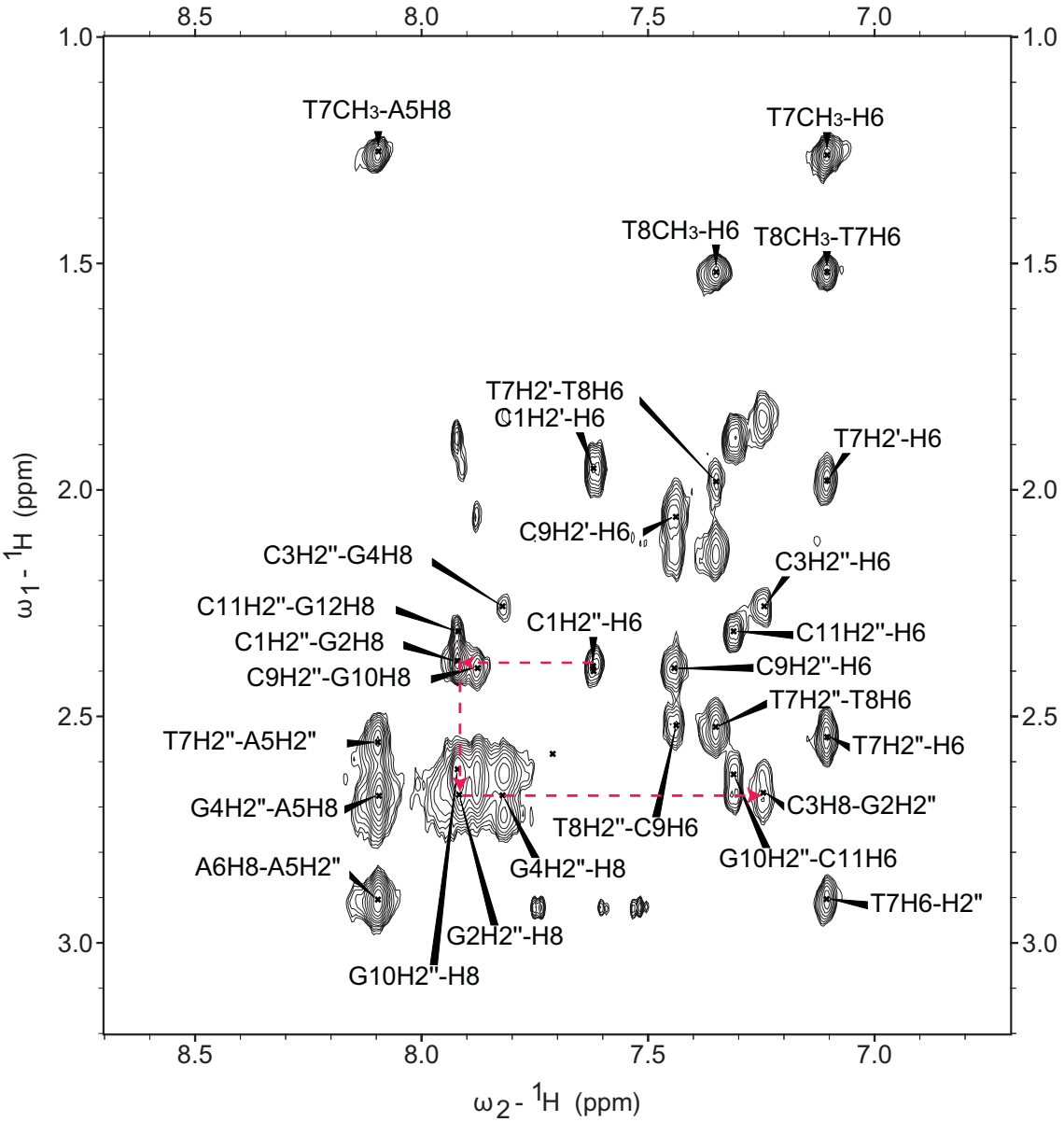

Figure 3.40: Expanded NOESY contour plot of the cross peaks between the GH8, CH6 region and the H2'-H2" and CH_3.

Starting at the established cross-peak between C1H6 and C1H2", we can follow a right hand NOE connectivity which allows us to assign all the cross-peak resonances with the exception of the missing NOE coupling between C3H6 and G4H8.

In particular from the spectrum in (Figure 3.40), it appears that the C3H2" is masked from interaction with G4H8. Because the C3H6 is still coupling with C3H2", the interaction with the metal complex seems to occur between the baseC3 and the immediate consecutive sugar unit of G4, which retains the NOE coupling with the A5H8. It was not possible to proceed with any evaluation in NOE

intensity (or volume) due to the severe overlap with the other guanines cross-peaks. If the intercalation on one strand occurs between C3 and G4, we should observe a NOE coupling with a reduced intensity for some of the couplings between C9 and G10 on the complementary strand. However in this part of the spectra we see that the C9H2" is still coupling with C9H6, while the coupling with the G10H8 is hard to evaluate because of the severe overlap.

3.2.6.2 Area b: NOE couplings by H1'

More information can be deduced using the region H1' of the NOESY spectrum (Figure 3.41), where no NOE connectivity was found between C3 and G4. In fact due to the intercalation of AATP the C3H1' does not display NOE coupling with the G4H8. Due to the employment of a self complementary 12-mer duplex a further disconnection was found between C9H1' and G10H8. In fact C9 and G10 are bases that are complementary to G4 and C3 respectively.

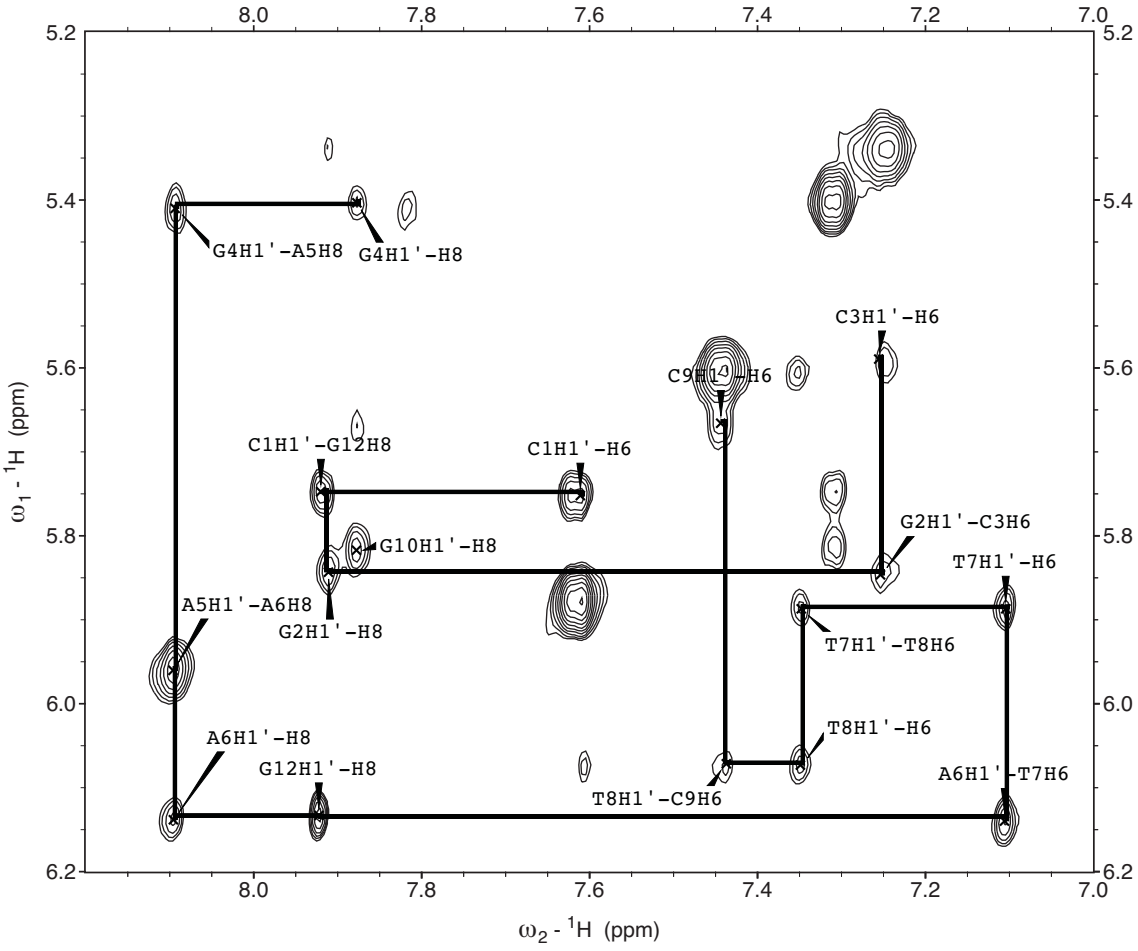

Figure 3.41: Expanded NOESY contour plot of the cross peaks between the GH8, CH6 region and the H1'.

The investigations on the NOESY spectrum are consistent with the explanation of AATP able to intercalate between the base pairs C3G4/C9G10; because we observe NOE interruption between C3/G4 and C9G10 we can argue the platinum terpyridine unit is lying parallel to the plane of the bases from both strands, which agrees with the X-ray data reported by Wang *et al*. using a similar complex to AATP ($[Pt(tpy)TPH]^{+}$) which was crystallised in between a base step of CpG dinucleotide (Figure 3.42).[36]

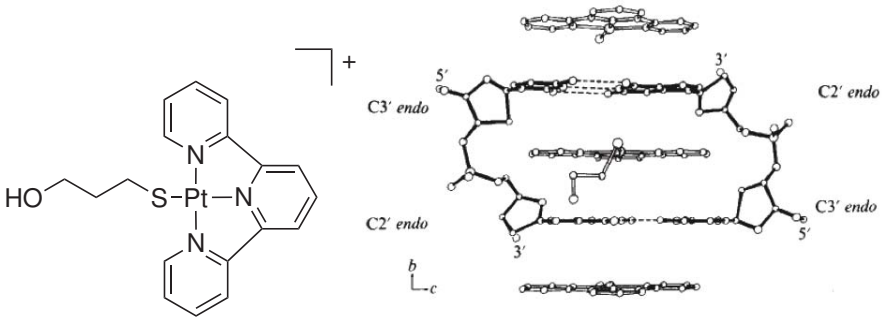

Figure 3.42: Structure of TPH on the left and crystal structure of the platinum terpyridine moiety intercalated in a CpG base step of a dinucleotide.

Based on a crystal structure of AATP previously reported[33] and a refined structure of the 12-mer oligonucleotides from the protein databank (PDB ID 1GIP), we can built a model of the interaction, which allows an estimations some of the possible NOE couplings between the binding site and the metal complex based on distances between nuclei in the model (Figure 3.43).

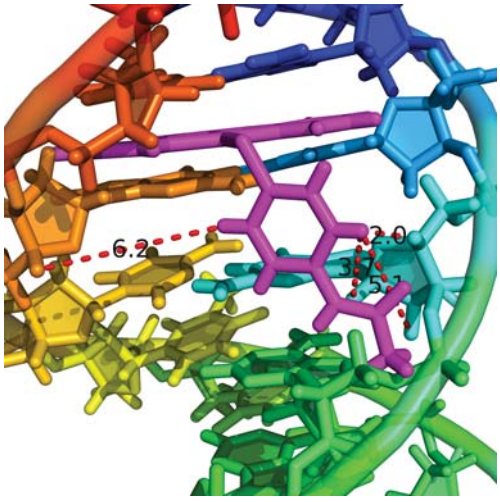

Figure 3.43: Model of the terpyridine intercalation based on image from the RCSB PDB[7] (www.pdb.org) of PDB ID 1GIP with AATP inserted in the intercalation site.

According to the NOE data where the intercalation of the AATP occurs from the major groove of the sequence, between C3 and G4 we can build a model where the platinum terpyridine is lying on the bases of the binding site. As a structural consequence we would observe the proton Hb arising from the 4'-amidothiophenol, having NOE coupling with the A6H2", A6H1' and A6H4' and consequently NOE interaction on the complementary strand, which involves T8H2", T8H1', T8H4'.

According to the ^{1}H-^{1}H COSY spectrum of AATP in water (see appendix to chapter 3, page 246), the figure 3.44 shows the aromatic region of the 12-mer oligonucleotide where the adduct with the AATP has its characteristic **Hb** at 7.5 giving NOE coupling with the vicinal **Ha**. Moving from Ha and Hb vertically to the H2", H2' region of the spectrum (area **a**) we found the **Hb** proton of the AATP unit having a clear NOE interaction with the A6H2", while for the proton **Ha** it was not possible to evaluate any NOE coupling because of the overlapped chemical shift with the T7H8.

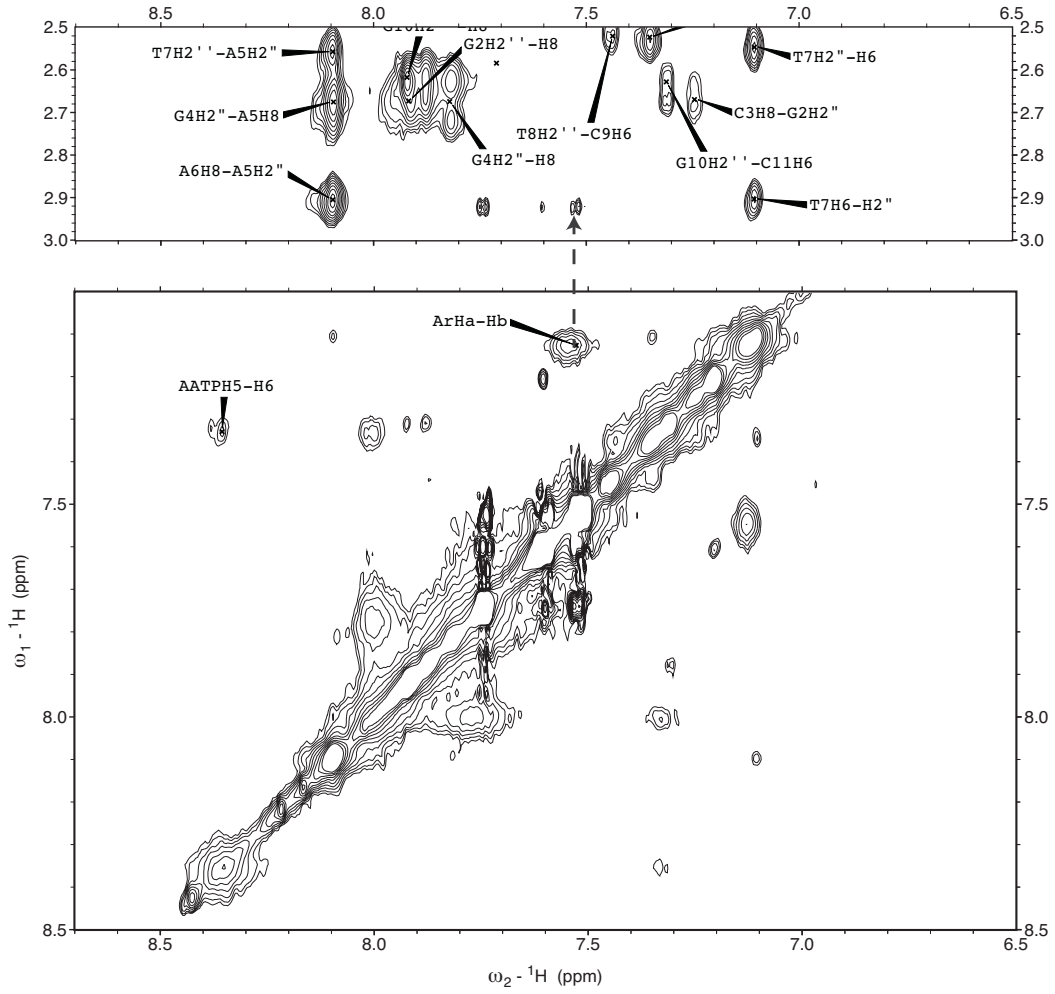

Figure 3.44: Model of the terpyridine intercalation based on image from the RCSB PDB[7] (www.pdb.org) of PDB ID 1GIP with AATP inserted in the intercalation site.

The NOESY spectrum did not show any NOE coupling between the T7CH_3 or T8CH_3 and the protons on the 4'-amidothiophenol, which allows us to speculate that when the platinum terpyridine complex intercalates from the major groove between C3 and G4, the 4-amido-thiophenol residue lies in the minor groove next to the binding site.

3.2.7 DNA binding studies by ^{31}P-NMR spectroscopy

A number of DNA sequences have been investigated by ^{31}P-NMR in order to understand the conformational changes.[37] Much of this work has been focused on the BI $\rightarrow$ BII transitions of the phosphate backbone. These conformations are defined by the ϵ and ζ, $C_{4'}$–$C_{3'}$–$O_{3'}$–P and $C_{3'}$–$O_{3'}$–P–O'_5, respectively, and the BI is the most common conformation in B DNA (Figure 3.45).[38]

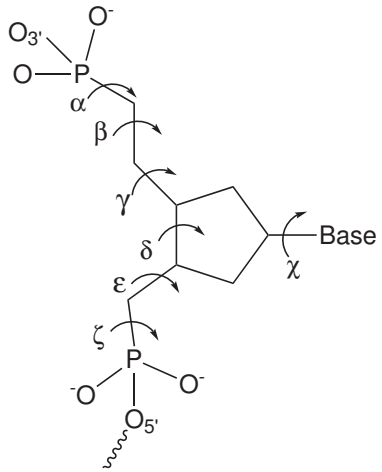

Figure 3.45: The backbone torsion angles in a unit nucleotide. Each rotatable bond is indicated by a curved arrow.

The phosphodiester backbone is the most flexible part of the DNA and it can be significantly distorted upon intercalation of small molecules such as [YPt_2]Cl_2 or AATP. There is good evidence that the factor that largely determines the chemical shift of ^{31}P NMR resonances is the phosphate ester torsional angle.[39] Figure 3.46 shows an overlay between the ^{31}P NMR of the d(5'-CGCGAATTCGCG-3')$_2$ oligonucleotide (bottom) and the 12-mer upon interaction with [YPt_2]Cl_2.

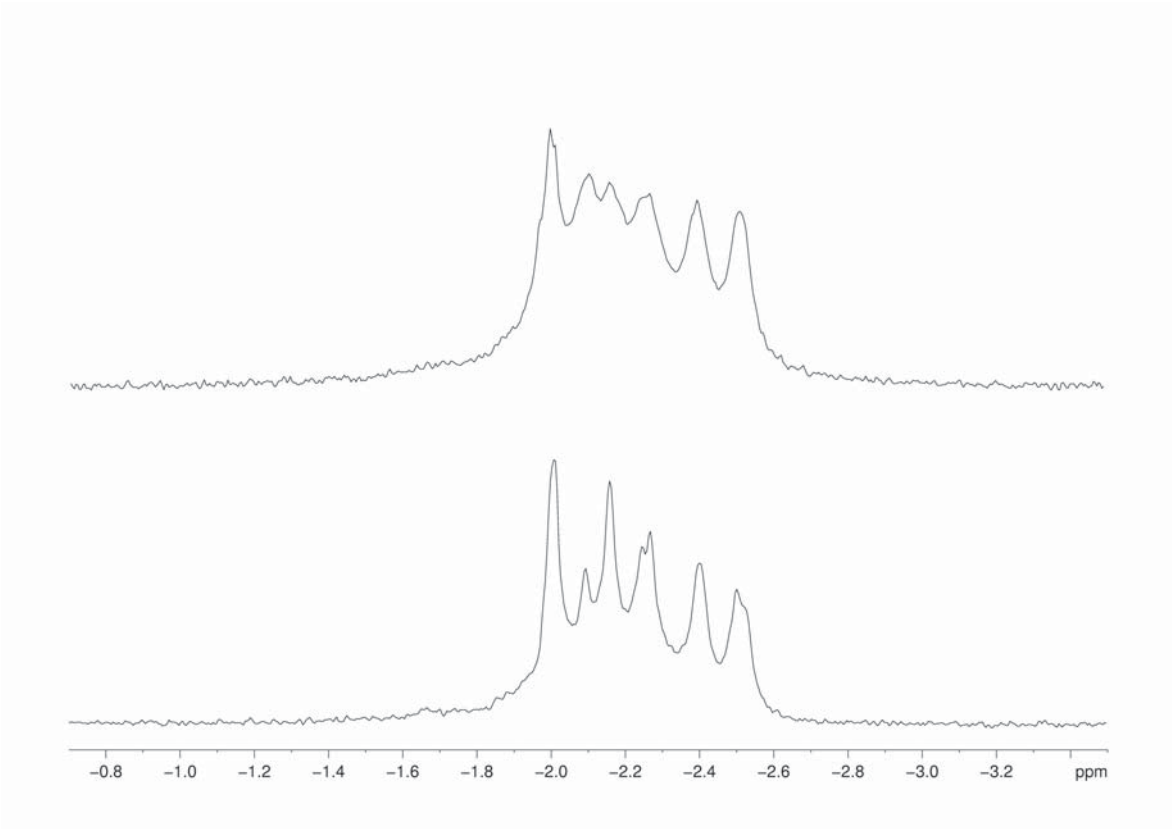

Figure 3.46: ^{31}P NMR of the free oligonucleotide (lower trace) and the $[YPt_2]Cl_2$ intercalated (upper trace). Chemical shifts are referenced to H_3PO_4. Experiment recorded at 27°C.

The intercalation of $[YPt_2]Cl_2$ between the bases of d(5'-CGCGAATTCGCG-3')$_2$, induces significant changes on the phosphate backbone of the duplex which lead to a 1D ^{31}P-NMR spectrum, where the resonance at -2.24 ppm shifts to -2.26 and the one from -2.39 to 2.40 ppm. The interaction of the metal complex with the 12-mer duplex induces one a further change to the ^{31}P NMR spectrum. Indeed, the intesity of the signal at -2.4 ppm increase upon addition of complex, while the resonance at -2.54 ppm is reduced. While the magnitude of the chemical shift depend on the relative positioning of the metal complex with respect to the duplex,[30] the shift to downfield of the signal at -2.54 is consistent with a transition from a conformation BI to a conformation BII.[38] This is consistent with a stiffening effect produced by the intercalation of the $[YPt_2]^{+2}$ between the 12-mer base pairs.

We performed the ^{31}P NMR experiment on the 12-mer duplex upon interaction with AATP and we recorded changes for the signal at -2.26 ppm, which in the presence of the metallo complex disappeared probably overlapping with the signal at -2.23 ppm. Chemical shifts to the upfield region of the spectrum are recorded for the signals at -2.39 and -2.49 which shift to -2.4 and -2.53 ppm

respectively (Figure 3.47).

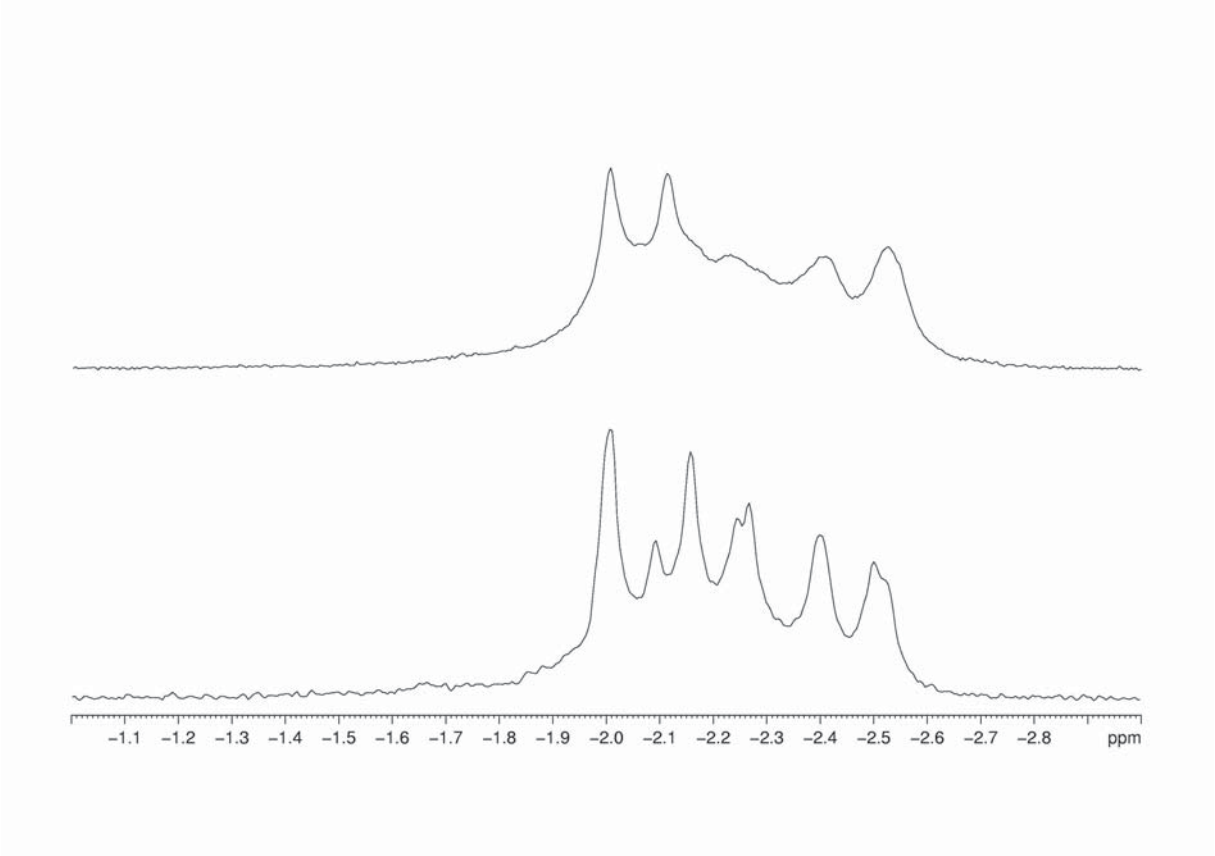

Figure 3.47: ^{31}P-NMR of the free oligonucleotide (lower trace) and the AATP intercalated (upper trace). Chemical shifts are referenced to H_3PO_4. Experiment recorded at 27°C.

Thus, upon interaction of the AATP with the 12-mer duplex we observe slighter bigger changes in chemical shifts than upon interaction with the $[YPt_2]^{+2}$, and an explanation can be found if the rigidity of the metal complexes is taken in account. The $[YPt_2]^{+2}$ is a rigid system compared to the AATP, and this can affect the intercalation process and consequently the magnitude of the chemical shifts. In first instance it is easier to accommodate the AATP than the $[YPt_2]^{+2}$ between the DNA base pairs. However due to the severe overlap of the signals is quite difficult to further speculate on the changes of the torsion angles and how they relate with the binding site.

3.2.8 Conclusions and Future work

In this chapter we have investigated the binding site of the heterometallic complex $[YPt_2]Cl_2$ upon interaction with the d(5'-CGCGAATTCGCG-3')$_2$ by ^{1}H-NMR. Following the results reported in the previous chapter, we have reinvestigated the Dickerson-Drew sequence and titrated it with $[YPt_2]Cl_2$. During the titration we observed changes in chemical shifts especially in the aromatic region for H8/H6 aromatic protons of the bases, which suggest a possible binding site involves the major groove of the sequence. The NOESY spectrum with a τ_m of 400 ms confirmed the bis-intercalation of $[YPt_2]Cl_2$ between C1/G2 and between G4/A5.

Evidence for the bis-intercalation binding of $[YPt_2]Cl_2$ arises also from the complementary strand, where the NOE pathway is interrupted in correspondence of the intercalation site.

The bases of the 12-mer contained between the metallo-intercalator unit, suffer a strong reduction of NOE coupling between the aromatic protons and the sugar; this is probably due to the stiffening effect produced on the 12-mer by the intercalation of $[YPt_2]Cl_2$. Indeed a previous study based on linear dichroism and ^{31}P-NMR showed that an important change is produced on the phosphate backbone of the 12-mer upon interaction with $[YPt_2]Cl_2$. Unfortunately due to severe signal overlap it was not possible in the case of $[YPt_2]Cl_2$ to assign any NOE coupling between the protons of the terpyridine units and the imino/amino protons of the bases in the oligonucleotide sequence.

Overall we can conclude, that the binding specificity of $[LnPt_2]$ observed upon interaction with a set of four oligonucleotides, is due to a combination of geometrics and rigidity of the complex with the distances offered from the 12-mer oligonucleotide. Due to a reduced thermodynamic stability of the π-π stacking between G4/A5 and T8/C9, we believe that this point of the sequence acts as a weak point to accommodate the intercalating unit from the rigid molecule $[YPt_2]Cl_2$; on the other side the second platinum terpyridine unit acts as an anchor unit making a thermodynamically favourite π-π stacking with the cytosines and the guanines of the binding site.[40] Since all the NOESY data has been collected using a mixing time τ_m at the maximum of the NOE enhancement, would be extremely useful in the future to employ this data for a restrained molecular dynamics modelling, which would describe the $[YPt_2]Cl_2$ intercalated between the base pairs with higher resolution.

Moreover the final results would yields more physical data, which would describe how the arms

interact independently when intercalated in the binding site.

New oligonucleotides should be designed and investigated, where the AT sequence is moved along the sequence, in order to weight the importance of this fragment as an attachment point on the sequence for the bis-intercalator and to investigate if the preference for the major groove binding is retained making the fluorescent [$LnPt_2$] have unique binding properties in its field.

3.3 Experimental

The DNA dodecamer d(5'-CGCGAATTCGCG-3')$_2$ with HPLC grade of purity was purchased from WG Eurofins and the D_2O 99.99% was provided by Cambridge Isotopic Inc.,while the metal complexes [YPt_2]Cl_2 and AATP were obtained following the synthetic reported in the previous chapter.

3.3.1 Sample Preparation for NMR Spectroscopy.

The oligonucleotide was buffered in 10 mM sodium phosphate, pD 7.2 (uncorrected for isotope effects) containing 10 mM NaCl. The DNA was annealed in the NMR tube by heating to 80 °C in a water bath, followed by cooling to room temperature over several hours. Sample concentrations were quantified by measuring the absorbance of a 1 mL solution at 260 nm (20 °C) and the final concentration calculated with the nearest neighbour principle.[41] All DNA and complexes samples were exchanged twice with D_2O (99.9%, Aldrich) and then made up to 550 μL with D_2O (99.96%, Aldrich). Stock solution of [YPt_2]Cl_2 and AATP were prepared using deuterated water and treated as DNA with three cycles of freeze drying. The final concentration was double checked by absorption spectroscopy. The titration was performed directly in the solvent and performed directly in the NMR tube by aliquots additions of stock solutions.

3.3.2 Acquisition of NMR Data

One-dimensional(1D) and NOESY spectra of the imino protons were acquired on a Bruker DRX 500 spectrometer, equipped with inverse probe. The sample temperature was regulated at 27 °C for all experiments in D_2O. The NOESY spectra in D_2O, with mixing times of 50, 100, 200, 300 400 and 500 ms, the TOCSY and ROESY spectra were collected without removing the sample from the spectrometer or changing any frequencies or gain settings. The pure absorption NOESY spectra were collected using the phase-sensitive methods STATES TPPI into 2048 complex points in $\omega 2$ and into 512 points in $\omega 1$. For each transient 32 scans were collected with a relaxation delay of 2.0 s between the transients. All the NOESY experiments in D_2O were carried out suppressing the residual resonance of the water peak using a partial CW water presaturation. Using the same settings the TOCSY and ROESY spectra were recorded using a mixing time of 100 ms. ^{31}P-NMR were

recorded using 512 scan and proton decoupling and referencing it to the chemical shift of the H_3PO_4.

The 1D NMR titrations were carried out for each complex with the 12-mer oligonucletode. The metal complexes were added in aliquots to oligonucleotide samples in the NMR tube to a maximum complex : duplex ratio (R) of 0.5. The complex was added in increments of 0.1 molar equiv, and a ^{1}H NMR spectrum was recorded after each addition. Temperatures were held constant throughout the course of the titrations and are specified in the relevant figure captions for each experiment. For the final high-R solution, 2D NOESY (τ_m = 100 - 400 ms), TOCSY and ROESY (τ_m = 100 ms) spectra were collected.

3.3.3 Data Processing

All the raw data and the one ^{1}H-NMR were processed using Bruker TOP SPIN 2.1 running on x32 Intel based workstation, which was employed for Fourier transform and phasing of the spectra. All the NOESY and TOCSY cross-peaks were assigned using SPARKY NMR 3.1, which is a free software specifically designed for NMR of proteins and oligonucleotides. All the chemical shifts values were obtained during the NOESY spectra assignment as an average of at least four single chemical shifts, and finally automatically reported in a correlation table of chemical shifts. All the intensity of NOE couplings were evaluated as manual integral of the NOE cone and then fitted using the Gaussian fit function of SPARKY.[42]

References

[1] Wuthrich, K.; Wider, G.; Wagner, G.; Braun, W. *J. Mol. Biol.* **1982**, *155*, 311.

[2] Scheek, R. M.; Boelens, R.; Russo, N.; Boom, J. H. V.; R.Kaptein, *Biochemistry* **1984**, *23*, 1371.

[3] Martinez, R.; Chacon-Garcia, L. *Curr. Med. Chem.* **2005**, *12*, 127–151.

[4] Jacobsen, J. P.; Pedersen, J. B.; Hansen, L. F.; Wemmer, D. E. *Nucleic Acids Res.* **1995**, *23*, 753.

[5] Braunlin, W. H.; Anderson, C. F.; Record, M. T. *Biopolymers* **1986**, *25*, 205.

[6] Padmanabhan, S.; Brushaber, V. M.; Anderson, C. F.; Record, M. T. *Biochemistry* **1991**, *30*, 7550–7559.

[7] Berman, H.; Westbrook, J.; Feng, Z.; Gilliland, G.; Bhat, T.; Weissig, H.; Shidyalov, I.; Bourne, P. *Nucleic Acid Res.* **2000**, *28*, 235.

[8] Blake, A.; Peacocke, A. R. *Biopolymers* **1961**, *6*, 1125.

[9] Fkyerat, A.; Demeunynck, M.; Michon, J. F. C. P.; Lhomme, J. *J. Am. Chem. Soc.* **1993**, *115*, 9952.

[10] Coppel, Y.; Constant, J. F.; Coulombeau, C.; Demeunynck, M.; Garcia, J. *Biochemistry* **1997**, *36*, 4831.

[11] Robinson, H.; Priebe, W.; Chaires, J. B.; Wang, A. H. *Biochemistry* **1997**, *36*, 8663.

[12] Collins, J. G.; Shieldsand, T. P.; Barton, J. K. *J. Am. Chem. Soc.* **1994**, *116*, 9840.

[13] Eriksson, M.; Leijon, M.; Hiort, C.; Norden, B.; Graslund, A. *Biochemistry* **1994**, *33*, 5031.

[14] Hudson, B. P.; Dupureur, C. M.; Barton, J. K. *J. Am. Chem. Soc.* **1995**, *117*, 9379.

[15] Zeglis, B. M.; Pierre, V. C.; Barton, J. K. *Chem. Commun.* **2007**, 4565.

[16] Franklin, S. J.; Barton, J. K. *Biochemistry* **1998**, *37*, 16093.

[17] Collins, J. G.; Aldrich-Wright, J. R.; Greguric, I. D.; Pellegrini, P. A. *Inorg. Chem.* **1999**, *38*, 5502.

[18] Waywell, P.; Gonzalez, V.; Gill, M. R.; Adams, H.; Meijer, A. J. H. M.; Williamson, M. P.; Thomas, J. A. *Chem. Eur. J.* **2010**, *16*, 2407.

[19] Baruah, H.; Wright, M. W.; Bierbach, U. *Biochemistry* **2005**, *44*, 4138.

[20] Choudhury, J. R.; Bierbach, U. *Nucleic Acids Res.* **2005**, *33*, 5622.

[21] Baruah, H.; Bierbach, *Nucleic Acids Res.* **2003**, *31*, 4138.

[22] Wing, R.; Drew, H.; Takano, T.; Broka, C.; ad K. Itakura, S. T.; Dickerson, R. E. *Nature* **1980**, *287*, 755.

[23] Sapienza, P. J.; Rosenberg, J. M.; Jen-Jacobson, L. *Structure* **2007**, *15*, 1368.

[24] Brevard, C.; Granger, P. *Handbook of high resolution multinuclear NMR*; Wiley New York, 1981.

[25] Hare, D. R.; Wemmer, D. E.; Chou, S. H.; Drobny, G.; Reid, B. R. *J. Mol. Biol.* **1983**, *171*, 319.

[26] Pardi, A.; Morden, K. M.; Patel, D. J.; Tinoco, I. *Biochemistry* **1983**, *22*, 1107.

[27] Deva, P. U.; Alexander, D. M. *J. Am. Chem. Soc.* **2006**, *128*, 678.

[28] Feigon, J.; Denny, W. A.; Leupin, W.; Kearns, D. R. *Biochemistry* **1983**, *22*, 5930.

[29] Nerdal, W.; Hare, D. R.; Reid, B. R. *Biochemistry* **1989**, *28*, 10008.

[30] Teng, Q. *Structural biology : practical NMR applications*; Springer New York, 2005.

[31] Claridge, T. D. W. *High-resolution NMR techniques in organic chemistry*; Pergamon, 1999.

[32] Kalk, A.; Berendsen, H. J. C. *J. Magn. Reson.* **1976**, *24*, 343.

[33] Glover, P. B.; Ashton, P. R.; Childs, L. J.; Rodger, A.; Kercher, M.; Williams, R. M.; Cola, L. D.; Pikramenou, Z. *J. Am. Chem. Soc.* **2003**, *125*, 9918.

[34] Arena, G.; Scolaro, L. M.; Pasternack, R. F.; Romeo, R. *Inorg. Chem.* **1995**, *34*, 2994.

[35] Jennette, K. W.; Gill, J. T.; Sadownick, J. A.; Lippard, S. J. *J. Am. Chem. Soc.* **1976**, *98*, 6159.

[36] Wang, A. H. J.; Nathans, J.; Vandermarel, G.; Vanboom, J. H.; Rich, A. *Nature* **1978**, *276*, 471.

[37] (a) Bax, A.; Lerner, L. *J. Magn. Reson.* **1988**, *79*, 429; (b) Mauffret, O.; Hartmann, B.; Convert, O.; Lavery, R.; Fermandjian, S. *J. Mol. Biol.* **1992**, *227*, 852; (c) Dingley, A. J.; Peterson, R. D.; Grzesiek, S.; Feigon, J. *J. Am. Chem. Soc.* **2005**, *127*, 14466.

[38] Tian, Y.; Kayatta, M.; Shultis, K.; Gonzalez, A.; Mueller, L. J.; Hatcher, M. E. *J. Phys. Chem. B* **2009**, *113*, 2596.

[39] Ott, J.; Eckstein, F. *Biochemistry* **1985**, *24*, 2530.

[40] Packer, M. J.; Hunter, C. A. *J. Mol. Biol.* **1998**, *280*, 407.

[41] Arshinoff, B. I.; Suen, G.; Just, E. M.; Merchant, S. M.; Kibbe, W. A.; Chisholm, R. L.; Welch, R. D. *Nucleic Acids Res.* **2007**, *35*, 422.

[42] Goddard, T. D.; Kneller, D. G. *SPARKY NMR Software, University of California (San Francisco)*

Chapter 4

Lanthanide bis-intercalators based on platinum acetylide moiety.

4.1 Introduction

Transition metal complexes have been used as photosensitisers in energy conversion and extensively studied in order to develop luminescent sensors. In particular the square planar nature of d^8 Pt(II) complexes have properties that are not available to d^6 metal complexes.[1] For example the d^8 complexes are characterised by axial intermolecular interactions, and in many cases they being responsible for leading to unique photophysical properties such as the formation of excimers. Thus, several groups have turned their attention on the photophysical properties of the platinum(II) terpyridine (Pt-tpy) complexes, bearing an acetylide group as co-ligand (Figure 4.1).

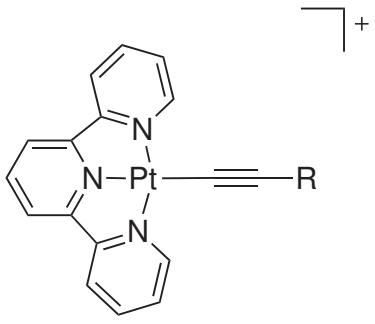

Figure 4.1: Generic structure of $[Pt(tpy)(C{\equiv}CR)]^{+1}$.

Indeed, the use of acetylide based moieties as co-ligands introduces a number of advantages:

- the large spin-orbit coupling of Pt(II) improves the singlet-triplet intersystem crossing and luminescence efficiency
- the strong ligand field properties of acetylide leads to a high energy gap of the $d-d$ transitions
- the p_π-orbitals of the acetylide ligand mix with the d_π(Pt) orbitals through π-conjugation, which facilitates charge migration and energy transfer.

However, despite all of the photophysical investigations, the Pt-tpy application as a metal drug or its use as a luminescent probe in biology still remain sparse.[2]

4.1.1 Photophysical properties of Pt-tpy acetylide complexes

The Pt-tpy complexes have been known since 1934[3] and their derivatives have been widely investigated.[4] Due to their intriguing photophysical properties such as a relatively long lifetime (order of μs), particular attention was given to platinum(II) diimine acetylide complexes. In 2001 Schanze and co-workers reported few examples of platinum diimine complexes bearing an aryl acetilide as coligand (Figure 4.2).[5][6]

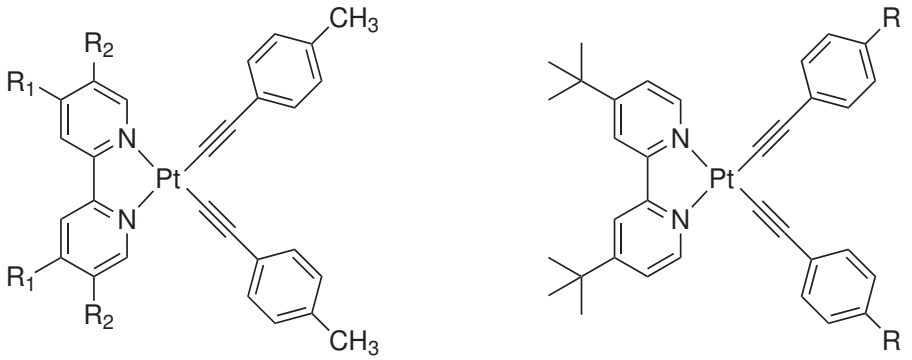

1

a: $R_1 = R_2 = CH_3$
b: $R_1 = RC(CH_3)_3$, $R_2 = H$
c: $R_1 = C(O)NEt_2$, $R_2 = H$
d: $R_1 = COOEt$, $R_2 = H$

2

a: $R = CF_3$
b: $R = NO_2$
c: $R = NMe_2$
d: $R = OCH_3$

Figure 4.2: Examples of luminescent platinum diimine complexes bearing an aryl acetilide as coligand.

The results of this study reveal that in most cases the photophysics of the complexes is dominated by the energetically low lying Pt→bpy ^{3}MLCT state. Some of the complexes also feature a low-lying intraligand (IL) $\pi \rightarrow \pi*$ excited state that is derived from transitions localized largely on the aryl acetylide ligands.

Since the original report of [Pt(phen)(C≡CPh)$_2$] (Figure 4.3) by Che and coworkers in 1994[7], the number of related platinum(II) acetylide complexes with a polyimine ligand has enormously expanded.[6] However in some cases the use of bypiridine ligands may be responsible for the thermal activation of $d-d$ transitions which provide a facile non-radiative deactivation pathway (see chapter 1 page 13). With the use of terpyridine as a polyimine ligand, it is possible to increase the structural rigidity of the platinum(II) complex, thus minimising the non-radiative decay, typically associated with the distortion of the complex.[8] [6]

The acetylide ligand allows to tune the photoluminescence properties by raising the HOMO of the metal centre and consequently reducing the energy level of the MLCT excited state. Moreover, the acetylide based co-ligands are strong σ and π donors that are able to raise the energy of the *d* orbitals, higher in energy than the ^{3}MLCT, which will decay by a luminescent pathway.[9]

Yam *et al*. have reported some of the luminescent complexes in this research field. They were the first to present the luminescence of [Pt(phen)(C≡CPh)$_2$]$_2$ and [Pt(tpy)(C≡CPh)] (**4**), that were luminescent in solution at room temperature (Figure 4.3).[10]

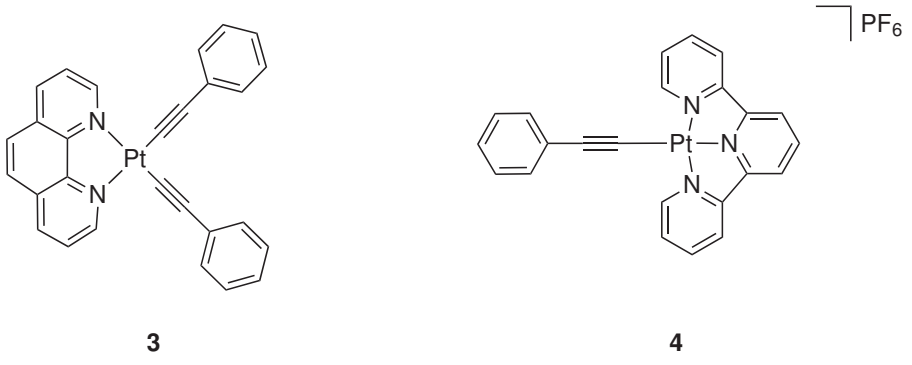

3 **4**

Figure 4.3: Structure [Pt(phen)(C≡C-Ph)$_2$] (**1**) and [Pt(tpy)(C≡CPh)]PF$_6$ (**2**).

In their first study of complexes of this type, Yam and co-workers prepared [Pt(tpy)(C≡CPh)]$^+$ salts with a range of para substituted aryl groups.[10] The emission energies follow the trend that would be expected for luminescence from a ^{3}MLCT state; e.g., the energies in MeCN solution at RT

decrease in the order Ph = -$C_6H_4NO_2$ > -C_6H_4Cl > -C_6H_5 > -C_6H_4Me, as the electrondonating power of the acetylide substituent increases (Figure 4.4 **a-e**). This was reinforced by the results obtained from theoretical studies using by TD-DFT calculations.[11,12]

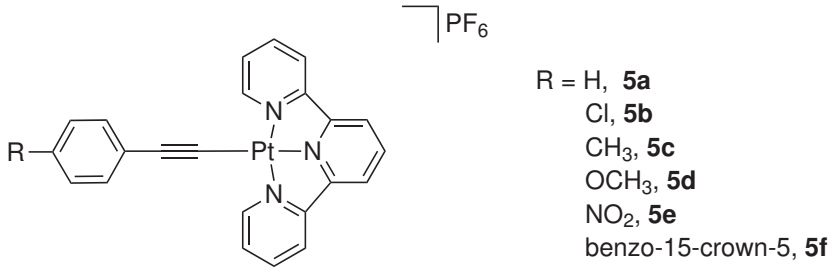

R = H, **5a**
Cl, **5b**
CH_3, **5c**
OCH_3, **5d**
NO_2, **5e**
benzo-15-crown-5, **5f**

5

Figure 4.4: Early Pt(II) acetylide complexes exhibiting luminescence in solution designed by Yam and coworkers.[10]

Castellano and co-workers have used a Pt-(tpy) acetylide platform to introduce tert-butyl substituents on the terpyridine ligand, in order to obtain complexes that would be soluble in non-polar solvents such as dichloromethane (Figure 4.5). Interestingly, they showed that the complexes exhibit bright photoluminescence with an excited state lifetime in the range of μs. It was demonstrated that the nature of the acetylide co-ligand plays a key role in modulating the luminescent properties of these complexes. The tert-butyl substituent that was initially introduced for solubility reasons, was found to play an important role, making the charge delocalisation upon excitation of the complex more favourable.[13]

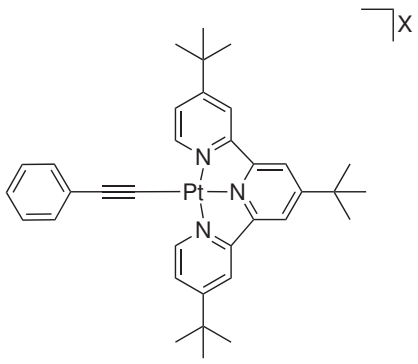

X = BF_4 , PF_6

6

Figure 4.5: Structure of [Pt(tpy)(tert-Bu)(C≡CPh)]X (X = BF_4, PF_6).

Tung *et al*. demonstrated that substitution on the terpyridine ligand together with tuning the electron density of the acetylide co-ligand, enhances the excited-state lifetime and the luminescence quantum yield of the terpyridylplatinum(II) derivatives. An example is the 4'-tolyl-terpyridines used in conjuction with different alkyl and aryl acetylide substituents, that rendered complexes with relatively high luminescence quantum yields (Figure 4.6).[14]

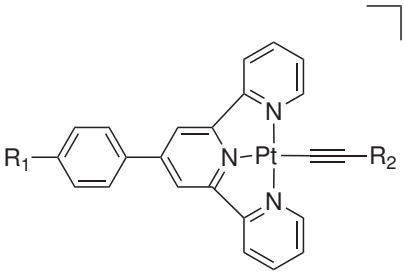

7

a R_1 = p-tolyl, R_2 = CH_2OH

b R_1 = p-tolyl, R_2 = n-propyl

c R_1 = p-tolyl, R_2 = C_6H_4Cl

d R_1 = p-tolyl, R_2 = C_6H_5

e R_1 = p-tolyl, R_2 = $C_6H_5CH_3$

f R_1 = H, R_2 = C_6H_5

Figure 4.6: Structure of [Pt(tpy−tolylil)(C≡CPh)]ClO_4.

Recently, photophysical and DFT studies of Pt-tpy acetylide complexes, were reported from Che *et al*. which showed the effects of substitutions on the terpyridine and on the acetylide moiety on the absorption and emission spectra.[15] In agreement with previous studies,[12,11] Che rationalised that aryl-acetylide ligands with electron-withdrawing substitutions are responsible for the increase in energy of the ^{1}MLCT and ^{1}LLCT transitions. On the other hand when strong electron-donating groups are used, the two energy levels are lowered followed by an increase of the energy gap between them. As mentioned before (see Chapter 1) the electron-donating groups are able to modify the energy

of the $d - d$ transitions as well. When a strong electron-donor is used the *d* orbitals are destabilised in energy, and if the electron-donating effect is strong enough the *d* orbitals can go higher in energy than the ligand excited state. This situation is the most suitable in order to obtain the ^{3}MLCT a the luminescent excited state.[15]

Despite all this work, the photophysical processes occurring in the terpyridylplatinum(II) acetylide complexes are still not fully understood, due to the overlapping of several photophysical processes that can compete with the luminescence from the ^{3}MLCT of the platimun(II) terpyridine.

4.1.2 Luminescent sensors based on Pt-tpy acetylide

Based on the previously reported photophysical properties, several luminescent sensors have been isolated that behave as 'switch on' metal complex. The general strategy is to derive a fluorescent terpyridylplatinum(II) complex with a binding site able to quench the platinum fluorescence when no substrate is bound to it. An example of this application is the fluorescent sensor for metal ions proposed by Yam *et al*. (Figure 4.7).[16]

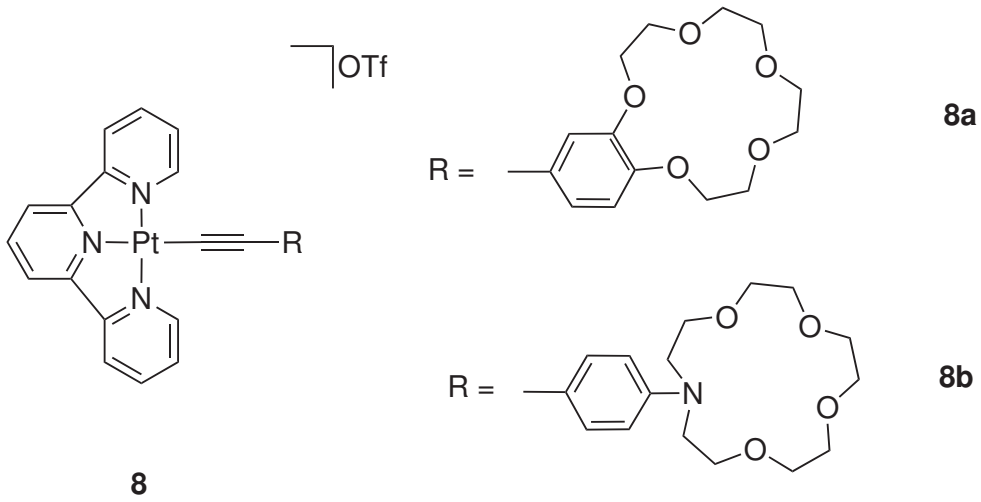

Figure 4.7: Luminescent sensor for metal ions by Yam *et al*..[16]

The complex shows an intense, low energy absorption band in solution, around 550 nm, which is attributed to a low-lying excited state of LLCT state. It is presumed that this state is able to deactivate the ^{3}MLCT state *via* non-radiative decay. In the event of Mg^{2+} or Ca^{2+} binding to the benzo-15-crown-5, the LLCT band is raised in energy and hence the luminescence is switched on.

Tung *et al*. also reported luminescent platinum(II) terpyridine complexes where the modulation of the charge transfer state could be obtained by the control of the solution pH. Furthermore they also investigated how an aromatic substituent on the 4' position of terpyridine can contribute to an increased stabilisation of the excited state, delocalising the hole generated during the irradiation of the complex (Figure 4.8).[17]

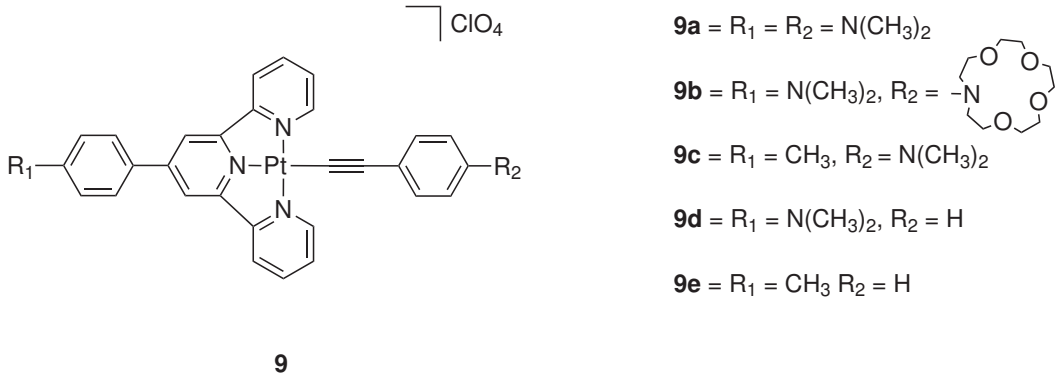

Figure 4.8: Amino derivatives used to monitor pH changes and detect metal ions.

The absorption spectra show that when the amino groups of the platinum co-ligand are protonated, the lowest energy excited state is switched from the LLCT to the MLCT and as a consequence luminescence is observed.

4.1.3 Luminescent heteronuclear complexes based on platinum acetylide

Taking advantage of the tunable photophysical properties of the Pt-tpy complexes, a series of transition metal complexes have been created with potential application in the optoelectronic field.[18] Particularly active in this field are Ziessel and coworkers, who have designed a Pt-tpy acetylide motif in order to develop bimetallic complexes of Fe(II) and Zn(II) (Figure 4.9).[19] [20]

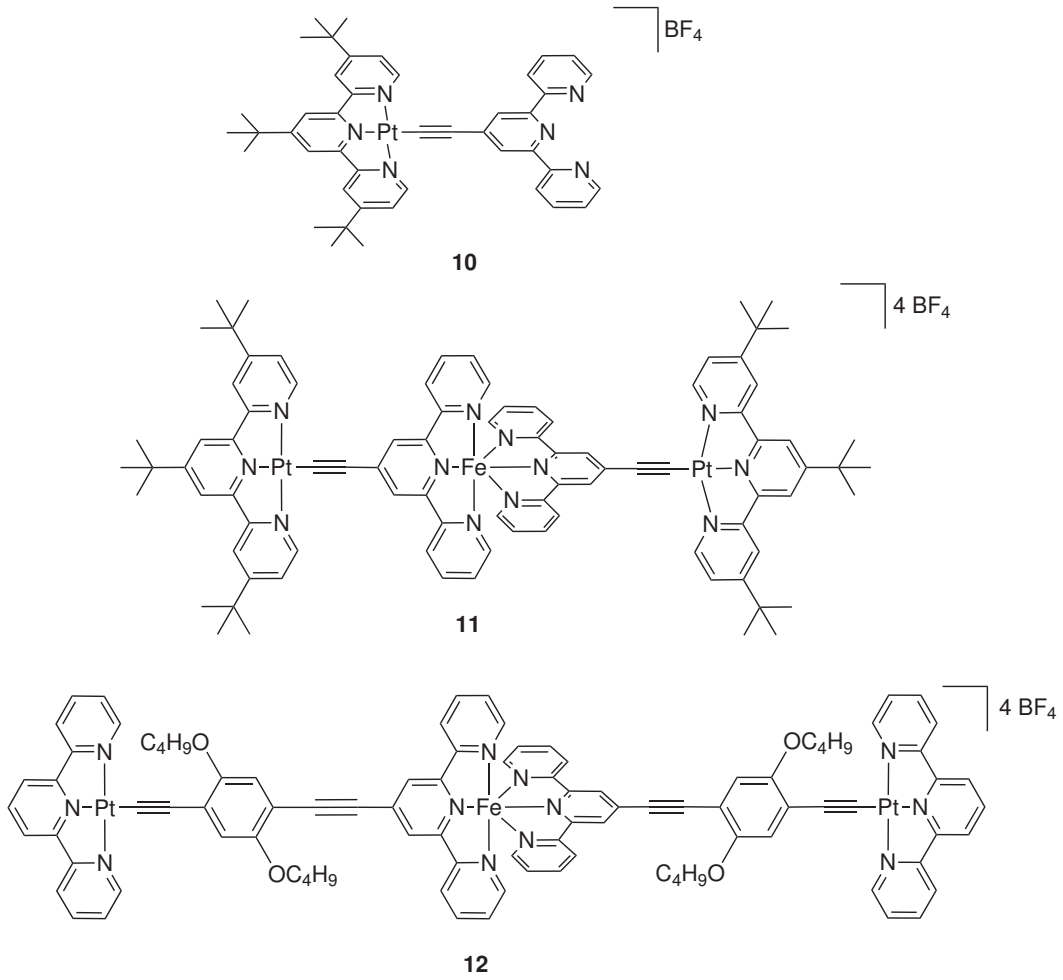

Figure 4.9: Heterometallic complexes containing $[Pt(tpy)_2(C{\equiv}C)]^+$ units developed by Ziessel *et al*.

The photophysical studies of these complexes showed that the fluorescence of complex **10** arising from the ^{3}CT becomes quenched by a favoured non-radiative decay pathway when the Fe(II) is co-ordinated to give complex **11**. The decay of the ^{3}CT by a non radiative pathway is in agreement with the presence of the low lying Fe-based ligand-field states which provide an efficient non radiative deactivation. Indeed luminescence was observed when a d^{12} metal such as Zn(II) was coordinated to the terpyridine moieties; thus the excited state generated was still a ^{3}CT, with the Zn(II) simply acting as a Lewis acid.[21]

In 2007 Ziessel and coworkers proposed a ligand for lanthanides where a terpyridylplatinum(II) acetylide motif was introduced as an antenna system to sensitise visible and NIR emitting lanthanides (Figure 4.10). The hexafluoroacetylacetonate was used in order to fully coordinate the lanthanide ion and avoid any quenching arising from the interaction with the solvent.[22]

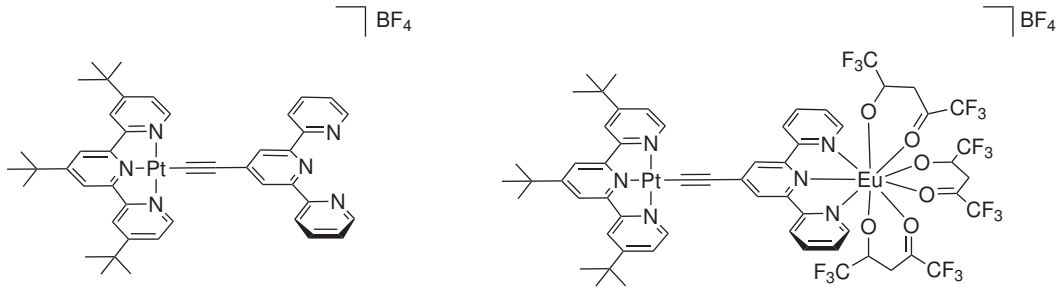

13 14

Figure 4.10: Structures of [PtLEu(hfac)$_3$]BF_4.

The complex **13** shows a platinum based emission upon excitation of the CT band. However in the presence of the Eu(III) the energy transfer from the ^{3}MLCT to the $^5D_0$ becomes the most efficient process, followed by lanthanide based luminescence. In 2009 the same group proposed a new ligand (**15**) based on the same scaffold of complex **13** which does not require any free ligand as the hexafluoroacetylacetonate fully coordinates the lanthanide ion (Figure 4.11).[23] Photophysical studies performed on complex **16** showed the ability of the ^{3}CT to sensitise the europium luminescence.

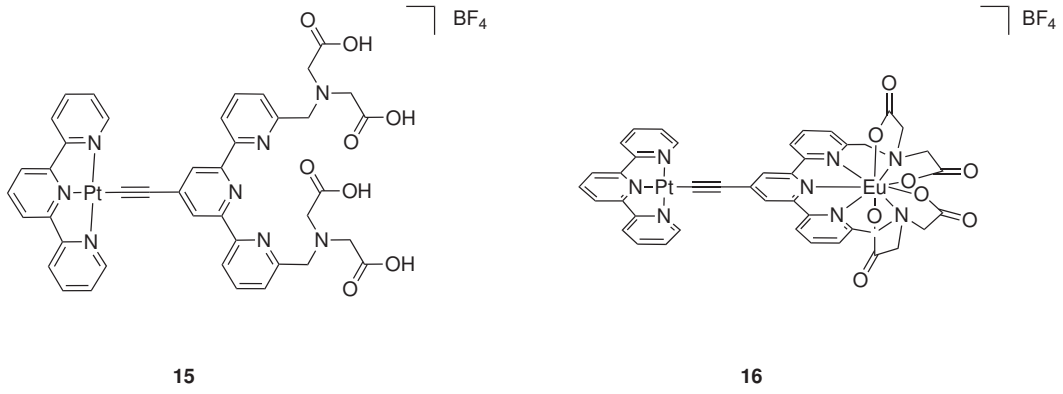

15 16

Figure 4.11: Structures of [Pt(tpy)L$_2$Eu]BF_4.

4.1.4 Terpyridylplatinum(II) acetylide complexes of biological interest

The Pt-tpy acetylide motifs are also attractive for biomolecule labelling as their long emission lifetimes mean that gated detection can be employed to suppress biological fluorescence. In fact, the longer wavelengths of light required to excite such complexes are ideal for use with biological samples as the lower energy reduces the effects of photo-degradation.

Yam and coworkers have developed a platinum(II) terpyridine complex bearing an acetylide motif functionalised with thiocyanate (**17a**) or iodoacetamide (**17b**) for protein labelling (Figure 4.12).[24]

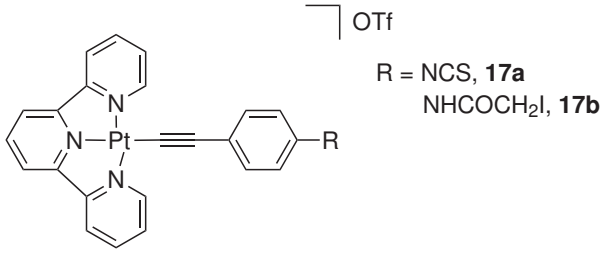

17

Figure 4.12: Strucure of [Pt(tpy)(tert-Bu)(C≡C-R)]OTf (R = NH_2, NCS, $NHCOCH_2I$).

Photophysical studies performed on complexes **17a** and **17b** in degassed acetonitrile, demonstrated that the strong luminescence, was arising from the dπ(Pt)$\rightarrow\pi^*$(^{t}Bu$_3$tpy) ^{3}MLCT excited state with some contribution from a π(C≡CR)$\rightarrow\pi^*$(tpy-^{t}Bu$_3$) ^{3}LLCT. Both bioconjugates retained luminescent properties but exhibited changes upon protein labelling. Complex **15a** gave a different luminescence colour to the derivative whereas **17b** displayed an increase luminescence in intensity when conjugated to the protein.

Pikramenou and co-workers in collaboration with Ziessel have developed a cyclodextrin(CD) platinum(II) terpyridine acetylide complex which, in dichloromethane, showed emission centred at 545 nm with a quantum yield (Φ) of 0.032% and a lifetime (τ) of 7.5 μs, in line with complexes bearing the same motif.[13] The DNA binding studies performed by linear and circular dichroism and gel electrophoresis, showed that the intercalative properties of the platinum(II) terpyridine moiety were retained and when the complex is placed in water it acts as a ”switch on” complex upon interaction with DNA (Figure 4.13).[25]

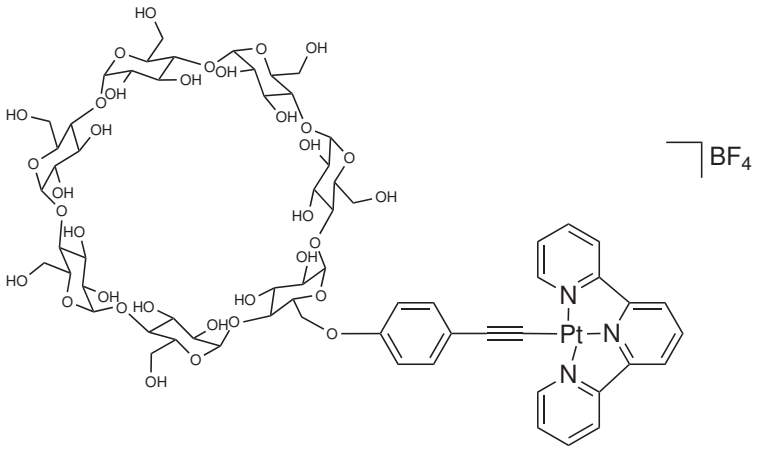

18

Figure 4.13: The structures of the [Pt(tpy)(tert-Bu)(C≡C)]BF_4 complexes with β-cyclodextrin attachments from Pikramenou *et al*.

Che and coworkers have isolated a group of water soluble platinum terpyridine metallo-intercalators for DNA recognition (Figure 4.14).[26] The photophysical properties of these complexes were examined upon interaction with DNA, followed by further examination of their cytotoxicity against cancer cells.

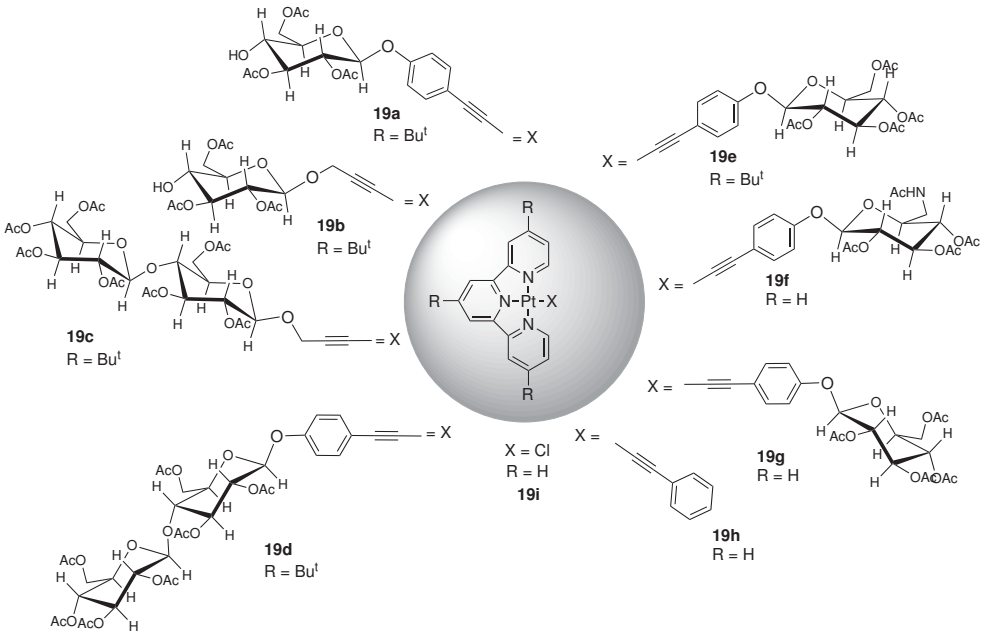

Figure 4.14: Structures of glycosylated [Pt(tpyR_3)X designed by Che and coworkers.[26]

Derivatives **19a**, **19d** and **19e** bearing an aryl acetylide group, were all emissive in aqueous solutions, while **19g** demonstrated an eight fold increase in emission intensity after the addition of CT-DNA. All Pt(II)-glycosylated arylacetilide complexes were found to have higher cytotoxic activity

against human cancer cells than cisplatin whereas the other derivatives did not.

In 2009 Hannon and co-workers reported a novel class of terpyridylplatinum(II) complexes bearing an acetylide derivatised steroid as the fourth position ligand. A set of terpyridylplatinum(II) steroids derivatives were isolated and tested against the ovarian cancer cell lines (T-47D) (Figure 4.15).[27]

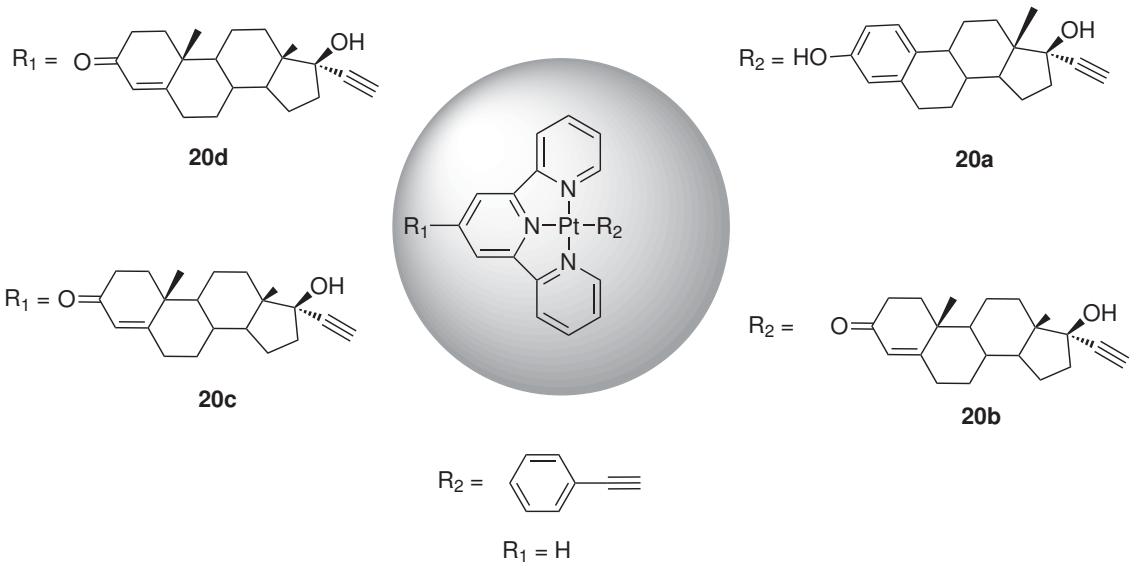

Figure 4.15: Set of steroidal and non steroidal terpyridine intercalators.

Coupling the steroidal moiety to the platinum(II) terpyridine moiety, they found that the final complex had a reduced cytotoxic activity when compared to the active non-steroidal compounds, that may be related to the interaction with proteins located in the cell cytoplasm. However complex **20a** and **20b** were found to be more active than **20c** and **20d**, demonstrating that the ability to intercalate between DNA bases was of high importance. In fact complexes **20c** and **20d** did not show any intercalative properties when studied with DNA by LD.

4.1.5 Project overview

The aim of this chapter is to develop a new high luminescent heterometallic complex [LnC≡CPt$_2$] $(CH_3SO_3)_2$ that interacts with DNA *via* an intercalative mode, and thus exploit it as a luminescent label for DNA recognition. The [LnC≡CPt$_2$]$(CH_3SO_3)_2$ retains the hairpin geometry, while new photophysical properties like the sensitisation of lanthanide luminescence with visible light can be activated (Figure 4.16).

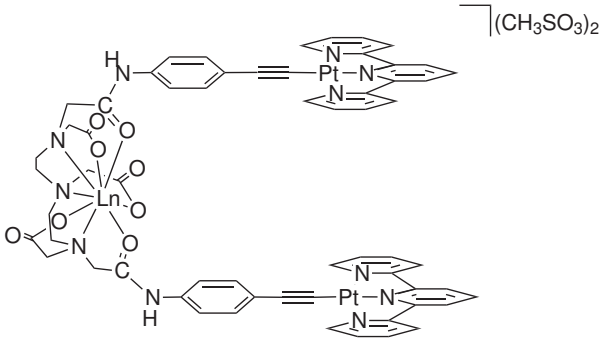

Figure 4.16: Structure of [LnC≡CPt$_2$]$(CH_3SO_3)_2$.

As seen in chapter 2, the LLCT transition relative to the Ph–S$^-$→tpy* is responsible for the partial quenching of the lanthanide emission in [LnPt$_2$] by back energy transfer. Herein we want to take advantage of a strong σ and π donor such as 4-ethynylaniline, and use it as the platinum(II) co-ligand instead of the thiol ones. With this strategy we aim to modify the energy levels of the LLCT transition compared to the luminescent platinum ^{3}MLCT in order to obtain an efficient sensitiser for lanthanide emitters.

Previously, Ziessel *et al*. have reported examples of platinum(II) acetylide complexes used to sensitise the lanthanide luminescence upon excitation in the visible region of light. Furthermore, if we consider that one of the limitations arising from single molecule fluorescence imaging is that the excitation wavelength is in the range of visible light, this class of complexes might become interesting luminescent probe that may be employed in techniques such as time resolved fluorescence microscopy (TRFM).

4.2 Results and discussion

The $[LnC{\equiv}CPt_2](CH_3SO_3)_2$ can be prepared by the addition of different components in two ways (Scheme 4.1).

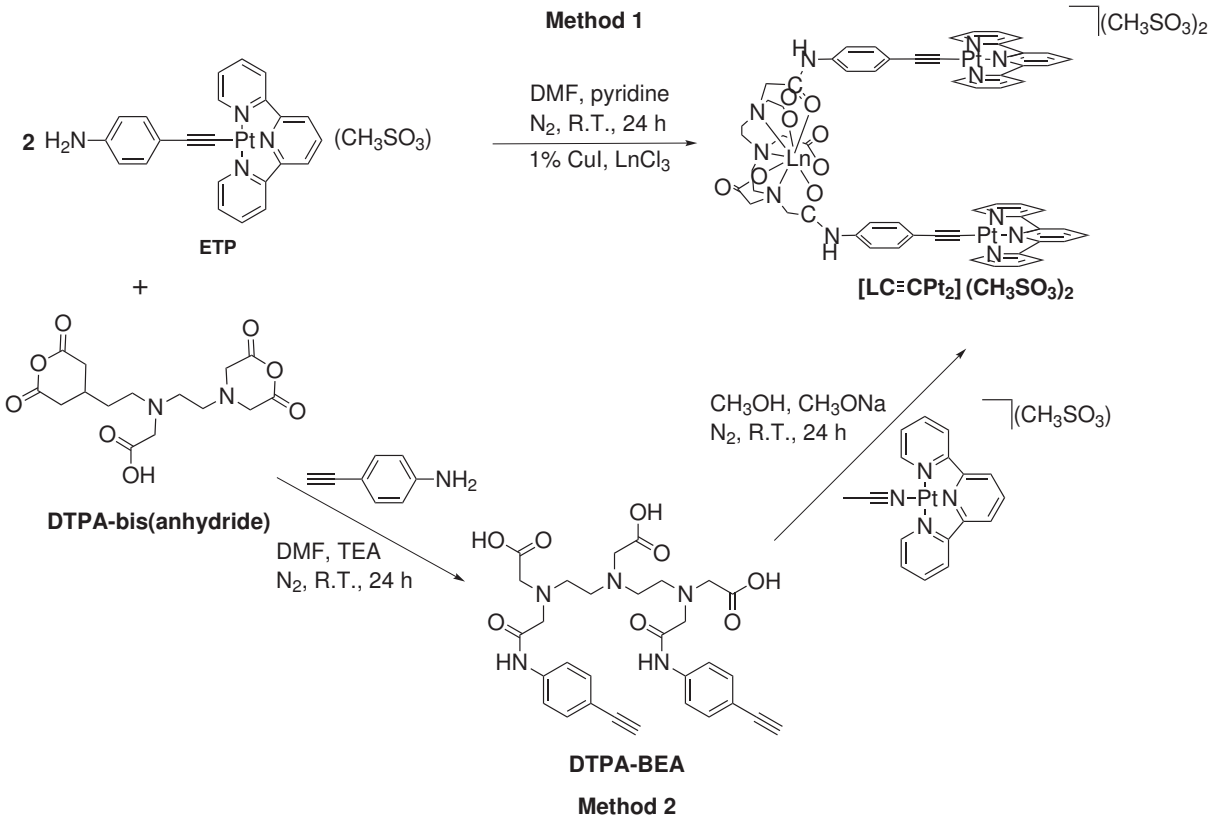

Scheme 4.1: Synthetic route to $[LnC{\equiv}CPt_2](CH_3SO_3)_2$ *via* Method 1 or Method 2.

The first step of method 1 is the isolation of the ETP complex that can be obtained by reacting the $[Pt(tpyCl)](CF_3SO_3)_2$ with two equivalents of 4-ethynylaniline in anhydrous DMF and TEA with a catalytic amount of CuI. After 16 hours stirring in the dark and under nitrogen at room temperature the final product was isolated as a red solid.

Full ^{1}H-NMR assignments were made in d_3-acetonitrile (Figure 4.17). The signal at 8.79 ppm is characteristic for terpyridyl **H6**, while the two satellite broad signals at 8.88 and 8.70 ppm are due to coupling with ^{195}Pt ion. Between 8.25 and 8.18 ppm there is a multiplet, which corresponds to the protons **H3'** and **H3** while between 8.08 and 8.02 ppm a multiplet is originating from the overlapping signal of **H4** and **H4'**. The characteristic doublet of doublets of **H5** from the terpyridine appears at 7.62 ppm and it overlaps with **Hb** from the ethhynylaniline ligand, which has **Ha** at 7.27 ppm. The

electrospray mass spectrum shows singularly charged species m/z = 559 [M - CF_3SO_3]$^+$. These data are in agreement with the characterisation reported by Yam et al. in 2005.[16]

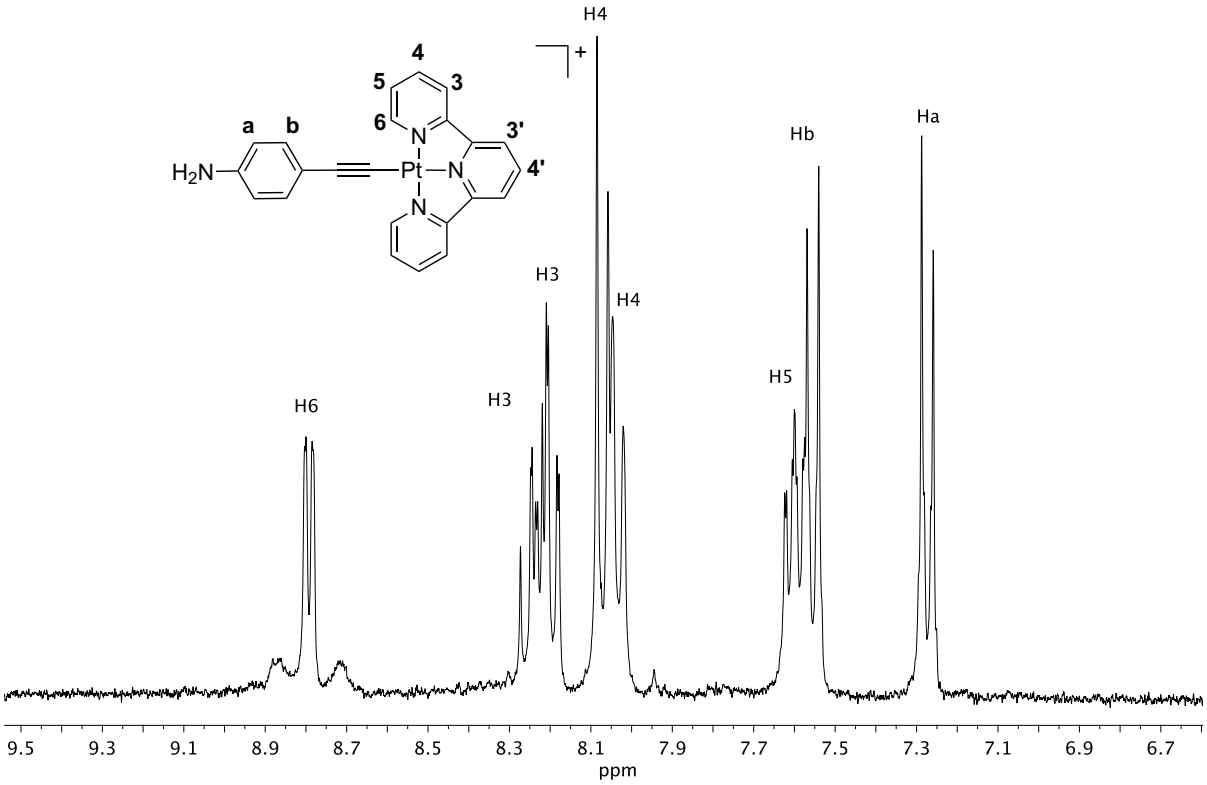

Figure 4.17: ^{1}H-NMR at 300MHz in d_3-acetonitrile of [4'-ethynylanilinePt(tpy)](CH_3SO_3).

The reaction between DTPA-bis(anydride) and [4-ethynylanilinePt(tpy)] (CF_3SO_3) was performed in dry DMF and dry pyridine (1:2), stirring for 24 hours in the dark, at room temperature. The reaction was monitored by mass spectrometry (ES), but we could not observe any peak characteristic of the desired product.

An excess of [4-ethynylanilinePt(tpy)](CF_3SO_3) in a final ratio of 4:1 with DTPA-bis(anhydride) and an increased reaction temperature at 40 °C, did not produce the desired effect by shifting the reaction towards the final product. We can ascribe the failure of the last step of the synthesis due to the mild conditions of the reaction.

However the synthesis of [LnC≡CPt_2](CH_3SO_3)$_2$ could still be attempted *via* method 2, which involved the isolation of a new DTPA derivative (DTPA-BEA) and the [Pt(tpy)MeCN](CH_3SO_3)$_2$.

4.2.1 Synthesis of DTPA-BEA

The DTPA-BEA was synthesised by reacting DTPA-bis(anhydride) with the 4-ethynyl aniline in DMF, while TEA was used as a base/nucleophilic catalyst.(Scheme 4.3).

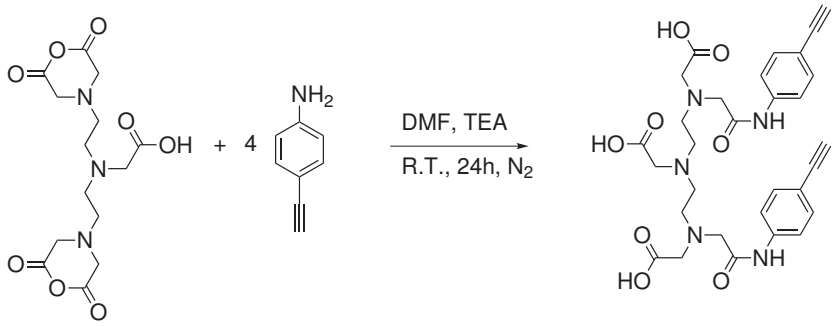

Scheme 4.2: Synthesis of DTPA-bis(4-ethynylaniline).

The ^{1}H-NMR show the characteristic doublets of the phenyl rings at 7.52 and 7.23 ppm respectively for **CH10** and **CH11** of the phenyl ring, while all the DTPA signals are included in their usual high field part of the spectrum between 3.0 and 3.6 ppm (Figure 4.18). The singlet at 3.78 ppm can be assigned to **2** on the DTPA aliphatic chain, while the two singlets at 349 and 3.41 ppm were assigned respectively to **5** and **7**. Protons **4** and **3** were observed as a triplet at 3.35 and 3.12 ppm respectively. The characteristic acetylide protons **14** were observed as a singlet integrating for two protons at 3.28 ppm. The electrospray mass spectrum shows a singly charged species at m/z = 590 $[M\text{-}H]^{+}$ and at m/z= 612 $[M\text{-}Na]^{+}$. The infrared absorption spectrum showed the characteristic C≡C stretch at 2103 cm^{-1} and C=O stretch at 1730 cm^{-1}, 1600 and 1520 cm^{-1} (see appendix page 265).

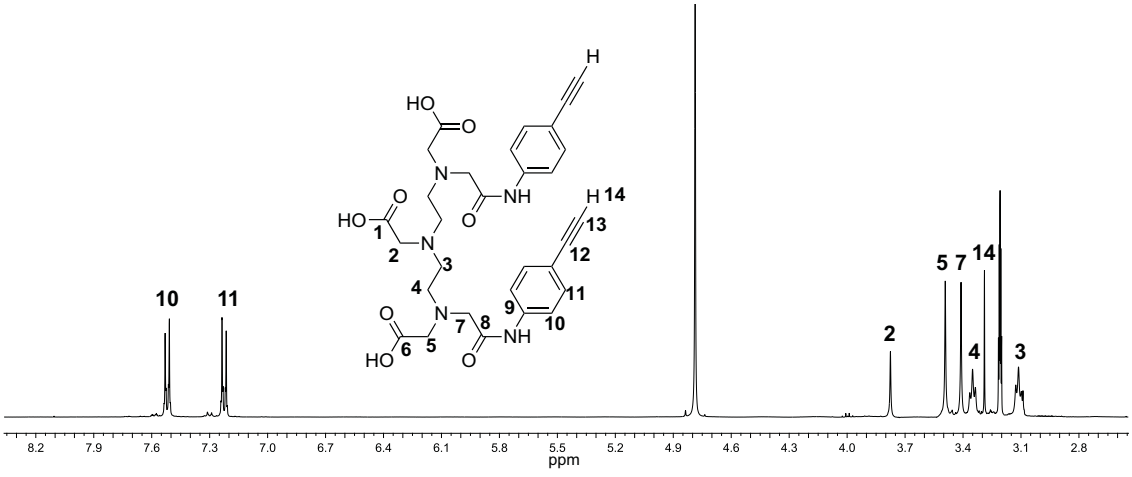

Figure 4.18: ^{1}H-NMR at 400 MHz in d^{3}-methanol of DTPA-bis(4-ethynylaniline).

The UV-vis absorption spectrum showed a strong band at 280 nm, which is assigned to the $\pi \rightarrow \pi^*$ transition of the phenyl moiety (Figure 4.19).

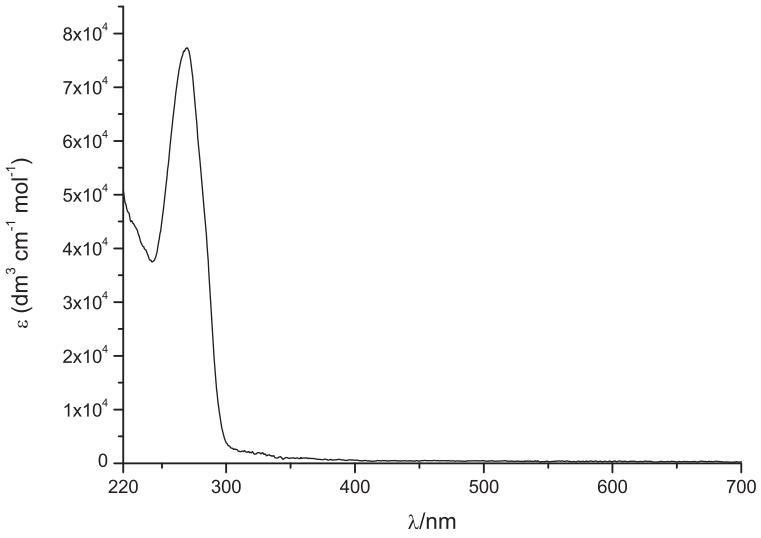

Figure 4.19: Absorption spectrum of 10 μM DTPA-bis(4-ethynylaniline) in methanol.

4.2.2 Preparation and photophysical properties of [EuDTPA-bis(ethynylaniline)]

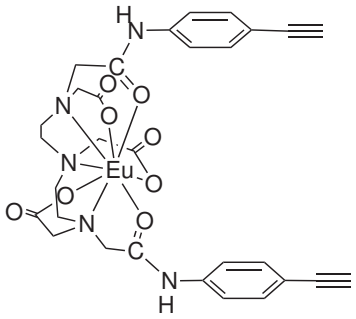

Figure 4.20: Structure of [EuDTPA-BEA].

The [EuDTPA-BEA] complex (Figure 4.20) was isolated by dissolving DTPA-BEA and $EuCl_3 \cdot 6H_2O$ in a mixture of methanol and water (1:1) after raising the pH to 5. The final complex was isolated by reducing the solvent volume followed by precipitation upon addition of acetonitrile and characterised by mass spectrometry, which showed a characteristic isotope pattern for a europium complex at m/z = 739 corresponding to $[M]^+$.

The UV-vis absorption spectrum of [EuDTPA-bis(4-ethynylacetilide)] showed the characteristic

π - π* transition at 270 nm, while the excitation spectrum that was recorded monitoring the $^5D_0 \rightarrow {}^7F_2$ at 615 nm demonstrated that the energy transfer arises from the ethynylaniline moieties to the lanthanide (Figure 4.21).

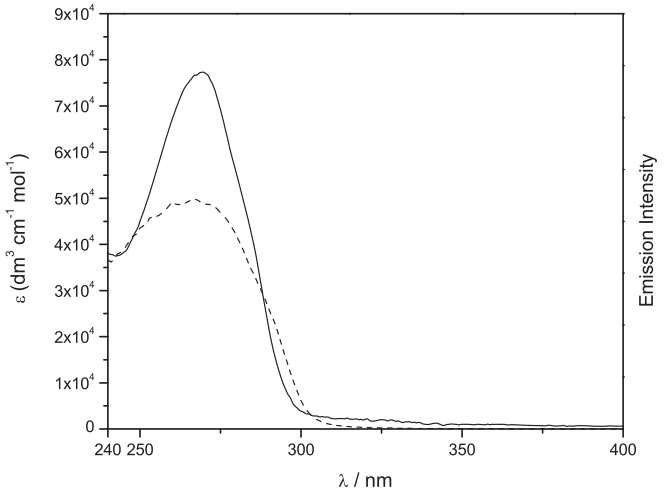

Figure 4.21: Absorption (dash line) and corrected excitation spectra (straight line) of [EuDTPA-bis(ethynylaniline)] (EuDTPA-BEA) in methanol. Excitation Spectrum: λ_{em} = 615 nm, corrected for lamp response.

Upon excitation of the visible emitting lanthanide complex at 270 nm, characteristic narrow red emission bands were observed for the Eu(III) complex (Figure 4.22). The emission spectrum for the Eu(III) complex has 5 sharp bands corresponding to the $^5D_0 \rightarrow {}^7F_J$ (J = 0 - 4) transitions, with the $^5D_0 \rightarrow {}^4F_2$ hypersensitive band at 615 nm being the most intense.

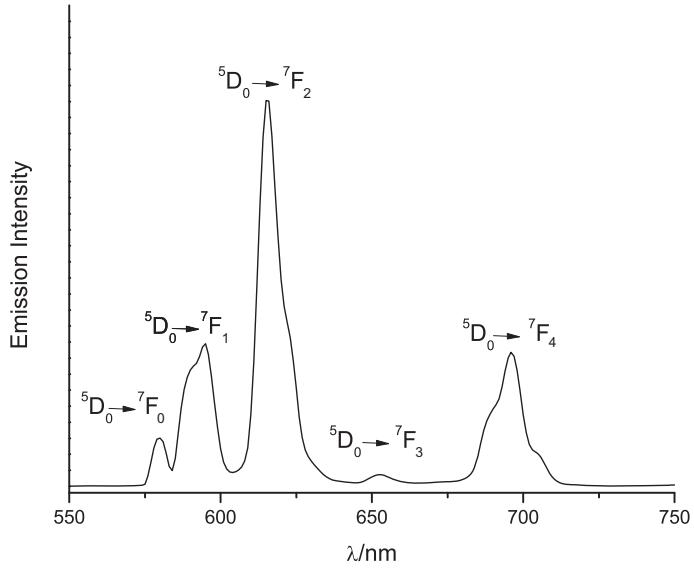

Figure 4.22: Emission spectrum of [EuDTPA-bis(ethynylaniline)] 10 μM in methanol ; λ_{exc} = 290 nm, corrected for PMT response.

In order to probe the coordination environment around the lanthanide ion, time resolved luminescence studies have been carried out in d_1-methanol and methanol. The samples were excited directly on the lanthanide at 355 nm and the resulting lifetimes recorded and fitted, giving a mono-exponential decay (Figure 4.23).

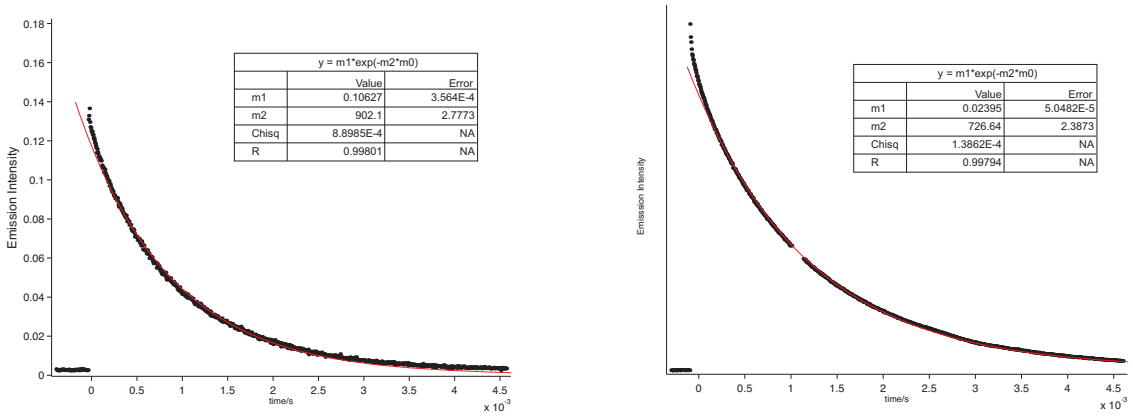

Figure 4.23: Emission decay trace of [EuDTPA-bis(ethynylaniline)] in methanol (left) and in d_1-methanol (right).

The Horrocks equation reported in chapter 1 has been used to determine the number of methanol solvent molecules coordinated to the Eu(III),[28] where the coefficient of A for Eu(III) in methanol is 2.10 ms.[29]

$$\mathrm{m} = \mathrm{A} \cdot (\tau^{-1}_{\mathrm{MeOH}} - \tau^{-1}_{\mathrm{MeOD}})$$

The fitted lifetimes and the number of solvent molecules (m) surrounding the lanthanide ion are summarised in table 4.1. The value of 0.7 $\pm$ 0.5 is expected as the ligand provides eight donors for the coordination of the lanthanide, with one vacant coordination site for the binding of a solvent molecule.

	τ(ms)		
Complex	MeOH	MeOD	m $\pm$ 0.5
[EuDTPA-BEA]	1.39	1.10	0.7

Table 4.1: Lifetime for [EuDTPA-BEA] in methanol and and d_1-methanol.

The shorter lifetime of the complexes in methanol is a result of the coordinated solvent molecules, bringing an O–H oscillator into the primary coordination sphere of the lanthanide, leading to the quenching of the lanthanide excited state (chapter 1 page 22). The ability of a given bond to quench luminescence is related to the frequency of the vibrational states, which is dependent upon the number of vibrational degrees of freedom of the bond in question. For example, the lower energy vibrational overtone (ν = 3) of an O–H bond, deactivates the Eu(III) $^5D_0$ excited state far more efficiently than the higher energy vibrational overtone (ν = 5) arising from an O–D bond. This explains why in the case of the d_1-methanol, the energy of the O–D oscillator is poorly matched to the lanthanide excited state making quenching inefficient.[30]

The preliminary photophysical studies showed that DTPA-BEA provides a well suited complexation pocket which excludes water molecules from the first coordination sphere and presents adequate energy levels for the energy transfer from the ligand to the europium excited state $^5D_0$. The presence of the acetylene moieties makes DTPA-BEA a good starting material also for click chemistry, which would allow the introduction of new functionalities and new features especially for lanthanide sensitisation.[31,32,33]

4.2.3 Synthesis of [LnC≡CPt$_2$](CH$_3$SO$_3$)$_2$

The most popular synthetic route to isolate platinum(II) acetylide complexes is mainly based on the Sonogashira reaction. Herein, we are concerned by the possibility of coordinating copper in the DTPA coordination site,[34] thus we preferred to use an alternative synthetic route that is based on the use of a labile co-ligand for the platinum(II) terpyridine starting material ([Pt(tpy)(MeCN)](CH$_3$SO$_3$).[24] Indeed, the use of even 1$\%_{mol}$ of Cu(I) could possibly lead to a secondary product such as [CuC≡CPt$_2$], which is difficult to remove due to its high similarity with [LnC≡CPt$_2$] as well as bearing an undesired secondary effect upon binding to the DNA, such as cleavage.[35]

Preparation of the trimetallic complex was achieved by the combination of three components: DTPA-BEA. LnCl$_3$ · 6H$_2$O, and [Pt(tpy)(CH$_3$CN)] (CH$_3$SO$_3$)$_2$ in a 1:1:2 molar ratio. The pure complex can be isolated after the formation of the heterometallic complex by repricipitation from the addition of acetonitrile to the aqueous solution (Scheme 4.3).

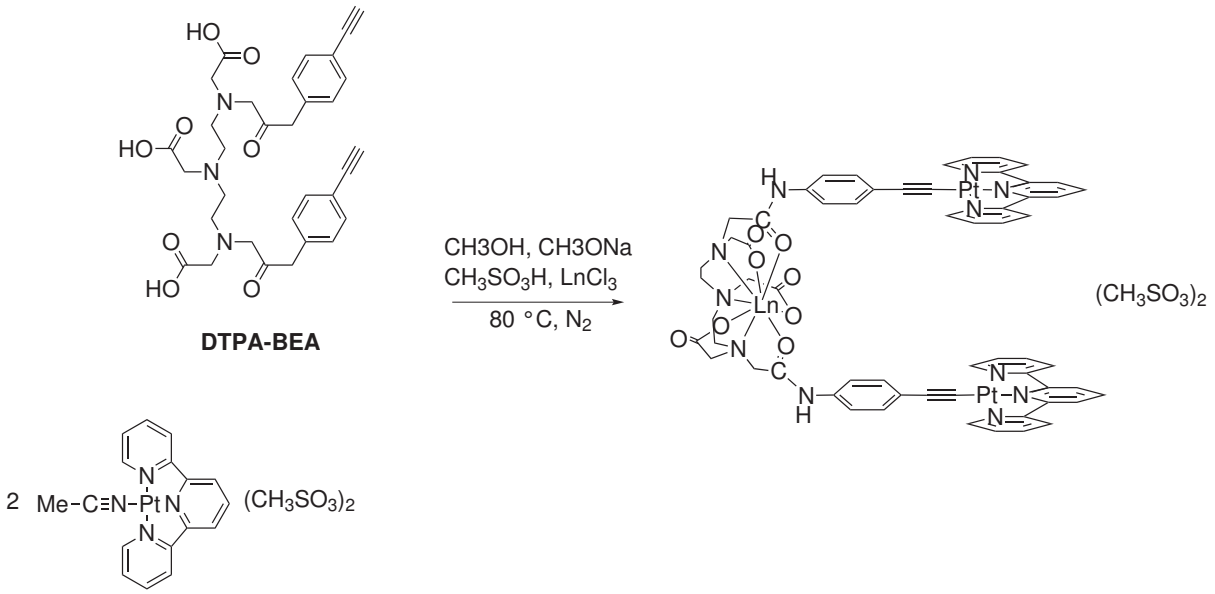

Scheme 4.3: Synthetic route to $[LnC{\equiv}CPt_2](CH_3SO_3)$.

The[Pt(tpy)MeCN] (CH_3SO_3) intermediate was prepared by a modified procedure of Annibale *et al.*,[36] where [Pt(tpy)Cl] (CH_3SO_3) was stirred at 90 °C for 4 h in presence of $AgCH_3SO_3$ in dry acetonitrile and under an inert atmosphere. The reaction yielded the desired [Pt(tpy)MeCN] (CH_3SO_3) in good yield as a crystalline pale yellow solid (Scheme 4.4).

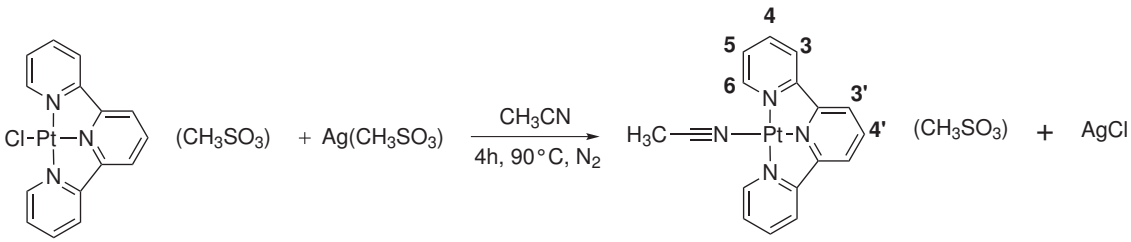

Scheme 4.4: Synthetic route to $[MeCNPt(tpy)]^{+}$.

We have attached platinum(II) terpyridyl moieties onto the DTPA-BEA, using the preferred interaction of platinum with soft Lewis bases.[37]

Initially, the $[LnC{\equiv}CPt_2]$ complex was synthesised by addition of DTPA-BEA to [Pt(tpy)MeCN] $(CH_3SO_3)_2$ in methanol. Sodium methoxide was added to activate the ethylene moieties in the reaction mixture.

It was observed that the characteristic deep red colour of the complex formed in the first 30 minutes; the reaction was completed in 2 hours time. The order of addition of the components was also optimised by firstly reacting DTPA-BEA with sodium methoxide followed by addition to the

[Pt(tpy)MeCN] $(CH_3SO_3)_2$. The lanthanide was then added to the complex, leading to the formation of the heterometallic complex. The pH of the solution was then adjusted to 5 by addition of CH_3SO_3H followed by addition of the lanthanide. Finally the product was precipitated by addition of acetonitrile to the water/methanol solution, yielding the desired complex in quantitative yield. The use of $CH_3SO_3^-$ as a counterion aids solubility of the complex in aqueous solution, which is essential for DNA binding studies and other biological applications.

4.2.4 Characterisations

[Pt(tpy)MeCN](CH_3SO_3)

The [Pt(tpy)MeCN]$(CH_3SO_3)_2$ was characterised by ^{1}H-NMR in d_3-acetonitrile (Figure 4.24) and mass spectrometry. The positive electrospray mass spectrum shows a peak at $m/z = 469$, corresponding to the [M - (CH_3SO_3)]$^+$. The integration of the aromatic resonance matches that expected for the complex and agrees with data previously published.[36] The doublet at 8.81 ppm is the **H6** of the platinum(II) terpyridine, which is able to couple with the ^{195}Pt which gives the two characteristic broad resonances at 8.86 and 8.77 ppm. The **H6** is the only proton in the compound that can have a three bond coupling with platinum. A $^3J_{H-H}$ coupling constant of 5.3 Hz is observed with the adjacent **H5** proton and is consistent with literature.[36] The **H5** proton at 7.92 ppm is the most shielded tpy proton. It has a complex coupling pattern (ddd) as it is coupled to both **H4** and **H6**, with a long range coupling to the **H3** proton. The **H4** at 8.48 ppm is coupled to the **H3** (8.40 ppm) and **H5** protons giving a doublet-doublet multiplicity, and is also split by a long range coupling. The **H4'** arises at 8.54 ppm and the overall integral between **H4** and **H4'** is equivalent to three protons. The **H4'** couples with the **H3'** at 8.35 ppm, where it gives a severe overlap with the proton **H3**; again the overall integral between **H3** and **H3'** is equivalent to three protons.

The methyl groups arising from the acetonitrile and from the mesilate counter-anion are the characteristic signals for these complexes and we found them at 2.11 and at 2.21 ppm respectively. Both singlets integrate for three protons when the **H6** integral was used as a reference for the integrals of two protons, which confirms that no excess of mesylate was present in the final isolated product.

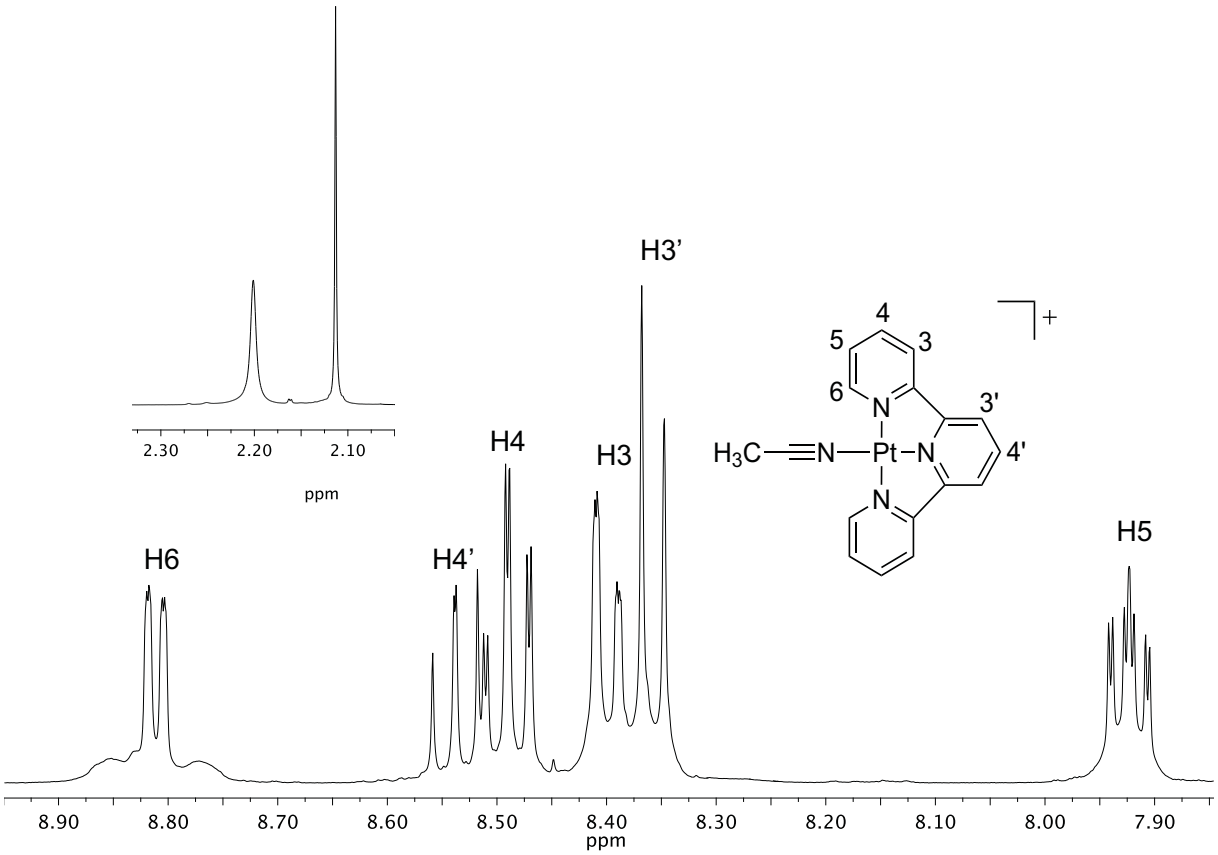

Figure 4.24: ^{1}H-NMR at 400 MHz of [Pt(tpy)MeCN](CH$_3$SO$_3$) in d^3-acetonitrile.

[LnC≡CPt$_2$](CH$_3$SO$_3$)$_2$

[LC≡CPt$_2$](CH$_3$SO$_3$)$_2$ has been fully characterised by ^{1}H-NMR and 2D ^{1}H-^{1}H COSY NMR, mass spectrometry and elemental analysis, while the [EuC≡CPt$_2$](CH$_3$SO$_3$)$_2$ was not investigated by ^{1}H-NMR due to the paramagnetism arising from the lanthanide metal centre.

Mass spectra for [LC≡CPt$_2$](CH$_3$SO$_3$)$_2$ and [EuC≡CPt$_2$](CH$_3$SO$_3$)$_2$ reveal peaks corresponding to a number of species for the same heterometallic complex, and thet are usually observed with the loss of both anions to give [M - 2(CH$_3$SO$_3$)]$^{2+}$ (Figure 4.25).

Due to the high viscosity of [LC≡CPt$_2$](CH$_3$SO$_3$)$_2$ in water at high concentration[38], the heterometallic complex was dissolved in a mixture of D$_2$O with d_4-methanol in the presence of NaOD and was characterised by ^{1}H and 2D ^{1}H-^{1}H COSY spectroscopy. Since the severe overlap of the signals characterise the aromatic region of the ^{1}H-NMR spectrum, assignments were only possible by using ^{1}H-^{1}H COSY, as a complementary technique (Figure 4.26).

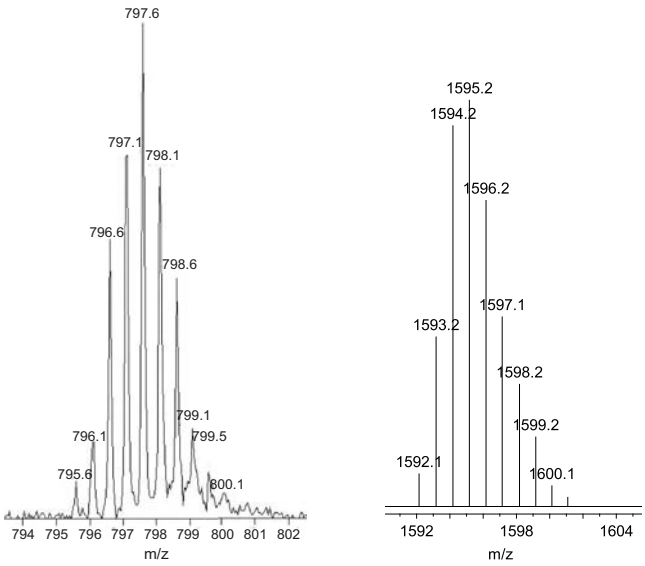

Figure 4.25: ES-MS(+) spectra of $[EuC{\equiv}CPt_2]^{2+}$ ($[M - 2(CH_3SO^-)]^+$)(left) and MALDI of $[EuC{\equiv}CPt_2]^{2+}$ ($[M - 2(CH_3SO_3)\text{-}H]^+$) (right).

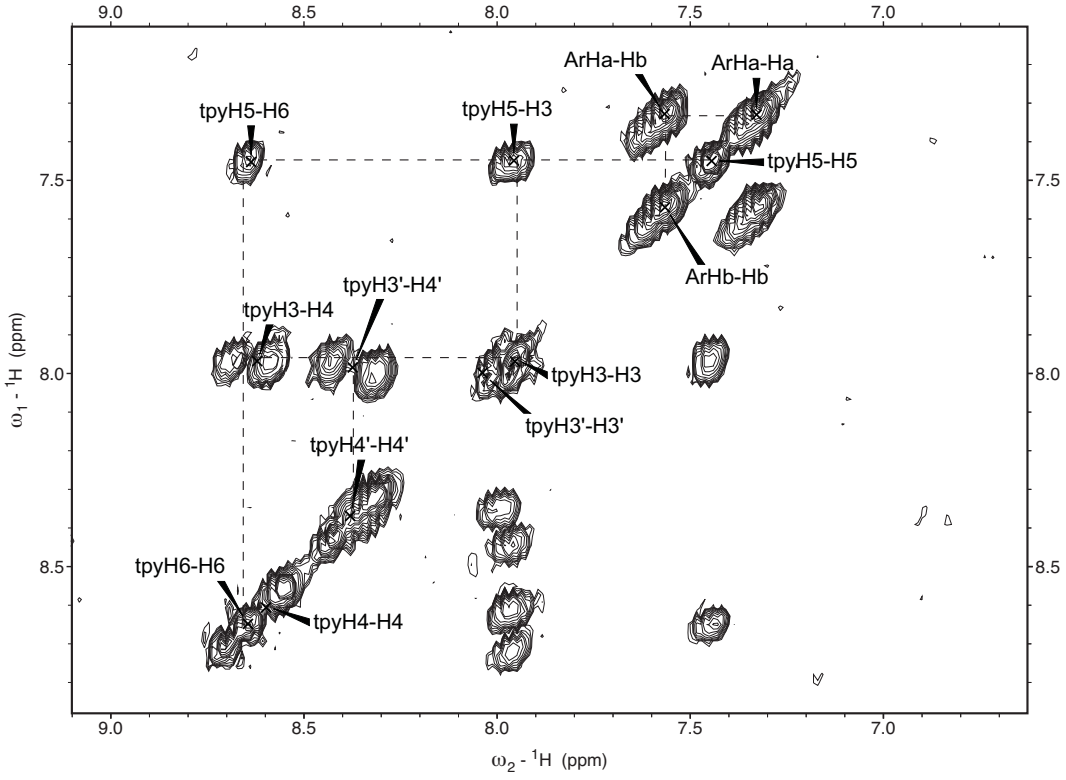

Figure 4.26: ^{1}H-^{1}H COSY NMR of $[LC{\equiv}CCPt_2](CH_3SO_3)_2$ in D_2O and d_4-methanol and in the presence of NaOD.

The aromatic region of the spectrum shows the **H6** at 8.65 ppm which couples with to **H4** and **H5** at 8.57 and 7.44 ppm respectively, while the **H4'** and **H3'** were observed at 8.55 and 8.45 ppm respectively. The H3 was observed at 7.98 ppm while the protons arising from the ethynilaniline **Hb** and **Ha** were at 7.57 ppm and 7.33 ppm respectively.

The chemical shifts of the aliphatic protons have previously been shown to be dependent on pH, with protons becoming more deshielded at higher pH.[39] The DTPA region appears as a manifold in the region in between 2.5 and 4.0 ppm, with the -CH_2-CH_2- backbone at 2.40 and 2.60 ppm, while the singlets for CH_2-CONH are expected at 3.00 and 3.20 ppm partially obscured by the residual peak of the NMR solvent, and the most deshielded CH_2COO^- appears at 3.73 ppm.

A mononuclear Pt acetylide complex as control compound

To study the effect of $[LnC{\equiv}CPt_2]^{2+}$ binding to DNA, it was necessary to have a control compound to assess the binding properties of the positively charged terpyridyl moiety which is the DNA intercalating unit. For this reason the [(4-amidoethynylaniline)(2,2':6'2"-terpyridine)platinum(II)](X) (X = BF_4, CH_3SO_3) was isolated from a reaction in methanol (Scheme 4.5).

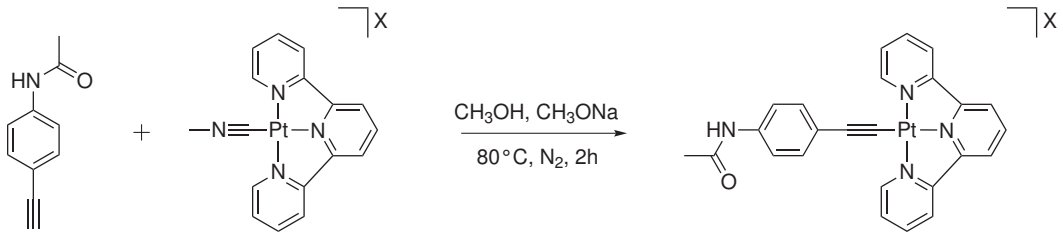

X = ($CH_3SO_3^-$), (BF_4^-)

Scheme 4.5: Synthetic route to [Pt(tpy)(C≡C)]X (X = BF_4, CH_3SO_3) complex.

The 4-acetamidoethynylaniline, obtained by a modified procedure of Che *et al.*[40] was reacted with [Pt(tpy)(MeCN)]$(BF_4)_2$ in methanol and in the presence of an equimolar amount of sodium methoxide. The final tetrafluoroborate complex was isolated by precipitation with a methanolic solution of NH_4BF_4, yielding the product as a deep red solid. The [Pt(tpy)(C≡C)](CH_3SO_3) was synthesised in a similar maner to the BF_4, while the isolation process was performed by drop wise addition of acetonitrile to a highly concentrated solution of the crude in water.

The desired products were characterised by ^{1}H-NMR spectrscopy, electrospray mass spectrometry, infrared spectroscopy (IR) and elemental analysis.

The ^{1}H-NMR spectrum of [Pt(tpy)(C≡C)](BF_4) in d_3-acetonitrile (Figure 4.27), displays the doublet centred at 8.79 ppm that can unequivocally be assigned to **H6** due to the platinum satellites and has an integral value of two. The **H4'** and **H4** appeared between 8.30 and 8.14 ppm as a doublet of doublets while the **H3'** and **H3** doublets appeared in between 8.10 and 8.00 ppm. The **H5** is clearly observed at 7.60 ppm with an integral value of two, and has a coupling pattern that is consistent with coupling to both **H6** and **H4** as well as long range coupling to **H3**. The phenyl proton signals are seen as double doublet signals, upfield from the terpyridine signals. The phenyl **Hb** signal is observed at 7.60 ppm being partially overlapped with **H5**, while the **Ha** proton of the phenyl is observed at 7.28 ppm. The aliphatic region of the spectrum displays a singlet at 2.14 ppm with an integration value of three, that can be confidently assigned as the methyl proton shift arising from the 4-acetamidoethynylaniline.

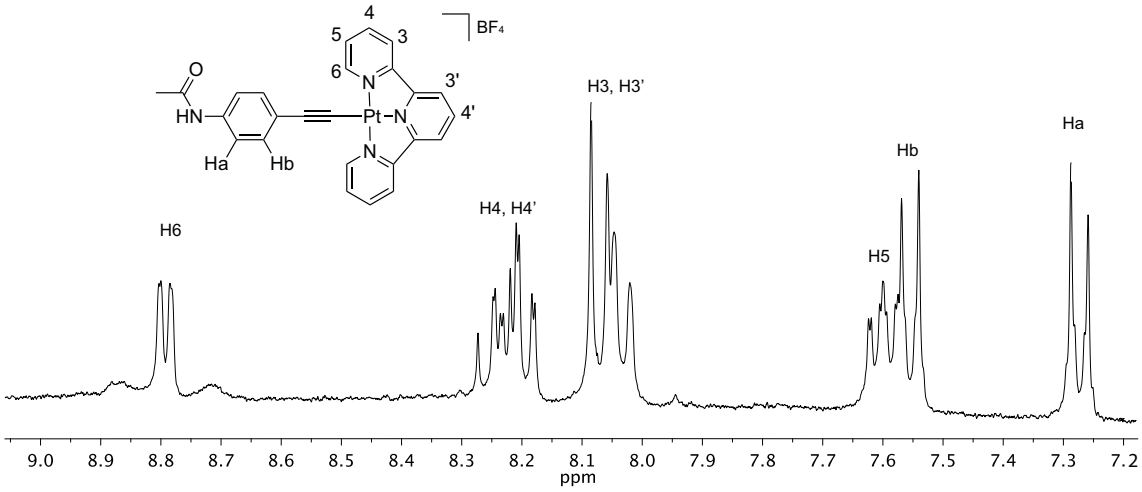

Figure 4.27: The aromatic region of the ^{1}H-NMR for [Pt(tpy)(C≡C)](BF_4) complex in d_3-acetonitrile.

Electrospray mass spectrometry showed a peak at 586 *m/z* containing the characteristic platinum isotopic pattern for the species $[M - BF_4^-]^+$.

While the tetrafluoroborate salt was isolated in order to improve the solubility of the [Pt(tpy)(C≡C)](BF_4) complex in organic solvents such as acetonitrile, the mesylate ones were isolated for their water solubility that is necessary for the DNA binding studies. However, the ^{1}H-NMR of the mesylate salt in D_2O is characterised by a severe signal overlapping in the aromatic region of the spectrum,

which can be due to the π - π stacking occurring between platinum terpyridine complexes in particular conditions of solvent polarity and compound concentration.[41,42,43] The aliphatic region of the ^1H-NMR spectrum shows two broad overlapping singlets at 2.49 and 2.29 ppm, that can be assigned to the methyl groups of mesilate and N-phenylacetamide respectively (see Appendix 7, Figure 25).

The [Pt(tpy)(C≡C)](CH_3SO_3) was observed by electrospray mass spectrometry with the isotopic pattern for the desired product at m/z = 586. This is consistent with the species [M - ($CH_3SO_3^-$)]$^+$, and it is also in agreement with the one observed for the [Pt(tpy)(C≡C)](BF_4). Furthermore, the solid state IR spectra for both [Pt(tpy)(C≡C)]X (X= BF_4, CH_3SO_3) are characterised by weak signals at ν=2127 cm^{-1} and ν=2123 cm^{-1} respectively, that belongs to the C≡C stretching of the platinum(II) acetylide complex (Appendix to chapter 4, Figure 28 and Figure 29). These values are in agreement with the previously reported ones by Yam *et al*. for similar platinum(II) acetylide complexes.[10]

4.2.5 Photophysical properties

The UV-vis absorbance spectrum of [Pt(tpy)(C≡C)](BF_4) recorded in acetonitrile (Figure 4.28), displays an absorption at 250 nm arising from the $\pi \rightarrow \pi^*$ transition within the ethynyl-aniline moiety, while the $\pi \rightarrow \pi^*$ intraligand terpyridine transitions were observed at 280, 330 and 345 nm. Characteristic of the terpyridylplatinum(II) acetylide complexes is the quite broad charge transfer band (CT) between 400 and 500 nm, that literature usually assigns to a mixture of MLCT ($dz^2 \rightarrow$tpy*) and LLCT (PhC≡C$\rightarrow$tpy*).[24]

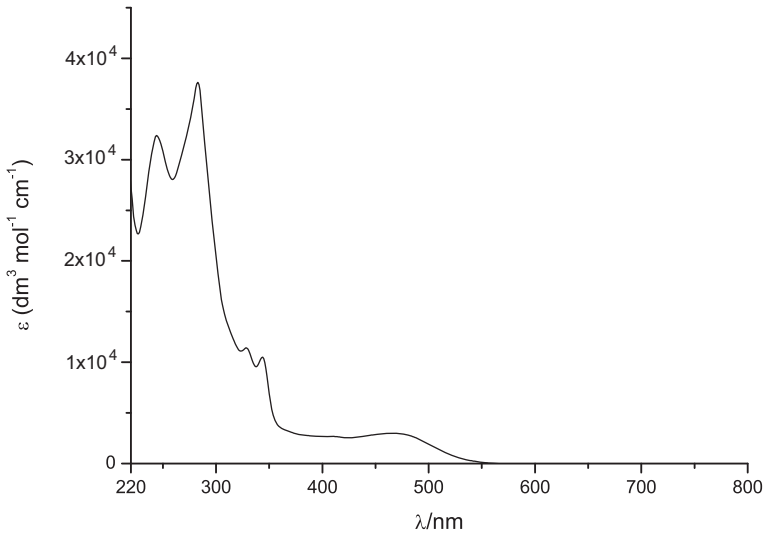

Figure 4.28: Absorption spectrum of 20 μM [Pt(tpy)(C≡C)](BF_4) in MeCN.

The UV-vis absorption spectrum of [EuC≡CPt_2](CH_3SO_3)$_2$ was recorded in MeOH (Figure 4.29), and it shows the main absorption band at 280 nm which is relative to the $\pi \rightarrow \pi^*$ intraligand phenyl-acetylide and terpyridine transitions, while the shoulder at 330 and 345 nm can be assigned to intraligand terpyridine transitions. Again a broad CT band is observed between 400 and 500 nm, and it can be assigned to a mixture of LLCT (PhC≡C→tpy*) and MLCT (dz^2 →tpy*) transitions.

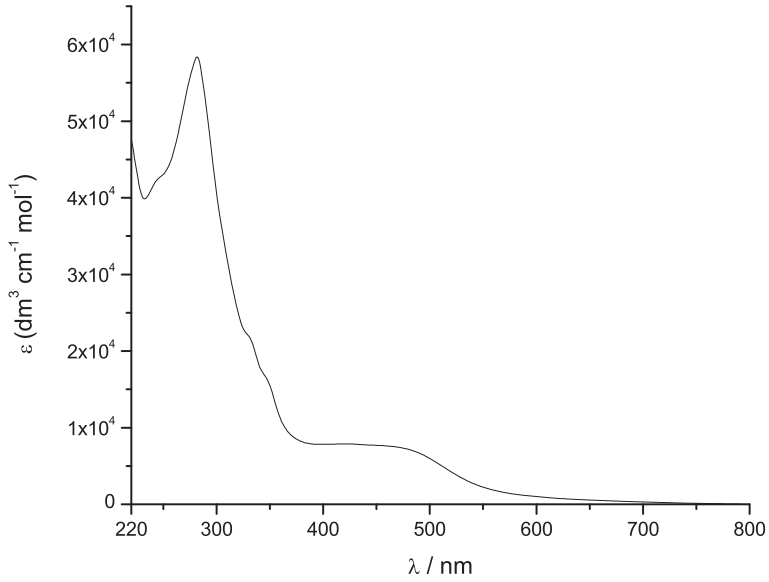

Figure 4.29: UV-vis absorption spectrum of [EuC≡CPt_2](CH_3SO_3)$_2$ in MeOH (25 μM).

The molar absorptivity coefficients of [EuC≡CPt_2](CH_3SO_3)$_2$ at λ_{max} = 280, 330, 345 nm and

the broad CT band between 400 and 500 nm are doubled when compared to the [Pt(tpy)(C≡C)]BF_4, which confirms the presence of two terpyridylplatinum(II) acetylide units in each [EuC≡CPt_2](CH_3SO_3)$_2$ complex.

Herein it is interesting the possibility of the use of the CT band at 450 nm to sensitise the lanthanide(III) ion emission. An example was reported in 2009 by Ziessel *et al*. where a platinum acetylide moiety was used as an antenna system, in order to sensitise a NIR emitting lanthanide ion.[23] However, the complex proposed by Ziessel et al. was limited by its solubility in a small range of organic solvents, which compromised its use as a luminescent probe for DNA recognition; in contrast [EuC≡CPt_2] (CH_3SO_3)$_2$ is characterised by a relatively good solubility in water and methanol.

Typical europium based luminescence in solution could be observed upon excitation of [EuC≡CPt_2] (CH_3SO_3)$_2$ at λ_{max} = 280 nm. The red emission was observed as a result of the luminescent transitions $^5D_0 \rightarrow {}^7F_J$ (J= 0, 1, 2, 3, 4) at 580, 590, 615, 650 and 695 nm respectively.

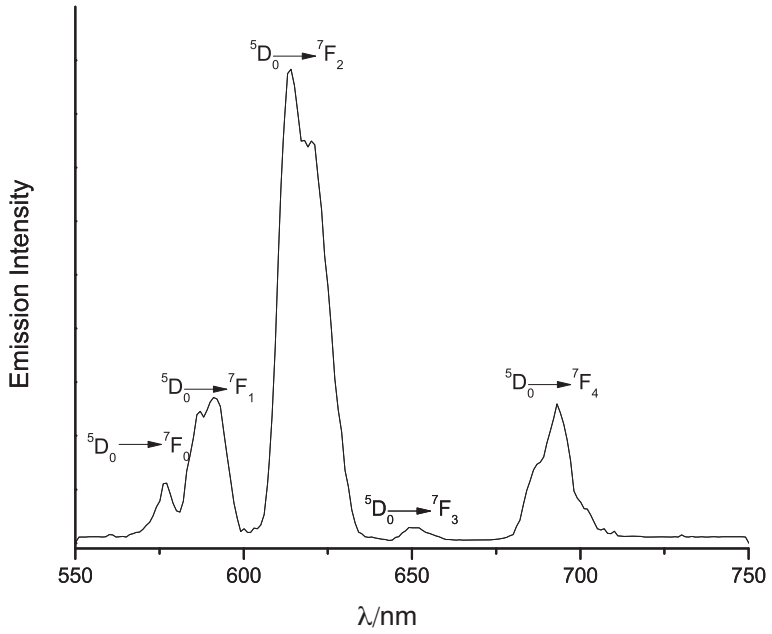

Figure 4.30: Emission spectra of [EuC≡CPt_2](CH_3SO_3)$_2$ 25μM in methanol. λ_{exc} = 280 nm.

Other excitation wavelengths were tested too (Figure 4.31), and while the intraligand terpyridine transitions at 330 and 345 nm led to a weak europium luminescence, no Eu(III) based emission could be detected upon excitation of the CT band at 450 nm.

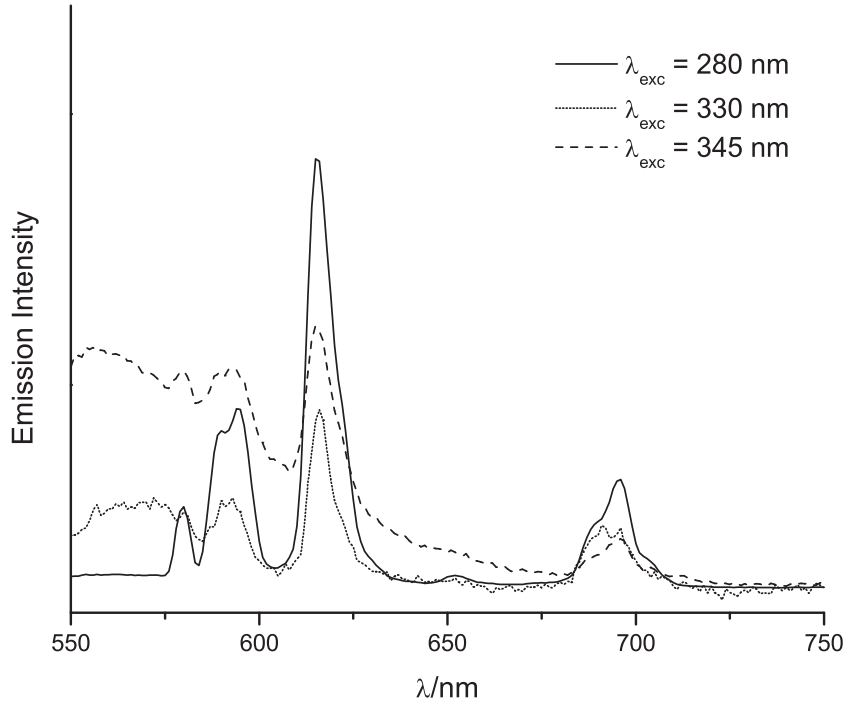

Figure 4.31: Emission spectra of [EuC≡CPt$_2$](CH$_3$SO$_3$)$_2$ in MeOH, upon excitation at λ_{exc} = 280 (25 μM, solid line), 330 nm (40μM, dotted line) and 345 nm (40μM, dashed line).

The excitation spectrum of [EuC≡CPt$_2$](CH$_3$SO$_3$)$_2$ was obtained by monitoring the Eu(III) emission at 615 nm (Figure 4.32). The spectrum shows a peak at 280 nm which is linked to the $\pi \rightarrow \pi^*$ intraligand phenyl-acetylide and terpyridine transitions. This is consistent with the energy transfer process operating from the terpyridylplatinum(II) acetylide group to the luminescent excited state of Eu(III). The most efficient energy transfer occurs upon excitation at 280 nm, although energy transfer can also operate upon excitation of the terpyridine transitions at 330 and 345 nm, while no Eu(III) based emission was observed upon excitation of the CT band at 450 nm.

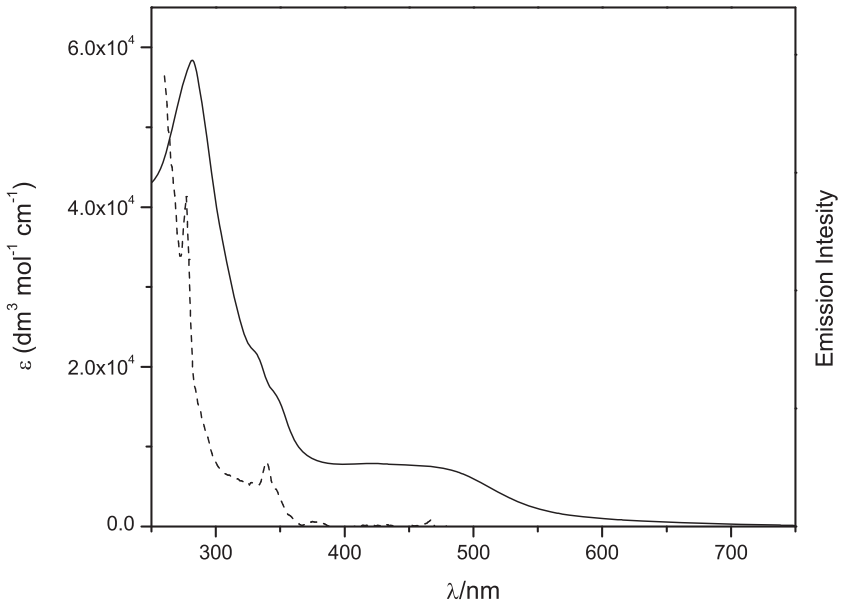

Figure 4.32: Overlay of absorption (solid line) and excitation spectra (dashed line) recorded by monitoring the europium fluorescence at 615 nm of $[EuC{\equiv}CPt_2](CH_3SO_3)_2$ in methanol (40 μM). The excitation spectrum is corrected for lamp profile.

The emission studies were also performed for $[NdC{\equiv}CPt_2](CH_3SO_3)_2$ in methanol solutions; however excitation at 280, 330, 345 or 450 nm did not lead to any Nd(III) based emission. Neither was any emission observed using deuterated water as solvent in order to minimise the quenching effects arising from the O–H oscillators (see chapter 1). The methanolic solutions of $[LnC{\equiv}CPt_2](CH_3SO_3)_2$ (Ln = Eu(III), Nd(III)) were degassed using the freeze pump thaw technique and the emission experiment repeated, but no lanthanide(III) based emission could be observed upon excitation of the CT band.

We investigated the luminescent properties of the [Pt(tpy)(C≡C)]X ($X = BF_4^-, CH_3SO_3^-$) complex upon excitation at 430 nm. Emission spectra were firstly recorded in methanol using [Pt(tpy)(C≡C)] (CH_3SO_3) which did not show any platinum based luminescence. Using a freeze pump thaw (FPT) degassed acetonitrile solution of $[Pt(tpy)(C{\equiv}C)](BF_4)$, a broad emission centred at 585 nm was recorded upon excitation at 430 nm. However, under the same experimental conditions no emission was observed upon excitation at 280 and 330 nm.

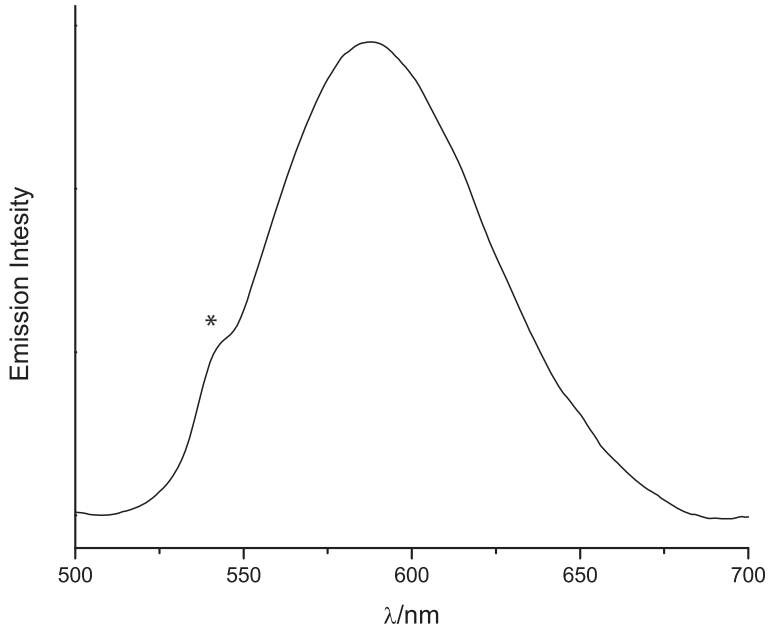

Figure 4.33: Emission spectrum of [Pt(tpy)(C≡C)]BF_4, in degassed acetonitrile (FPT). λ_{exc} = 430 nm. Emission corrected for PMT response. The * indicates an artefact signal.

When monitoring the emission at 585 nm, an excitation spectrum was recorded, which displays a broad band with maximum at 390 and 430 nm (Figure 4.34). These results are in agreement with the ones reported in literature by Yam *et al*., where for similar complexes the luminescence was assigned as arising from the ^{3}MLCT (Figure 4.34).[10]

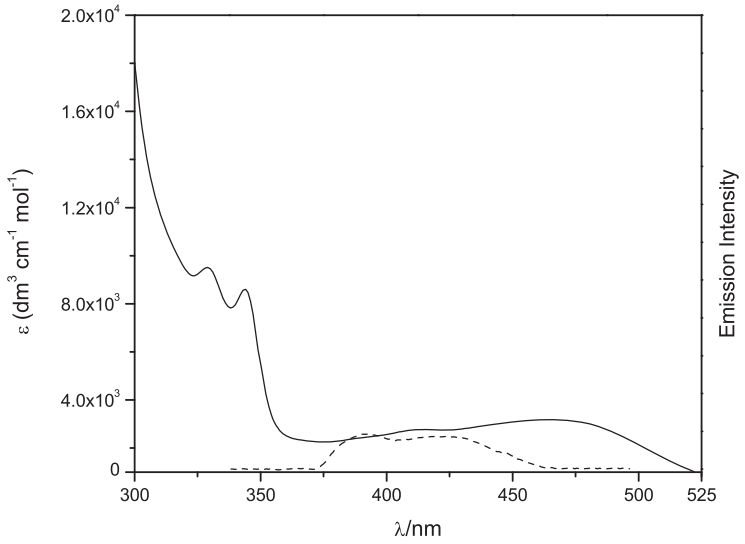

Figure 4.34: Overlay of absorption (solid line) and excitation spectra (dashed line) of [Pt(tpy)(C≡C)]BF_4, recorded by monitoring the emission at 615 nm. The excitation spectrum is uncorrected for lamp profile.

There are several factors that can be responsible for the lack of Eu(III), Nd(III) and Pt(II) emission upon excitation of the CT band. The solvent polarity plays an important role, since it would be able to deactivate the excited state simply by interacting with the metal centre through the axial positions of the square planar complex. Furthermore the nature of the platinum(II) co-ligand,[10] the presence of oxygen[24] and the thermal activation of the $d \rightarrow d$ transitions can also contribute to the non-radiative pathway deactivation of the platinum(II) excited state.

However due to the insolubility of $[LnC{\equiv}CPt_2](CH_3SO_3)_2$ (Ln = Eu, Nd) in apolar solvents, we could not test which is the effect of this class of solvents on the emission properties of the complex.[44] We attempted the isolation of the $[LnC{\equiv}CPt_2]X_2$ ($X = BF_4, PF_6$) *via* a metathesis reaction of $[LnC{\equiv}CPt_2](CH_3SO_3)_2$ with NH_4BF_4 or NH_4PF_6, but the red solid thus obtained would not dissolve in a broad range of organic solvents.

At this stage the interaction with DNA can play a crucial role. Indeed intercalation of the platinum(II) terpyridine units arising from $[LnC{\equiv}CPt_2](CH_3SO_3)_2$ (Ln= Eu, Nd) in the DNA hydrophobic environment, might protect the Pt(II) axial positions from interaction with the aqueous buffer or with oxygen leading to a "switch on" of the platinum based luminescence.[26]

4.2.6 Molecular Modelling

Several unsuccessful attempts have been tried to obtain single crystals of $[EuC{\equiv}CPt_2](CH_3SO_3)_2$ for X-ray diffraction. Thus we tried to model the structure of $[EuC{\equiv}CPt_2]^{2+}$ by semi empirical calculation using Chem3D and MOPAC.[45,46] The molecular model for the complex was built on results from two published crystal structures. The lanthanide complex moiety was based on the single x-ray structure of [Bi(DTPA-bis(4,5-diamino-6-hydroxy-2-mercaptopyrimidine)].[47] This complex was chosen as the pyrimidine arms of the ligand are directly bound to the amide giving it a structure that is easily adaptable to the structure of $[LnC{\equiv}CPt_2]^{+2}$. The Bi(III) metal ion was changed for Eu(III) while the pyrimidine arms were changed for the acetylide moieties, and the geometry optimised for the minimum energy by restricted molecular mechanics, and successively with the semi empirical methods. The PM6 Hamiltonian, was employed to model the lanthanide complex and a correction for the CONH energy barrier was employed (MMOK) (Figure 4.35).

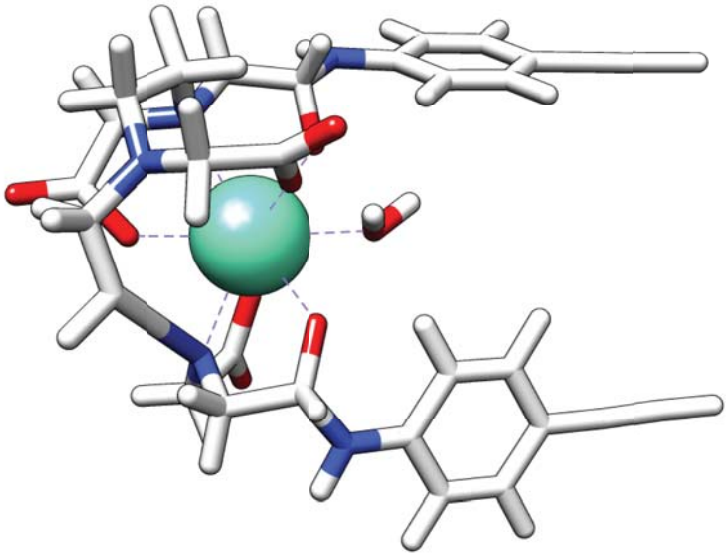

Figure 4.35: A 3D model of the minimised [EuDTPA-BEA] structure.

An X-ray crystal structure of the terpyridylplatinum(II) acetylide complex[48] was obtained from the CDS crystallographic database, and the crystal structure of $[Pt(tpy)C{\equiv}CN(CH_3)_2]^+$ modified by replacing the two methyl groups with an acetamide group. The optimal geometry was elucidated by restricted molecular mechanics followed by semi empirical minimisation employing the PM6 Hamiltonian and a correction for the CONH energy barrier was employed (MMOK). The optimised structure is in good agreement with the distances reported for the crystal structure (Figure 4.36).

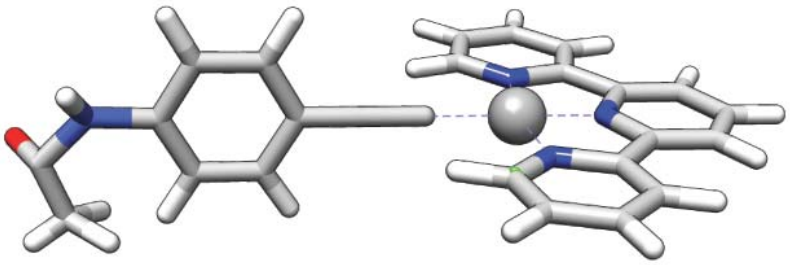

Figure 4.36: A 3D model of the minimised [4-amidoethynylanilinePt(tpy)]$^+$ structure.

The final structure of $[LnC{\equiv}CPt_2]^{2+}$ was obtained by replacing the phenyl-acetylide moiety with the one arising from the DTPA-BEA. The $[EuC{\equiv}CPt_2]^{2+}$ obtained was then optimised in its geometry by the employment of the semi empirical calculation. The final structure obtained is comparable has

distances and angles comparable to the original complexes used to built it. The distances between the two Pt(II) centres in the model is measured to be approximately 8 Å (Figure 4.37).

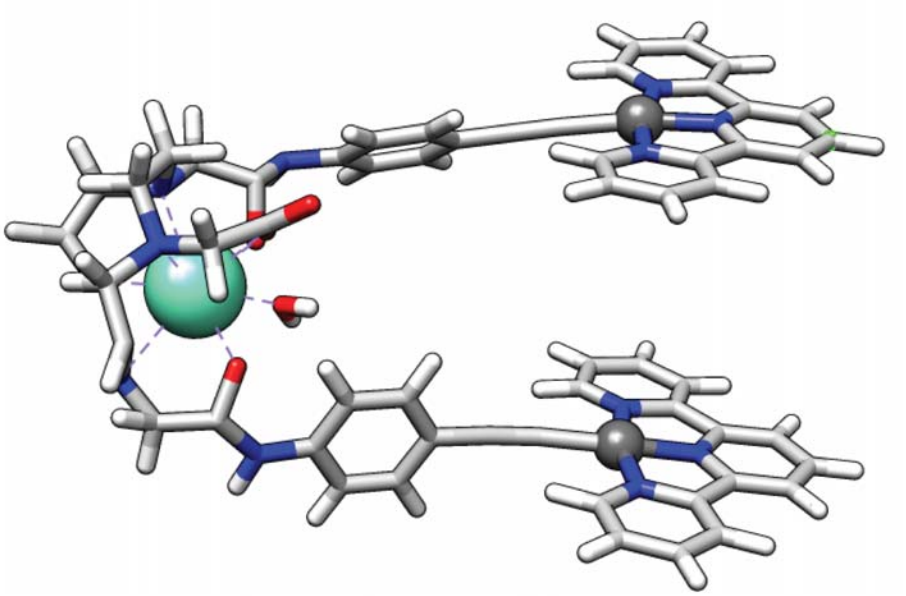

Figure 4.37: A 3D model of the minimised $[EuC{\equiv}CPt_2]^{2+}$ structure.

4.3 DNA binding studies

The binding of [LnC≡CPt$_2$] to calf thymus DNA (CT-DNA) has been investigated by absorption spectroscopy, luminescence, linear dichroism, melting point and gel electrophoresis. The beauty of [LnC≡CPt$_2$] is in the retained properties that we saw earlier for the [LnPt$_2$] hairpin system. The most important part of the molecule used in DNA recognition remains in its square planar geometry, which is essential for intercalation between the DNA base pairs.

4.3.1 UV-vis absorption of spectroscopy [EuC≡CPt$_2$] (CH$_3$SO$_3$)$_2$ and [Pt(tpy)(C≡C)] (CH$_3$SO$_3$) upon interaction with CT-DNA

UV-vis absorption spectroscopy was used to determine the binding of [EuC≡CPt$_2$](CH$_3$SO$_3$)$_2$ to CT-DNA (Figure 4.38). The addition of CT-DNA to [EuC≡CPt$_2$](CH$_3$SO$_3$)$_2$ resulted in a hypochromicity effect on the intraligand terpyridine $\pi \rightarrow \pi^*$ transition bands at 330 and 345 nm, with interesting changes occurring on the CT band at 470 nm. In fact the spectra indicate that there is a 20 nm bathochromic shift of the CT band upon the addition of CT-DNA.

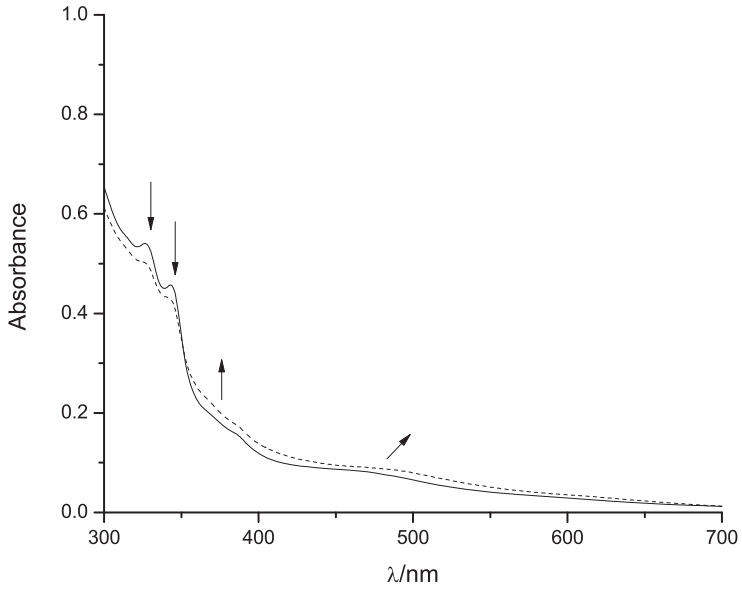

Figure 4.38: Absorption spectra of [EuC≡CPt$_2$](CH$_3$SO$_3$)$_2$ 10 μM (dash line) and in the presence of CT-DNA (ratio 1-4 solid line) in 10 mM HEPES buffer and 10 mM NaCl.

Using the the same experimental conditions the experiment was repeated for [Pt(tpy)(C≡C)](CH_3SO_3) (Figure 4.39). The addition of CT-DNA to [Pt(tpy)(C≡C)](CH_3SO_3) resulted in a bathochromic shift of $\sim$ 20 nm occurring on the CT band.

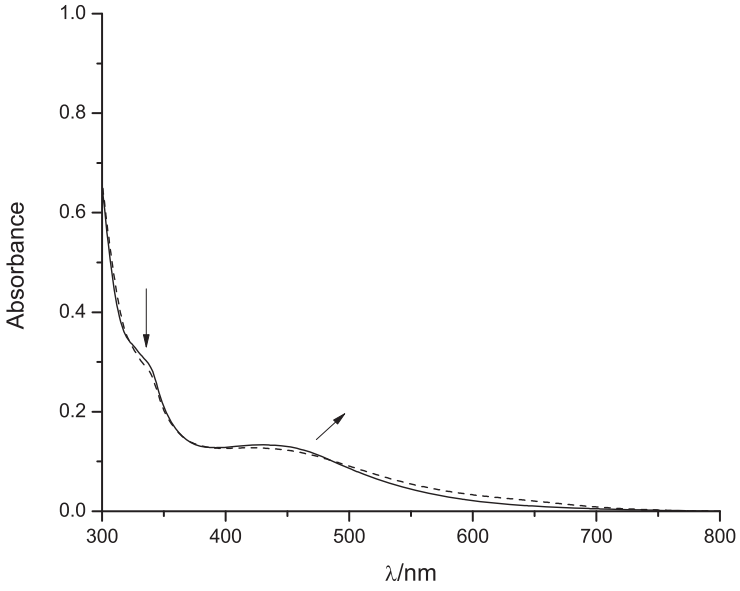

Figure 4.39: Absorption spectra of [Pt(tpy)(C≡C)](CH_3SO_3) (solid line) and in presence of CT-DNA (ratio 1-4 dashed line) in 10 mM HEPES buffer and 10 mM NaCl.

The bathochromic shifts observed for both [Pt(tpy)(C≡C)](CH_3SO_3) and [EuC≡CPt_2](CH_3SO_3)$_2$ are consistent with the intercalation of the platinum(II) terpyridine units in a hydrophobic enviroment such as the internal part of DNA.[11,49,38,50,51]

4.3.2 Melting point of [EuC≡CPt_2](CH_3SO_3)$_2$ upon interaction with CT-DNA

At high temperatures double stranded DNA can be denatured to a randomly coiled single stranded DNA by making the hydrogen bonds between the base pairs of the helix less favourable.[52,53] Since DNA bases absorb UV light in the 260 nm region, it is possible to monitor the hyperchromicity effect *via* absorption of the UV light.

This experiment has been used to assess the intercalative properties of [EuC≡CPt_2](CH_3SO_3)$_2$ with CT-DNA. The DNA absorption was measured at 260 nm, and a derivative method was used to calculate the melting point value (T_m). The melting curves for CT-DNA, both alone and with

[EuC≡CPt$_2$] $(CH_3SO_3)_2$ exhibit sigmoid behaviour (Figure 4.40). The results indicate that the double helix DNA becomes highly stabilised at high ratios DNA:complex. Indeed for the ratio of 20 : 1 we observed a ΔT_m of 10 °C, while further addition of the complex in order to bring the ratio to 4 : 1 produced smaller stabilisation of the double helix ($\sim \Delta T_m = 2°C$).

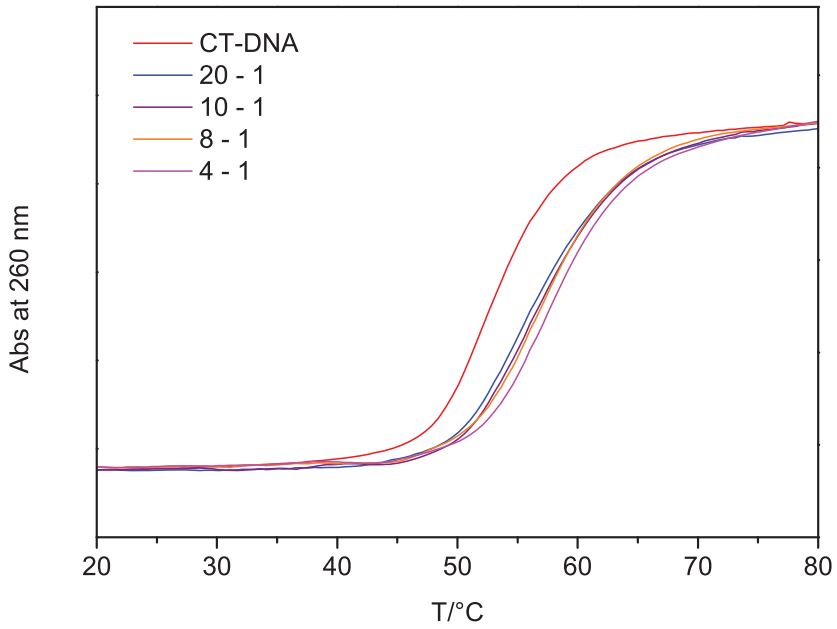

Figure 4.40: Melting curves of CT-DNA (60 μM) in the presence of [EuC≡CPt$_2$]$(CH_3SO_3)_2$ (the ratio DNA:complex is 4-1) in 10 mM HEPES buffer and 10 mM NaCl.

Thus in the event of intercalation, the π - π interaction between the DNA bases and the terpyridylplatinum(II) complex increases the stabilisation of the CT-DNA double stranded structure. Hence, a higher temperature is required in order to pass from a double stranded DNA to a random coiled single stranded one. However, previous studies based on a DNA monointercalator of Ru and Re showed a ΔT_m of 20 °C.[54] Kumar *et al.* have reported an anthryl intercalator with a ΔT_m which showed an increase of 6.4 °C.[55]

4.3.3 Flow linear dichroism

We have used flow linear dichroism (LD) studies to detect the binding of [LnC≡CPt$_2$] and of the [Pt(tpy)(C≡C)](CH_3SO_3) complex to CT-DNA. Linear dichroism is used to study the difference in absorption of linearly polarised light parallel and perpendicular to the orientation axis of the DNA,

where:

$$LD = A_{\parallel} - A_{\perp}$$

DNA gives a negative LD signal at λ = 260 nm as its bases are perpendicular to the orientation axis of the DNA. Transitions that are more parallel than perpendicular to the DNA helix axis will have a positive LD signals while transition moments greater than a certain angle from the main helix axis will result in negative signal. Upon addition of [EuC≡CPt$_2$](CH$_3$SO$_3$)$_2$ to CT-DNA, the LD signal displayed changes at 260, 330 and 450 nm which corresponds to the absorption band of the complex (Figure 4.41).

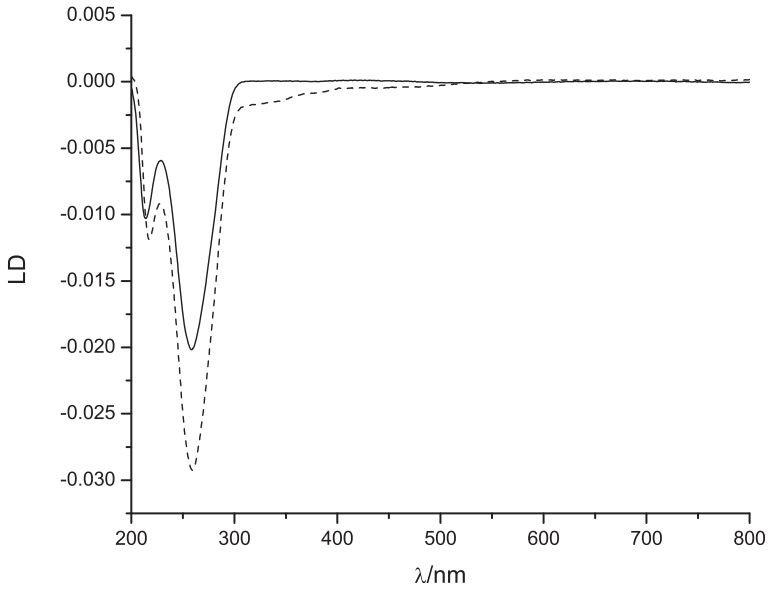

Figure 4.41: LD spectra of CT-DNA (solid line) upon addition of [EuC≡CPt$_2$](CH$_3$SO$_3$)$_2$ (dashed line) (40:1) in 10 mM HEPES buffer and 10 mM NaCl.

The LD spectrum of CT-DNA shows an increase in the intensity of the signal at 260 nm at a ratio of DNA:complex 40-1. This increase is attributed to the stiffening of the DNA double helix structure, as a result of the simultaneous stacking of the two platinum(II) terpyridine units between the DNA bases. Furthermore, we observed ILD bands in the 330 nm region that are the characteristic transitions of the terpyridine moiety, while the broad ILD band observed between 400 and 500 nm can be assigned to the CT transition. All the ILD signals were characterised by a negative sign, which

indicates that the two intercalating units are perpendicular to the main B-DNA axis.

Under the same experimental conditions we recorded the LD spectra of CT-DNA alone and upon interaction with [Pt(tpy)(C≡C)](CH_3SO_3) (Figure 4.42). The spectrum shows that the largest increase of the negative signal at 260 nm is obtained at a ratio of DNA:complex 5-1, while almost no changes are observed at ratio 40-1. Furthermore, induced LD signals can be observed at 330 and 450 nm which can be assigned to the intraligand terpyridine and CT transitions respectively. Since all the ILD signals are negative, this is consistent with the platinum(II) terpyridine complex lying orthogonal to the main B-DNA axis.

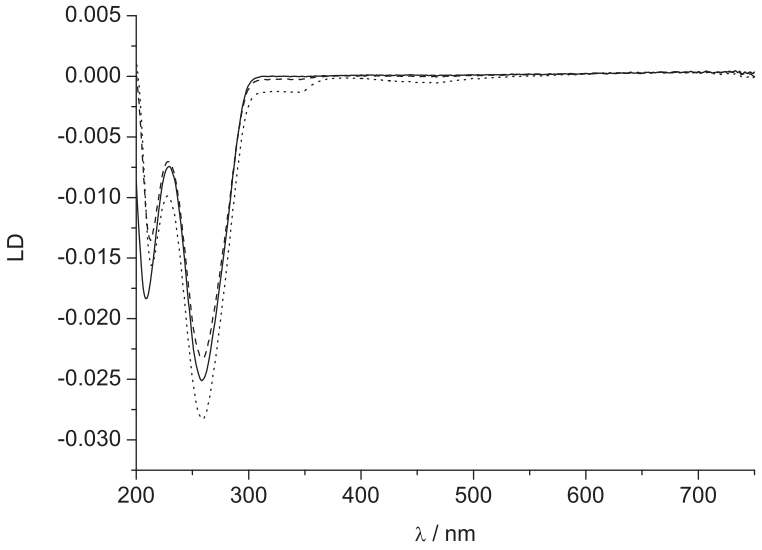

Figure 4.42: LD spectra of CT-DNA (solid line) upon addition of [Pt(tpy)(C≡C)](CH_3SO_3) at ratio DNA:complex 40:1 (dashed line) tand at 5:1 (dotted line) in 10 mM HEPES buffer and 10 mM NaCl.

From these results and from the shape of the [EuC≡CPt_2](CH_3SO_3)$_2$, we conclude that the complex binds to DNA *via* an intercalative mode. Furthermore, the large stiffening effect observed for [EuC≡CPt_2](CH_3SO_3)$_2$ is not only consistent with intercalation but suggests the bis-intercalation of the two platinum(II) terpyridine units.

4.3.4 Gel electrophoresis

Agarose gel electrophoresis has previously been used to detect DNA cleavage by macrocyclic transition metal complexes of Cu(II), Zn(II) and (Ru(II). The cleavage mechanism involves an oxidative process arising from $^1O_2$ generated under aerobic conditions.[56] This method has been previ-

ously used to detect a mono-intercalative interaction of DNA with terpyridylplatinum(II) glygosil-acetylide.[26] Gel electrophoresis should confirm whether our complexes are inert in the presence of DNA or can induce cleavage.

The gel electrophoresis experiments were performed on [EuC≡CPt$_2$] and EAP complex using 1% agarose gel in 1 mM TEA buffer and plasmid pBR322 DNA, and the results visualised by staining with ethidium bromide. The ratios of complex to DNA base pairs used were 15:1, 10:1, 8:1, 6:1, 5:1, 3:1. In each case the complex was incubated with the plasmid DNA at 37 °C for 2h prior to loading. By using super-coiled plasmid DNA, the degree of DNA stiffening upon addition of the complex can be determined.

The [EuC≡CPt$_2$] was found to be able to uncoil DNA already at low concentrations of complex (Figure 4.43). Indeed, most of the supercoiled DNA is already unwound to uncoiled DNA at 12:1 (DNA : complex ratio). The gel experiment did not show any DNA fragmentation which would be characteristic of a complex that is able to cleave DNA. However the DNA cleavage properties are a feature that can also be introduced if required, for example by replacement of the luminescent lanthanide ion with Ce(IV).[57]

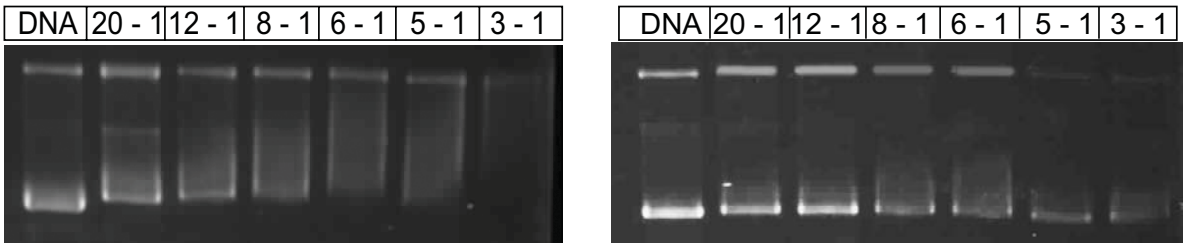

Figure 4.43: Gel image of pBR322 DNA treated with [EuC≡CPt$_2$](CH$_3$SO$_3$)$_2$ (left) and [Pt(tpy)(C≡C)](CH$_3$SO$_3$) (right).

The experiment was repeated under the same conditions with the [Pt(tpy)(C≡C)](CH$_3$SO$_3$) complex (Figure 4.43). The [Pt(tpy)(C≡C)](CH$_3$SO$_3$) complex showed the retained ability to interact with DNA by intercalation, with the uncoiling effect starting at higher concentrations of the complex. Almost double the amount of [Pt(tpy)(C≡C)](CH$_3$SO$_3$) has to be used to cause the same uncoiling effect observed for [EuC≡CPt$_2$]. Hence the stronger interaction of [EuC≡CPt$_2$] with DNA could be assigned to its high binding constant and to the rigid hairpin shape of the complex.

As reported in chapter 2 (page 86), the gel electrophoresis of supercoiled and open-circle plasmid

DNA can be used to assess the unwinding angle of the DNA helix produced upon the binding of platinum(II) complexes.[58] [59] Upon the binding of [EuC≡CPt$_2$](CH$_3$SO$_3$)$_2$ or upon interaction with the EAP complex, a retardation of the supercoiled band and an acceleration of the open circle band can be observed.

Using the appropriate ratio complex : plasmid DNA, the two bands relative to the supercoiled and uncoiled DNA can co-migrate. This particular ratio can be used to assess the unwinding angle by applying the equation 4.1:[60]

$$\phi = -18 \times \frac{\sigma}{r_c} \tag{4.1}$$

Where ϕ is the unwinding angle and σ the superhelicity constant, while r_c is the base complex ratio where supercoiled and relaxed DNA co-migrate. Using a σ value of -0.074,[61] [58] we determined an unwinding angle of 13° for [EuPt$_2$]Cl$_2$, while an angle of 7.5 ° was determined for the EAP complex. These results match with previously reported for the [LnPt$_2$]Cl$_2$ complex, and it confirms the retained DNA binding properties after the DTPA-BATP was replaced with the DTPA-BEA. Furthermore, as for the [EuPt$_2$]Cl$_2$, the [EuC≡CPt$_2$](CH$_3$SO$_3$)$_2$ is able to produce an unwinding of the double helix almost similar to the cis-platinum (13°) due to its bulk steric effect.[62]

4.3.5 Fluorescence studies of [EuC≡CPt$_2$](CH$_3$SO$_3$)$_2$ and [Pt(tpy)(C≡C)](CH$_3$SO$_3$) in presence of CT-DNA

Photophysical studies to investigate the effects of DNA intercalation on lanthanide emission intensity have been undertaken in both the visible and near-infrared regions of the spectrum. In each case the emission signal of the complex is recorded before and after the addition of CT-DNA.

The excitation wavelength selected for the visible emission was 300 nm, where the DNA absorption is the least and excitation of the chromophore is still efficient for energy transfer to the lanthanide. Excitation at 330 nm leads to relatively weak europium emission when the complex is alone in solution. Upon addition of CT-DNA to the complex there is an increase in the emission signal intensity (Figure 4.44). A comparison of the peak area integration values confirms an increase of about three times the original emission intensity. However, no emission was observed when the excitation oc-

curred at 450 nm (CT), and at the same excitation wavelength the addition of CT-DNA did not lead to any Eu(III) based emission.

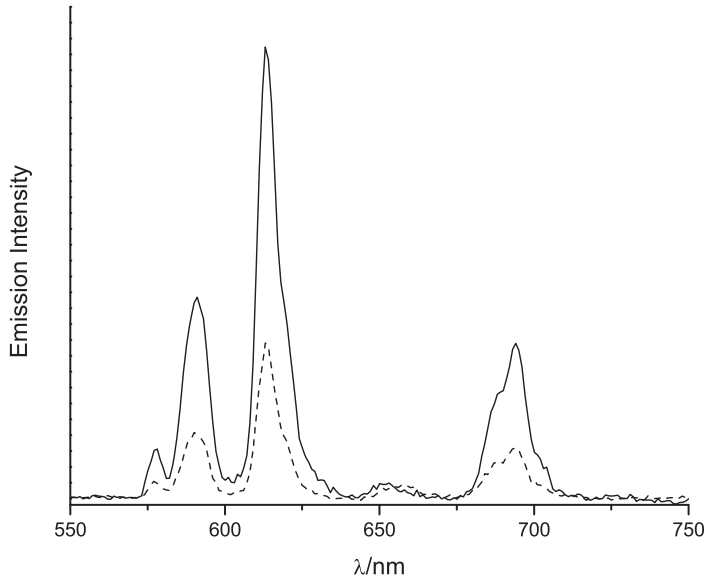

Figure 4.44: Emission experiment of [EuC≡CPt$_2$](CH$_3$SO$_3$)$_2$ (dashed line) and of [EuC≡CPt$_2$](CH$_3$SO$_3$)$_2$ (solid line) in presence of CT-DNA in a ratio (1-4), in 10 mM sodium phosphate buffer. λ_{exc}=330 nm cutoff filter 550nm, uncorrected for PMT response.

The experiment was repeated for [NdC≡CPt$_2$](CH$_3$SO$_3$)$_2$ and was performed in deuterated phosphate saline buffer, to minimise quenching by any appropriate bond oscillators. The photophysical studies were performed on both aerated and de-aerated solutions (10 min purge with nitrogen), and the excitation wavelength maintained at 330 nm. Nevertheless, we could not observe any Nd(III) based emission which may be due to the weakness of the signal. Furthermore, the excitation of the lanthanide emission through the CT band at 450 nm did not lead to any Nd(III) based emission. This might be due to a favourite non-radiative pathway which still remain active even when D_2O is used as solvent system.

Studies with [EuC≡CPt$_2$](CH$_3$SO$_3$)$_2$ and CT-DNA showed an increase in emission intensity. Thus, the visible luminescent [EuC≡CPt$_2$](CH$_3$SO$_3$)$_2$ can act as a luminescent labels to detect intercalative DNA recognition. Near infrared emission intensity of [NdC≡CPt$_2$](CH$_3$SO$_3$)$_2$ is too weak to be detected, even when quenching by bond oscillators is tentatively reduced using a deuterated environment (chapter:1, section 1.4).

4.4 Conclusion and future work

In this chapter we reported the synthesis and characterisation of a heterometallic hairpin complex, where the 4-aminothiophenol groups characteristic for the [$LnPt_2$] complex were replaced with 4-ethynylaniline. In order to introduce platinum(II) acetylide bonds in our hairpin photosystem, a new DTPA ligand (DTPA-BEA) having two acetylene terminal units has been isolated and fully characterised.

The DTPA-BEA showed interesting photophysical properties, and is a very useful starting material from which to obtain other interesting derivatives. The DTPA-BEA has been designed to be a versatile building block to be used in a one-pot reaction to isolate the DTPA-bis-terpyridylplatinum(II) acetylide in a quantitative yield. The [$EuC{\equiv}CPt_2$]$(CH_3SO_3)_2$ retains most of the properties seen before for [$LnPt_2$]Cl_2 (Ln = Eu, Nd). Indeed, the [$EuC{\equiv}CPt_2$]$(CH_3SO_3)_2$ is able to produce most of the large DNA stiffening already at low concentrations. Evaluation of the DNA unwinding angle by gel electrophoresis shows that the [$EuC{\equiv}CPt_2$]$(CH_3SO_3)_2$ is able to uncoil the DNA similarly to the parent complex [$EuPt_2$]Cl_2. However, the most important feature retained is the luminescence enhancement that is still observed upon interaction with DNA, when excitation occurs in the UV region. A possible explanation for this behaviour is that the energy levels of the terpyridine transitions are slightly modified due to the $\pi - \pi$ stacking interaction occurring upon intercalation between DNA bases. This results in a more efficient energy transfer operating between the sensitiser and the lanthanide emitter. Unfortunately this was not observed for the NIR emitter [$NdC{\equiv}CPt_2$]$(CH_3SO_3)_2$, which may be due to the weak emission signal of Nd(III).

Future work might be oriented on more detailed photophysical studies of [$LnC{\equiv}CPt_2$]$(CH_3SO_3)_2$. It will be particularly interesting to isolate a complex which has solubility in solvents such as acetonitrile or ideally dichloromethane. One possible way could be the use of organic counter anions (i.e. ammonium tetraphenylborate) or alternatively it may be possible to modify the DTPA aliphatic chain in order to control the solubility properties.

Not so many examples of lanthanide-platinum acetylide complexes are reported in literature for biological applications. In this sense, the [$LnC{\equiv}CPt_2$]$(CH_3SO_3)_2$ appears to be a good candidate

due to its reasonably good water solubility. This provides advantages in biological tests, such as cytotoxicity studies and investigation for mutagenesis (AMES test). Moreover, it would be interesting to see how these complexes are able to inhibit the PCR.

4.5 Experimental

4.5.1 Synthesis of 1,11-(bis(4-aminoethynylaniline)-1,11-dioxo-3,6,9-triaza-3,6,9-triscarboxymethyl) undecane

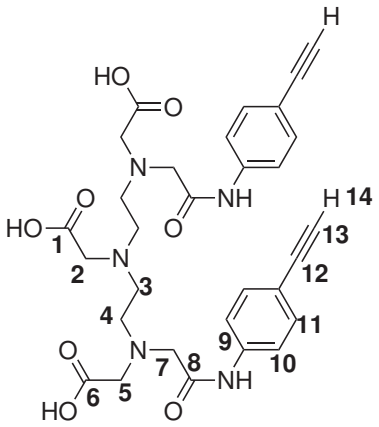

4-Aminoethynylaniline (1.32 g, 11.2 mmol) was added to a stirring suspension of diethylene triamine pentaacetic acid bis(anhydride) DTPA (1 g, 2.8 mmol) in triaethylamine (10 cm^3). The solution was stirred under nitrogen for 24 h at room temperature. A cloudy pale yellow solution was obtained. The solvent was removed under *vacuo* at 40 °C and a yellow solid was obtained. The solid was triturated in ethyl acetate and left stirring overnight at room temperature. A pale yellow precipitate was isolated by filtration and further washing occurred (2 $\times$ 25 cm^3) with ethylacetate and (2 $\times$ 25 cm^3) diethyl ether. The crude ligand was redissolved in the minimum amount of water and the pH lowered to 3 via the dropwise addition of 0.1 M hydrochloric acid. The solution was then refrigerated to encourage precipitation and the solid bottom layer was collected by decanting. The resulting off-white suspension was then stirred vigorously in 25 cm^3 of ethylacetate to afford an off-white powder. The powder was collected by filtration and washed with diethyl ether (2 $\times$ 20 cm^3). The crude product was isolated as an off-white powder.

^{1}H NMR (400 MHz, [D3]CD_3Cl, 24°C, TMS) δ = 7.52 (d, ^{3}J(H,H) = 9.0 Hz, 2H, H10), 7.23 (d, ^{3}J(H,H)=9.0 Hz, 2H, H11), 3.78 (s, 2H, H1), 3.49 (s, 4H, H5), 3.41 (s, 4H, H7), 3.35 (t, ^{3}J(H,H) = 5.7 Hz 4H, H4), 3.29 (s, 2H, H14), 3.28 (s, 4H, Hc), 3.12 (t, ^{3}J(H,H) = 5.7 Hz, 4H, H2); ^{13}C {^{1}H} NMR (100 MHz, [D3]CD_3OD+NaOD, 24°C,TMS) δ= 173.4 (C1), 169.0 (C6), 168.0(C8), 137.3 (C9), 130.9 (C11), 118.6 (C10), 116.6 (C11), 132.9 (C11), 121.1 (C10), 117.4 (C12), 81.7 (C13), 75.4 (C14), 64.3 (C5), 57.7 (C7), 55.0 (C2), 53.5 (C4), 52.9 (C3); IR (KBr): $\tilde{\nu}$ = 3277 cm^{-1} (s), 2103 cm^{-1} (m), 1670 cm^{-1} (s); MS (ES^{+}) = *m/z* 590 [*M* - H]$^{+}$, 295.5 [*M* - 2H]$^{2+}$; UV-Vis (CH_3OH): λ_{max} in nm (log ε) 270 (4.8); Elemental Analysis calcd (%) for $C_{30}H_{33}N_5O_8$ $(Cl)_2$ $(H_2O)_2$: C, 51.58; H, 5.34, N 9.75; found: C, 51.33; H, 5.34; N, 9.75.

4.5.2 Synthesis of [Pt(tpy)Cl] (CH_3SO_3)

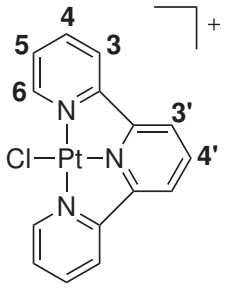

A solution of Ag(CH_3SO_3) (0.054 g, 0.210 mmol) in dry acetonitrile (5 cm^3) was added to a suspension of [$PtCl_2(PhCN)_2$] (0.100 g, 0.210 mmol) in dry acetonitrile (10 cm^3). The solution was heated under reflux at 90 °C for 6 h and underwent a colour change from clear yellow to clear and colourless with a white precipitate. The precipitate was removed by filtration and 2,2': 6',2"-terpyridine (tpy) (0.049 g, 0.210 mmol) added. A clear yellow solution resulted and was heated under reflux at 90 °C for 16 h. The volume of the solution was reduced *in vacuo* to afford an orange solid. The product was collected by filtration, washed with diethyl ether and dried under vacuum. Yield 70%

^{1}H NMR (300 MHz, [D3]CD_3CN, 24°C), δ = 9.10-8.98 (m, 2H, H6); 8.55 (t, 1H, ^{3}J = 8.1 Hz, H4'); 8.46 (dt, 2H, ^{3}J(H,H) = 8.1 Hz, ^{3}J(H,H) = 2Hz, H4); 8.37-8.33 (4H, m, H3/H3'); 7.84 (dt, 2H, ^{3} J(H,H) = 8.1 Hz, ^{3} J(H,H) = 2Hz, H5). ^{13}C {^{1}H} NMR (100 MHz, CD_3CN, 24°C),

δ= 127.6, 122.72 (C2, C2'); 149.3 (C6); 141, 140.7 (C4', C4); 127.7 (C5); 126.7, 125.4 (C3, C3'). MS (ES^+) = *m/z* 464 [M^+ - (CF_3SO_3)], 463 [M^+ - (CF_3SO_3) - H]. UV-Vis (CH_3OH:H_2O), 4:1): λ_{max} in nm (log ε) 540 (2.2), 380 (3.3), 330 (4.1), 280 (4.4), 255 (4.3).

4.5.3 Synthesis of N-(4-ethynylphenyl)acetamide.

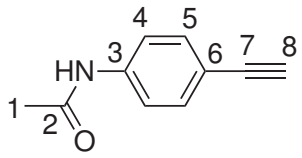

A solution of 2-ethynylaniline (1g, 8.5 mmol) and acetic anhydride (0.96 g, 0.0095 mmol) in dry CH_2Cl_2 (25 cm^3) was stirred at room temperature for 6 h under nitrogen atmosphere. The organic layer was extracted with a water based saturated solution of $KHCO_3$ (3 $\times$ 50 cm^3), brine (1$\times$50 cm^3) and then dried over $MgSO_4$. 1.23 g of final product has been isolated by evaporation of the solvent under vacuum. Yield 93%

^{1}H NMR (300 MHz, [D3]$CDCl_3$, 24°C,TMS) δ ppm = 8.38 (s, 1H, NH), 7.49 (d, ^3J(H,H) = 6.0 Hz, H4), 7.40 (d, ^3J(H,H) = 6.0 Hz, H5), 3.05 (s, 1H, H8), 2.1 (s, 3H, CH_3); ^{13}C {1H} NMR (75 MHz, [D3]CD_3Cl, 24 °C, TMS) δ ppm = 169.3 ppm (C=O), 138.5 ppm (C3), 132.8 (C4), 119.5 (C5), 83.4, (C7), 76.82 (C8), 50.53 (CH_3); IR (KBr): $\tilde{\nu}$ = 3316 cm^{-1} (s), 2108 cm^{-1} (m), 1669 cm^{-1} (s).

4.5.4 Synthesis of [Pt(tpy)(C≡C)]BF_4

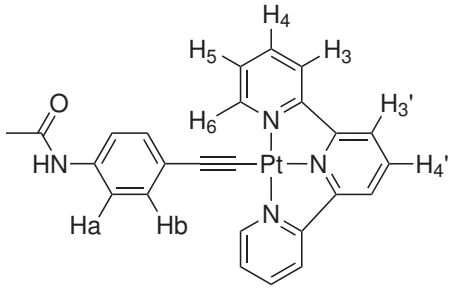

Sodium methoxide (9.57 mg 0.177 mmol) was added to a stirred solution of N-(4-ethynylphenyl) acetamide (28 mg 0.177 mmol) in methanol. The resultant solution was stirred at room temperature for 30 min. [Pt(tpy)MeCN](CH_3SO_3) (50 mg 0.088 mmol) was added to the reaction mixture which turned to red solution and was refluxed for 2h at 80 °C under nitrogen. The solvent was reduced by vacuum to 2 cm^3 and a saturated methanolic solution of NH_4BF_4 was added drop wise. The fine deep red precipitate was collected by filtration and washed with methanol (20 cm^3) and diethyl ether (20 cm^3) to obtain 39.13 mg. Yield 73 %.

^{1}H NMR (300 MHz, [D4]CD_3OD, 24°C, TMS) δ = 8.79 (d, ^3J(Pt,H) = 46 Hz, ^3J(H,H) = 5.6 Hz, H6), 8.30 - 8.14 (m, 4H, H3, H3'), 8.10 - 8.00 (m, 3H, H4', H4), 7.60 (ddd, 2H, ^3J(H,H) = 8.1 Hz, ^3J(H,H) = 5.6 Hz, H5), 7.60 (d, 2H, ^3J(H,H) = 8.5 Hz, Ar-Ha), 7.28 (d, 2H, ^3J(H,H) = 8.5 Hz, Hb), 2.11 (3H, s, CH_3); IR (KBr): $\tilde{\nu}$ = 3081 cm^{-1} (m), 2127 cm^{-1} (m), 1669 (s) cm^{-1}, 1593 (s) cm^{-1} ; MS (ES^+) = *m/z*= 586 [M^+-(CH_3SO_3)]; UV-Vis (CH_3CN): λ_{max} in nm (log ε) 470 (3.4), 345 (3.3), 330 (4.1), 280 (4.7), 255 (4.7). Elemental Analysis calcd (%) for $C_{25}H_{19}BF_4N_4OPt$ (Na): C 43.12, H 2.75, N 8.05; found C 43.56, H 2.75, N 8.05.

4.5.5 Synthesis of [Pt(tpy)(C≡C)](CH_3SO_3)

Sodium methoxide (9.57 mg 0.177 mmol) was added to a stirred solution of N-(4-ethynylphenyl)acetamide (28 mg 0.177 mmol) in methanol. The resultant solution was stirred at room temperature for 30 min. [Pt(tpy)MeCN](CH_3SO_3) (50 mg 0.088 mmol) was added to the reaction mixture which turned to a red solution and was reflux for 2h at 80 °C under nitrogen.The solvent was removed by vacuum and

the deep red precipitate was dissolved in the minimum amount of water. By drop wise addition of acetonitrile a red precipitate was afforded that was isolated by filtration and washed with 20 cm^3 of acetonitrile and 20 cm^3 of diethyl ether. Yield 68%.

^{1}H NMR (300 MHz, [D2]D_2O, 24 °C,TMS) δ = 8.50 - 7.20 (m, 9H, H6, H5, H4, H4', H4, H3, H3', Ha, Hb), 2.49 (s, br, CH_3, CH_3SO_3Pt), 2.29 (s, br, $CH_3SO_3^-$); MS (ES^+) *m/z* 586 [M^+)]; IR (KBr) $\tilde{\nu}$ = 3075 cm^{-1} (m), 2115 cm^{-1} (m), 1659 (s) cm^{-1}, 1601 (s) cm^{-1}, 1054 (s) cm^{-1}; UV-Vis (CH_3OH): λ_{max} in nm (log ε) 470 (3.4), 345 (3.3), 330 (4.1), 280 (4.7), 255 (4.7).

4.5.6 Synthesis of [DTPA-bis(Pt(tpy)N-(4-ethynylphenyl)(acetamide)](CH_3SO_3)$_2$

Sodium methoxide (10 mg 0.2 mmol) was added to a stirred solution of DTPA-bis-N-(4-ethynylphenyl) acetamide (23 mg 0.04 mmol) in methanol was added sodium methoxide (10 mg 0.2 mmol). The resulting solution was stirred at room temperature for 30 min. [Pt(tpy)MeCN](CH_3SO_3) (50 mg 0.09 mmol) was added to the reaction mixture which turned to red colour and was heated under refluxed for 2h at 80 °C under a nitrogen atmosphere. The solvent was removed by vacuum and the deep red precipitate was dissolved in deionised water (10 cm^3). The pH was lowered to 3.0 by dropwise addition of methane sulfonic acid 0.1 M. The solvent was then reduced by vacuum to approximately 2 ml and dropwise addition of acetonitrile afforded a red precipitate that was isolated by filtration and washed with acetonitrile (2 $\times$ 10 cm^3) and diethyl ether (20 cm^3). Yield 58%.

MS (MALDI) = *m/z* 1446.3 [M^+]; MS (ES^+): *m/z* 739.7 [M^++Na]; IR (KBr) $\tilde{\nu}$ = 3074 cm^{-1} (m), 2109 cm^{-1} (m), 1609 (s) cm^{-1}, 1601 (s) cm^{-1}, 1173 (s) cm^{-1}; UV-Vis (H_2O): λ_{max} in nm (log ε) 420 (4.2), 280 (4.7); Elemental Analysis calcd (%) for $C_{62}H_{59}N_{11}O_{14}Pt_2S_2$ (H_2O) ($CH_3SO_3^-$)$_2$ Na: C, 41.67; H, 3.36; N, 8.25; found: C, 41.79; H, 3.25; N, 8.00;

4.5.7 Synthesis of $[LnC{\equiv}CPt_2](CH_3SO_3)_2$ (Ln = Eu, Nd)

[DTPA-bis(Pt(tpy)N-(4-ethynylphenyl)acetamide)]$(CH_3SO_3)_2$ (50 mg 0.03 mmol) was dissolved in minimum amount of deionised water and the pH corrected to 5.5 by the drop wise addition of tetrabutyl ammonium hydroxide followed by the addition of 40 %w in water, and $LnCl_3 \cdot 6\ H_2O$ (0.03 mmol) to the solution keeping the pH stable around 5. Solvent was then reduced by vacuum to approximately 2 ml followed with drop wise addition of acetonitrile. The fine red precipitate was isolated by filtration and washed with acetonitrile (2×10 cm^3) and diethyl ether (2×20 cm^3).

[Eu(C≡CPt)$_2$] MS (ES$^+$): *m/z* 797.6 [M$^+$]; UV-Vis (H_2O): λ_{max} in nm (log ε) 420 (4.2), 280 (4.7); Elemental Analysis calcd (%) for $C_{60}H_{59}EuN_{11}O_{14}Pt_2S_2\ (H_2O)_2\ (CH_3SO_3)_2$ Na: C, 37,78; H, 3.27; N, 7.57; found: C, 37.66; H, 3.12; N 7.56; Yield 65%

[Nd(C≡CPt)$_2$] MS ES$^+$: *m/z* 792.1 [M^{2+}]; UV-Vis (H_2O): λ_{max} in nm (log ε) 420 (4.2), 280 (4.7); Elemental Analysis calcd (%) for $C_{62}H_{59}NdN_{11}O_{14}Pt_2S_2\ (H_2O)$ (Cl): C, 40.67; H, 3.19; N, 8.41; found: C, 40.62; H, 3.39; N 8.27; Yield 53%

References

[1] Jarosz, P.; Du, P. W.; Schneider, J.; Lee, S. H.; McCamant, D.; Eisenberg, R. *Inorg. Chem.* **2009**, *48*, 9653.

[2] (a) Lippard, S. J. *Acc. Chem. Res.* **1978**, *11*, 211; (b) Mcfadyen, W. D.; Wakelin, L. P. G.; Roos, I. A. G.; Leopold, V. A. *J. Med. Chem.* **1985**, *28*, 1113.

[3] Morgan, G. T.; Burstall, F. H. *J. Chem. Soc.* **1934**, 1498.

[4] Cummings, S. D. *Coord. Chem. Rev.* **2009**, *253*, 1968.

[5] Whittle, C. E.; Weinstein, J. A.; George, M. W.; Schanze, K. S. *Inorg. Chem.* **2001**, *40*, 405.

[6] Muro, M. L.; Rachford, A. A.; Wang, X. H.; Castellano, F. N. *Photophysics of Organometallics*; Springer-Verlag Berlin, 2010; Vol. 29; p 159.

[7] Chan, C. W.; Cheng, L. K.; Che, C. M. *Coord. Chem. Rev.* **1994**, *132*, 87.

[8] (a) Constable, E. C. *Chem. Soc. Rev.* **2007**, *36*, 246; (b) Ballhaus.Cj.; Bjerrum, N.; Dingle, R.; Erik, K.; Hare, C. R. *Inorg. Chem.* **1965**, *4*, 514; (c) Balzani, V.; Carassiti.V, *J. Phys. Chem.* **1968**, *72*, 383.

[9] Castellano, F. N.; Pomestchenko, I. E.; Shikhova, E.; Hua, F.; Muro, M. L.; Rajapakse, N. *Coord. Chem. Rev.* **2006**, *250*, 1819.

[10] Yam, V. W. W.; Tang, R. P. L.; Wong, K. M. C.; Cheung, K. K. *Organometallics* **2001**, *20*, 4476.

[11] Liu, X. J.; Feng, J. K.; Meng, J.; Pan, Q. J.; Ren, A. M.; Zhou, X.; Zhang, H. X. *Eur. J. Inorg. Chem.* **2005**, 1856.

[12] Zhou, X.; Zhang, H. X.; Pan, Q. J.; Xia, B. H.; Tang, A. C. *J. Phys. Chem. A* **2005**, *109*, 8809.

[13] Shikhova, E.; Danilov, E. O.; Kinayyigit, S.; Pomestchenko, I. E.; Tregubov, A. D.; Camerel, F.; Retailleau, P.; Ziessel, R.; Castellano, F. N. *Inorg. Chem.* **2007**, *46*, 3038.

[14] Yang, Q. Z.; Wu, L. Z.; Wu, Z. X.; Zhang, L. P.; Tung, C. H. *Inorg. Chem.* **2002**, *41*, 5653.

[15] Tong, G. S. M.; Law, Y. C.; Kui, S. C. F.; Zhu, N. Y.; Leung, K. H.; Phillips, D. L.; Che, C. M. *Chem-Eur. J*. **2010**, *16*, 6540.

[16] Tang, W. S.; Lu, X. X.; Wong, K. M. C.; Yam, V. W. W. *J. Mater. Chem*. **2005**, *15*, 2714.

[17] Han, X.; Wu, L. Z.; Si, G.; Pan, J.; Yang, Q. Z.; Zhang, L. P.; Tung, C. H. *Chem. Eur. J*. **2007**, *13*, 1231.

[18] Nishihara, H.; Kanaizuka, K.; Nishimori, Y.; Yamanoi, Y. *Coord. Chem. Rev*. **2007**, *251*, 2674.

[19] Ziessel, R.; Diring, S. *Tetrahedron Lett*. **2006**, *47*, 4687.

[20] Ziessel, R.; Diring, S.; Retailleau, P. *Dalton Trans*. **2006**, 3285.

[21] Muro, M. L.; Diring, S.; Wang, X.; Ziessel, R.; Castellano, F. N. *Inorg. Chem*. **2008**, *47*, 6796.

[22] Ziessel, R.; Diring, S.; Kadjane, P.; Charbonniere, L.; Retailleau, P.; Philouze, C. *Chem. Asian. J*. **2007**, *2*, 975.

[23] Kadjane, P.; Platas-Iglesias, C.; Ziessel, R.; Charbonniere, L. J. *Dalton Trans*. **2009**, 5688.

[24] Wong, K. M. C.; Tang, W. S.; Chu, B. W. K.; Zhu, N. Y.; Yam, V. W. W. *Organometallics* **2004**, *23*, 3459.

[25] Solomons, M. Ph.D. thesis, University of Birmingham, Birmingham UK, 2008.

[26] Ma, D. L.; Shum, T. Y. T.; Zhang, F. Y.; Che, C. M.; Yang, M. S. *Chem. Commun*. **2005**, 4675.

[27] Sanchez-Cano, C.; Hannon, M. *Dalton Trans*. **2009**, 10765.

[28] Holz, R. C.; Chang, C. A.; Horrocks, W. D. *Inorg. Chem*. **1991**, *30*, 3270.

[29] Glover, P. B.; Ashton, P. R.; Childs, L. J.; Rodger, A.; Kercher, M.; Williams, R. M.; Cola, L. D.; Pikramenou, Z. *J. Am. Chem. Soc*. **2003**, *125*, 9918.

[30] Bunzli, J. C. G.; Choppin, G. R. *Lanthanide Probes in Life, Chemical and Earth Sciences*; Elsevier Science LTD., 1990.

[31] Moses, J. E.; Moorhouse, A. D. *Chem. Soc. rev.* **2007**, *36*, 1249.

[32] Stasiuk, G. J.; Lowe, M. P. *Dalton Trans.* **2009**, 9725.

[33] Jauregui, M.; Perry, W. S.; Allain, C.; Vidler, L. R.; Willis, M. C.; Kenwright, A. M.; Snaith, J. S.; Stasiuk, G. J.; Lowe, M. P.; Faulkner, S. *Dalton Trans.* **2009**, 6283.

[34] Seccombe, R. C.; Lee, B.; Henry, G. M. *Inorg. Chem.* **1975**, *14*, 1147.

[35] Chen, C. H. B.; Milne, L.; Landgraf, R.; Perrin, D. M.; Sigman, D. S. *ChemBioChem* **2001**, *2*, 735.

[36] Annibale, G.; Bergamini, P.; Bertolasi, V.; Bortoluzzi, M.; Cattabriga, M.; Pitteri, B. *Eur. J. Inorg. Chem.* **2007**, 5743.

[37] Huheey, J. E.; Keiter, E. A.; Keiter, R. L. *Inorganic chemistry : principles of structure and reactivity, 5th ed.*; Addison Wesley, 2005.

[38] Arena, G.; Scolaro, L. M.; Pasternack, R. F.; Romeo, R. *Inorg. Chem.* **1995**, *34*, 2994.

[39] Aime, S.; Fasano, M.; Paoletti, S.; Terreno, E. *Gazz. Chim. Ital.* **1995**, *125*, 125.

[40] Chan, W. K.; Ho, C. M.; Wong, M. K.; Che, C. M. *J. Am. Chem. Soc.* **2006**, *128*, 14796.

[41] Yam, V. W. W.; Wong, K. M. C.; Zhu, N. Y. *J. Am. Chem. Soc.* **2002**, *124*, 6506.

[42] Tam, A. Y. Y.; Wong, K. M. C.; Zhu, N. Y.; Wang, G. X.; Yam, V. W. W. *Langmuir* **2009**, *25*, 8685.

[43] Yam, V. W. W.; Chan, K. H. Y.; Wong, K. M. C.; Zhu, N. Y. *Chem. Eur. J.* **2005**, *11*, 4535.

[44] Tears, D. K. C.; McMillin, D. R. *Coord. Chem. Rev.* **2001**, *211*, 195.

[45] Kieltyka, R.; Fakhoury, J.; Moitessier, N.; Sleiman, H. F. *Chemistry* **2008**, *14*, 1145.

[46] 12.0, V. *CambridgeSoftware, Chem3D*; 2010.

[47] Georgopoulou, A. S.; Ulvenlund, S.; Mingos, D. P.; Baxter, I.; Williams, D. J. *J. Chem. Soc., Dalton Tans*. **1999**, 547.

[48] Yang, Q. Z.; Tong, Q. X.; Wu, L. Z.; Wu, Z. X.; Zhang, L. P.; Tung, C. H. *Eur. J. Inorg. Chem*. **2004**, 1948.

[49] Lu, W.; Mi, B. X.; Chan, M. C. W.; Hui, Z.; Che, C. M.; Zhu, N. Y.; Lee, S. T. *J. Am. Chem. Soc*. **2004**, *126*, 4958.

[50] Clark, M. L.; Green, R. L.; Johnson, O. E.; Fanwick, P. E.; McMillin, D. R. *Inorg. Chem*. **2008**, *47*, 9410.

[51] Suntharalingam, K.; White, A. J. P.; Vilar, R. *Inorg. Chem*. **2010**, *49*, 8371.

[52] Wetmur, J. G. *Crit. Rev. Biochem. Mol. Bio*. **1991**, *26*, 227.

[53] Breslauer, K. J.; Frank, R.; Blocker, H.; Marky, L. A. *Proc. Natl. Acad. Sci. U.S.A*. **1986**, *83*, 3746.

[54] Kumar, C. V.; Asuncion, E. H. *J. Am. Chem. Soc*. **1993**, *115*, 8547.

[55] Wang, Y. P.; Che, C. M.; Wong, K. Y.; Peng, S. M. *Inorg. Chem*. **1993**, *32*, 5827.

[56] Foxon, S. P.; Phillips, T.; Gill, M. R.; Towrie, M.; Parker, A. W.; Webb, M.; Thomas, J. A. *Angew Chem Int Edit* **2007**, *46*, 3686.

[57] Chen, W.; Kitamura, Y.; Zhou, J.-M.; Sumaoka, J.; Komiyama, M. *J. Am. Chem. Soc*. **2004**, *126*, 10285.

[58] Jennette, K. W.; Lippard, S. J.; Vassilades, G. A.; Baueri, W. R. *Proc. Nat. Acad. Sci. USA* **1974**, *71*, 3829.

[59] Ramos-Lima, F. J.; Vrana, O.; Quiroga, A. G.; Navarro-Ranninger, C. N.; Halamikova, A.; Rybnickova, H.; L. Hejmalova, V. B. *J. Med. Chem*. **2006**, *49*, 2640.

[60] Bauer, W. R. *Annual Rev. of Biophys. and Bioeng*. **1978**, *7*, 287.

[61] Newman, J. *Biopolymers* **1984**, *23*, 1113 – 1119.

[62] Bellon, S. F.; Coleman, J. H.; Lippard, S. J. *Biochemistry* **1991**, *30*, 8026.

Chapter 5

Lanthanide-platinum monointercalator based on an asymmetric DTPA ligand

5.1 Project overview

The aim of the work presented in this chapter is to prepare a diethylene triamine pentaacetic acid (DTPA) bis(amide) derivatives, which bears only one soft ligand for binding to the terpyridylplatinum(II) moiety in order to obtain [LnH_3LPt]; a luminescent lanthanide probe with a single DNA intercalator unit (Figure 5.1).

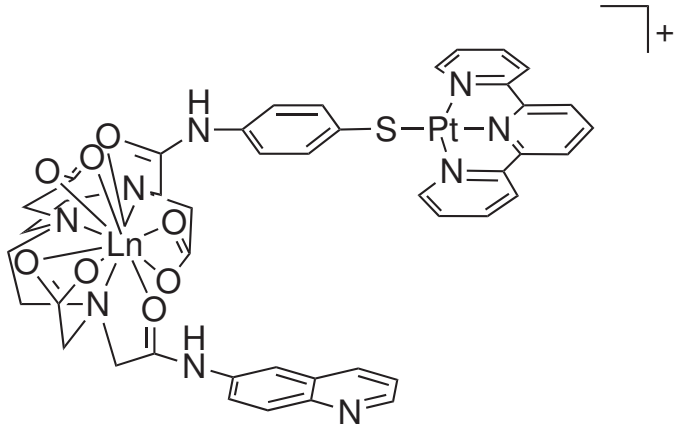

[LnH_3LPt]

Figure 5.1: Structure of the monointercalator incorporating both a *d* and *f*-block metal for binding to DNA.

Comparing the bis-intercalator complex [$LnPt_2$]Cl_2 with [LnLPt]PF_6, we replaced one intercalating unit with a quinoline moiety, although the hairpin design and its rigidity were left unchanged. With this complex we aim to investigate the effect upon interaction with DNA and how this affects the photophysical properties.

5.2 Results and discussion

5.2.1 Synthesis and characterisation of the asymmetric ligand H_3L

In order to synthesise the $[EuH_3LPt]PF_6$ complex, the synthesis and isolation of the asymmetric ligand $\mathbf{H_3L}$ was carried out according to a previously reported procedure.[1,2] The synthetic approach used the co-condensation of 6-aminoquinoline with DTPA-bis(anhydride) and 4-aminothiophenol. This reaction led to a mixture of the desired asymmetric ligand $\mathbf{H_3L}$ and symmetric bisamides $\mathbf{H_3L}^a$ and $\mathbf{H_3L}^b$ (Scheme 5.1),

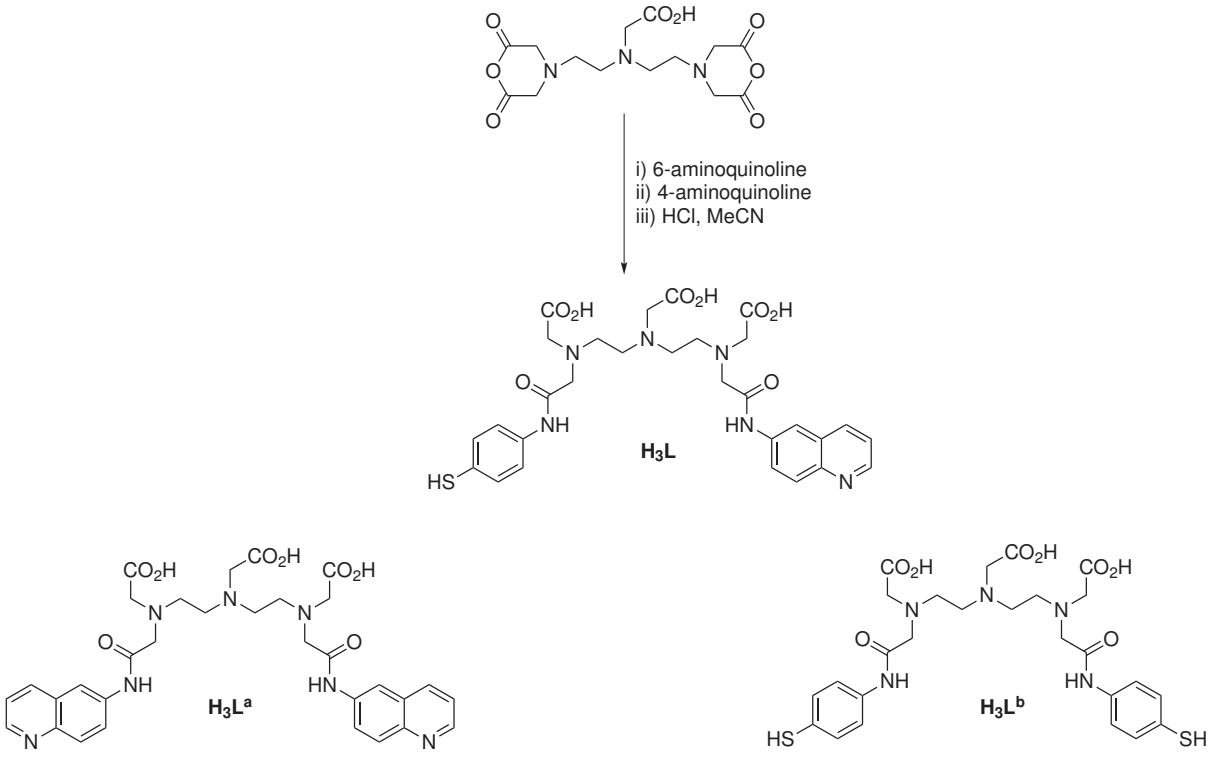

Scheme 5.1: Synthesis of the asymmetric **L** and the symmetric bisamides $\mathbf{L}^a$ and $\mathbf{L}^b$.

The mixture of asymmetric and symmetric ligands was separated into the different compounds by High Pressure Liquid Chromatography (RP-HPLC, Figure 5.2) using a C18 reverse phase column. The mixture of **L**, $\mathbf{L}^a$ and $\mathbf{L}^b$ was eluted by running a gradient from water to acetone over 40 minutes at a flow rate of 10 ml/min. The bisamidoquinolyl derivative $\mathbf{L}^a$ elutes first at 16.0 minutes due to its hydrophilic nature. The more hydrophobic bisamidothiophenyl derivative $\mathbf{L}^b$ elutes much later at 33.2 minutes when the amount of acetone was increased. The ligand $\mathbf{H_3L}$ elutes in between the two symmetric bisamides at 25.0 minutes.

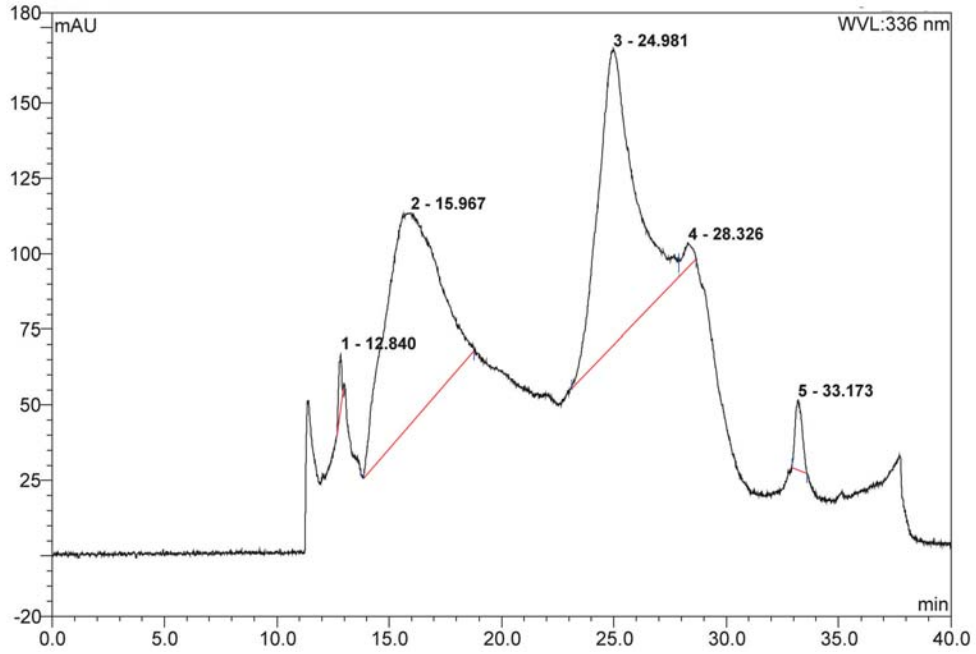

Figure 5.2: RP-HPLC separation of **L** (25.0 min) from **La** (16.0 min) and **Lb** (33.2 min) monitored from UV absorbance at 336 nm.

The ^{1}H NMR of $\mathbf{H_3L}$ was recorded in D_2O/NaOD and it is in agreement with the previously reported ones.[1] The signal at 8.41 ppm is assigned to the **Hf** proton which is observed as a doublet of doublets due to coupling with **He** at 7.19 ppm and with **Hd** at 7.98 ppm, while the **Hh** proton was observed at 7.45 ppm as a doublet of doublets due to the coupling with **Hc** and **Hg** respectively at 7.64 and 7.71 ppm. The aminothiophenyl protons were observed as doublets at 6.95 and 6.60 ppm which can be respectively assigned as **Hb** and **Ha**. While characteristic DTPA signals were observed at 3.14 (**Hm**, **Hp**, **Hk**), at 2.85 (**q**, **x**) and 2.44 ppm (**Hj, Ho, Hn, Hl**). The integration of the aminothiophenyl resonances (**Ha** and **Hb**) resulted to be exactly double when compared to the protons arising from the quinolin moiety (Figure 5.3).[1] [2]

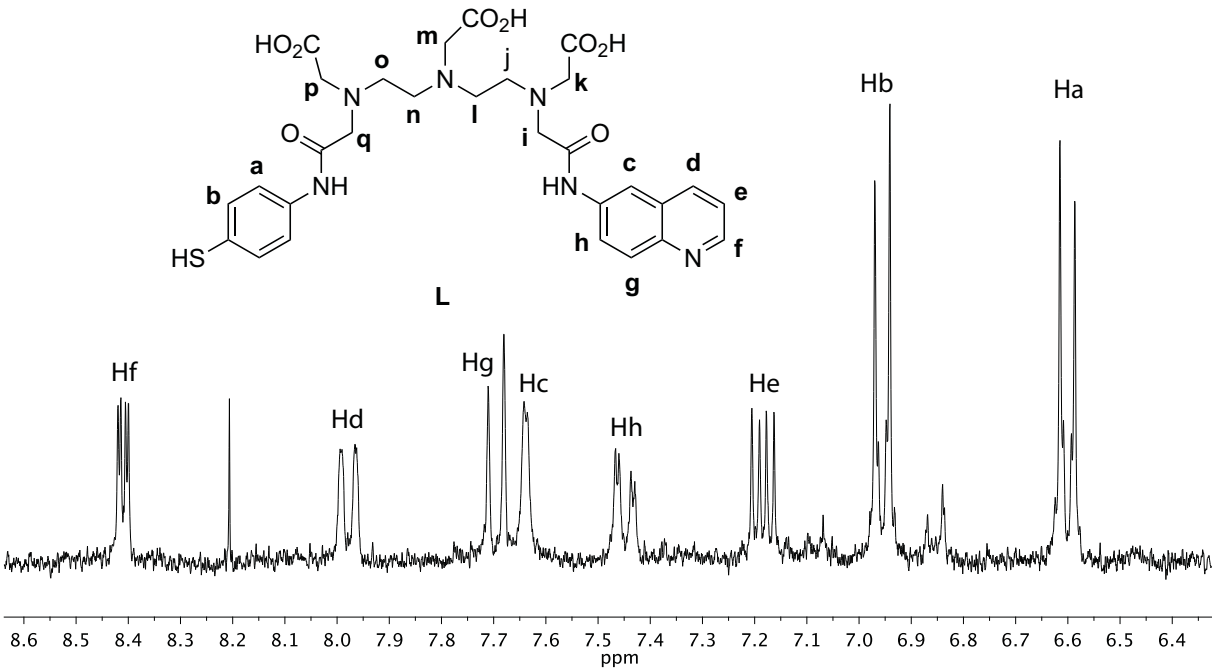

Figure 5.3: The 300 MHz ^{1}H NMR spectrum of the aromatic region of **L** in D_2O/ NaOD.

5.2.2 Synthesis of the heterometallic luminescent lanthanide complex [EuH$_3$LPt]

The synthesis of [EuH$_3$LPt] could be achieved by self assembly using stoichiometric control by combining the three components L, [Pt(tpy)Cl] (CF_3SO_3) and $LnCl_3 \cdot 6H_2O$ in a 1:1:1 ratio. A variety of different approaches, both sequential and one-pot synthetic routes, can be successfully employed to isolate the final product. However, the procedure predominantly employed in this work involved prior assembly of the ligand [LPt] in order to confirm that the first step was successful (Scheme 5.2)

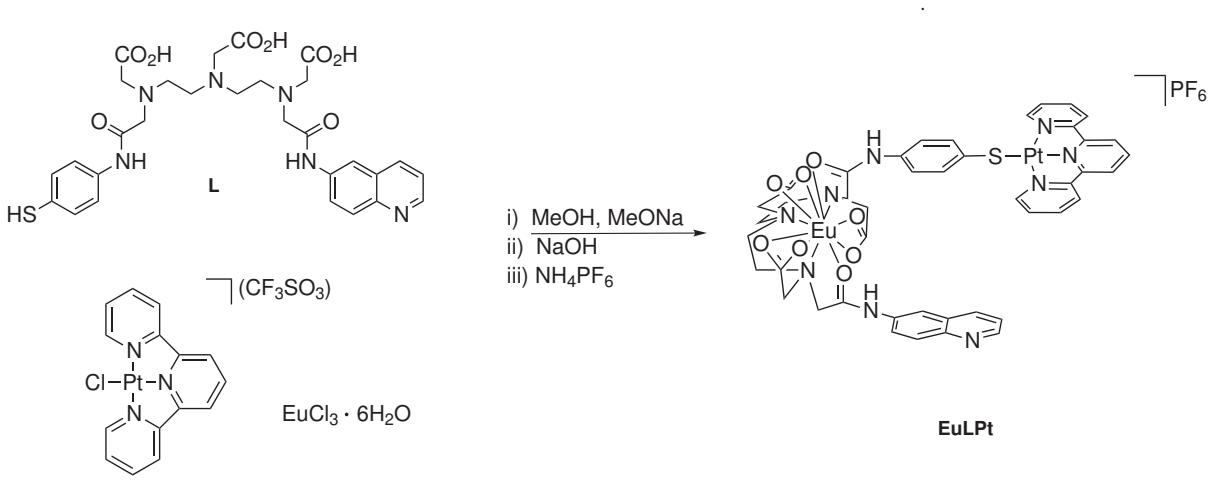

Scheme 5.2: Synthetic routes to [EuH$_3$LPt](PF$_6$).

The synthesis proceeded by deprotonation of ligand **L** at sulphur by employing sodium methoxide and was successively combined with [Pt(tpy)Cl](CF_3SO_3) to form the Pt–S bond linkage. The reaction was refluxed for 2 hours under an inert atmosphere and finally the pH of the solution was raised to 4 by addition of NaOH. The final product was isolated by a metathesis reaction using a saturated methanolic solution of ammonium hexafluorophosphate to precipitate [LPt] as the PF_6 salt. [LPt](PF_6) was characterised by electrospray spectrometry, ^{1}H NMR and UV-vis spectroscopy. A peak at *m/z* 534 is assigned to [M -(PF_6)+ H]$^{2+}$ as the doubly charged species. The characteristic isotope pattern with a half point gap between the peaks was observed at *m/z* = 535, which corresponds to the doubly charged species [M-(PF_6)+ H]$^{2+}$ (Figure 5.4).

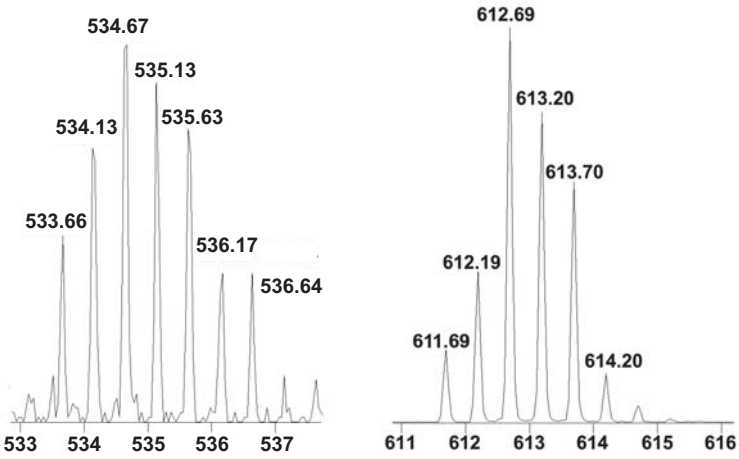

Figure 5.4: Electrospray mass spectra of [LPt](PF_6) (left) and of [EuH_3LPt](PF_6) (right)

A second peak containing a Pt isotopic pattern was found at *m/z* = 464, which belongs to the [Pt(tpy)Cl]$^+$. However since the elemental analysis and ^{1}H-NMR excluded the presence of any secondary product, the pattern at *m/z* = 464 can be assigned to the fragmentation product [Pt(tpy)Cl]$^+$.

[EuH_3LPt](PF_6) was also characterised by electrospray mass spectrometry. It is expected as [M - PF_6 + H + Na] with a characteristic isotopic pattern at *m/z* 613 (Figure 5.3). The peak at *m/z* = 464 was again observed in the mass spectrum of [EuH_3LPt](PF_6) correspondig to the fragmentation product [Pt(tpy)Cl]$^+$.

^{1}H-NMR recorded in d_4-methanol showed the characteristic doublet arising from **H6** of terpyridylplatinum(II) unit at 8.79 ppm, while in between 8.60 and 8.25 ppm are the **Hf** from the quinoline and **H4/H4'** from the terpyridine. We found **Hd** and **Hc** respectively at 8.12 and 7.95 ppm, while the **Hh**

at 7.75 ppm overlapped with **H5** arising from quinoline. Upon coordination to platinum(II) the **Hb** resulted in being downshielded to 7.50 ppm while the **Ha** was found at 7.30 ppm overlapped with **He** from quinoline (Figure 5.5). A comparison of **Hd** and **H6** integrals showed the expected ratio 1:2.

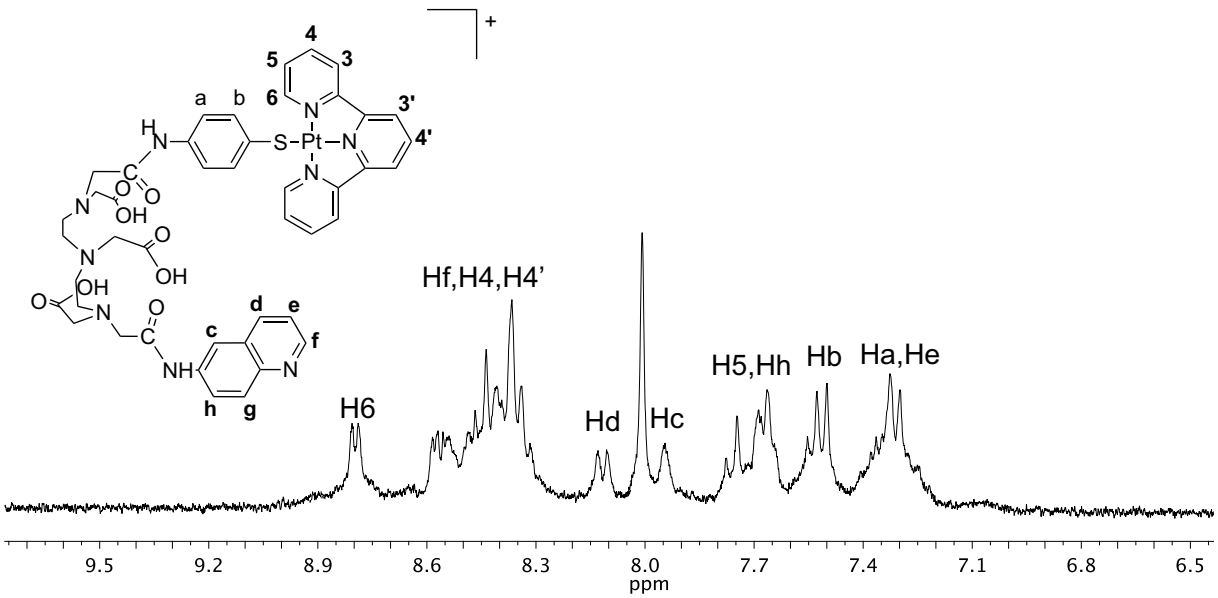

Figure 5.5: 300 MHz ^{1}H NMR spectrum of the aromatic region of **L** in D_2O/ NaOD.

5.2.3 Luminescence studies of [LPt](PF_6)

The UV-vis absorption spectrum of [LPt](PF_6) has two main absorption features, one at 250 - 380 nm in the UV region of the spectrum, while the other is in the visible region between 400 - 700 nm (Figure 5.6). The band at 250 nm belongs to the $\pi \rightarrow \pi^*$ transitions localised on on the thiophenyl ring and the bands at 280 and 345 nm can be attributed to the $\pi \rightarrow \pi^*$ transitions of the terpyridine ring. The band at 330 nm is due to the absorption from the $\pi \rightarrow \pi^*$ of the quinoline moiety which overlaps with the terpyridine absorption; a slight shoulder is observed at 380 nm, which arises from the metal to ligand charge transfer transition (MLCT).[3]

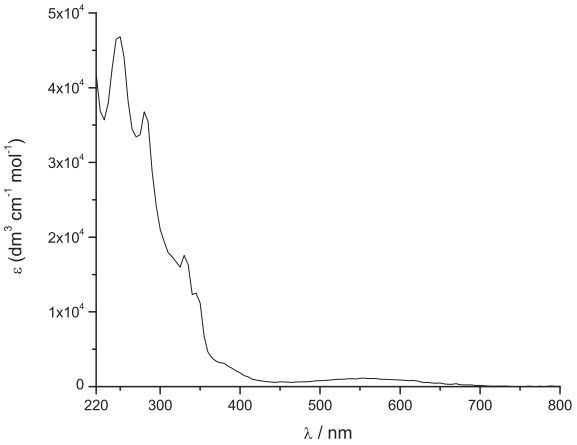

Figure 5.6: UV-vis absorption spectrum of $[H_3L–Pt](PF_6)$ (25 μM) in methanol.

The low energy band centred at 550 nm is due to ligand to ligand charge transfer (LLCT). The appearance of this band is illustrative of complex formation and its colour is dependent on solvent polarity.[4]

5.2.4 Emission Studies of $[EuH_3LPt](PF_6)$

Typical Eu(III) luminescence was observed upon excitation of $[EuH_3LPt]PF_6$ at 330 nm and red emission was observed as a result of the luminescent $^5D_0 \rightarrow {}^7F_J$ (J = 0, 1, 2, 3, 4) transition observed at 580, 590, 615, 650, 695 nm (Figure 5.7)

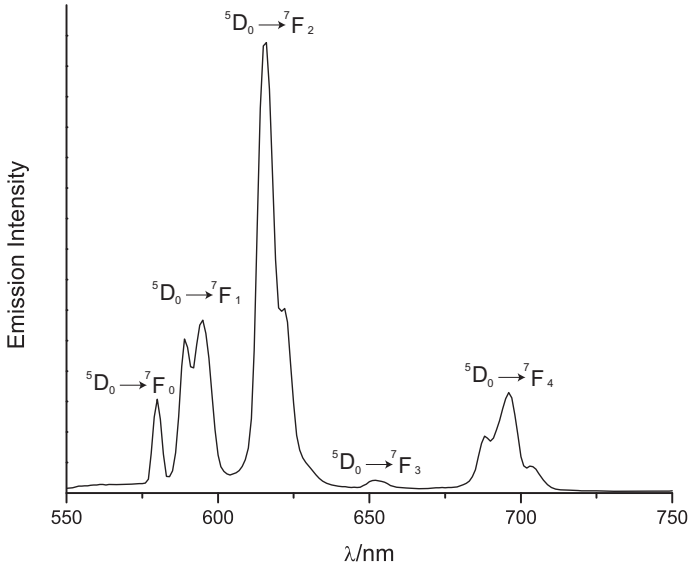

Figure 5.7: Emission spectrum of $[EuH_3LPt](PF_6)$ in MeOH (25 μM), λ_{exc} = 330 nm (corrected for PMT response).

However Eu(III) emission could also be obtained through excitation of the amidothiophenol group at 250 nm, and with excitation at 280 and 345 nm, which are absorption maxima that belongs to the terpyridyl and quinoline moieties. Indeed the excitation profile of [EuH_3LPt](PF_6) shows two clear peaks, one at 330 nm and the other at 345 nm (Figure 5.8), with the latter peak being attributed to the $\pi \rightarrow \pi^*$ transition of the terpyridine ring. Thus both quinoline and platinum(II) entities contribute with energy transfer to the central europium ion with the quinoline excited state dominating the process.

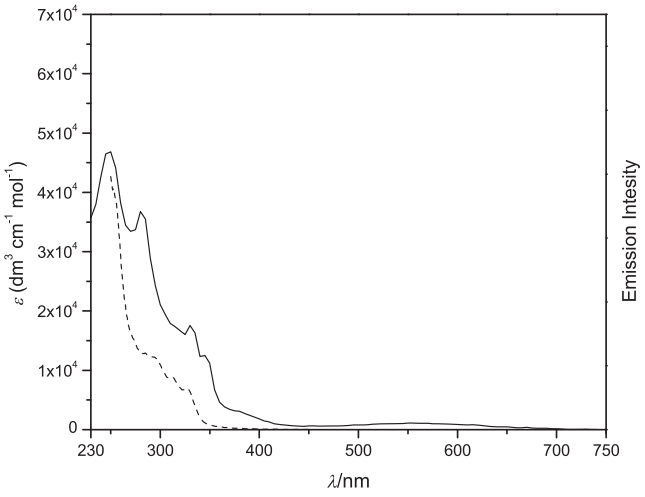

Figure 5.8: UV-vis absorption spectrum of [EuH_3LPt](PF_6) in MeOH(solid line)(25 μM) and excitation spectrum (dashed line) recorded by monitoring emission at 615 nm (corrected for lamp profile).

5.2.5 DNA binding studies

Emission studies

Luminescence studies were performed to investigate how the addition of CT-DNA to the [EuH_3LPt](PF_6) affects the Eu(III) ion emission. The excitation wavelength selected was 330 nm, where the DNA molar extinction coefficient is the smallest and the energy transfer for the lanthanide sensitisation is still efficient. Upon excitation at 330 nm we observed a relatively weak lanthanide based emission which was enhanced by almost double upon addition of CT-DNA to the [EuH_3LPt] (Figure 5.9).

The same emission experiments were performed with poly (dAdT) DNA and we observed changes similar to those recorded upon interaction with CT-DNA. The Eu(III) emission was initially weak but

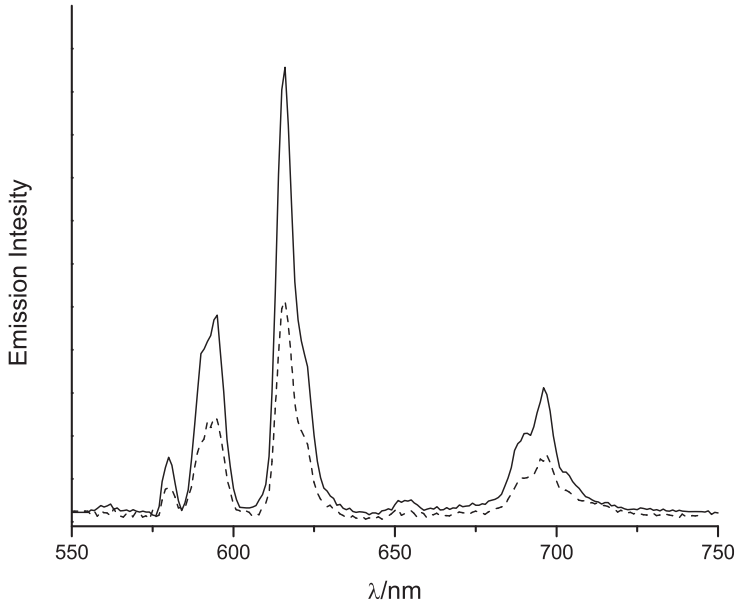

Figure 5.9: An emission spectra of [EuH$_3$LPt](PF$_6$) (180 μM) (dashed line), 4:1 CT-DNA:[EuH$_3$LPt](PF$_6$) complex (solid line) in H$_2$O, 20 mM sodium phosphate buffer. λ_{exc} = 330 nm (Corrected for PMT response).

enhanced by double upon interaction of the complex with poly(dAdT), while the luminescence was enhanced by almost 2.5 times upon addition of poly(dGdC) (Figure5.10).

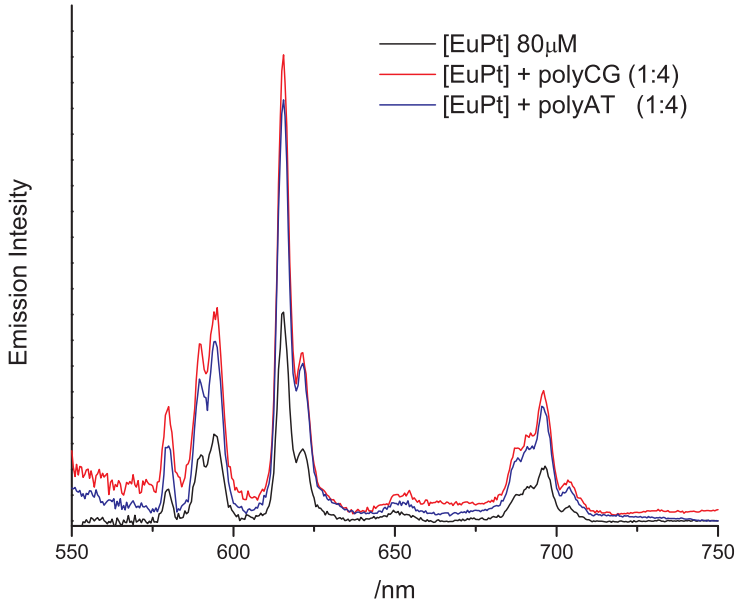

Figure 5.10: Emission spectra of [EuH$_3$LPt](PF$_6$) (80 μM) with 4:1 poly(dAdT) (4:1) and poly(dGdC) (4:1) in H$_2$O, 20 mM sodium phosphate buffer. λ_{exc} = 330 nm, uncorrected.

When excitation of [EuH_3LPt](PF_6) occurs at 330 nm, energy transfer from the quinoline-terpyridine moiety to the lanthanide ion is realised. However the efficiency of the energy transfer process is dramatically affected by the quenching effect which arises from the O–H oscillators leading to a relatively weak europium emission. However addition of DNA to the [EuH_3LPt](PF_6) leads to the intercalation of the platinum(II) terpyridine units between the DNA base pairs. The DNA hydrophobic environment reduces the quenching effect arising from the aqueous buffer, realising a more efficient energy transfer which is observed as luminescent enhancement of the lanthanide ion. Addition of poly(dAdT) and poly(dGdC) to [EuH_3LPt](PF_6) resulted in a non specific DNA binding, since a luminescence enhancement of almost double was observed in both cases.

Circular dichroism

The DNA binding of [EuH_3LPt](PF_6) was investigated by circular dichroism (CD), which measures the difference in absorbance between the right and left circularly polarised light, and hence is able to measure the molar extinction coefficients differences ($\Delta\varepsilon$) between enantiomers of chiral compounds.[5] This concept is summarised within equation 5.1:

$$CD = A_l - A_r \tag{5.1}$$

where A_l and A_r are the absorbances for the light polarised left and right respectively. As shown in chapter 2, only molecules which are chiral will be able to exhibit a CD signal. While achiral molecules are not detected by CD simply because they are not able to change the phase for one of the two components of the circularly polarised light. However an achiral molecule can become active in CD spectroscopy as long as interaction with a chiral molecule can be realiesed (i.e supramolecular interaction).

The circular dichroism of CT-DNA showed the characteristic B-DNA shape with the negative and positive signals respectively at 245 and 276 nm.[6] The addition of CT-DNA and formation of the [EuH_3LPt]/CT-DNA adduct showed small changes in the DNA region of the CD spectrum, while a weak induced CD signal was observed in the terpyridine and LLCT region (Figure 5.11).

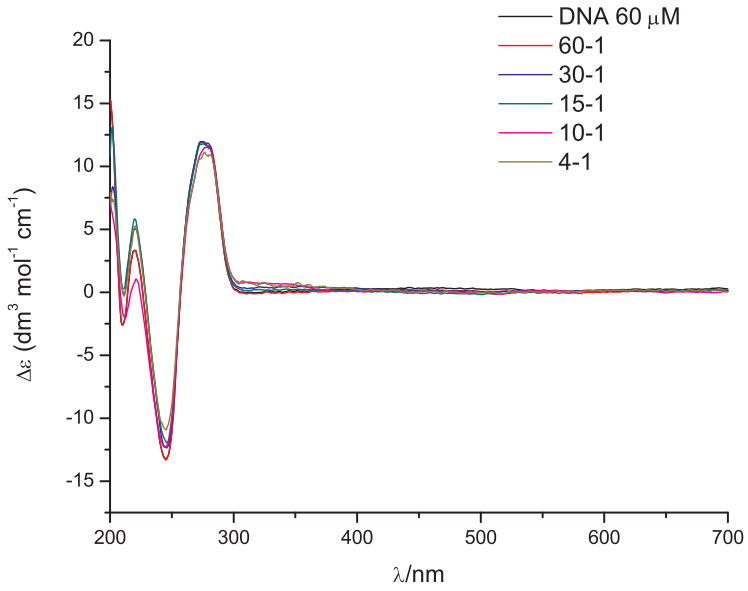

Figure 5.11: CD spectra of 60 μM CT-DNA upon interaction with [EuH_3LPt] range from 60:1 to 4:1, in 20 mM sodium phosphate buffer.

The ICD signal observed in the region in between 300 and 400 nm, can be assigned to a non degenerate coupling of the transition moment arising from the platinum(II) terpyridine with those originating from the CT-DNA bases. However the DNA region between 220 and 300 nm showed only slight changes upon interaction with [EuH_3LPt], which may be ascribed to the reduced DNA stiffening ability of [EuH_3LPt] when compared to the hairpin shaped complexes ([$LnPt_2$] and [$LnC{\equiv}CPt_2$]). Hence these results are consistent with the mono-intercalator behaviour expected after replacing one of the platinum terpyridine unit with the quinoline moiety.

Linear dichroism

Linear dichroism (LD) can be defined as the difference in absorption of linearly polarised light both parallel and perpendicular to a chosen plane and can be used to probe the orientation of molecules (see chapter 2 page 68). The B-DNA conformation is characterised by a negative signal in the region between 220 and 300 nm, which arises from the $\pi \rightarrow \pi^*$ with transitions moments at an angle of greater than 54° compared to the DNA helix axis. The intensity of the LD signal is dependent on the degree to which the DNA is oriented, being reduced by effects such as DNA-bending, and increased by intercalation between the bases of the DNA. This latter effect is better known as stiffening of the

DNA double helix.

The CT-DNA usually exhibits a negative LD signal at λ = 260 nm as its bases are orthogonal to the main axis of the DNA helix. Since the $[EuH_3LPt]PF_6$ is randomly oriented in solution, its LD signal can be observed only upon interaction with DNA, which is oriented by the viscous drag.Thus, when $[EuH_3LPt]PF_6$ is added to CT-DNA three negative signals are observed at 260, 340 and 515 nm (Figure 5.12).

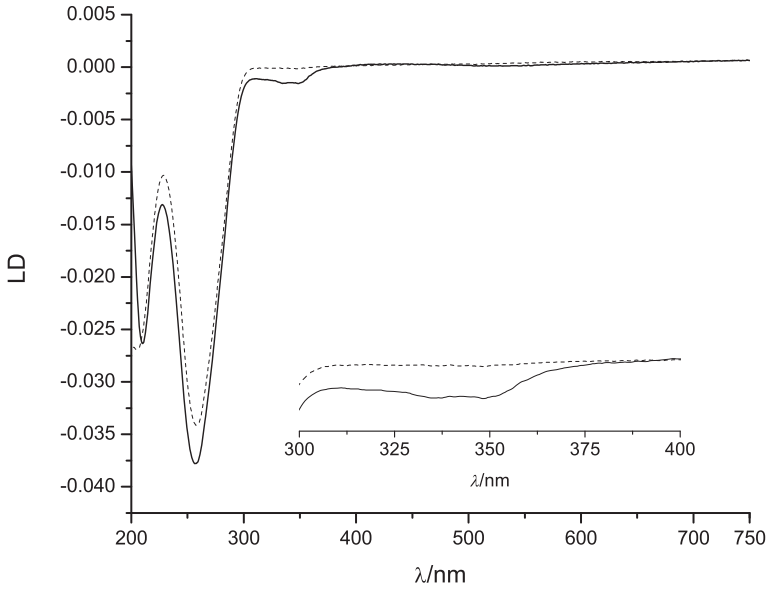

Figure 5.12: LD spectra of 300 μM CT-DNA (dashed line) upon interaction with $[EuH_3LPt]$ at ratio CT-DNA : complex 4-1 (solid line), in 20 mM sodium phosphate buffer.

The 300–520 nm region is characterised by a negative signal arising from transition moments oriented in the plane of the platinum(II) terpyridine unit, which is consistent with the platinum(II) tepryridine intercalating unit lying orthogonal to the DNA helix axis, while the LLCT transition between 400 and 700 nm is characterised by a weak induced linear dichroism (ILD) signal.[6]

The reduced linear dichroism LD^r is often a convenient path length and concentration independent summary of LD data, and it can be calculated according to equation 5.2

$$LD^r = \frac{LD}{A} = \frac{A_{||} - A_{perp}}{A} = \frac{3}{2} S cos^2\alpha - 1 \tag{5.2}$$

where A is the absorption of the sample under isotropic conditions, S the DNA orientation factor

(when S equals 1 we have perfect orientation, while 0 represents the random orientation) and α the angle between the transition moment responsible for the absorption of light at a particular wavelength and the orientation axis which usually corresponds to the main B-DNA axis.[7]

The LD^r signal for $[EuH_3LPt]PF_6$ bound to CT-DNA (Figure 5.13) shows negative signals indicating that the the different terpyridine transitions all lie at the the same angle with the DNA helix axis. This indicates the molecule is lying perpendicular to the helix axis. Furthermore, the LD signal of DNA with $[EuH_3LPt]PF_6$ increases more than the absorbance signal upon $[EuH_3LPt]PF_6$ binding showing that the DNA stiffens upon binding. The magnitude of the LD^r signal is significantly reduced if compared to the one reported for $\mathbf{LnPt_2}$.

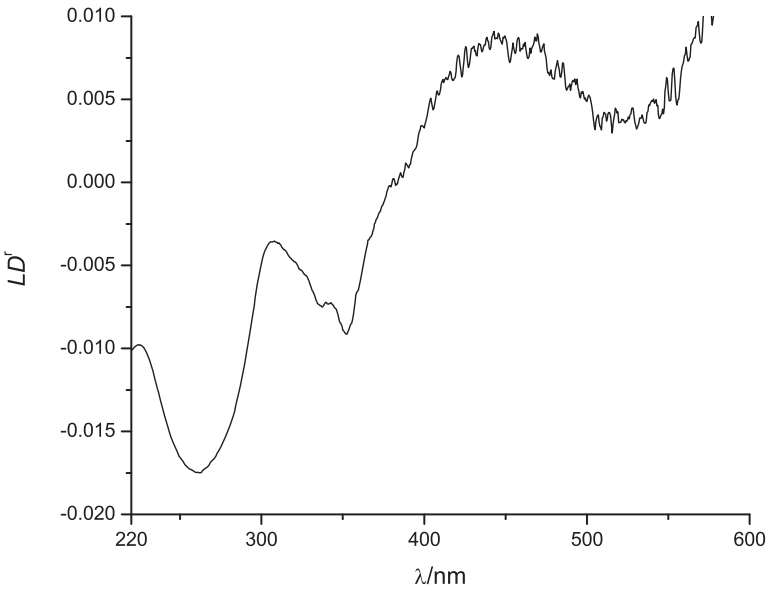

Figure 5.13: Calculated LD^r spectrum of CT-DNA upon interaction with $[EuH_3LPt]PF_6$ (4:1), in 20 mM sodium phosphate buffer.

From these results and the shape of $[EuH_3LPt]PF_6$ we can conclude that the $[EuH_3LPt]PF_6$ binds to DNA *via* an intercalative mode that results in a significant reduced stiffening effect of the DNA when compared to the parent complex $[LnPt_2]Cl_2$.[8]

Gel Electrophoresis

The gel electrophoresis experiments were performed on $[EuH_3LPt]$ complex using 1% agarose gels in 1 mM TEA buffer and plasmid pBR322 DNA, and the results visualised by staining with ethidium

bromide. The ratios of complex to DNA base pairs used were 20:1, 12:1, 8:1, 6:1, 5:1, 3:1. In each case the complex was incubated with the plasmid DNA at 37 °C for 2h prior to loading. By using super-coiled plasmid DNA the unwinding angle of the helix upon addition of the complex can be determined (Figure 5.14).[9]

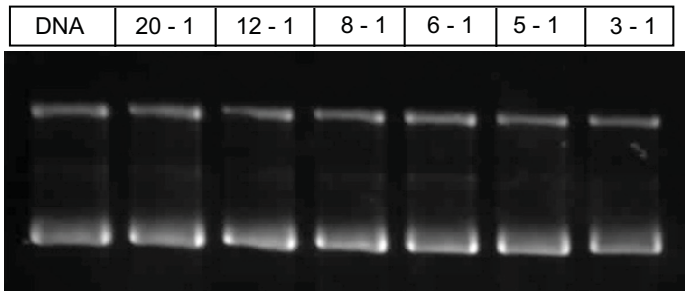

Figure 5.14: Gel image of pBR322 DNA treated with [EuLPt].

The $[EuH_3LPt]PF_6$ complex was found to uncoil DNA into a circular form which travels faster through the gel matrix than the open-circular form, which will be the most retarded. The $[EuH_3LPt]$ showed the ability to interact with DNA by intercalation, however the replacement of one of the terpyridylplatinum(II) recognition units with the quinoline moiety reduced the DNA stiffening dramatically.[10]

A gel electrophoresis experiment for plasmid DNA upon interaction with AATP, was run parallel to the $[EuH_3LPt]PF_6$ ones (Figure 2.50). This experiment suggests that both complexes interacts with DNA in the same way and both are able to produce the same modification on the DNA double helix, and possibly they are characterised with a binding constant of the same order of magnitude.

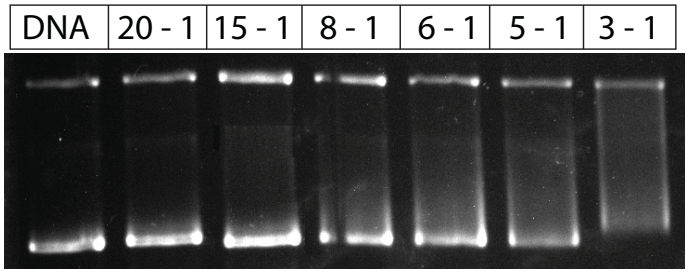

Figure 5.15: Gel image of pBR322 DNA treated with [AATP].

This could be confirmed numerically by calculating the unwinding angle using equation 5.3 where ϕ is the unwinding angle and σ is the superhelicity constant, while r_c is the base complex ratio where supercoiled and relaxed DNA co-migrate.[11] [9]

$$\phi = -18 \times \frac{\sigma}{r_c} \tag{5.3}$$

Using a superhelicity value of –0.074 we found the unwinding angle for [EuH_3LPt] to be 8°, which is similar to that 7.5 ° arising from the AATP and it is almost half the value obtained for [$EuPt_2$]Cl_2 (see chapter 2.2.8 page 86).

Melting point

Based on the hypercromicity effect which is characteristic when a DNA double helix is denatured into a randomly coiled single stranded DNA, we performed a DNA melting point experiment monitoring by UV-vis spectroscopy the absorbance at 260 nm while the sample was heated with and without the [EuH_3LPt] complex. Plotting the absorbance versus temperature, the characteristic sigmoidal behaviour for a DNA melting point was found (Figure 5.16) .

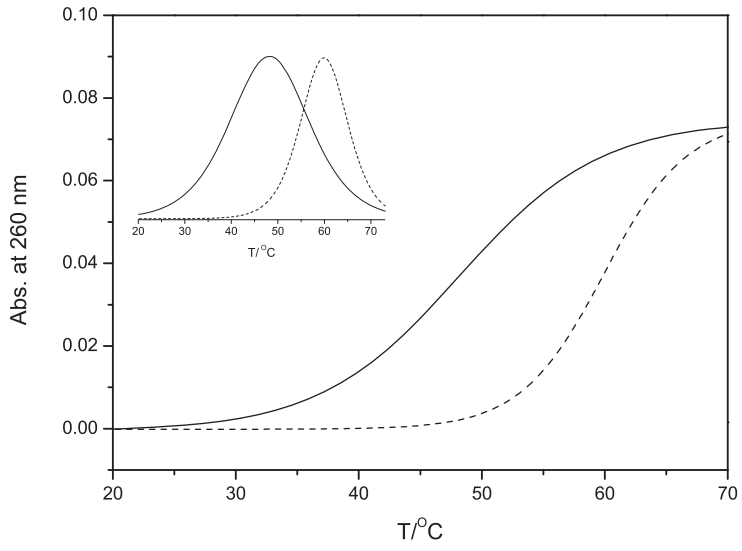

Figure 5.16: Melting curves of CT-DNA (60 μM) (solid line) and in presence of [EuH_3LPt] 4:1 (dashed line), in 10 mM HEPES, 10 mM NaCl. Inset plot the first order derivative used to determine the T_m.

Considering that T_m corresponds to the mid point of the sigmoidal curve at which 50% of the double stranded DNA denatures into the random coiled single strand form, we can determine the melting temperature using the first order derivative plots, where an increase of 14 °C of CT-DNA T_m was observed upon addition of [EuH_3LPt]. This effect can be ascribed to the stabilisation of the double helix arising from the π - π stacking interaction of the terpyridylplatinum(II) unit with the DNA bases. However the ΔT_m for [EuH_3LPt] resulted in a bigger value than for the [$EuPt_2$]Cl_2 complex (12 °C see chapter 2), and this might be due to the less rigid structure that characterises the [EuH_3LPt] complex. While the [$EuPt_2$]Cl_2 is constricted in its hairpin geometry upon interaction with DNA, the [EuH_3LPt] has a greater degree of freedom to accommodate itself upon interaction with CT-DNA.

5.3 Conclusions

The [EuH_3LPt] was obtained by one pot reaction between a previously reported asymmetric DTPA-(quinoline) moiety[1] (**H_3L**) and the [Pt(tpy)Cl](CF_3SO_3) followed by addition of $EuCl_3 \cdot 6\ H_2O$.[2] The [EuH_3LPt]PF_6 was fully characterised and its luminescent properties investigated showing that efficient sensitisation of the lanthanide ion can be obtained upon excitation of the quinoline moiety at 330 nm. Luminescence studies of [EuH_3LPt](PF_6) with DNA were characterised by luminescence enhancement upon interaction with CT-DNA and polynucleotide DNA. This may further confirm what was observed for [$LnPt_2$]Cl_2 (Chapter 2), where the terpyridine transitions are modified upon intercalation between the DNA bases, leading to a more efficient energy transfer process occurring between the sensitiser and the lanthanide ion.

The DNA binding studies performed by flow LD, circular dichroism and melting point are consistent with the intercalation of the platinum terpyridine unit of the [EuH_3LPt]PF_6. Due to the presence of only one DNA intercalating unit, the grade of DNA stiffening produced by interaction of [EuH_3LPt]PF_6 with CT-DNA is sensitively reduced when compared to the [$LnPt_2$]Cl_2. Further, the gel experiment highlighted that by removing one DNA recognition site, the ability to uncoil to DNA is highly affected. Indeed, almost double the amount of [EuH_3LPt]PF_6 is required compared to the [$EuPt_2$]Cl_2 in order to obtain the same grade of unwinding angle.

An ongoing work is oriented to investigate the biological properties of [EuH_3LPt]PF_6 in comparison with the bis-intercalator species [$EuPt_2$]Cl_2 and [$EuC{\equiv}CPt_2$]CH_3SO_3. It would be particularly interesting to test all the complexes as cell stain for fluorescence microscopy experiments. In this sense the [EuH_3LPt]PF_6 is one of the best candidates since the quinoline moiety is a good lanthanide sensitiser.

5.4 Experimental

5.4.1 Synthesis of 1-(6-amidoquinoline),11-(4-amidothiophenol)-1,11-dioxo-3,6,9-triaza-3,6,9 tris carboxymethyl) undecane : L

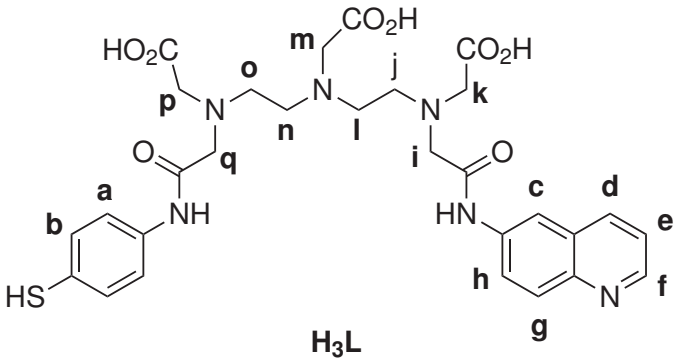

H_3L

Kugelröhr distillation of 4-aminothiophenol

A sample of 4-aminothiophenol (0.91 g) was separated by Kugelröhr distillation at 180 °C under reduced pressure. The resulting white crystalline solid (0.71 g, 78%) was dried *in vacuo* and stored under a nitrogen atmosphere at -5 °C.

Synthesis of L and purification of H_3L

6-aminoquinoline (1.58 g, 10.9 mmol) was added to a suspension of DTPA-bisanhydride (3.94 g, 11.0 mmol) in anhydrous pyridine (100 cm^3). The resulting mixture was stirred for 45 min at room temperature under nitrogen. Distilled 4-aminothiophenol (0.71 g, 5.7 mmol) was added and the solution stirred for 2 h. Water (80 cm^3) was added and the solution was stirred for 30 min. The solvent was removed *in vacuo* to yield a yellow solid (2.94 g). This was dissolved in degassed water (50 cm^3) and filtered *in vacuo* to leave a clear yellow solution. The solution was acidified to pH = 3 with concentrated HCl (32%, 10.2 M) under nitrogen, precipitating a yellow solid. The residual supernatant water was discarded and the yellow solid washed with degassed water (10 cm^3) and acetonitrile (10 cm^3) which were both discarded. Degassed acetonitrile (200 cm^3) was added and the solid was triturated for 5 h to form a bright yellow powder. This was collected by suction filtration under nitrogen and washed with degassed acetonitrile (2 $\times$ 25 cm^3) and diethyl ether (2 $\times$ 10 cm^3) yielding a mixture of bisamides $\mathbf{L}^b$, $\mathbf{L}^a$ and the asymmetric **L** (753 mg, 11 %);

RP-HPLC was used to separate the DTPA bisamides $\mathbf{L}^a$, $\mathbf{L}^b$ and the asymmetric **L**. A typical operation involved the crude mixture (20 mg, 0.03 mmol) being dissolved in 1 cm^3 THF/ degassed water (1:1) and injected into a HPLC system running a water/ acetone solvent gradient (0 min 100 % water 40 min 100 % acetone) with a flow rate of 10 cm^3/min on a Luna 10u C18(2) 100 A. AXIA reverse phase column. Detection of the eluting bisamides was achieved by monitoring UV absorbance at 336 nm. After a run was complete the column was washed with acetone and water until a UV baseline was re-established and the injection procedure repeated. Mass spectrometry (ES^+) was used to identify the 3 bisamides. **La** (*m/z* = 646) eluted at 16.0 min, the asymmetric **L** (*m/z* = 626) eluted at 25.0 min and **Lb** (*m/z* = 607) eluted at 33.2 min. **L** was collected and dried under vacuum to yield **L** as a pale yellow powder (6 mg, 30%).

^{1}H (300 MHz, [D2]D2O/NaOD, 24 °C) 8.42 (d,1H, ^3J(HH) = 4.4 Hz, Hf), 7.95 (d, 1H, ^3J(HH) = 8.5 Hz, Hd) 7.70 (d,1H, ^3J(HH) = 9.1 Hz, Hg), 7.65 (d, 1H, ^4J(HH) = 1.8 Hz, Hc), 7.45 (dd, 1H, ^3J(HH) = 9.1 Hz, ^4J(HH)= 1.8 Hz, Hh), 7.20 (dd, 1 H, ^3J(HH) = 8.5 Hz, ^{4}J(HH) = 4.4 Hz, He), 6.95 (d, 2H, ^3J(HH) = 8.4 Hz, Hb), 6.60 (d, 2H, ^3J(HH) = 8.4 Hz, Ha), 3.10 (s, 2H, Hi), 3.00 (2 H, s, Hq), 2.85-2.95 (m, 6H, Hk,m,p) 2.35-2.55 (s, 8H, Hj,l,n,o) ; MS (ES^+) *m/z* 627 $[M + H]^+$, 649 $[M + Na]^+$; UV-vis (1:1 THF/H_2O) λ_{max} in nm (log ε): 248 (4.5), 317 (3.78), 330 (3.7).

5.4.2 Synthetic procedure for [LPt](PF$_6$)

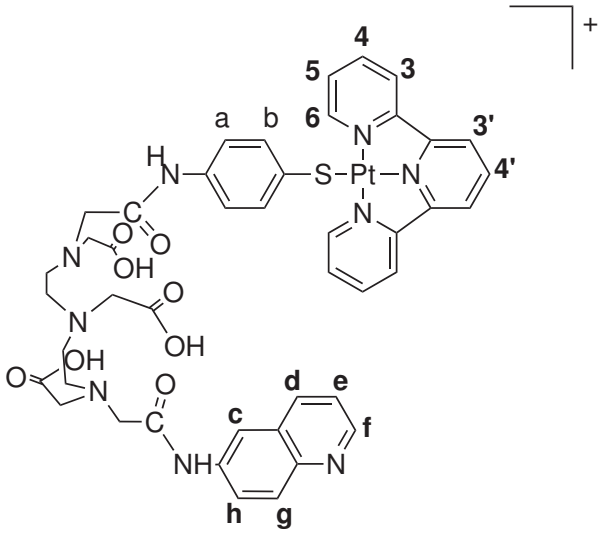

To a solution of [Pt(terpy)Cl](CF$_3$SO$_3$) (31 mg, 0.05 mmol), in hot methanol (20 cm^3) was added a solution of L (31.6 mg, 0.05 mmol) in methanol (25 cm^3) and dry DMF (2 cm^3) followed by addition of sodium methoxide (2.7 mg, 0.05 mmol) in methanol (1 cm^3). The solution gave a rapid colour change from yellow to a deep purple. The solution was heated under reflux for 5 h at 80 °C after which it was allowed to cool to room temperature. The solvent was removed *in vacuo* and methanol (25 cm^3) added followed by raising the pH from 1 to 4 by dropwise addition of aqueous sodium hydroxide (0.1 M). The volume of the solution was reduced to 1 cm^3 *in vacuo* and the anion was exchanged with a saturated methanolic solution of ammonium hexafluorophosphate to give a fine deep purple precipitate. The product was collected by filtration *in vacuo* and washed with ethanol (10 cm^3), methanol (10 cm^3) and ether (20 cm^3) and dried under vacuum (37 mg, 62 %);

^{1}H NMR (300 MHz, [D4]MeOD/NaOD, 24 °C), 8.88 (1H, d, ^3J(HH) = 3.0 Hz, H7), 8.78 (d, 1H, ^3J(HH) = 6 Hz, H12), 8.25 – 8.55 (m, 13H, m, H3/3', 5, 6, 8, 9, 10, 11), 7.95 – 8.05 (m, 4H, H 4/4'), 7.50 – 7.75 (m, 4H, H 1, 2), 3.05 – 3.25 (m, 6H, H14, 17, 20), 2.55 – 2.80 (m, 5H, 15, 16, 18, 19); MS (ES$^+$) m/z = 526 [M – (PF$_6$) + H]$^{2+}$. UV-vis (MeOH): λ_{max} in nm (log ε) 550 (3.08), 345 (4.09), 330 (4.24), 281 (4.57), 249 (4.67). Analysis calcd (%) for C$_{45}$H$_{47}$F$_6$N$_9$O$_8$PPtS · (HCl) · (H$_2$O): C, 42.1; H, 3.7; N, 10.1; found: C, 42.1; H, 3.7; N, 9.8.

5.4.3 Synthetic procedure for [EuH$_3$LPt](PF$_6$)

To a solution of [LPt](PF$_6$) (10 mg, 0.01 mmol) dissolved in 10 cm^3 MeOH/ H$_2$O (1:1), EuCl$_3$ · 6H$_2$O (3 mg, 0.01 mmol) at room temperature was added. The pH of the solution was increased from 3 to 5 by dropwise addition of aqueous sodium hydroxide (0.1 M) and the volume of the solution was reduced to 1 cm^3 *in vacuo*. Dropwise addition of acetonitrile precipitated the product as a deep purple fine solid.

MS (ES$^+$) m/z = 613 [M – (PF$_6$) + H + Na]$^{2+}$. UV-vis (H$_2$O): λ_{max} in nm (log ε) 491 (2.65), 345 (3.43), 330 (3.49), 281 (3.87), 244 (4.01). Analysis calcd (%) for C$_{45}$H$_{44}$EuF$_6$N$_9$O$_8$PPtS · (H$_2$O): C, 38.4; H, 3.2; N, 9.1; found: C, 38.3; H, 3.2; N, 9.1.

References

[1] Lewis, D. J. Luminescent lanthanide (III) DTPA complexes : modulating selectivity efficiency asymmetry and nanoscale properties. Ph.D. thesis, University of Birmingham, Birmingham, 2006.

[2] Mann, G. M.Sc. thesis, University of Birmingham, 2010.

[3] (a) Aldridge, T. K.; Stacy, E.; McMillin, D. R. *Inorg. Chem.* **1994**, *33*, 722; (b) Yip, H.-K.; Cheung, L.-K.; Cheung, K.-K.; Che, C.-M. J. *Dalton Trans.* **1993**, 2933.

[4] (a) Tzeng, B. C.; Fu, W. F.; Che, C. M.; Chao, H. Y.; Cheung, K. K.; Peng, S. M. *Dalton Trans.* **1999**, 1017; (b) Howe-Grant, M.; Lippard, S. J.; Chalipoyil, P.; Marzilli, L. *Inorg. Synth.* **1980**, *20*, 101.

[5] Steed, J. W.; Atwood, J. L. *Supramolecular Chemistry Second Edition*; John Wiley and Sons, 2009.

[6] Rodger, A.; Norden, B. *Crcular Dichroism and Linear Dichroism*; Oxford University Press, 1997, 25.

[7] Rodger, A.; Marrington, R.; Geeves, M. A.; Hicks, M.; de Alwis, L.; Halsall, D. J.; Dafforn, T. R. *Phys. Chem. Chem. Phys.* **2006**, *8*, 3161.

[8] Glover, P. B.; Ashton, P. R.; Childs, L. J.; Rodger, A.; Kercher, M.; Williams, R. M.; Cola, L. D.; Pikramenou, Z. *J. Am. Chem. Soc.* **2003**, *125*, 9918.

[9] (a) Jennette, K. W.; Lippard, S. J.; Vassiliades, G. A.; Bauer, W. R. *Proc. Natl. Acad. Sci. U. S. A.* **1974**, *71*, 3839; (b) Ramos-Lima, F. J.; Vrana, O.; Quiroga, A. G.; Navarro-Ranninger, C.; Halamikova, A.; Rybnickova, H.; Hejmalova, L.; Brabec, V. *J. Med. Chem.* **2006**, *49*, 2640.

[10] Bauer, W. R. *Annual Rev. of Biophys. and Bioeng.* **1978**, *7*, 287.

[11] Newman, J. *Biopolymers* **1984**, *23*, 1113.

Chapter 6

General Experimental

6.0.4 Materials and methods

All chemicals were purchased from Aldrich, Acros, or Alfa Aesar and were used without further purification unless otherwise stated.

All solvents were purchased from Aldrich or Fisher. CH_3CN was dried over P_2O_5 (5% w/v) and freshly distilled prior to use. NMR solvents were purchased from Goss Scientific or Aldrich and used as received. Solvents used in photophysical studies were HPLC grade and were purchased from Fisher. Water was deionised using an Elga Option 3 water purifier.

Column chromatography was performed on silica gel (Fluorochem of Merck 40-63 μM). Thin layer chromatography was carried out using Merck silica gel 60 F254 aluminium sheets.

Nitrogen gas used was supplied by BOC-gases. All reactions were performed under dinitrogen using standard Schlenk and high vacuum techniques. Air sensitive reactions were carried out using degassed solvents and dried over the appropriate molecular sieves.

6.0.5 Instrumentation

^{1}H NMR and ^{13}C NMR spectra were obtained using 300 MHz Brüker AC 300, AV 300, AV 400 or DRX 500 spectrometers. ES-TOF mass spectra were recorded on a Micromass LC-TOF machine. MALDI-TOF mass spectra were recorded on a Brüker Biflex IV mass spectrometer. Elemental analyses were recorded on a Carlo Erber EA1110 Simultaneous CHNS elemental analyser. Absorption spectra were recorded on a Varian Cary UV 5000

6.0.6 Photophysical studies

Luminescence experiments were carried out using a PTI fluorescence system. The illumination source was a PTI L-201M 75 W xenon arc lamp. The detection system was a PTI 814 with a Shimadzu R928 in a photon-counting photomultiplier tube. The emission monochromator was equipped with 500 and 750 nm blazed gratings. Emission was recorded at 90° to the excitation source, and after passing through appropriate long pass filters. Excitation spectra were corrected for variation in lamp output in real time by using a reference beam correction profile. Spectra were recorded using PTI Felix fluorescence analysis software for Windows.[1]

Steady state near-infrared measurements were performed using a similar set up with a double excitation monochromator (1200 lines mm^{-1}), an emission monochromator (600 lines mm^{-1}) equipped with a 1.25 μM blazed grating, a high sensitivity thermoelectric-cooled InGaAs detector, Stanford research systems SR510 lock-in amplifier and PTI OC-4000 optical chopper for noise suppression.

Typically visible emission spectra were recorded using an excitation band-pass of 5 nm and an emission band-pass of 2 nm. Excitation spectra were recorded using an excitation band-pass of 2 mm and an emission band-pass of 5 nm. All near-infrared emission and excitation spectra were recorded with 5 nm band-pass settings. Luminescence spectra of solutions at ambient temperature were carried out using a 1 $\times$ 1 cm path length quartz cuvette with 4 transparent polished faces. Solvent had been degassed by three freeze-pump-thaw cycles.

6.0.7 Time resolved emission spectroscopy

Visible emission lifetime spectra were recorded using a Continuum Surelite I SSP class 4 pulsed Nd-YAG laser (10 Hz) as the excitation source using the 355 nm harmonic. The signal was collected as a direct output from the PMT to minimise the response time of the apparatus. Data were recorded on a LeCroy 9350AM 500 MHz oscilloscope, which was triggered by the laser, as an average of 500 shots.

Lifetime data was analysed using Kaleidagraph software for the PC and fitted using a non-linear least-squares iterative technique (Marquardt-Levenberg algorithm).[2]

6.0.8 DNA preparation

The ct-DNA (highly polymerised) was purchased from Sigma□Aldrich and it was dissolved in water without any further purification and the poly(dAdT) and poly(dGdC) DNA from Sigma-Aldrich. The concentration was determined spectroscopically using the molar extinction coefficients at the wavelength of maximum absorption[3]: CT-DNA ϵ_{258} = 6600 $mol^{-1} \cdot dm^3 \cdot cm^{-1}$, poly(dGdC) DNA ϵ_{254} = 8400 $mol^{-1} \cdot dm^3 \cdot cm^{-1}$, poly(dAdT) DNA ϵ_{262} = 6600 $mol^{-1} \cdot dm^3 \cdot cm^{-1}$. All DNA experiments were performed using a HEPES buffer which is effective over a neutral pH range. Aqueous sodium chloride was used to stabilise the negatively charged phosphate backbone.

6.0.9 Circular dichroism and linear dichroism experiments

Circular dichroism (CD) spectra were collected on a JASCO J-810 spectropolarimeter using quartz emission cells (10.00 mm). All CD spectra were recorded at 20 oC internal temperature. The parameters used were; standard sensitivity, continuous scanning mode, 0.5 nm data pitch, 200 nm/sec scanning speed, 1 sec response time, 1 nm band width and 20 accumulations.

Linear dichroism (LD) spectra were collected on a Jasco J-715 spectropolarimeter adapted for LD measurements. For flow linear dichroism experiments the samples were orientated in a radial cuvette flow cell. This is a specialised small volume cylindrical quartz cell, pathlength 1 mm, which is rotated by an electric motor during the course of the experiment. All LD spectra were recorded at 20 °C and 5.8 V.

6.0.10 DNA melting studies

DNA melting studies were carried out using a Varian Cary 5000 UV-Vis-NIR spectrophotometer equipped with Cary temperature controller. Spectra were recorded using Cary WinUV software.[4] Helix melting was monitored by following the absorption of the sample at 260 nm, as a function of temperature. The melting temperature (T_m) was determined from the first derivative of a plot of absorption versus temperature. The following parameters were used; 0.5 °C data interval and 0.5 °C/min rate.

6.0.11 Gel electrophoresis

Electrophoresis experiments were carried out using an Amersham Biosciences HE 99X Max Submarine unit with a 15 $\times$ 20 cm gel casting tray and a 15 well comb. The power supply used was an Amersham Biosciences electrophoresis power supply model EPS 301.

The gel employed was a 1% agarose gel matrix. The agarose used was ultra pure microbiology grade for separation $\geq$ 500 base pairs purchased from usb. The buffer used was Tris-acetate EDTA buffer, microbiology grade, purchased from Sigma and diluted to 10% in ultra pure water (Fluka) prior to use. The dye used was bromophenol blue. The plasmid DNA used was pBR322 purchased for New England Biolabs.

The gels were stained with ethidium bromide (HPLC grade) and imaged using an UVipro platinum 2.0 gel documentation system, version 12.7a for windows, consisting of a CCD camera and UV transilluminator.

The unwinding assay was obtained integrating the pixel area[5] and the resuting values plotted against the base pair/complex ratio in order to determine the co-migrate concentration.

References

[1] 32, F. *Photon Technology International Software* **2001**,

[2] 4.0, K. *Synergy Software* **2000**,

[3] Rodger, K. K., A.and Patel; Sanders, K. J.; Datt, M.; Sacht, C.; Hannon, M. J. *Dalton Trans.* **2002**, 3656.

[4] 3, C. *Varian Australia Pty Ltd* **2002**,

[5] W.S., R. In ; http://rsb.info.nih.gov/ij/,, Ed.; ImageJ, U. S. National Institutes of Health, 2009.

Chapter 7

Conclusions and future work

In this thesis we have reported the synthesis, photophysical studies and DNA binding studies of hairpin shaped lanthanide heterometallic complexes. All the complexes were obtained by self-assembly of different components in a one pot reaction. This led us to isolate heterometallic complexes, where a lanthanide DTPA complex was assembled with a platinum terpyridine moiety, which works as DNA recognition unit and antenna system for lanthanide sensitisation. The complex named **LnPt**$_2$ showed the ability to bis-intercalate between the DNA base-pairs. Upon interaction with DNA a relatively strong luminescent enhancement could be observed for the visible and NIR emitting lanthanide complexes. We believe this is an effect of the polarity change of the sensitiser units upon interaction with DNA, leading to an improvement of the energy transfer process to the lanthanide.

We also investigated the interaction of **LnPt**$_2$ with four oligonucleotide sequences double stranded and of 12 bases length. The addition of **LnPt**$_2$ to the 12-mer duplexes showed the ability of the complex in stabilising the double stranded structure by increasing the values of their melting point. Further investigation on **LnPt**$_2$ upon interaction with DNA and oligonucleotides were performed by circular dichroism and luminescence. These studies were conducted parallel to DNA binding studies of a model compound named **AATP**, which resembles the DNA recognition units of the **LnPt**$_2$. These studies highlighted that the small differences observed upon interaction of **LnPt**$_2$ with the 12-mer duplexes can be ascribed to the rigidity of the hairpin structure induced by the lanthanide DTPA unit to the **LnPt**$_2$.

We also performed NMR studies of **LnPt**$_2$ and the monomer **AATP** upon interaction with a 12-mer duplex, thus we could investigate in detail the structural changes operated on the Dickerson-Drew duplex upon interaction with the complexes. It is important to highlight how the adenine and thymine

sequences plays a crucial role. It was surprising that although the **LnPt$_2$** gives a better interaction with the Dickerson-Drew sequence, we could not observe any NOE coupling occurring between the adenine and thymine arising from the central part of the sequence and the complexes. On the other hand, characteristic NOE couplings occurring between H8/H6 of cytosine and guanine and the relative deoxyribose disappeared upon interaction of **LnPt$_2$** and **AATP**. We believe that the central part of the Dickerson-Drew sequence plays a role in the flexibility of the sequence, that facilitates the intercalation process of **LnPt$_2$** between the DNA bases. The UV-vis, melting point and NMR experiments of **AATP** upon interaction with the Dickerson-Drew sequence support the model for the bis-intercalation described above, since we observed a preferred interaction with alternating sequence of cytosine and guanine through different spectroscopic techniques.

LnPt$_2$ inspired the synthesis of **LnC≡CPt$_2$** which retains the characteristic hairpin structure of the DTPA ligand, but introduces the acetylide as coligand of platinum(II). The isolation of this product was possible by designing a new DTPA-bis(acetylide) ligand which it is an interesting starting material for further studies, such as derivatisation of lanthanide complexes using click chemistry (e.g. cyclodextrins). Moreover, using the synthetic approach that involves DTPA-bis(acetylide) and [Pt(tpy)MeCN]$^{+2}$ we obtained **LnC≡CPt$_2$** by a one-pot reaction.

When the **LnC≡CPt$_2$** complex was investigated upon interaction with DNA we observed that most of the characteristic DNA binding features of its parent complex **LnPt$_2$** were retained. **LnC≡CPt$_2$** stabilises the B-DNA conformation of CT-DNA by increasing the melting point temperature by 10 °C. Moreover, the linear dichroism studies showed the retained ability of the complex to stiffen the double helix as its parent bis-intercalator. Parallel to this we isolated the relative Pt(tpy) acetylide complex which resembles the DNA recognition unit of **LnC≡CPt$_2$**. DNA binding studies of this complex highlight once again how the Ln-DTPA part of the molecule induces a structural rigidity which is responsible for structural changes on the DNA double helix.

The use of acetylide may give the advantage of sensitising the lanthanide luminescence in the visible region. However, in this case we could not observe lanthanide sensitisation arising from the CT band, which we ascribe to the weakness of the lanthanide signal mainly due to the poor solubility of **LnC≡CPt$_2$** in a wide range of solvents. However, visible lanthanide luminescence can be obtained

through excitation of the phenyl ring of **[EuC≡CPt$_2$]**$^{+2}$ leading to an europium based emission.

The importance of the hairpin rigidity in both **LnPt$_2$** and **LnC≡CPt$_2$** was better highlighted when a DNA mono-intercalator based on Ln-DTPA was isolated. The asymmetric **[EuLPt]**$^{+}$ compared to the **LnPt$_2$** is characterised by having only one Pt(tpy) as DNA recognition unit. Linear dichroism studies and gel electrophoresis studies, showed that the structural changes induced on the DNA upon interaction with the metal complexes resemble the behaviour of the **AATP** and the **EAP** complex. The **[EuLPt]**$^{+}$ retained the luminescent properties for the **[LnPt$_2$]**$^{+2}$ upon interaction,with DNA.

As general point of view, the rigid hairpin structure induced by DTPA ligand combined with the presence of two DNA metallo-intercalating units leads to an heterometallic complex that is able to produce larger DNA structural modification than the relative mono-intercalators. In this sense, it will be interesting for the future to explore the biological activity of this class of complexes and compare the results with parallel studies on the mono-intercalator species. Work is on going to evaluate the possibility of using this complexes as luminescent cell stains for imaging. In particular it would interesting to evaluate the possibility to stain the cell nucleus selectively. From this point of view the **[EuLPt]**$^{+}$ is a good candidate since it has a quite strong luminescence. Perhaps the quinoline ring allows allows introduction of peptides for drug delivery or introduction of suitable groups for surfaces studies.

The DTPA backbone may be also considered as a part of the molecule to derivatise. Even if this requires to revisit the synthesis of the DTPA ligand there are a lot of advantages that can be brought in, such as the combination of an improved solubility in water with drug delivery properties.

Despite of the many attempts we were not able to obtain crystal structures for these complexes. These data have a crucial importance since they can be used in combination with the NMR studies to better describe the interaction of **LnPt$_2$** with the Dickerson-Drew sequence. Furthermore, it will be interesting to use the NMR data here collected to refine the duplex structure, in order to understand the structural modifications induced by the interaction with complexes. In this sense further experiments including multinuclear NMR experiments, such ^{31}P and ^{1}H experiments that will allow a better understanding of the structural transitions between BI an BII upon induced by the interaction of the complex with the oligonucleotide.

Appendix to Chapter 2

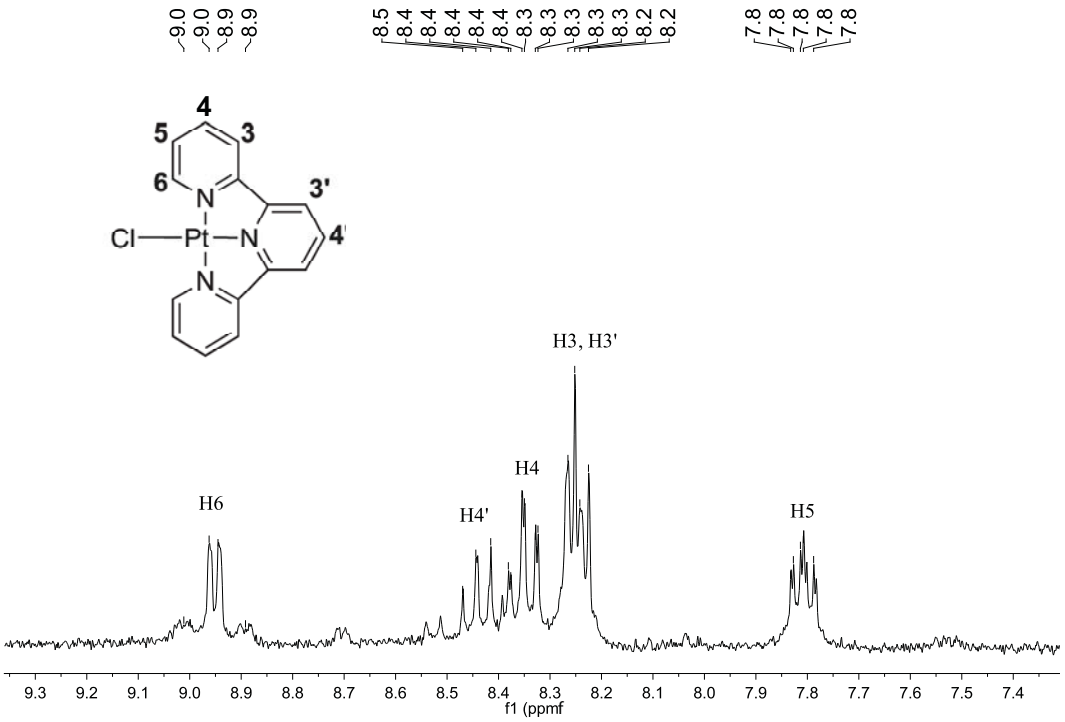

Figure 1: ^{1}H-NMR at 300 MHz of [Pt(tpy)Cl](CF_3SO_3) in CD_3CN.

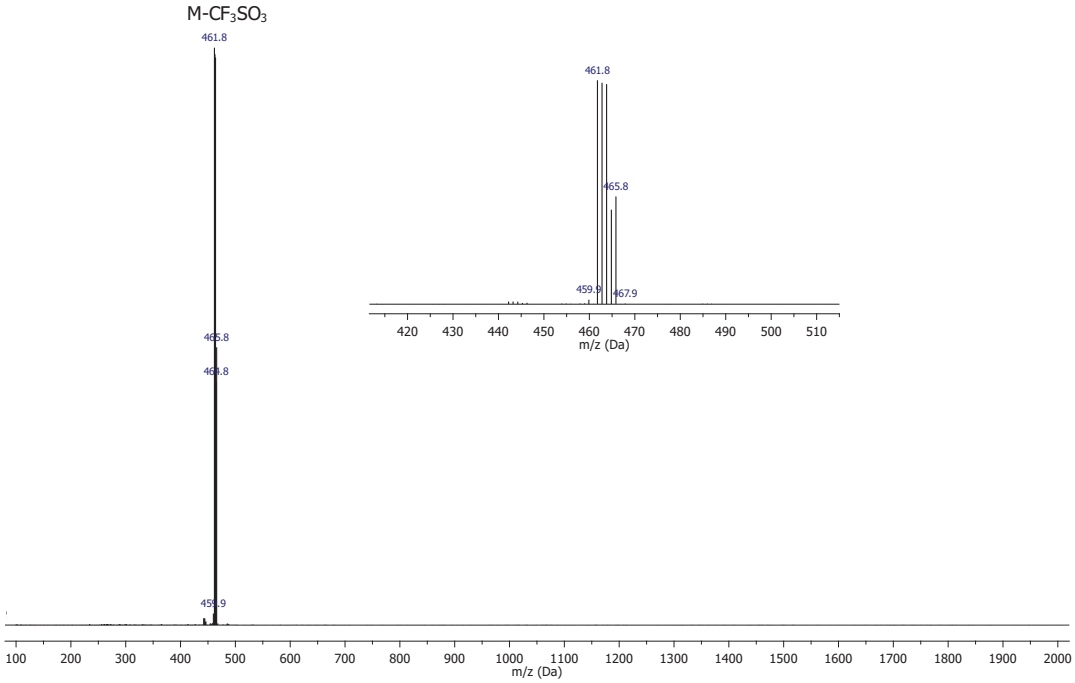

Figure 2: ESI-TOF of [Pt(tpy)Cl](CF$_3$SO$_3$).

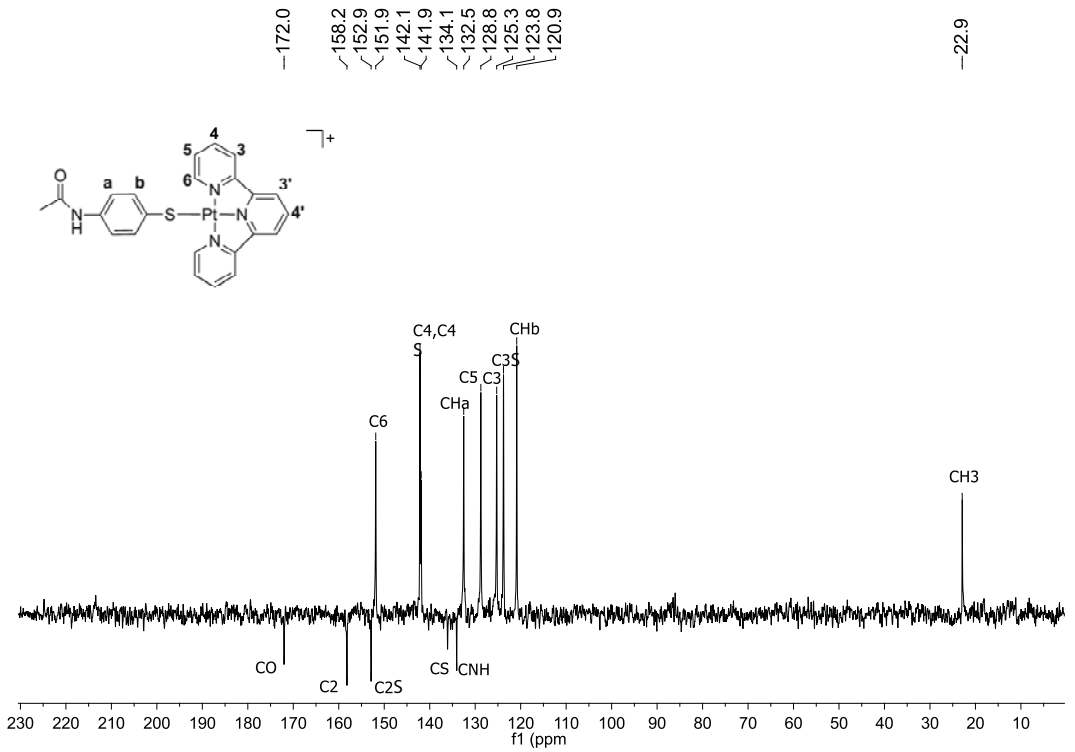

Figure 3: ^{13}C {H} NMR at 100MHz of AATP in D$_2$O.

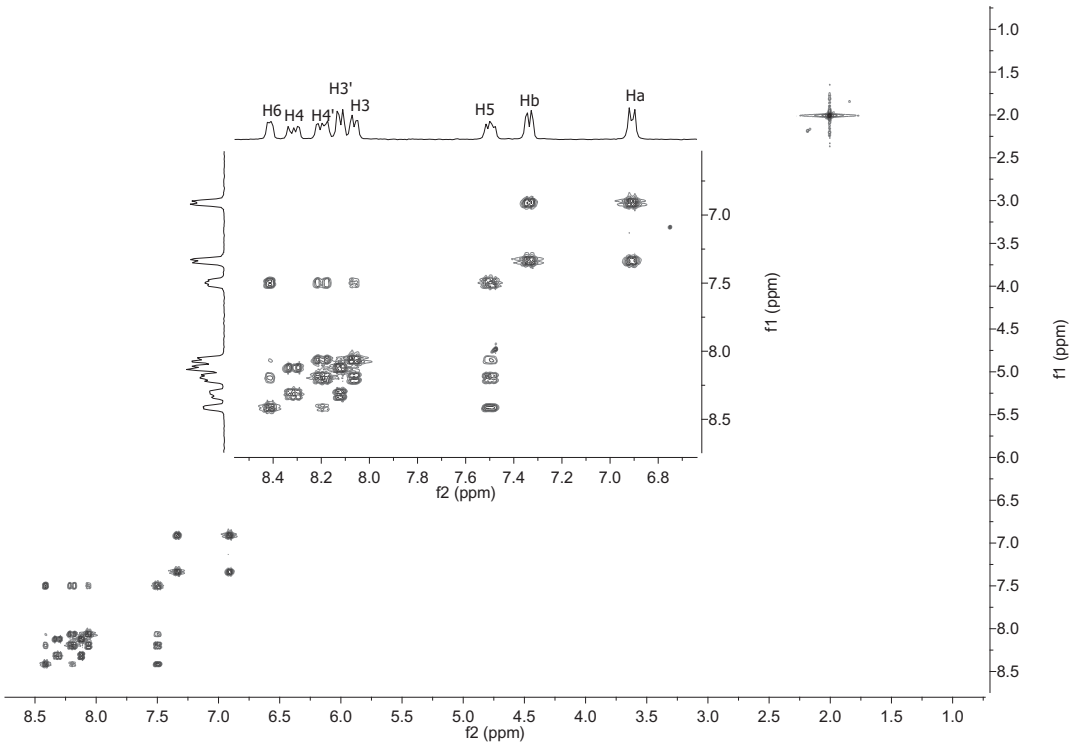

Figure 4: ^{1}H COSY NMR of AATP in D_2O at 400 MHz.

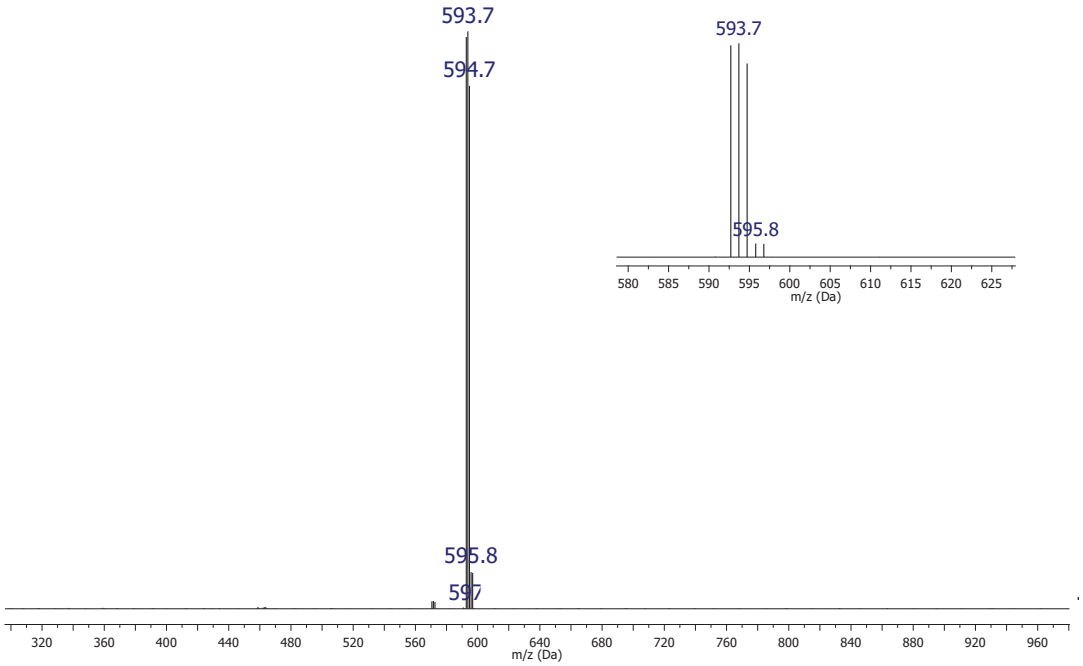

Figure 5: ESI-TOF spectra of AATP.

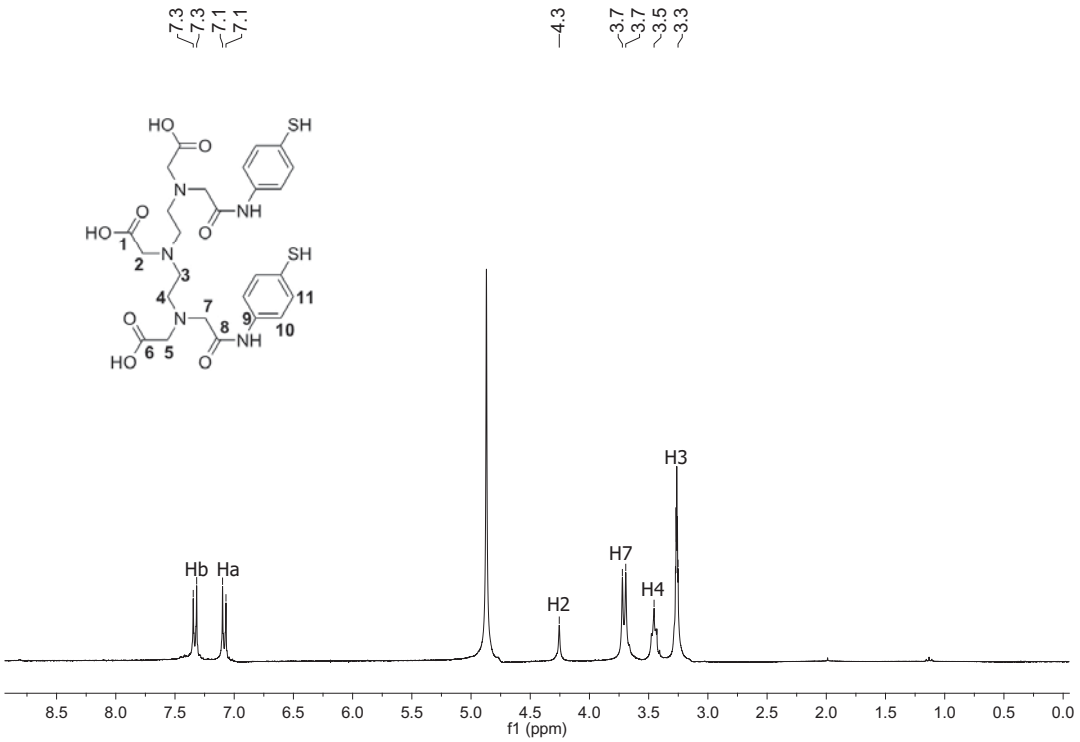

Figure 6: ^{1}H-NMR of DTPA-BATP in CD_3OD at 300 MHz.

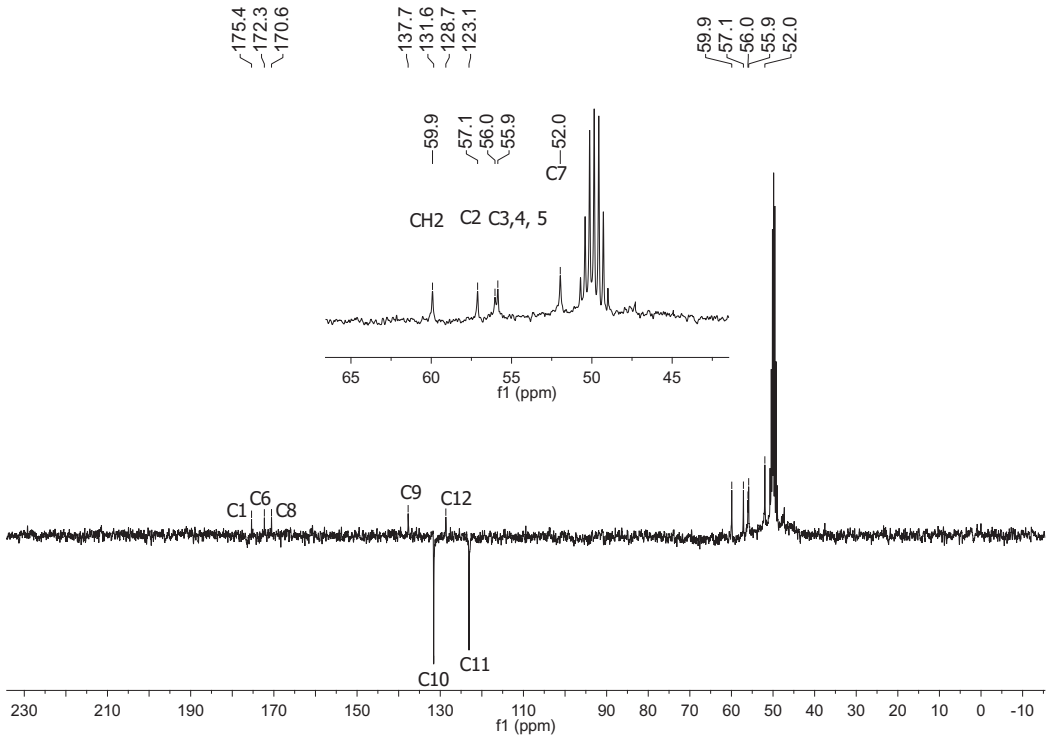

Figure 7: ^{13}C {H} NMR of DTPA-BATP in CD_3OD at 400 MHz.

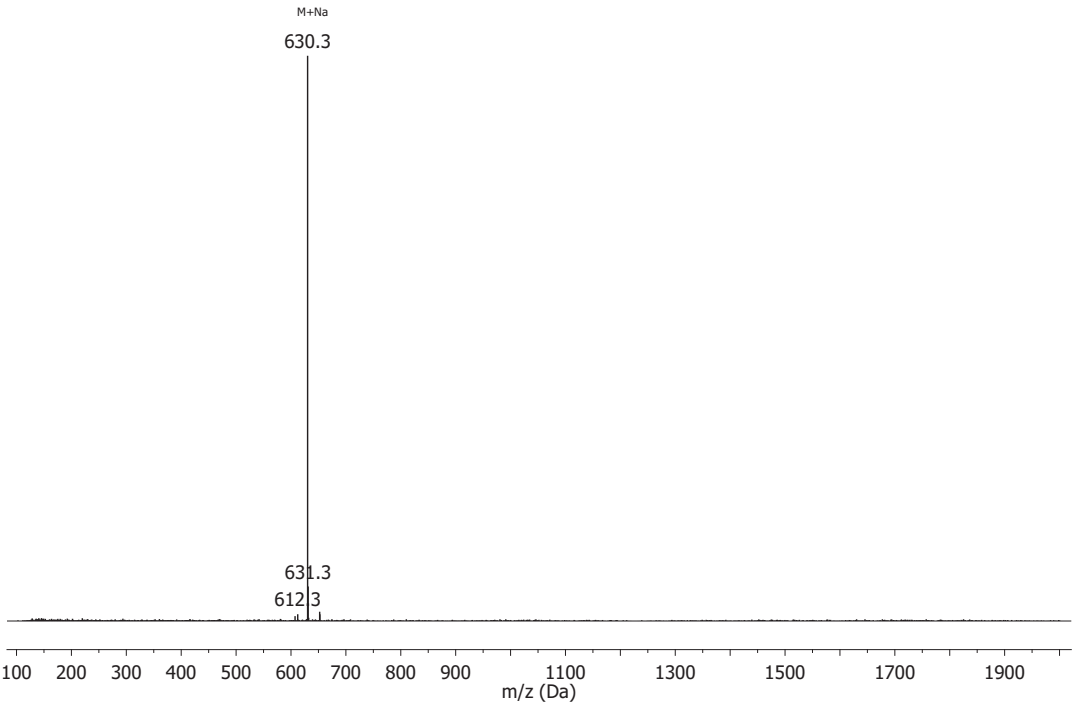

Figure 8: ESI-TOF of DTPA-BATP

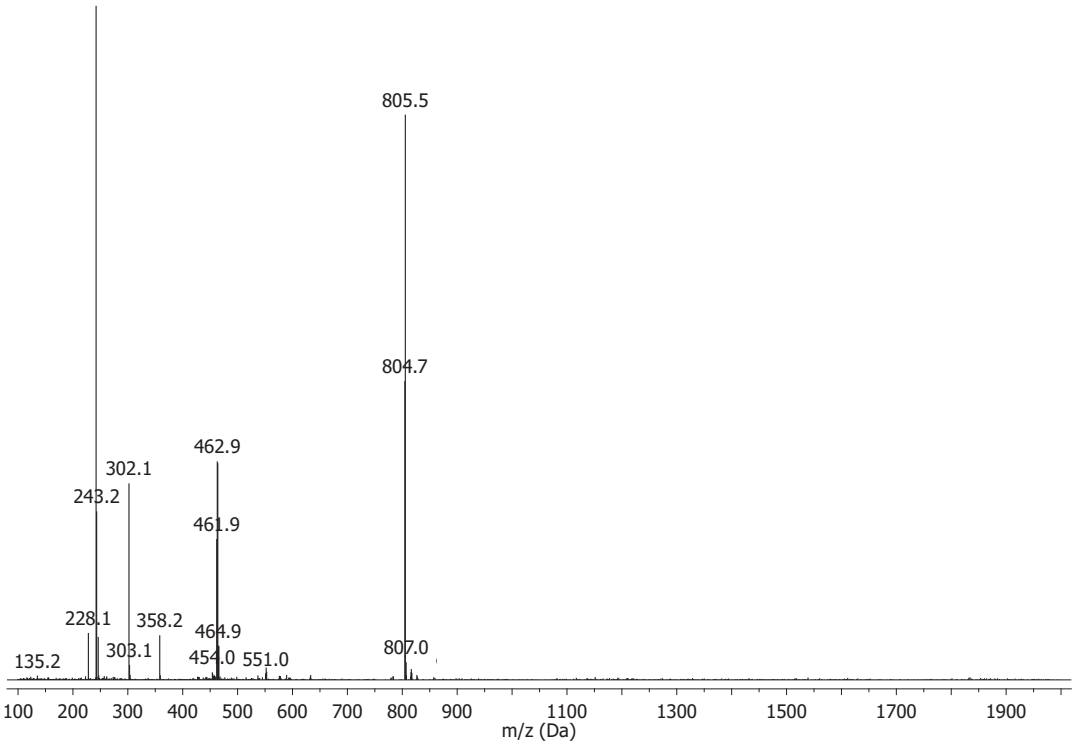

Figure 9: ESI-TOF of $[EuPt_2]Cl_2$.

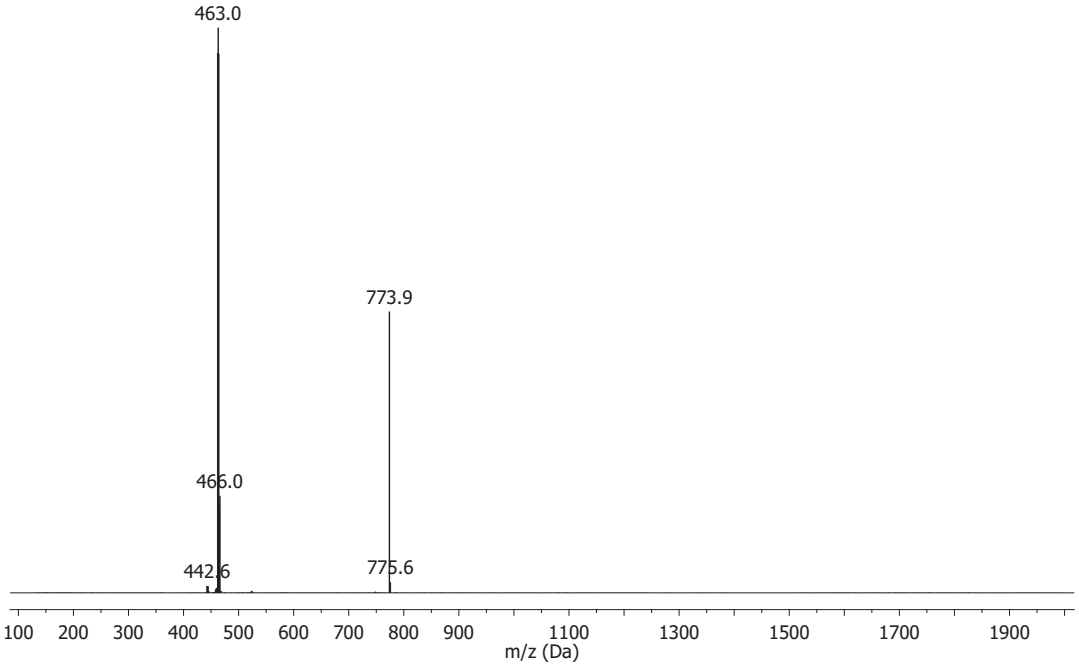

Figure 10: ESI-TOF of $[YPt_2]Cl_2$.

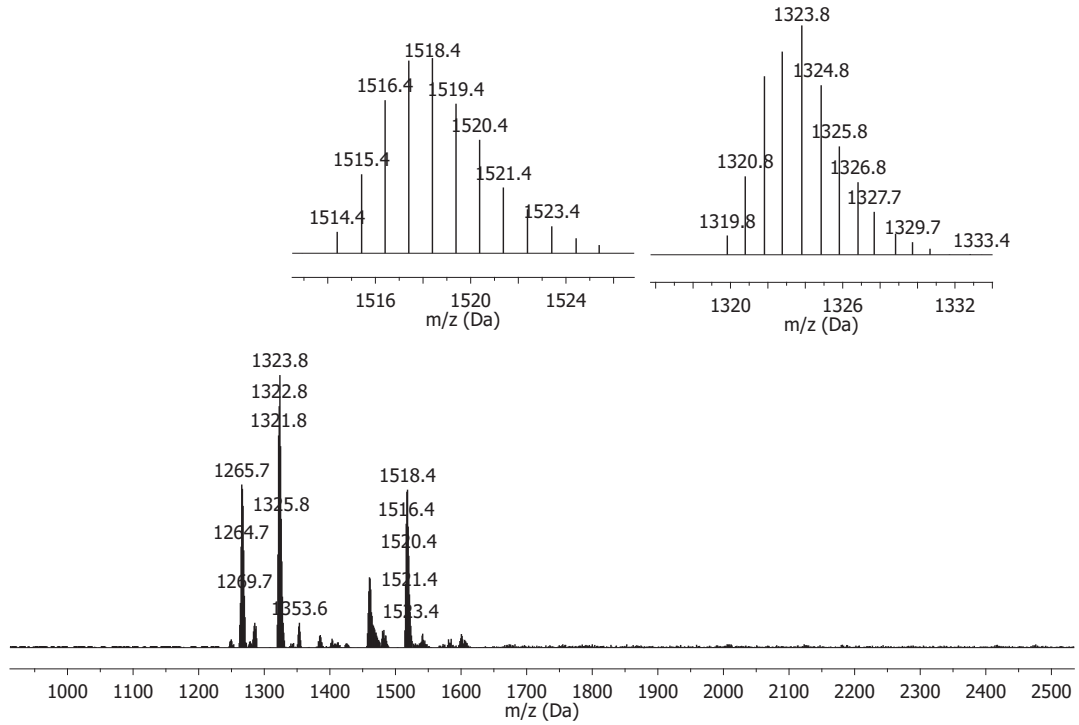

Figure 11: MALDI-TOF of $[LPt_2]Cl_2$.

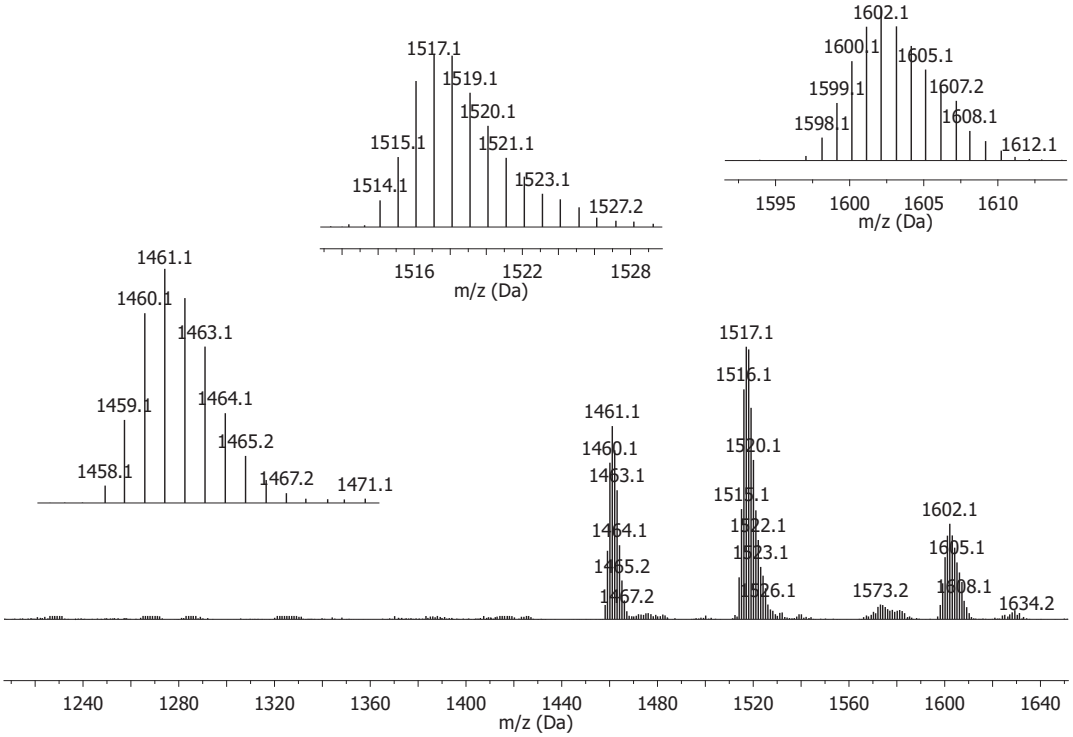

Figure 12: MALDI-TOF of $[NdPt_2]Cl_2$.

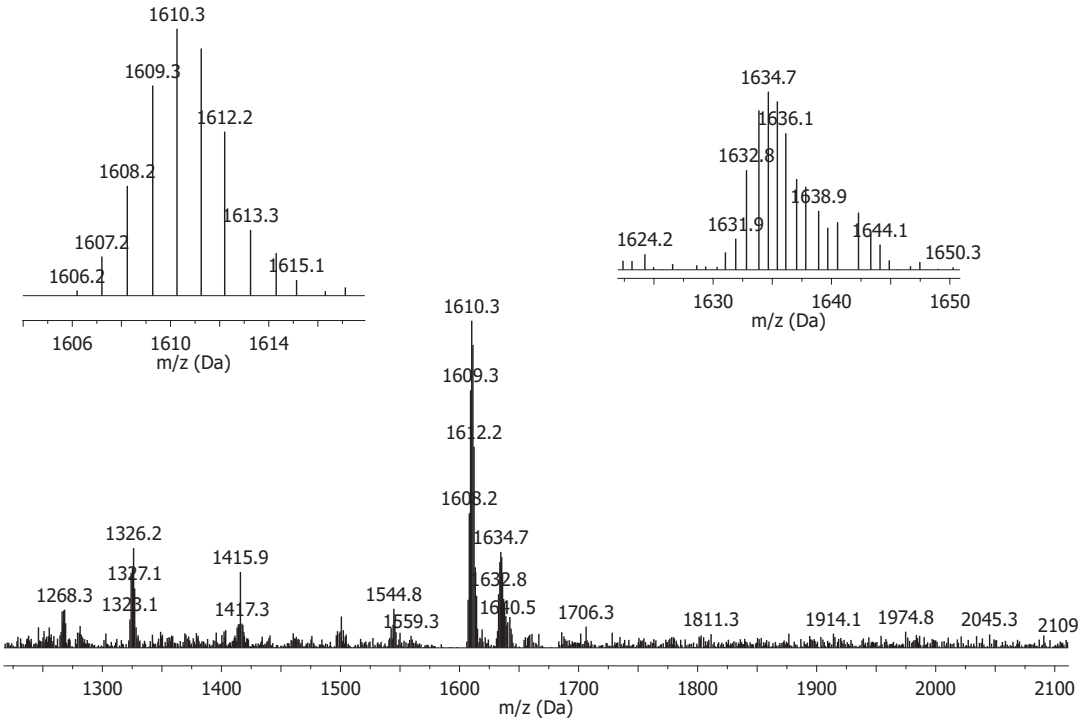

Figure 13: MALDI-TOF of $[EuPt_2]Cl_2$.

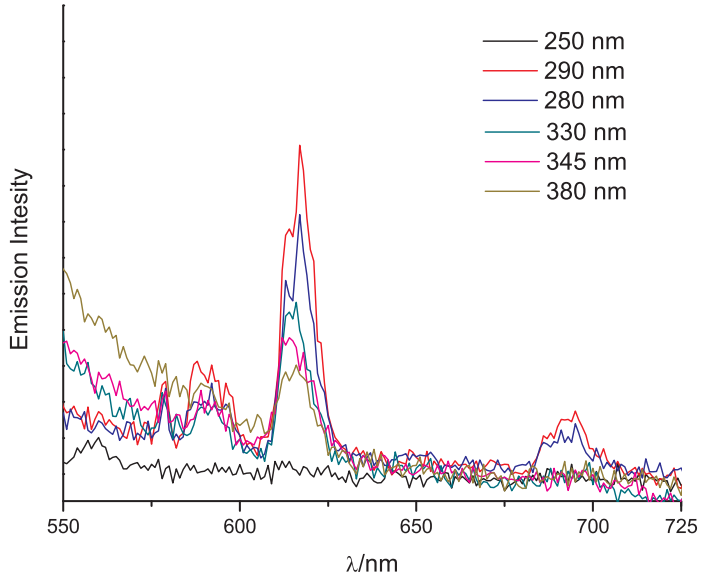

Figure 14: Emission spectra of $[EuPt_2]Cl_2$ in MeOH uncorrected for PMT response.

Sequence	Peak Area		
	$[NdPt_2]$	$[NdPt_2]$ + 12-mer	$\%_{en}$
d(5'-CGCGATATCGCG-3')$_2$	32,700	63,8662	95
d(5'-CGCGAATTCGCG-3')$_2$	31,5839	58,9673	86
d(5'-CGCGCCGGCGCG-3')$_2$	34,5361	48,7078	41
d(5'-CGCGCGCGCGCG-3')$_2$	34,6883	48,7078	36

Table 1: Integrated peak area of $[NdPt_2]$ emission over interaction with 12-mer oligonucleotides.

	Peak Area		
Sequence	[EuLPt]	[EuLPt] + DNA	$\%_{en}$
poly(dAdT)	108179	252938	133
poly(dGdC)	109308	290693	165

Table 2: Integrated peak area of [$NdPt_2$] emission over interaction with 12-mer oligonucleotides.

Appendix to Chapter 3

Listing 1: NOE volumes for the d(5'-CGCGAATTCGCG-3')$_2$ measured at τ_m = 400 ms.

w1	w2	Volume		ATOM1		ATOM2
5.755	7.625	−1.02e+07 ga	1 C	H1'	1 C	H6
5.750	7.932	−5.02e+06 ga	1 C	H1'	2 G	H8
2.395	5.756	−2.33e+07 ga	1 C	H2"	1 C	H1'
2.407	4.691		1 C	H2"	1 C	H3'
2.400	4.145		1 C	H2"	1 C	H4'
2.398	7.626	−1.11e+07 ga	1 C	H2"	1 C	H6
2.384	7.933	−1.22e+07 ga	1 C	H2"	2 G	H8
1.954	5.756	−7.40e+06 ga	1 C	H2'	1 C	H1'
1.955	4.696	−1.61e+07 ga	1 C	H2'	1 C	H3'
1.958	7.626	−1.94e+07 ga	1 C	H2'	1 C	H6
1.952	7.940	−3.86e+06 ga	1 C	H2'	2 G	H8
4.695	7.629	−6.65e+06 ga	1 C	H3'	1 C	H6
4.693	7.943		1 C	H3'	2 G	H8
5.875	7.942	−5.47e+06 ga	2 G	H1'	2 G	H8
5.876	7.260	−4.91e+06 ga	2 G	H1'	3 C	H6
2.702	5.864	−3.69e+07 ga	2 G	H2"	2 G	H1'
2.659	4.974	−1.55e+08 ga	2 G	H2"	2 G	H3'
2.666	4.345		2 G	H2"	2 G	H4'
2.679	7.261	−1.41e+07 ga	2 G	H2"	3 C	H6
2.616	4.974		2 G	H2'	2 G	H3'
2.678	7.943	−2.91e+07 ga	2 G	H2'	2 G	H8
4.959	7.942	−6.70e+06 ga	2 G	H3'	2 G	H8
5.591	7.259	−4.30e+06 ga	3 C	H1'	3 C	H6
5.591	7.837	−3.00e+06 ga	3 C	H1'	4 G	H8
2.261	5.593	−1.97e+07 ga	3 C	H2"	3 C	H1'
2.297	4.798	−3.33e+07 ga	3 C	H2"	3 C	H3'
2.268	4.118		3 C	H2"	3 C	H4'
2.260	7.260	−8.54e+06 ga	3 C	H2"	3 C	H6
2.258	7.838	−5.89e+06 ga	3 C	H2"	4 G	H8
1.828	5.592	−8.75e+06 ga	3 C	H2'	3 C	H1'
1.834	4.792		3 C	H2'	3 C	H3'
1.834	7.260	−1.84e+07 ga	3 C	H2'	3 C	H6
5.416	7.835		4 G	H1'	4 G	H8
5.414	8.100	−5.98e+06 ga	4 G	H1'	5 A	H8
2.739	5.415	−2.01e+07 ga	4 G	H2"	4 G	H1'
2.652	4.310		4 G	H2"	4 G	H4'

2.714	7.837	−4.67e+07	ga	4 G	H2”	4 G	H8
2.676	8.102	−7.23e+07	ga	4 G	H2”	5 A	H8
2.655	5.417			4 G	H2’	4 G	H1’
2.638	4.972			4 G	H2’	4 G	H3’
2.645	7.833			4 G	H2’	4 G	H8
4.978	7.837	−8.94e+06	ga	4 G	H3’	4 G	H8
5.981	8.102	−1.25e+07	ga	5 A	H1’	5 A	H8
2.927	5.983	−2.36e+07	ga	5 A	H2”	5 A	H1’
2.917	5.001	−1.73e+07	ga	5 A	H2”	5 A	H3’
2.689	4.443	−5.57e+06	ga	5 A	H2”	5 A	H4’
2.695	5.980	−2.86e+07	ga	5 A	H2’	5 A	H1’
2.688	5.051	−2.58e+07	ga	5 A	H2’	5 A	H3’
4.993	8.103	−8.97e+06	ga	5 A	H3’	6 A	H8
6.150	8.102	−3.28e+06	ga	6 A	H1’	6 A	H8
6.148	7.102	−4.62e+06	ga	6 A	H1’	7 T	H6
2.915	6.150	−1.57e+07	ga	6 A	H2”	6 A	H1’
2.927	5.051	−2.10e+07	ga	6 A	H2”	6 A	H3’
2.922	4.450	−1.08e+07	ga	6 A	H2”	6 A	H4’
2.922	8.102	−3.95e+07	ga	6 A	H2”	6 A	H8
2.916	7.104	−1.08e+07	ga	6 A	H2”	7 T	H6
2.558	4.456	−4.21e+06	ga	6 A	H2’	6 A	H4’
5.049	8.101	−1.12e+07	ga	6 A	H3’	6 A	H8
5.001	7.101	−2.41e+06	ga	6 A	H3’	7 T	H6
1.265	8.102	−1.45e+07	ga	7 T	CH3	6 A	H8
1.266	7.104	−2.11e+07	ga	7 T	CH3	7 T	H6
5.907	7.102	−3.52e+06	ga	7 T	H1’	7 T	H6
5.905	7.360	−5.50e+06	ga	7 T	H1’	8 T	H6
2.551	5.905	−2.23e+07	ga	7 T	H2”	7 T	H1’
2.553	4.817	−1.64e+07	ga	7 T	H2”	7 T	H3’
2.549	4.197			7 T	H2”	7 T	H4’
2.554	7.103	−1.60e+07	ga	7 T	H2”	7 T	H6
2.541	7.360	−2.29e+07	ga	7 T	H2”	8 T	H6
1.977	5.907	−1.75e+07	ga	7 T	H2’	7 T	H1’
1.990	4.817	−7.49e+06	ga	7 T	H2’	7 T	H3’
1.985	4.188			7 T	H2’	7 T	H4’
1.985	7.104	−1.04e+07	ga	7 T	H2’	7 T	H6
1.984	7.360	−7.12e+06	ga	7 T	H2’	8 T	H6
1.526	7.103	−1.16e+07	ga	8 T	CH3	7 T	H6
1.528	7.361	−1.98e+07	ga	8 T	CH3	8 T	H6
6.094	7.361	−4.24e+06	ga	8 T	H1’	8 T	H6
6.094	7.453	−3.10e+06	ga	8 T	H1’	9 C	H6
2.534	6.120	−2.94e+08	ga	8 T	H2”	8 T	H1’
2.535	4.890	−2.94e+07	ga	8 T	H2”	8 T	H3’
2.535	7.451	−8.41e+06	ga	8 T	H2”	9 C	H6
2.158	6.095	−1.49e+07	ga	8 T	H2’	8 T	H1’
2.157	4.890	−7.97e+06	ga	8 T	H2’	8 T	H3’
2.160	4.202			8 T	H2’	8 T	H4’
2.155	7.361	−1.97e+07	ga	8 T	H2’	8 T	H6
2.154	7.450	−5.11e+07	ga	8 T	H2’	9 C	H6
4.887	7.361	−7.57e+06	ga	8 T	H3’	8 T	H6

2.401	4.863	−2.09e+07	ga	8 T	H3’	9 C	H3’
5.617	7.361	−2.81e+06	ga	9 C	H1’	8 T	H6
5.625	7.454	−2.97e+07	ga	9 C	H1’	9 C	H6
5.647	7.896	−2.77e+06	ga	9 C	H1’	10 G	H8
2.402	5.650	−2.21e+07	ga	9 C	H2”	9 C	H1’
2.401	7.456	−1.27e+07	ga	9 C	H2”	9 C	H6
2.399	7.894	−6.73e+07	ga	9 C	H2”	10 G	H8
2.061	5.635	−5.21e+07	ga	9 C	H2’	9 C	H1’
2.063	4.861			9 C	H2’	9 C	H3’
2.056	7.456	−1.86e+07	ga	9 C	H2’	9 C	H6
1.987	4.200			9 C	H2’	9 c	H4’
2.060	7.897	−3.99e+06	ga	9 C	H2’	10 G	H8
4.870	7.454	−1.03e+07	ga	9 C	H3’	9 C	H6
5.843	7.897	−5.02e+06	ga	10 G	H1’	10 G	H8
5.844	7.312	−7.64e+06	ga	10 G	H1’	11 C	H6
2.643	5.852	−3.38e+07	ga	10 G	H2”	10 G	H1’
2.657	7.907	−2.17e+08	ga	10 G	H2”	10 G	H8
2.679	7.315	−1.64e+07	ga	10 G	H2”	11 C	H6
2.582	4.970			10 G	H2’	10 G	H3’
4.979	7.896	−8.83e+06	ga	10 G	H3’	10 G	H8
2.313	5.751	−2.33e+07	ga	11 C	H2”	11 C	H1’
2.312	7.316	−1.29e+07	ga	11 C	H2”	11 C	H6
2.319	7.929	−1.11e+07	ga	11 C	H2”	12 G	H8
1.877	5.752	−1.08e+07	ga	11 C	H2’	11 C	H1’
1.871	4.796			11 C	H2’	11 C	H3’
1.876	7.316	−2.15e+07	ga	11 C	H2’	11 C	H6
1.871	7.933			11 C	H2’	12 G	H8
6.144	7.929	−4.55e+06	ga	12 G	H1’	12 G	H8
2.588	6.144			12 G	H2”	12 G	H1’
2.370	6.144	−3.90e+07	ga	12 G	H2’	12 G	H1’
2.370	4.666			12 G	H2’	12 G	H3’
2.372	4.162			12 G	H2’	12 G	H4’

Listing 2: NOE volumes for the d(5'-CGCGAATTCGCG-3')$_2$ and **YPt$_2$** (1:0.5) measured at τ_m = 400 ms.

w1	w2	Volume	ATOM1		ATOM2	
5.723	7.605	7.83e+06 ga	1 C	H1'	1 C	H6
2.385	5.723		1 C	H2"	1 C	H1'
2.383	7.592	8.00e+06 ga	1 C	H2"	1 C	H6
2.377	7.899	4.40e+07 ga	1 C	H2"	2 G	H8
1.942	5.724		1 C	H2'	1 C	H1'
1.949	4.691		1 C	H2'	1 C	H3'
1.957	7.605	1.79e+07 ga	1 C	H2'	1 C	H6
2.677	7.899		2 C	H2"	2 G	H8
5.829	7.881	8.80e+06 ga	2 G	H1'	2 G	H8
5.831	7.239	7.55e+05 ga	2 G	H1'	3 C	H6
2.685	5.839		2 G	H2"	2 G	H1'
2.652	4.967		2 G	H2"	2 G	H3'
2.693	7.247		2 G	H2"	3 C	H6
2.266	5.582		3 C	H2"	3 C	H1'
2.284	4.788		3 C	H2"	3 C	H3'
2.269	7.247	7.71e+06 ga	3 C	H2"	3 C	H6
2.250	7.829	6.01e+06 ga	3 C	H2"	4 G	H8
1.825	5.574		3 C	H2'	3 C	H1'
1.820	7.245	3.15e+07 ga	3 C	H2'	3 C	H6
5.403	7.824	4.06e+06 ga	4 G	H1'	4 G	H8
5.410	8.091	8.81e+06 ga	4 G	H1'	5 A	H8
2.726	5.409		4 G	H2"	4 G	H1'
2.706	7.828		4 G	H2"	4 G	H8
2.687	8.098	9.94e+07 ga	4 G	H2"	5 A	H8
2.635	5.407		4 G	H2'	4 G	H1'
2.655	7.838	6.49e+08 ga	4 G	H2'	4 G	H8
5.973	8.096	1.46e+07 ga	5 A	H1'	5 A	H8
2.911	5.971		5 A	H2"	5 A	H1'
2.908	4.993		5 A	H2"	5 A	H3'
2.679	4.432		5 A	H2"	5 A	H4'
2.693	5.972		5 A	H2'	5 A	H1'
2.688	5.047		5 A	H2'	5 A	H3'
6.142	8.095	2.85e+06 ga	6 A	H1'	6 A	H8
6.143	7.096	7.07e+06 ga	6 A	H1'	7 T	H6
2.905	6.144		6 A	H2"	6 A	H1'
2.914	5.047		6 A	H2"	6 A	H3'
2.906	4.443		6 A	H2"	6 A	H4'
2.914	8.097	4.57e+07 ga	6 A	H2"	6 A	H8
2.905	7.100	1.90e+07 ga	6 A	H2"	7 T	H8
2.553	4.444		6 A	H2'	6 A	H4'
1.260	8.097	1.77e+07 ga	7 T	CH3	6 A	H8
1.260	7.098	2.64e+07 ga	7 T	CH3	7 T	H6
5.889	7.100	4.75e+06 ga	7 T	H1'	7 T	H6
5.891	7.345		7 T	H1'	8 T	H6
2.544	5.894		7 T	H2"	7 T	H1'
2.546	4.812		7 T	H2"	7 T	H3'

2.542	7.095	1.29e+07	ga	7 T	H2”	7 T	H6
2.535	7.355	2.11e+07	ga	7 T	H2”	8 T	H6
1.981	5.901			7 T	H2’	7 T	H1’
1.997	7.106			7 T	H2’	7 T	H6
1.979	4.810			7 T	H2’	8 T	H3’
1.520	7.098	2.10e+07	ga	8 T	CH3	7 T	H6
1.520	7.355	2.64e+07	ga	8 T	CH3	8 T	H6
6.083	7.359	1.16e+07	ga	8 T	H1’	8 T	H6
6.107	7.441	1.26e+06	ga	8 T	H1’	9 C	H6
2.523	6.084			8 T	H2”	8 T	H1’
2.530	4.860			8 T	H2”	8 T	H3’
2.524	7.445	5.52e+07	ga	8 T	H2”	9 C	H6
2.147	6.086			8 T	H2’	8 T	H1’
2.122	4.861			8 T	H2’	8 T	H3’
2.147	7.357	1.23e+07	ga	8 T	H2’	8 T	H6
2.164	7.451	4.95e+08	ga	8 T	H2’	9 C	H6
4.880	7.356	5.68e+06	ga	8 T	H3’	8 T	H6
5.614	7.444	3.88e+07	ga	9 C	H1’	9 C	H6
2.388	4.855			9 C	H2”	8 T	H3’
2.396	5.639			9 C	H2”	9 C	H1’
2.396	7.443	3.48e+07	ga	9 C	H2”	9 C	H6
2.053	5.643			9 C	H2’	9 C	H1’
2.052	4.868			9 C	H2’	9 C	H3’
2.071	7.446	4.57e+07	ga	9 C	H2’	9 C	H6
2.055	7.877	1.93e+06	ga	9 C	H2’	10 G	H8
2.636	5.830			10 G	H2”	2 G	H1’
2.632	7.901			10 G	H2”	10 G	H8
2.638	7.296	1.57e+07	ga	10 G	H2”	11 C	H6
2.296	5.732			11 C	H2”	11 C	H1’
2.295	7.291	4.36e+06	ga	11 C	H2”	11 C	H6
1.872	5.730			11 C	H2’	11 C	H1’
1.864	7.298	2.01e+07	ga	11 C	H2’	11 C	H6
6.101	7.898	1.34e+06	ga	12 G	H1’	12 G	H8
2.366	6.101			12 G	H2”	12 G	H1’
2.600	6.102			12 G	H2”	12 G	H1’
2.365	4.666			12 G	H2’	12 G	H3’

Listing 3: NOE volumes for the d(5’-CGCGAATTCGCG-3’)$_2$ and AATP (1:0.5) measured at τ_m = 400 ms.

w1	w2	Volume		ATOM1		ATOM2
5.752	7.616	2.74e+07	ga	1 C	H1’	1 C	H6
5.748	7.919	1.52e+07	ga	1 C	H1’	12 G	H8
1.953	4.693	5.30e+07	ga	1 C	H2’	1 C	H3’
1.953	7.616	6.28e+07	ga	1 C	H2’	1 C	H6
2.393	7.617	3.47e+07	ga	1 C	H2’’	1 C	H6
2.382	7.920	6.35e+07	ga	1 C	H2’’	2 G	H8
2.409	7.615	4.98e+06	ga	1 C	C1H2”	1 C	C1H2”
5.842	7.911	1.35e+07	ga	2 G	H1’	2 G	H8
5.844	7.251	1.73e+07	ga	2 G	H1’	3 C	H6
2.670	7.897	2.13e+08	ga	2 G	H2’’	2 G	H8

5.594	7.247	1.14e+07	ga	3	C	H1’	3	C H6
2.258	7.247	2.66e+07	ga	3	C	H2’’	3	C H6
2.260	7.820	9.46e+06	ga	3	C	H2’’	4	G H8
2.674	7.246	5.03e+07	ga	3	C	H8	2	G H2”
5.404	7.877	7.86e+06	ga	4	G	H1’	4	G H8
5.411	8.093	1.29e+07	ga	4	G	H1’	5	A H8
2.659	7.833	6.22e+08	ga	4	G	H2”	4	G H8
2.678	8.096	1.80e+08	ga	4	G	H2”	5	A H8
5.960	8.096	4.10e+07	ga	5	A	H1’	6	A H8
2.678	5.961	6.62e+07	ga	5	A	H2’	5	A H1’
2.909	5.961	7.40e+07	ga	5	A	H2’’	5	A H1’
6.138	8.096	1.31e+07	ga	6	A	H1’	6	A H8
6.140	7.106	1.59e+07	ga	6	A	H1’	7	T H6
2.904	6.140	6.46e+07	ga	6	A	H2”	6	A H1’
2.907	5.038	6.10e+08	ga	6	A	H2”	6	A H3’
2.908	8.097	1.43e+08	ga	6	A	H8	5	A H2”
1.260	8.098	4.81e+07	ga	7	T	CH3	5	A H8
1.261	7.105	7.96e+07	ga	7	T	CH3	7	T H6
5.886	7.105	1.19e+07	ga	7	T	H1’	7	T H6
5.886	7.348	8.95e+06	ga	7	T	H1’	8	T H6
2.546	7.106	6.00e+07	ga	7	T	H2”	7	T H6
2.528	7.351	7.00e+07	ga	7	T	H2”	8	T H6
1.974	5.886	6.28e+07	ga	7	T	H2’	7	T H1’
1.980	7.106	4.13e+07	ga	7	T	H2’	7	T H6
1.982	7.350	2.02e+07	ga	7	T	H2’	8	T H6
2.556	8.098	7.12e+07	ga	7	T	H2’’	5	A H2”
2.537	5.889	8.36e+07	ga	7	T	H2’’	7	T H1’
2.522	4.815	1.95e+09	ga	7	T	H2’’	7	T H3’
2.905	7.106	3.87e+07	ga	7	T	H6	7	T H2”
1.519	7.106	4.13e+07	ga	8	T	CH3	7	T H6
1.520	7.351	6.24e+07	ga	8	T	CH3	8	T H6
6.073	7.349	9.84e+06	ga	8	T	H1’	8	T H6
6.075	7.438	1.35e+07	ga	8	T	H1’	9	C H6
2.541	6.097	1.49e+09	ga	8	T	H2”	8	T H1’
2.142	6.073	4.47e+07	ga	8	T	H2’	8	T H1’
2.520	7.443	3.29e+07	ga	8	T	H2’’	9	C H6
5.646	7.444	4.01e+08	ga	9	C	H1’	9	C H6
2.061	5.671	3.32e+07	ga	9	C	H2’	9	C H1’
2.071	7.443	1.07e+08	ga	9	C	H2’	9	C H6
2.260	5.595	5.53e+07	ga	9	C	H2’’	3	C H1’
2.376	5.685	2.63e+09	ga	9	C	H2’’	9	C H1’
2.395	7.444	4.60e+07	ga	9	C	H2’’	9	C H6
2.392	7.879	3.40e+07	ga	9	C	H2’’	10	G H8
5.816	7.877	1.71e+07	ga	10	G	H1’	10	G H8
2.624	7.920	1.14e+08	ga	10	G	H2’’	10	G H8
2.648	7.311	5.71e+07	ga	10	G	H2’’	11	C H6
1.904	5.749	9.35e+07	ga	11	C	H2’	11	C H1’
2.314	7.310	4.02e+07	ga	11	C	H2’’	11	C H6
2.331	7.922	2.66e+07	ga	11	C	H2’’	12	G H8
6.133	7.923	1.54e+07	ga	12	G	H1’	12	G H8

2.376	6.133	1.26e+08	ga	12 G	H2'	12 G	H1'
2.380	4.676	9.51e+07	ga	12 G	H2'	12 G	H3'

	$\Delta\delta$		
Base	H2"	H2'	H1'
C1	0.006	0.006	0.031
G2	-0.009	0.04	0.04
C3	0.001	0.009	0.014
G4	-0.016	0.009	0.008
A5	0.003	0.001	0.009
A6	0.003	0.005	0.006
T7	0.001	-0.002	0.012
T8	0.001	0.012	0.011
C9	0.001	-0.013	0.003
G10	0.017	-0.003	
C11	0.012	0.006	0.021
G12	0.0025	0.006	0.043

Table 3: $\Delta\delta$ of d(5'-CGCGAATTCGCG-3')$_2$ and **YPt$_2$** (1:0.5) obtained from NOE resonances assignemets at τ_m = 400 ms.

Listing 4: Chemical shifts for d(5'-CGCGAATTCGCG-3')$_2$ determined by NOE experiment at τ_m = 400 ms.

Group	Atom	Nuc	Shift	SDev	Assignments
C1	H1'	1H	5.754	0.002	4
C1	H2"	1H	2.397	0.008	5
C1	H2'	1H	1.955	0.002	4
C1	H3'	1H	4.694	0.002	4
C1	H4'	1H	4.145	0	1
C1	H6	1H	7.627	0.002	4
G2	H1'	1H	5.872	0.005	3
G2	H2"	1H	2.676	0.016	4
G2	H2'	1H	2.647	0.031	2
G2	H3'	1H	4.969	0.007	3
G2	H4'	1H	4.345	0	1
G2	H8	1H	7.939	0.004	7
C3	H1'	1H	5.592	0.001	4
C3	H2"	1H	2.269	0.014	5
C3	H2'	1H	1.832	0.003	3
C3	H3'	1H	4.795	0.003	2
C3	H4'	1H	4.118	0	1
C3	H6	1H	7.26	0.001	5
G4	H1'	1H	5.415	0.001	4
G4	H2"	1H	2.706	0.043	4
G4	H2'	1H	2.646	0.007	3
G4	H3'	1H	4.975	0.003	2
G4	H4'	1H	4.31	0	1
G4	H8	1H	7.836	0.002	6
A5	H1'	1H	5.981	0.001	3
A5	H2"	1H	2.844	0.11	3
A5	H2'	1H	2.692	0.003	2
A5	H3'	1H	5.015	0.026	3
A5	H4'	1H	4.443	0	1
A5	H8	1H	8.101	0.001	3
A6	H1'	1H	6.149	0.001	3
A6	H2"	1H	2.92	0.004	5
A6	H2'	1H	2.558	0	1
A6	H3'	1H	5.034	0.023	3
A6	H4'	1H	4.453	0.003	2
A6	H8	1H	8.102	0.001	5
T7	CH3	1H	1.265	0.001	2
T7	H1'	1H	5.906	0.001	4
T7	H2"	1H	2.55	0.005	5
T7	H2'	1H	1.984	0.004	5
T7	H3'	1H	4.817	0	2
T7	H4'	1H	4.192	0.004	2
T7	H6	1H	7.103	0.001	8
T8	CH3	1H	1.527	0.001	2
T8	H1'	1H	6.101	0.011	4
T8	H2"	1H	2.535	0	3

T8	H2’	1H	2.157	0.002	5
T8	H3’	1H	4.267	1.077	4
T8	H4’	1H	4.202	0	1
T8	H6	1H	7.361	0	8
C9	H1’	1H	5.635	0.013	5
C9	H2”	1H	2.401	0.001	3
C9	H2’	1H	2.045	0.029	5
C9	H3’	1H	4.865	0.004	3
C9	H6	1H	7.453	0.002	7
c9	H4’	1H	4.2	0	1
G10	H1’	1H	5.846	0.004	3
G10	H2”	1H	2.66	0.015	3
G10	H2’	1H	2.582	0	1
G10	H3’	1H	4.974	0.004	2
G10	H8	1H	7.898	0.004	6
C11	H1’	1H	5.752	0	2
C11	H2”	1H	2.315	0.003	3
C11	H2’	1H	1.874	0.003	4
C11	H3’	1H	4.796	0	1
C11	H6	1H	7.315	0.002	4
G12	H1’	1H	6.144	0	3
G12	H2”	1H	2.588	0	1
G12	H2’	1H	2.371	0.001	3
G12	H3’	1H	4.666	0	1
G12	H4’	1H	4.162	0	1
G12	H8	1H	7.93	0.002	3

Listing 5: Chemical shifts for d(5'-CGCGAATTCGCG-3')$_2$ upon interaction with determined **YPt$_2$** by NOE experiment at τ_m = 400 ms.

Group	Atom	Nuc	Shift	SDev	Assignments
C1	H1'	1H	5.723	0	3
C1	H2"	1H	2.383	0.004	3
C1	H2'	1H	1.949	0.006	3
C1	H3'	1H	4.691	0	1
C1	H6	1H	7.601	0.006	3
C2	H2"	1H	2.706	0	1
G2	H1'	1H	5.832	0.004	4
G2	H2"	1H	2.677	0.018	3
G2	H3'	1H	4.967	0	1
G2	H8	1H	7.893	0.008	3
C3	H1'	1H	5.578	0.004	2
C3	H2"	1H	2.26	0.017	4
C3	H2'	1H	1.823	0.002	2
C3	H3'	1H	4.788	0	1
C3	H6	1H	7.245	0.003	4
G4	H1'	1H	5.407	0.003	4
G4	H2"	1H	2.714	0.019	3
G4	H2'	1H	2.645	0.01	2
G4	H8	1H	7.83	0.005	4
A5	H1'	1H	5.972	0.001	3
A5	H2"	1H	2.833	0.109	3
A5	H2'	1H	2.691	0.002	2
A5	H3'	1H	5.02	0.027	2
A5	H4'	1H	4.432	0	1
A5	H8	1H	8.095	0.003	3
A6	H1'	1H	6.143	0.001	3
A6	H2"	1H	2.909	0.004	5
A6	H2'	1H	2.553	0	1
A6	H3'	1H	5.047	0	1
A6	H4'	1H	4.444	0	2
A6	H8	1H	8.096	0.001	3
T7	CH3	1H	1.26	0	2
T7	H1'	1H	5.894	0.005	4
T7	H2"	1H	2.542	0.004	4
T7	H2'	1H	1.986	0.008	3
T7	H3'	1H	4.812	0	1
T7	H6	1H	7.099	0.003	6
T7	H8	1H	7.1	0	1
T8	CH3	1H	1.52	0	2
T8	H"	1H	2.523	0	0
T8	H1'	1H	6.09	0.01	4
T8	H2"	1H	2.526	0.003	3
T8	H2'	1H	2.145	0.015	4
T8	H3'	1H	4.853	0.023	5
T8	H6	1H	7.355	0.004	6

C9	H1’	1H	5.632	0.013	3
C9	H2”	1H	2.393	0.004	3
C9	H2’	1H	2.058	0.008	4
C9	H3’	1H	4.868	0	1
C9	H6	1H	7.445	0.003	6
G10	H2”	1H	2.635	0.002	3
G10	H8	1H	7.889	0.012	2
C11	H1’	1H	5.731	0.001	2
C11	H2”	1H	2.295	0.001	2
C11	H2’	1H	1.868	0.004	2
C11	H6	1H	7.295	0.003	3
G12	H1’	1H	6.101	0	3
G12	H2”	1H	2.483	0.117	2
G12	H2’	1H	2.365	0	1
G12	H3’	1H	4.666	0	1
G12	H8	1H	7.898	0	1

	$\Delta\delta$	
Base	H2”	H1’
C1	-0.005	0.005
G2	-0.032	-0.079
C3	0	1E-3
G4	-0.008	-0.036
A5	1E-3	-0.015
A6	-1E-3	-0.012
T7	-0.006	0.003
T8	-0.009	-0.002
C9	0.034	-0.007
G10	-0.003	-0.021
C11	-0.013	0.002
G12	-0.006	0.007

Table 4: $\Delta\delta$ of d(5’-CGCGAATTCGCG-3’)$_2$ and AATP (1:0.5) obtained from NOE resonances assignemets at τ_m = 400 ms.

Appendix to chapter 4

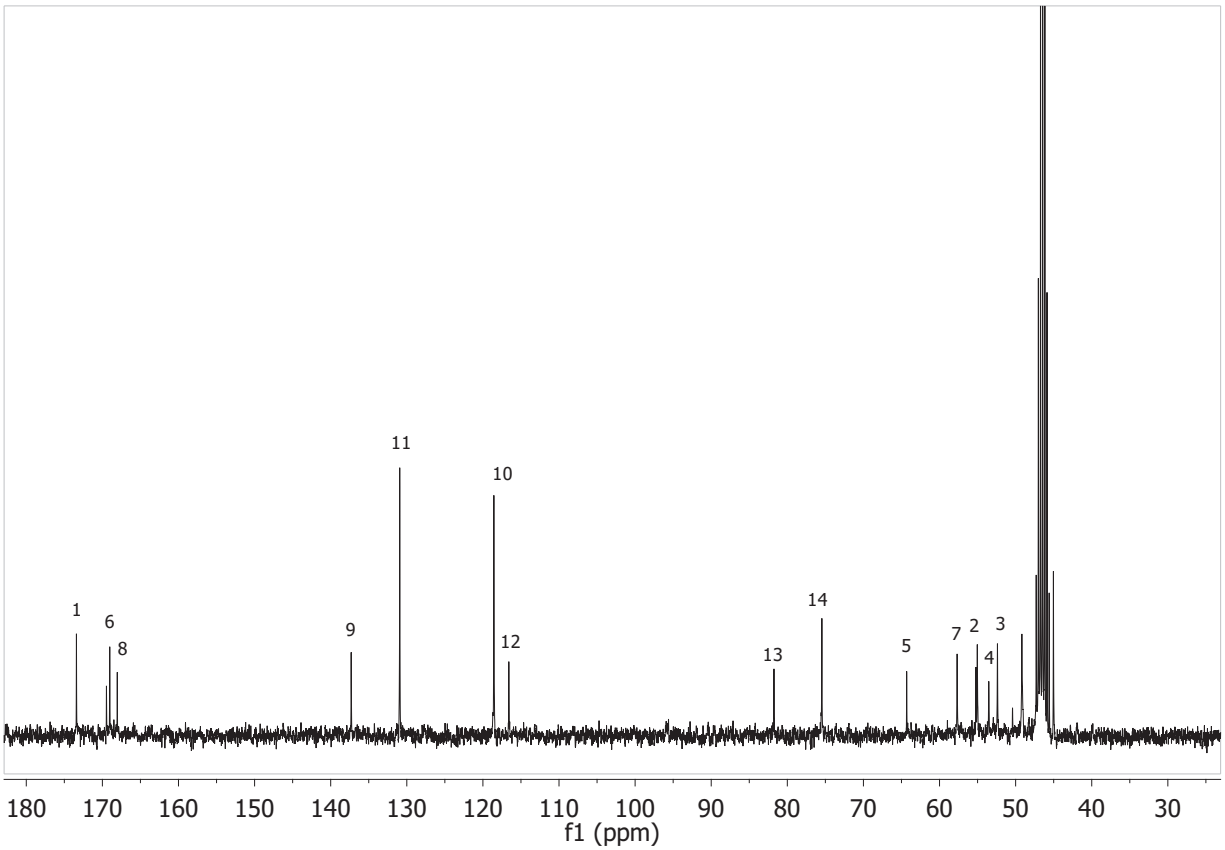

Figure 15: ^{13}C-NMR at 100MHz of DTPA-BEA in d_4-methanol.

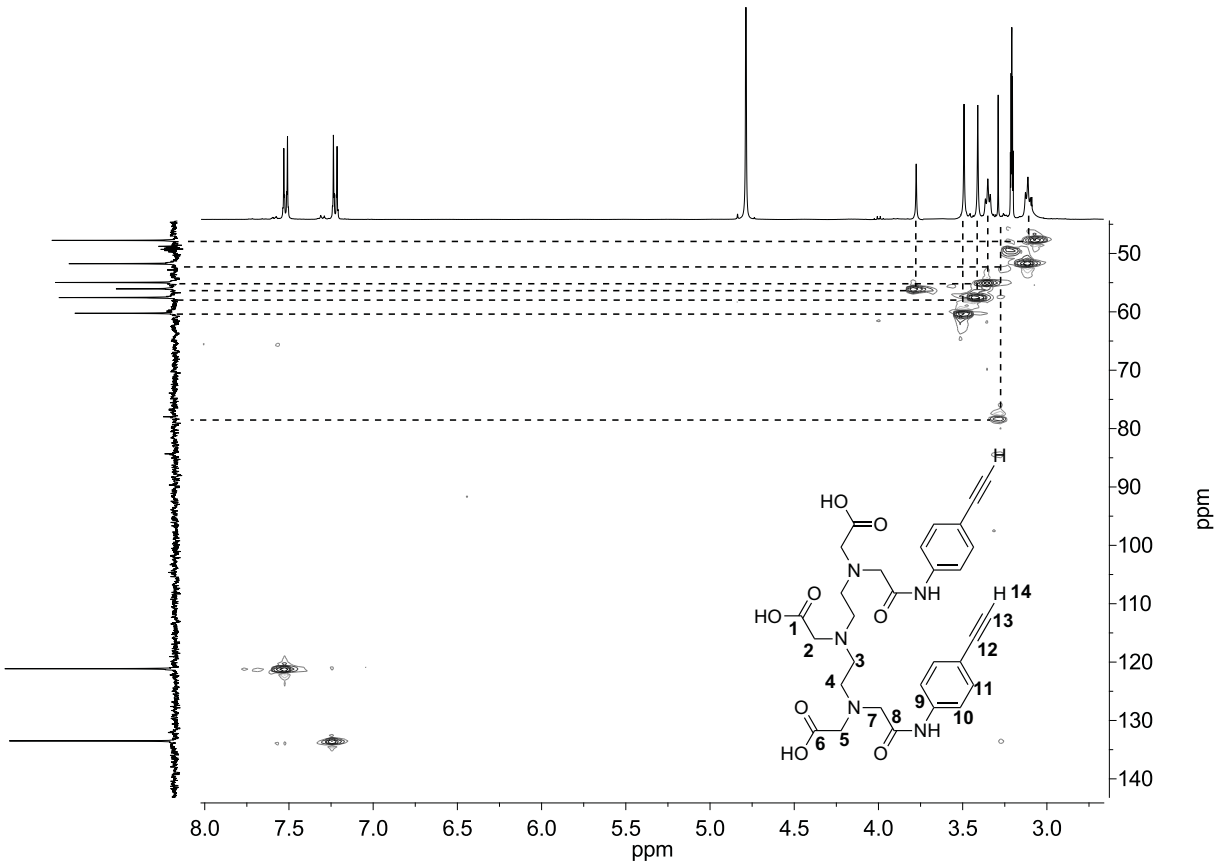

Figure 16: HSQC NMR at 400 MHz of DTPA-BEA in d_4-methanol.

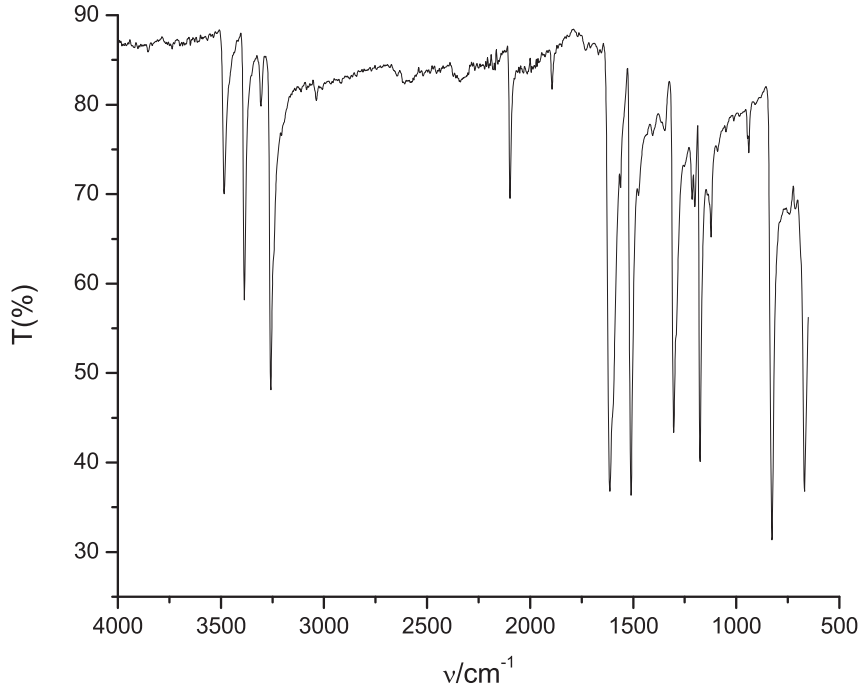

Figure 17: IR spectra of DTPA-bis(ethynylaniline).

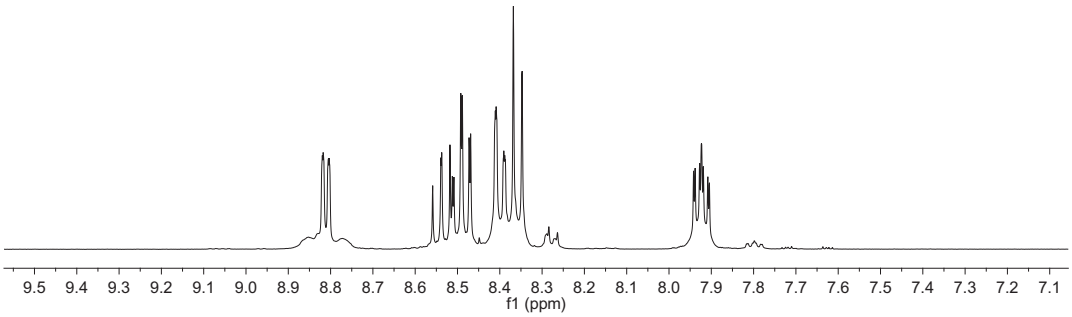

Figure 18: ^{1}H-NMR at 300 MHz of [Pt(tpy)MeCN]CH_3SO_3 d_3 MeCN.

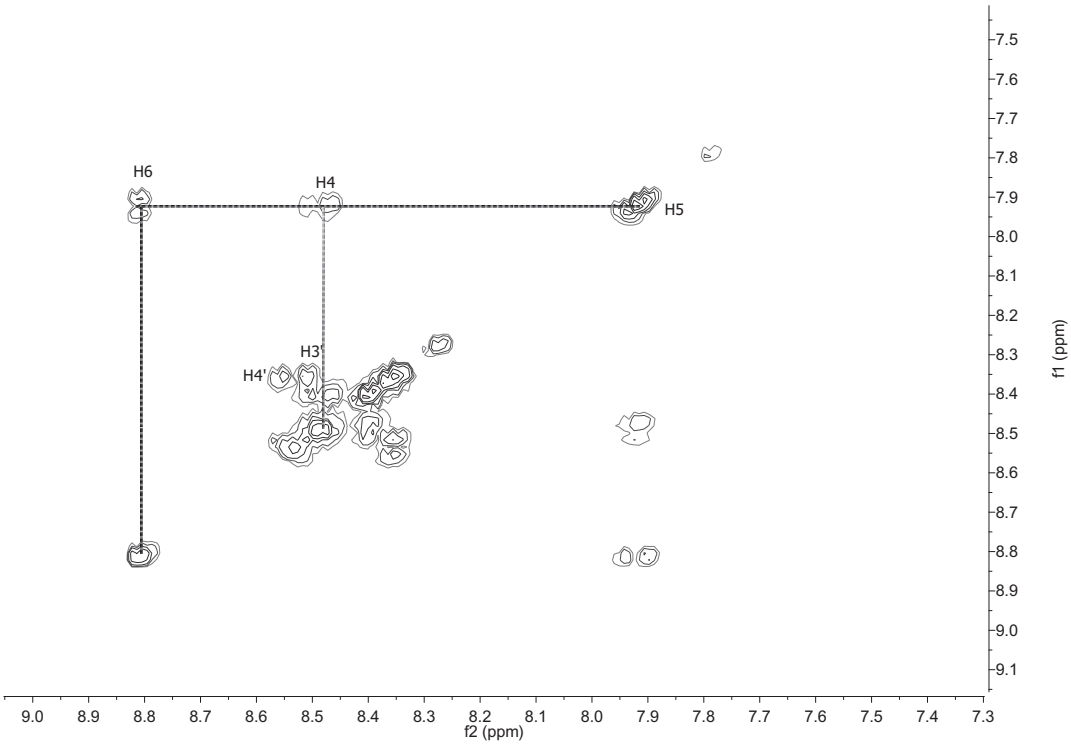

Figure 19: ^{1}H-^{1}H COSY NMR at 400 MHz of [Pt(tpy)MeCN]CH_3SO_3 d_3-MeCN.

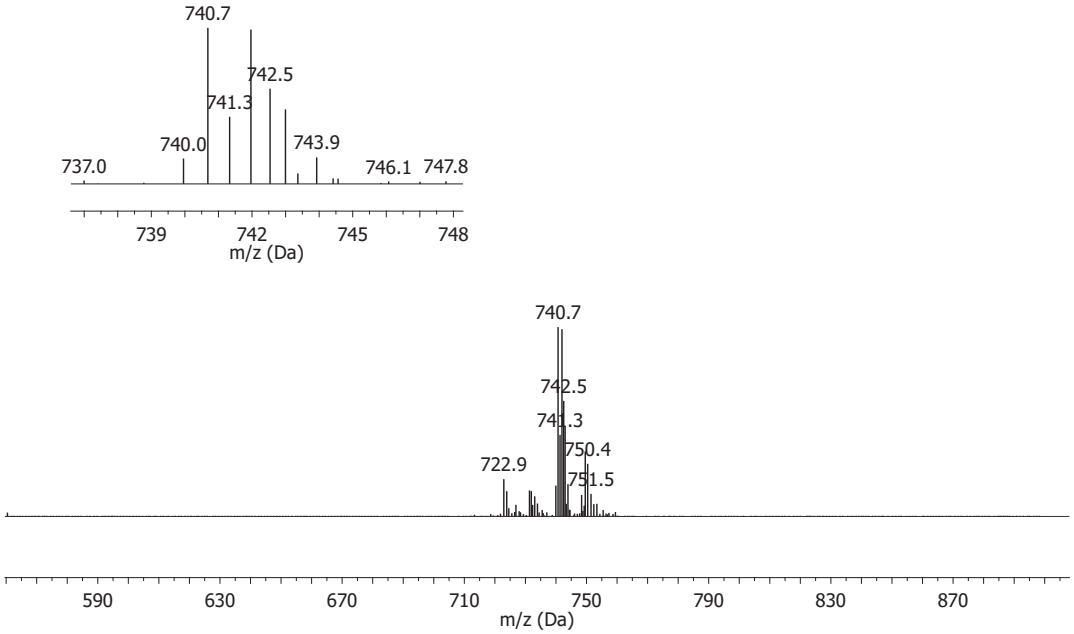

Figure 20: MS (ES^+) of $[LC{\equiv}CPt_2](CH_3SO_3)_2$.

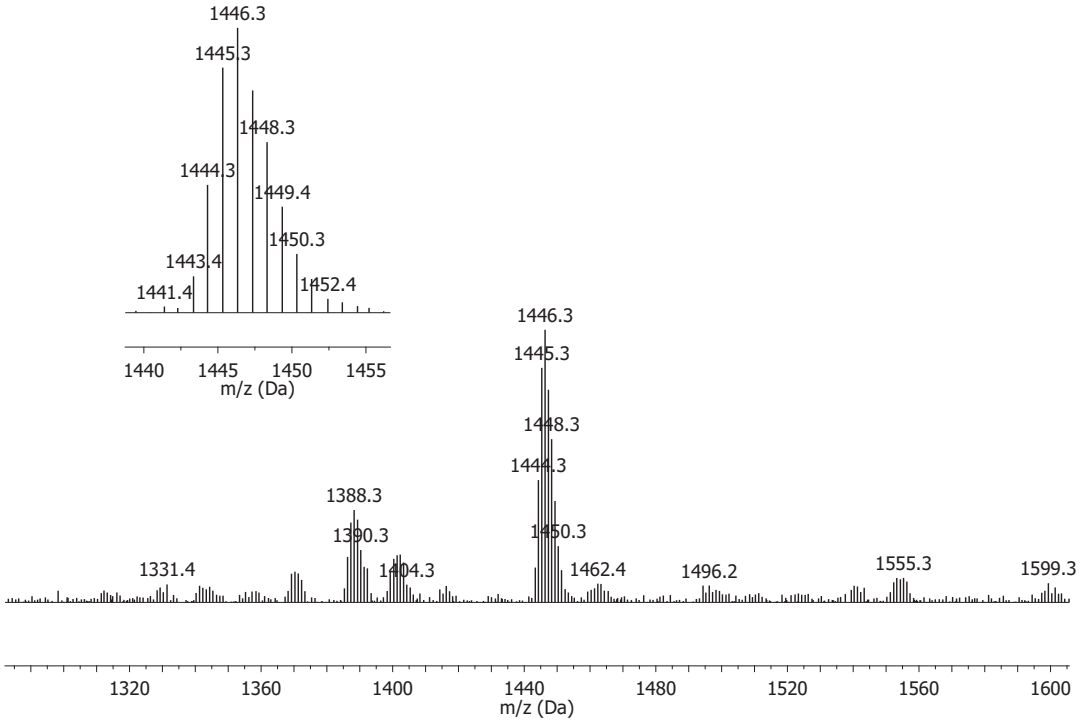

Figure 21: MS (MALDI) of $[LC{\equiv}CPt_2](CH_3SO_3)_2$.

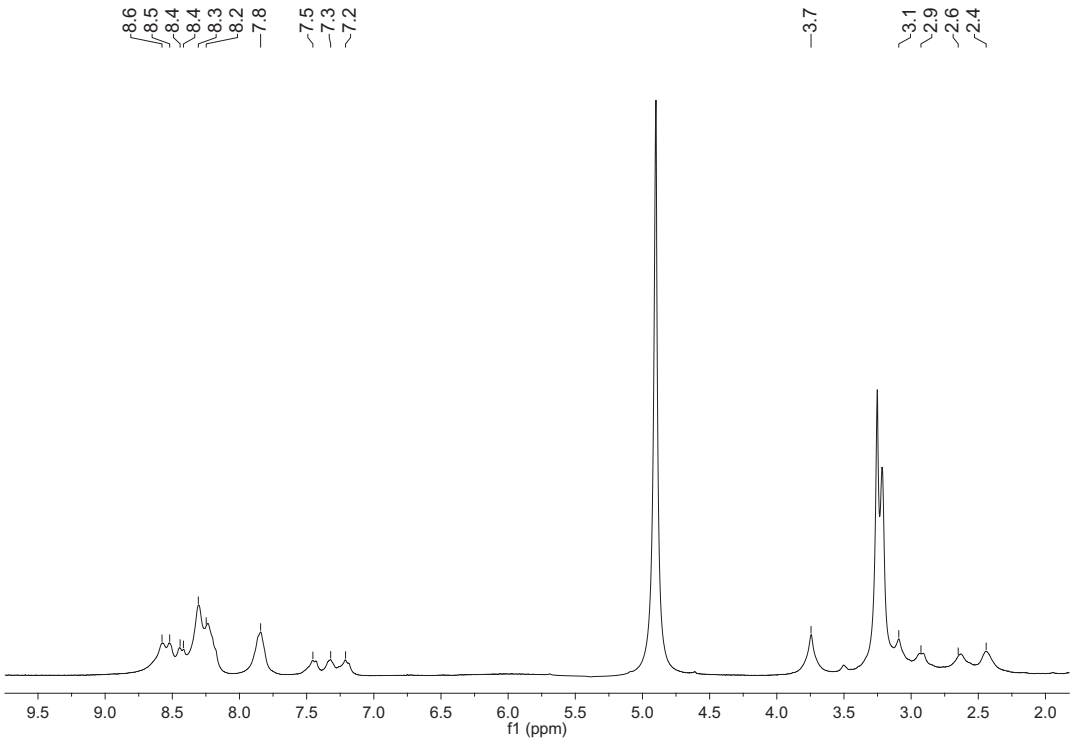

Figure 22: ^{1}H-NMR at 300 MHz of $[LC{\equiv}CPt_2](CH_3SO_3)_2$ in d_3-MeOH.

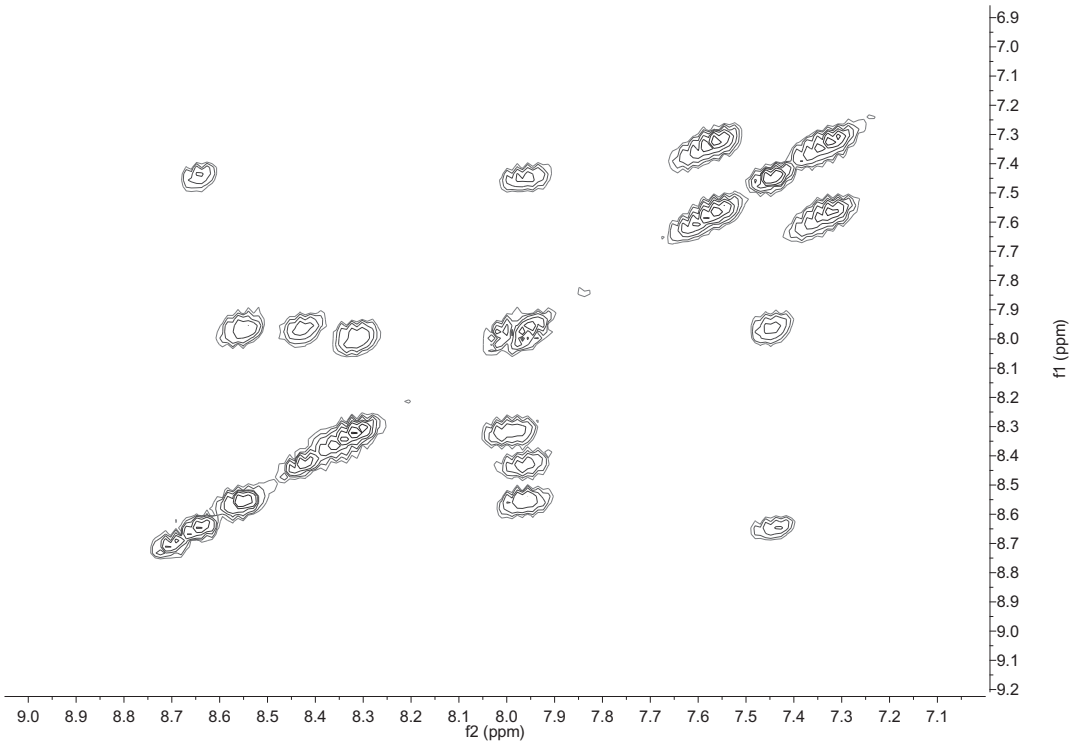

Figure 23: ^{1}H-^{1}H COSY NMR at 400 MHz of $[LC{\equiv}CPt_2](CH_3SO_3)_2$ d_3-MeOH.

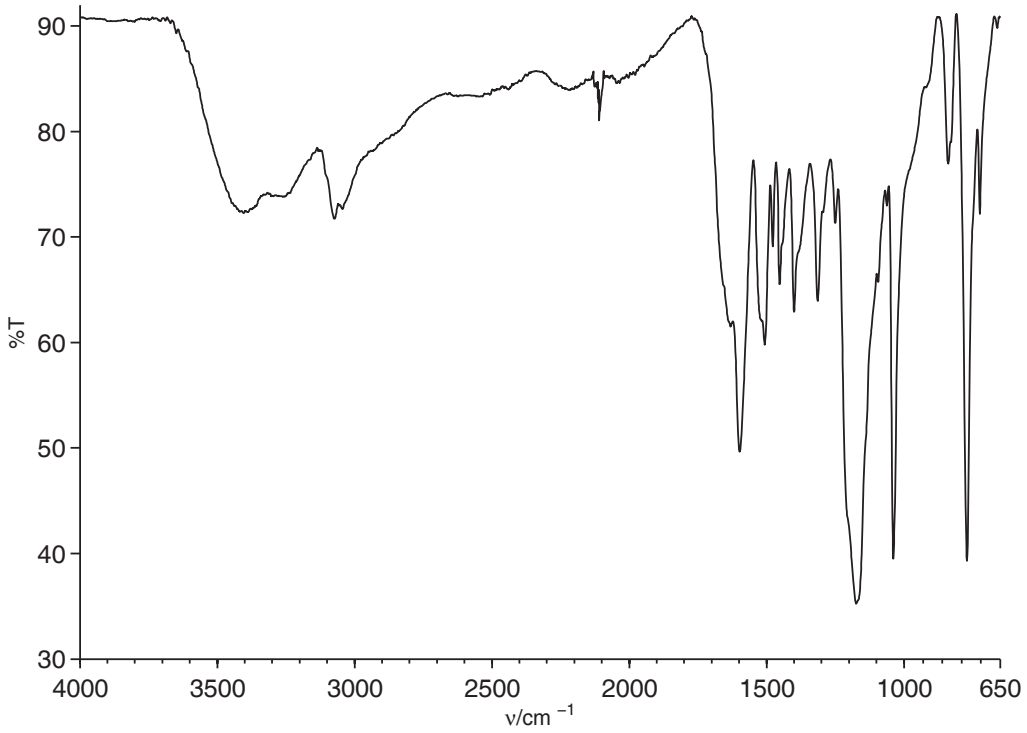

Figure 24: IR of $[LC{\equiv}CPt_2](CH_3SO_3)_2$.

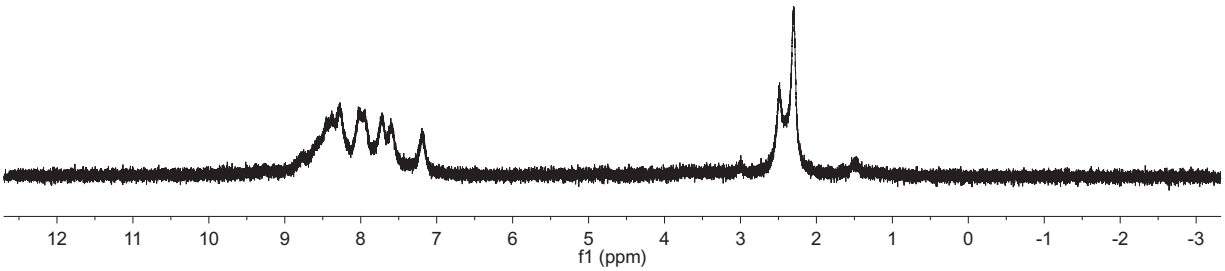

Figure 25: ^{1}H-NMR spectrum at 300MHz of [Pt(tpy)(C≡C)](CH_3SO_3) in D_2O.

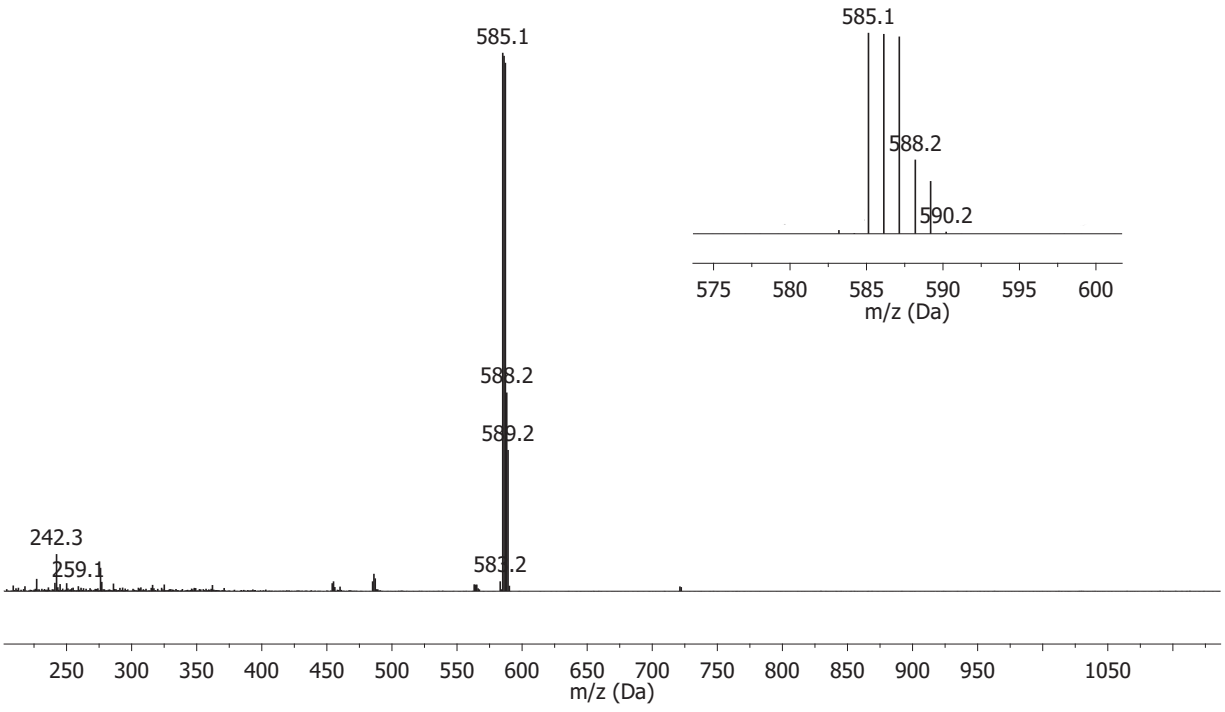

Figure 26: MS (ES^{+}) spectra of [Pt(tpy)(C≡C)](CH_3SO_3) complex.

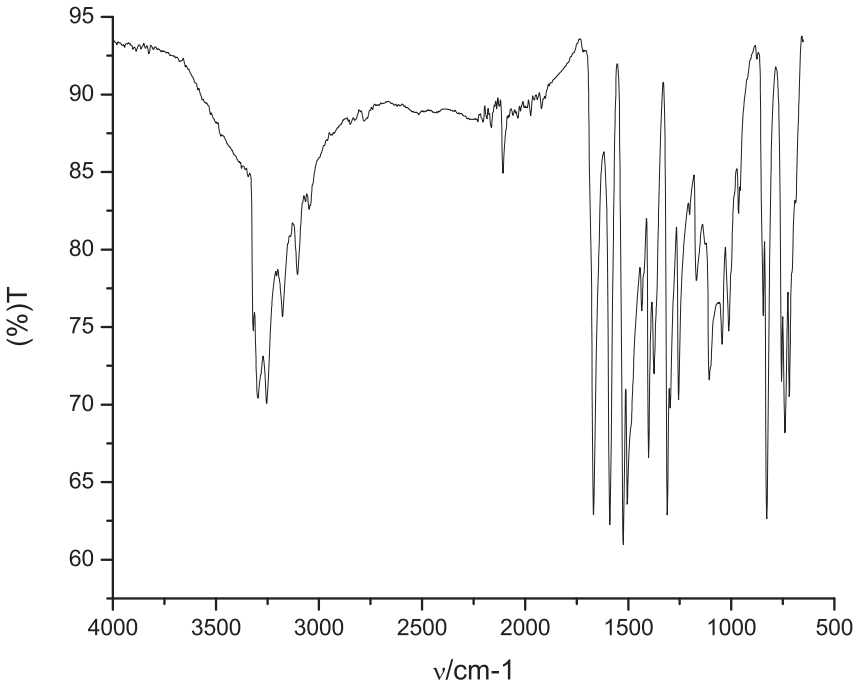

Figure 27: Solid state IR spectra of N-(4-ethynylphenyl)acetamide.

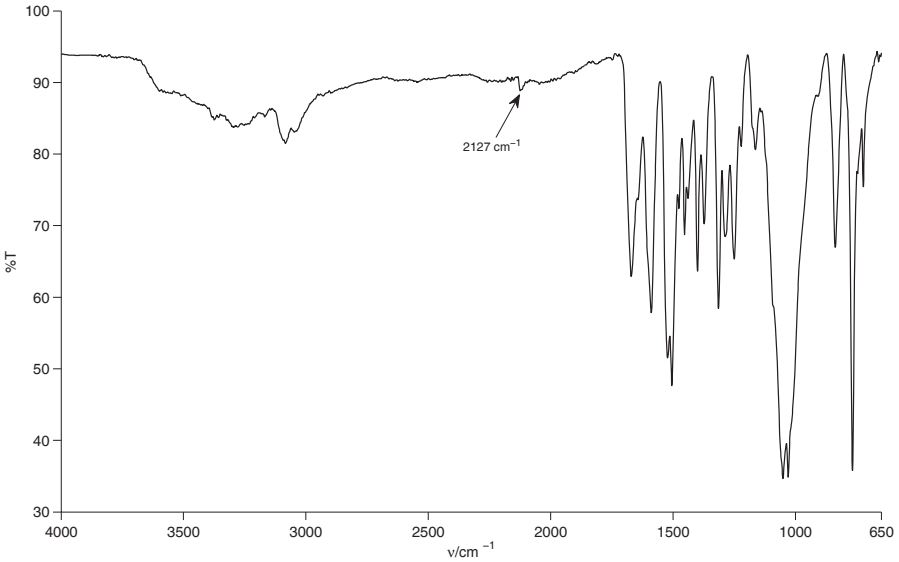

Figure 28: Solid state IR spectra of [Pt(tpy)C≡C](BF_4).

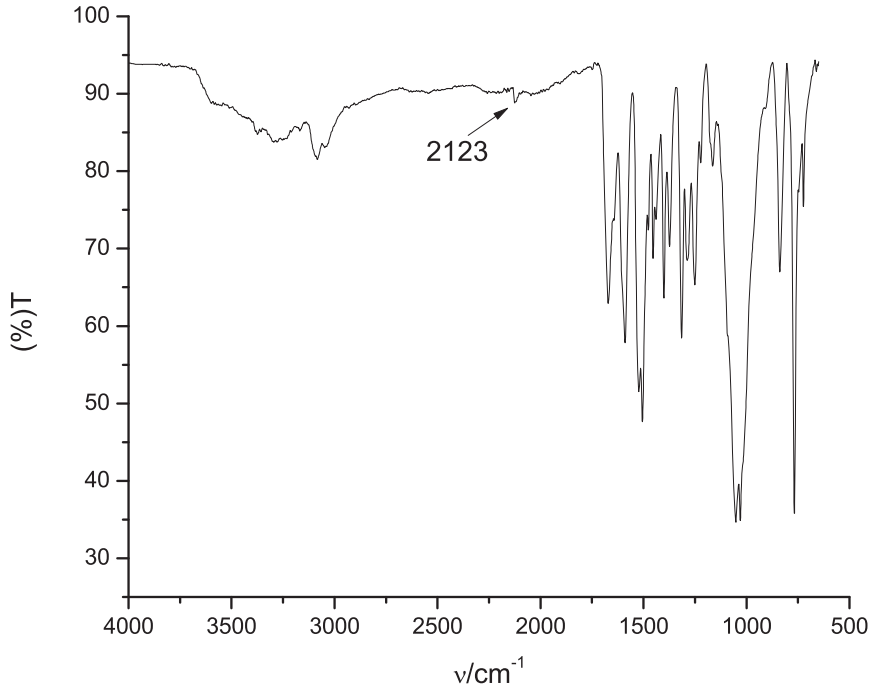

Figure 29: Solid state IR spectra of [Pt(tpy)C≡C](CH_3SO_3).

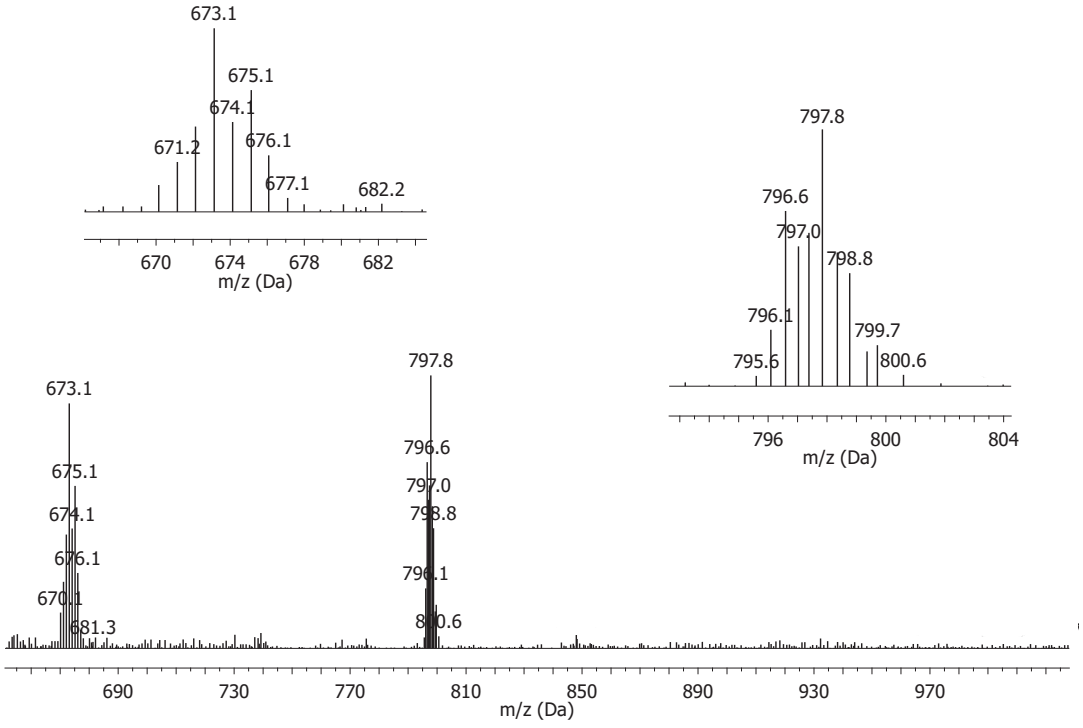

Figure 30: MS (ES^+) spectra of [Eu($CCPt)_2$]($CH_3SO_3)_2$.

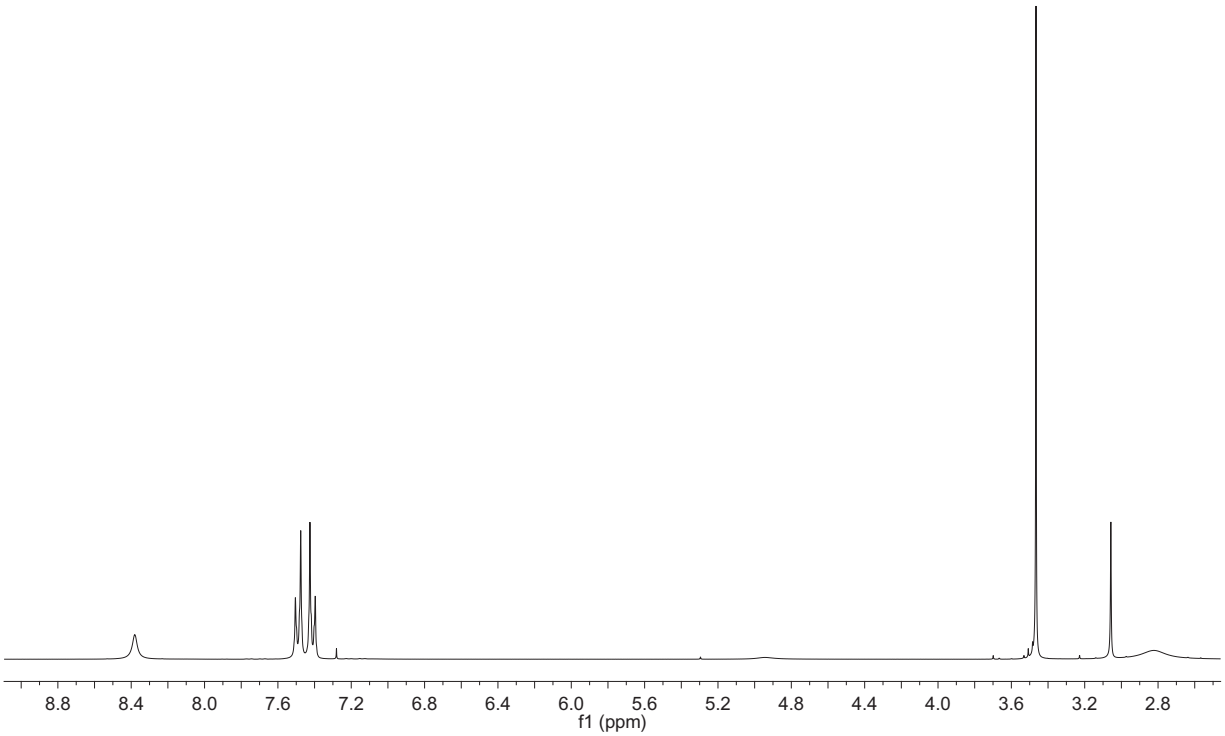

Figure 31: ^{1}H H-NMR spectrum at 300 MHz of N-(4-ethynylphenyl)acetimide in $CDCl_3$.

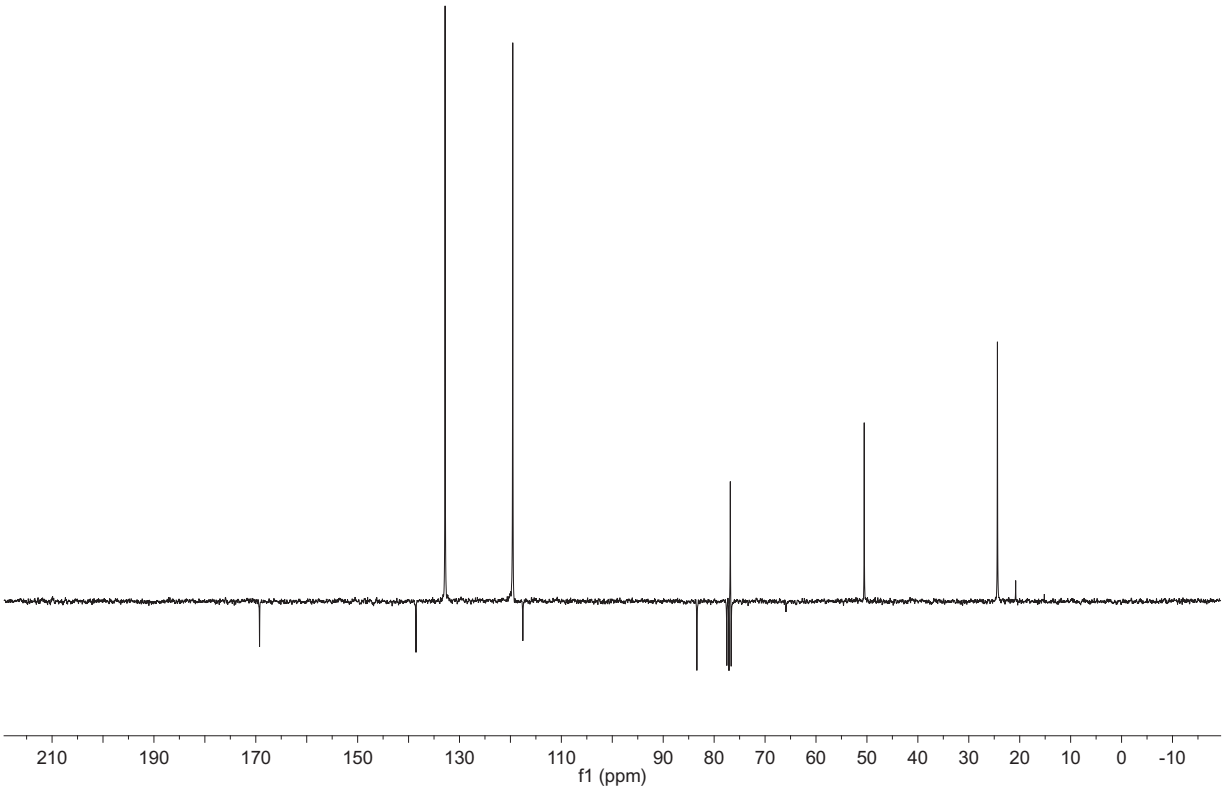

Figure 32: ^{13}C {H} PENDANT NMR spectrum at 75 MHz of N-(4-ethynylphenyl)acetimide in $CDCl_3$.

Appendix to chapter 5

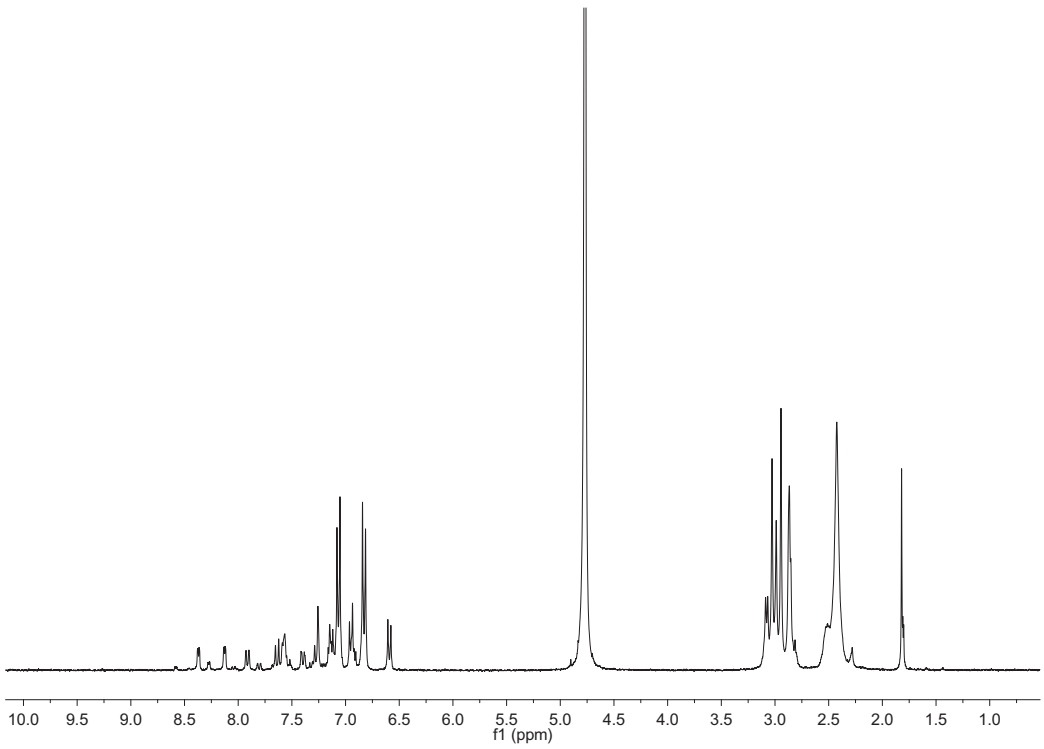

Figure 33: ^{1}H-NMR at 300 MHz of DTPAQ–SH, mixture of the crude ligands.

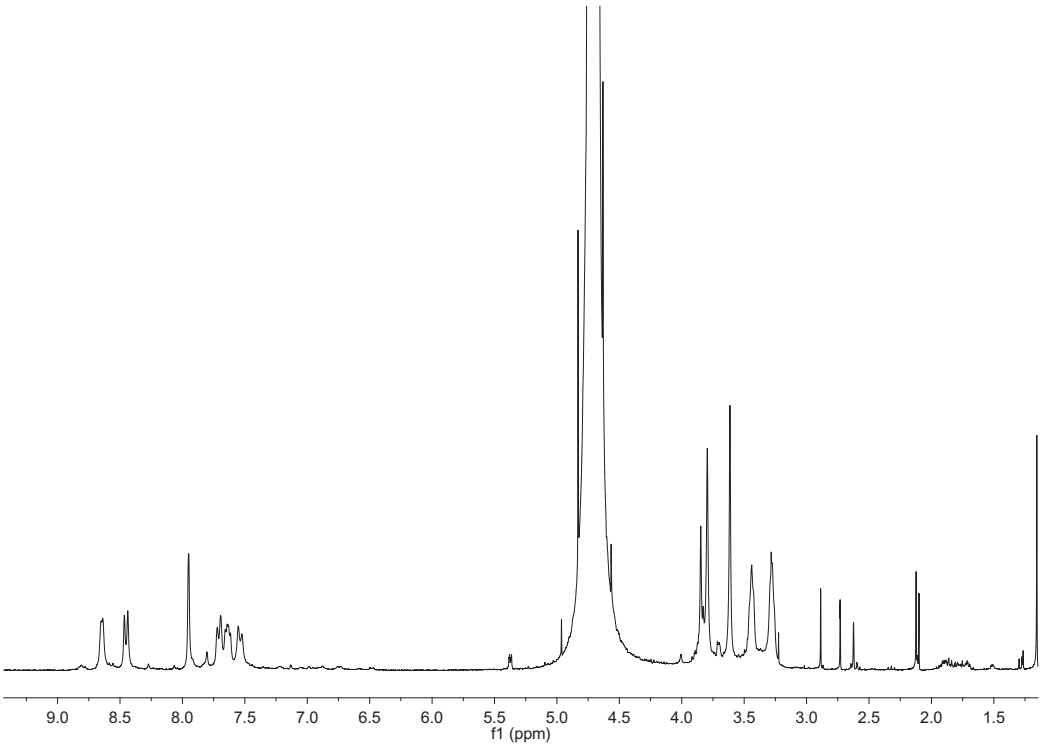

Figure 34: ^{1}H-NMR at 300 MHz of H_3L^a.

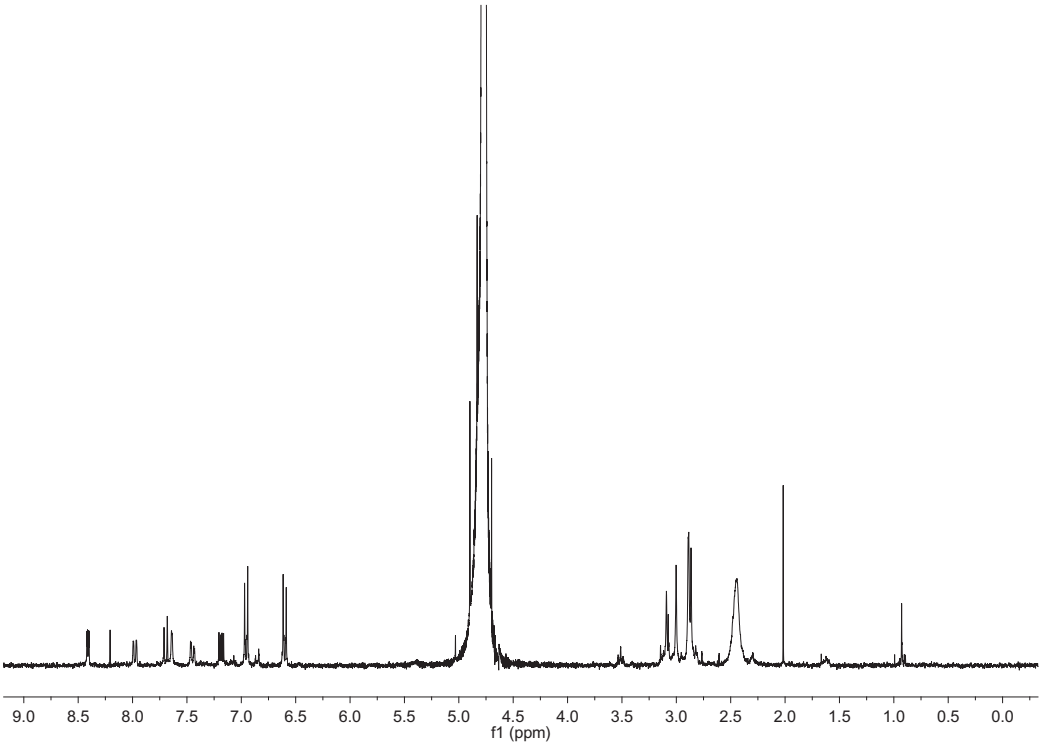

Figure 35: ^{1}H-NMR at 300MHz of H_3L^b with presence of H_3L^a .